

NISTIR 5241



**NIST
PUBLICATIONS**

RL/NIST Workshop On Moisture Measurement and Control for Microelectronics

**Proceedings of the RL/NIST Workshop
held at the National Institute of Standards and Technology
Gaithersburg, MD, April 5-7, 1993**

Benjamin A. Moore and Joseph A. Carpenter, Jr.



**United States Department of Commerce
Technology Administration
National Institute of Standards and Technology**

**QC
100
.U56
#5241
1993**

RL/NIST Workshop On Moisture Measurement and Control for Microelectronics

Proceedings of the RL/NIST Workshop
held at the National Institute of Standards and Technology
Gaithersburg, MD, April 5-7, 1993

Co-Chairmen:

Benjamin A. Moore
Joseph A. Carpenter, Jr.

Sponsored by:

Rome Laboratory
Griffiss AFB, NY 13441-5700
and
National Institute of Standards and Technology
Gaithersburg, MD 20899

August 1993



U.S. Department of Commerce

Ronald H. Brown, Secretary

Technology Administration

Mary L. Good, Under Secretary for Technology

National Institute of Standards and Technology

Arati Prabhakar, Director

Table of Contents

A Historical Review of Residual Gas Analysis R.W. Thomas, Technology Expert Network	1
Lab Correlation Study Status Benjamin A. Moore, Rome Laboratory/ERDR	12
Low-Density Water Vapor Measurements; The NIST Primary Standard and Instrument Response Stuart A. Tison and Charles R. Tilford, National Institute of Standards and Technology	19
Using Permeation Tubes to Calibrate Trace Moisture Analyzers James J. McKinley, Kin-Tek Laboratories, Inc.	30
Thermodynamic Properties of Moist Air Containing 1000 to 5000 PPMv of Water Vapor Peter H. Huang, National Institute of Standards and Technology	43
Studies on a Solvent Resistant Humidity Sensor with High Water Vapor Affinity: Important Implications for Microelectronics Gerald Schultz and Christopher Polla, Phys-Chem Scientific Corp.	52
Hydrogen Desorption from Base and Processed Packaging Alloy Philipp wh Schuessler and Stephen G. Gonya, IBM/FSC	67
Degreaser Fluid Induced Electrical Assembly Corrosion; Failure Analysis of a Moisture Limited Mechanism David O. Ross, Rome Laboratory	91
Moisture Effects on Interphase Conductivity J.E. Anderson and K.M. Adams, Ford Motor Co., P.R. Troyk, Pritzker Institute for Medical Engineering	115
Corrosion of Chip Resistors within a Hybrid Induced by Tantalum Chip Capacitor Outgassing Products Joe Abbott, Thomas J. Green, and Kerry Huntington, Martin Marietta	121

Moisture Effect and Measurement on Semiconductor Gas Process Anthony F. Amato, Yadan W. Chen, and Edward T. Flaherty, Matheson Gas Products, Inc.	134
Military Specifications and Laboratory Suitability for MIL-STD-883 Method 1018 Alan R. Clark, Defense Electronics Supply Center	159
Hermeticity Specifications and their Effects on Method 1018 A. Dermarderosian, Sr., Raytheon Company	163
Hermetic Package Moisture Control at Harris Semiconductor Robert K. Lowry, Harris Semiconductor	172
Improving Device Reliability Through Residual Gas Analysis (RGA) Arun Kumar and James O. McClain, Jr., SEAL Laboratories	185
Moisture Level Fluctuations within Hermetically Sealed Microelectronic Devices Larry Henke, Steve VanDerlick, Mark Alderton, Cardiac Pacemakers, Inc.	194
High Reliability Sealed Chip Technology, What's Needed for Determining Corrosion Protection David O. Ross and James F. Reilly, Rome Laboratory	203
Long Term Package Integrity in a Military Environment D. David Dylis and George H. Ebel, IIT Research Institute	210
Alternate Packaging Scheme to Guarantee Low Internal Moisture Content James C. Lau and Doug B. Nord, TRW	222
Decreasing Moisture Content of Epoxy After High Temperature Stress, by Altering Pre-Seal Bake Times Bill Vigrass, Jack Linn and Jim Walling, Harris Semiconductor	241
Effects of Process Variables on Moisture in Hermetic Packages Containing Organic Adhesives William H. Bardens, Beckman Industrial Corp. and Terry E. Phillips and Richard C. Benson, Johns Hopkins University	249
Low Moisture Polymer Die Attach Adhesive for Solder Seal Packages My N. Nguyen, Johnson Matthey Electronics	262

Interpretation of RGA Data - Including Recent Observations on the Outgassing Characteristics of New Materials Donald T. Shuman, Oneida Research Services, Inc.	275
Water Adsorption at a Polyimide/Silicon Wafer Interface Wen-li Wu, William J. Orts, Charles J. Majkrzak and Donald L. Hunston, National Institute of Standards and Technology	291
An Evaluation of the Moisture Content of Hermetically Sealed T05 Metallic Cans as a Function of Analysis Temperature Jack H. Linn and Josh Daar, Harris Semiconductor	313
Reliable Moisture Determination in the Presence of Hydrogen or Oxygen Using Method 1018.2 Bruce J. Gollob, Atlantic Analytical Laboratory, Inc.	326
Gas Composition Analysis of Hermetic Structures as a Non-Destructive Test John C. Pernicka, Pernicka Corp.	327
New Microelectronics Package Atmosphere Analysis System: Sample Analysis and Calibration Standards Stephen A. Ruatta, Julius Perel and John F. Mahoney	332
Microcircuit Hermeticity Testing Using the Bergquist Method Scot K. Anderson and Thomas J. Green, Martin Marietta Astronautics Group . . .	338

**A HISTORICAL REVIEW OF
RESIDUAL GAS ANALYSIS**

by

R.W. Thomas
Technology Expert Network
Rome, NY

HISTORICAL BACKGROUND

THE PLAYERS - A RICH HISTORY

**ROME AIR DEVELOPMENT CENTER -
Ben Moore, Bob Thomas, Chuck Messenger**

Atmospheric Sampling Probe

Epitaxial Reaction Chamber

Autonetics Oven Obtained

Rapid Cycle Tech Development &
Transfer to Industry

Dry Ceramic & Hybrid Technology

Viking Program

Certification Program

AUTONETICS - Phil Eisenberg - Monograph - Date

Multiple Sample Holder Oven

Gas Chromatography Detector

Concern About Failures Due to Moisture

TEXAS INSTRUMENTS - Don Meyer

Mass Spectrometry

Measuring Gas Line Purity

Made a Jig for Package Sampling

JOHN PERNICKA

Smoke Stack Sampling

TV Tubes

Earthquake Gas Evolution Measurements

AF Contract to Make First Commercial RGA

Three Volume Calibration Valve

NATIONAL BUREAU OF STANDARDS - Stan Ruthberg & Saburo Hasegawa

Pacemaker Symposium (Cordis & Medtronics)

Helium Leak Measurements

Moisture Measurement Symposium

Three Volume Calibration Valve

JEDEC - Phil Schuessler, IBM ; Connie Zierdt, AT&T

Method 1018 Task Force

Round Robin Correlation Tests

RAYTHEON - Aaron DerMaderosian

Moisture Standards

RH Experiments

GOLLOB ANALYTICAL -

Fred Gollob & Steve Carvellus

Round Robin Testing

**WEST COAST TECHNICAL SERVICES -
Dwight Fisher & Richard Merrell**

Magnetic Sector

**ONEIDA RESEARCH SERVICES -
Tom Rossiter & Diane Feliciano**

Commercialization of Method 1018

Dynamic Analysis Technique

AT&T - M. White & J. Mucha

Die Attach Reaction

Laser Absorption Technique

JPL - Alex Shumka - Dick Piety & Ray Haack

Au Migration

Viking Program

Delta Parameter Test

HARRIS - Bob Lowry

Dry Cerdips

KYOCERA

Vitreous Sealing Glass - (KC-1M)

Superdry - Dessicated

INTEL - Brad Sun

Sensitivity Factor in Mixtures

PANAMETRICS - Vic Fong

Solid State Sensor

MEDTRONICS - Steve Loukes

Integration Method

BRITISH TELECOM - Bob Merritt

ERICSSON - Orjan Halberg

CLARKSON UNIVERSITY - Naga Annamalai

... PROBLEMS NEEDING RESOLUTION

Moisture limits for hybrids or IC's that contain absorbing materials (i.e., epoxy or silicone coatings) will require new definition related to total water.

• Stable, inexpensive standards that cover the range of testing (i.e., 500 ppm - 20,000 ppm) available to customers to monitor their test labs.

A method for accurate calibration using hydrogen/nitrogen mixture.
Round Robin Correlation.

PROBLEMS NEEDING RESOLUTION ...

An understanding of the various leak mechanisms such as one-way leakers, capillary leak plugging, compression seals, stress cracking of glass to metal seals (both cerdip and hybrid).

Techniques for minimizing no-tests. (Sample opening procedures.)

More data on Procedure 2, Method 1018 for large volume samples (i.e., greater than 10cc).

LAB CORRELATION STUDY STATUS

by

Benjamin A. Moore
Rome Laboratory/ERDR
Griffiss AFB, NY

LAB CORRELATION STUDY

- TWO SERIES OF SAMPLES
- SAMPLE VOLUME RANGE: 0.01CC - 5.5CC
- VARYING MOISTURE CONCENTRATION
 - ONE SERIES ONLY
 - VOLUME DEPENDENT
- GAS MATRIX EFFECTS
- ORGANIC EFFECTS
- "SPECIAL" SAMPLES

LAB CORRELATION STUDY

0.01CC SAMPLES-MOISTURE IN PPMV

	<u>ROME LAB</u>	<u>LAB D</u>	<u>LAB G</u>	<u>LAB I</u>
X	13030	12130	16500	12830
S	1230	1680	1040	490
%OM	96.2	89.6	119.4	94.8

OVERALL MEAN (OM):13540

LAB CORRELATION STUDY

0.02CCA SAMPLES-MOISTURE IN PPMV

<u>LAB</u>	<u>X</u>	<u>S</u>	<u>%OM</u>
RL	8670	690	88.9
D	9770	470	100.2
G	10300	420	105.6
I	9500	220	97.4
X1	8401	293	86.1
X2	11878	1552	121.8

OVERALL MEAN (OM):9753

LAB CORRELATION STUDY

0.02CCB SAMPLES-MOISTURE IN PPMV

	<u>ROME LAB</u>	<u>LAB D</u>	<u>LAB G</u>	<u>LAB I</u>
X	6400	5850	8230	6530
S	200	460	250	150
%OM	94.8	86.7	121.9	96.7

OVERALL MEAN (OM):6750

LAB CORRELATION STUDY

0.1CC SAMPLES-MOISTURE IN PPMV

<u>LAB</u>	<u>X</u>	<u>S</u>	<u>%OM</u>
D	5970	320	94.8
G	7100	300	112.7
I	6300	210	100.6
X1	5442	276	86.4
X2	6648	375	105.5

OVERALL MEAN (OM):6300

Session I

Moisture Physics

LOW-DENSITY WATER VAPOR MEASUREMENTS; THE NIST PRIMARY STANDARD AND INSTRUMENT RESPONSE

Stuart A. Tison and Charles R. Tilford
National Institute of Standards and Technology
Thermophysics Division
Gaithersburg, MD 20899

ABSTRACT

A primary standard for low-density water vapor has been built using a Knudsen-effusion source and a calculated conductance. The effusion source uses arrays of laser-drilled holes to generate a known flow of water. This flow is passed through the calculated conductance to generate water pressures in the range 10^{-5} to 10^{-2} Pa (10^{-7} to 10^{-4} Torr). This standard has been used to examine the operating characteristics with water of several types of vacuum instruments: ionization gages, Spinning Rotor Gages, and Partial Pressure or Residual Gas Analyzers. In general, operation with water can cause significant changes in the sensitivity of these instruments, and also generate several other gas species that can cause misleading partial pressure or residual gas measurements. This work is continuing with the development of improved standards and further instrument performance studies.

1. INTRODUCTION

Water is the most common and one of the least desirable residual gases in low-pressure or vacuum environments. The water can be introduced with process gases, but more usually comes from within the vacuum system, desorbing from the copious quantities attached to surfaces after exposure to atmospheric air. Water can cause significant and generally undesirable changes in the properties of metal and semiconductor thin films, obscure optical components, and corrode components to the point of mechanical failure. These problems may occur during component fabrication, or accrue over periods of years during storage and service.

Various procedures are used to minimize water during vacuum processing and device storage. However, the sources of water are so varied that the efficacy of these procedures can vary significantly and it is desirable to directly monitor the residual water to test their effectiveness. A variety of vacuum instrumentation is used to monitor water, principally ionization gages and Residual Gas (RGA) or Partial Pressure Analyzers (PPAs). Unfortunately, the performance of these instruments can be seriously affected by exposure to or operation with water, and the reliability of their results is generally unknown.

In order to calibrate and evaluate the performance of vacuum instrumentation the Vacuum Group of the National Institute of Standards and Technology (NIST) has undertaken the development of primary high vacuum standards for water vapor. A prototype orifice-flow standard has been built using a Knudsen-effusion water source. This standard has been used to examine the performance of both hot- and cold-cathode ionization gages, quadrupole and magnetic-sector type PPAs, and Spinning Rotor Gages (SRGs), and has been used for the calibration of several instruments to be used in a satellite outgassing experiment. The success of the prototype standard encouraged the construction of a second-generation water effusion source, which is presently undergoing calibration and evaluation. Plans are also underway to use high-resolution infrared absorption to directly measure vapor-phase water.

This paper describes the design and calibration of the water effusion-source primary standard, and summarizes the results to date on instrument performance, with particular emphasis on PPAs and ion gages.

2. ORIFICE-FLOW PRIMARY STANDARD

2.1 Design and Construction

The National Institute of Standards and Technology has used the orifice-flow technique [1] to develop a series of primary standards for pressures between 10^{-7} and 10 Pa (10^{-9} and 10^{-1} Torr; 1 Torr = 133.322 Pa). These standards generate a pressure by passing a known flow of gas through an orifice, in most cases a nominal 11 mm diameter orifice that is fabricated with a shape that allows the calculation of its molecular conductance. Known flows between 10^{-12} and 10^{-6} mol/s (10^{-8} and 10^{-2} std cc/s) are generated by constant-pressure, variable-volume flowmeters [2].

The constant-pressure flowmeters will work only with "permanent" gases. To generate known water pressures the system has been modified to include a calibrated molecular-effusion source, as shown in figure 1. The principal component of the water effusion source is a molecular, or near-molecular conductance; an array of holes, 3-5 micrometers in diameter, drilled by a laser in a 25 micrometer thick stainless steel foil. A 10-Torr capacitance diaphragm gage (CDG) measures the water pressure upstream from the conductance. The conductance and CDG are maintained at a temperature of 70 °C. As discussed below, the flow rate through the conductance is calibrated

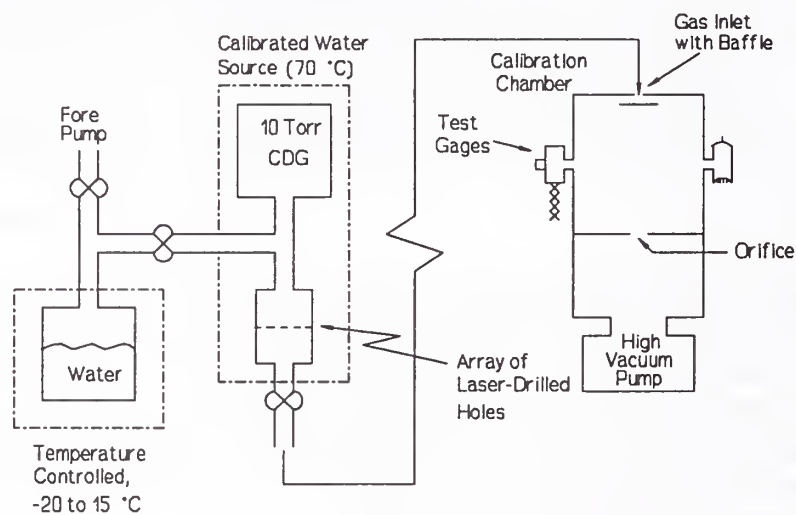


Figure 1: Schematic of the vacuum calibration apparatus configured to generate known water pressures.

as a function of the CDG reading for one or more permanent gases using one of our constant-pressure flow standards. The calibrated water source is separated from the calibration chamber by a bakeable valve so that the flow of water can be completely turned off. The source has been used with three different calibration chambers. The chamber generally used is a 45 cm diameter, 50 cm long cylinder, equipped with twelve metal-gasketed mounting flanges that permit a number of instruments to be calibrated at the same time, and the volume downstream from the orifice is pumped by a 500 l/s turbomolecular pump (High Vacuum Pump). The entire system is of bakeable all-metal construction.

Water is supplied to the effusion source from a temperature-controlled container of distilled and deionized water. The water is outgassed by pumping on it for several days while it is repeatedly frozen and melted. As with the rest of the system, all-metal construction is used throughout. By varying the temperature of the water, and pumping on it with an auxiliary mechanical pump, the water supply pressure can be varied between 6 and 1000 Pa.

The prototype water source employs a single array with 100 holes with a water conductance of 4.2×10^{-5} l/s at 70°C . This allows the generation of water calibration pressures between 1.8×10^{-5} and 3×10^{-3} Pa. The success of this system prompted the construction of a new source, shown in figure 2, with three arrays of 5, 50, and 500 holes. The multiple conductances will allow an extension of the water calibration range, and permit intercomparison of the different conductances to check on stability and determine viscosity corrections at higher water supply pressures.

2.2 Conductance Calibration

Determination of the array conductances is a critical element of the standard. As noted, we cannot directly determine the water conductance using primary standard flowmeters and it is necessary to derive the conductance from data for other gases. In the simplest case, a thin orifice, kinetic theory predicts that in the low-pressure or molecular-flow limit the conductance scales with the inverse square-root of the gas molecular weight. However, the laser drilled holes are hardly thin orifices; they are fairly steep conic sections with relatively small length-diameter ratios between 5 and 10, intermediate in geometry between thin orifices and long tubes. For such geometries, collisions between the gas molecules and the surfaces of the conductance element will cause deviations from the kinetic theory predictions for thin orifices. Even at very low pressures, where collisions between gas molecules are rare, differences in molecular scattering characteristics, the ratio of specular to diffuse scattering at the conductance surfaces, and surface adsorption can be important. It is possible to account for some of these effects; Tison has demonstrated [3] that if mean free path corrections are taken into account, the sulfur hexafluoride, nitrogen, argon, and helium conductances of long metal capillaries can be modeled to within $\pm 2.5\%$ for Knudsen numbers (the ratio of the molecular mean-free path to the conductance dimension) between 0.01 and 10. However, water has an exceptionally high sticking probability and different scattering characteristics, so the possibility of larger deviations from these conductance models must be examined.

The calibration of the conductance used in the prototype system was limited to nitrogen and helium for supply pressures up to 1 kPa. A much more extensive calibration has been carried out for the three arrays in the second-generation system. Conductances have been determined for helium, nitrogen, argon, and sulfur hexafluoride with upstream pressures as high as 10 kPa. Sulfur hexafluoride and helium were selected to include a large range of molecular weights and because of their different adsorption energies or sticking coefficients. As can be seen in figure 3, for the 500 hole array the helium, nitrogen, argon and sulfur hexafluoride conductances scale with the mean free path for inverse Knudsen numbers greater than 0.4. In figures 3 and 4 the conductance is expressed in equivalent nitrogen molar flow per Pascal; this may be converted to m^3/s by multiplying by the Universal Gas Constant ($R = 8.3144 \text{ J/mol K}$) and the appropriate temperature in kelvin. In this range the flow approaches slip flow, for which molecule-molecule collisions become important [4]. For inverse Knudsen numbers less than 0.4 the conductances of the various gases diverge, with helium increasing and sulfur hexafluoride decreasing relative to nitrogen and argon. For these non-zero length tubes we believe this is because of the increasing importance of gas-surface interactions as the mean free path increases. Molecules which tend to specular

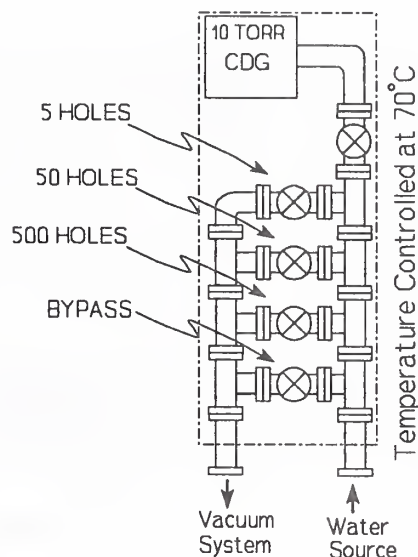


Figure 2: Schematic of the new effusion source. Solenoid-operated valves are used to select individual laser-drilled arrays. The bypass valve allows zero setting of the CDG.

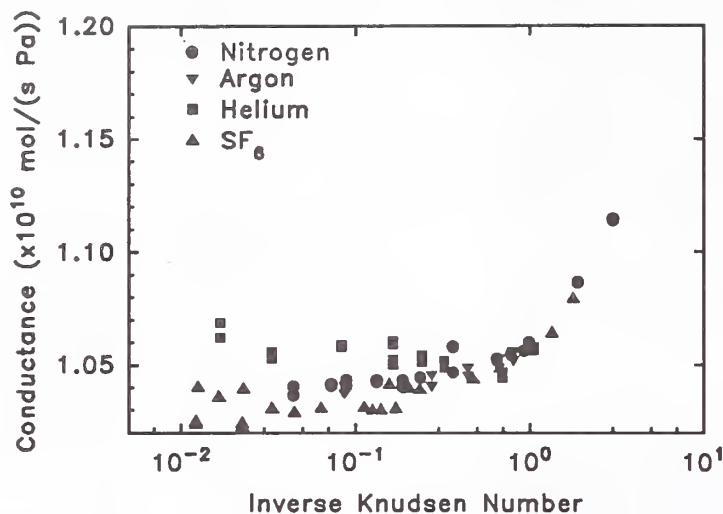


Figure 3: Nitrogen equivalent conductance of an array of 500 laser-drilled holes with nominal 5 μm diameters.

scattering, e.g., helium, will have a higher conductance. This is seen in figure 3 where the conductance of the array increases for helium, relative to nitrogen, which has a higher accommodation. The difference in conductance between helium and nitrogen agrees well with data available in the literature [5-7] for similar geometries. However, the molecular conductance of a tube will be reduced for gases such as sulfur hexafluoride and water where gas adsorption on the wall is a significant factor. The sulfur hexafluoride conductance is 1% lower than the nitrogen conductance for small values of the inverse Knudsen number. This difference in conductance dissipates at larger inverse Knudsen numbers where molecule-molecule collision effects become appreciable.

The theory to predict the effect of molecular adsorption (residence time) on the conductance of tubes is very involved [8] and closed form solutions do not exist for most experimental conditions. However, the effects of adsorption on the molecular conductance can be estimated [9]. The model of de Boer predicts that the adsorption effects on the water molecular conductance will be 10 times greater than the effects for sulfur hexafluoride. Since the observed effect for sulfur hexafluoride is 1%; this predicts that for small inverse Knudsen numbers the water conductance will decrease by as much as 10% below the value derived using simple kinetic theory models and the measured nitrogen conductance. This effect will become negligible for inverse Knudsen numbers greater than 1.

The conductance for the 50 hole array in shown in figure 4 and the Knudsen number dependence of the conductance is very similar to that of the 500 hole array. Although the scatter in the data is larger, the same trends can be identified. The molecular helium conductance is slightly higher than for nitrogen while the sulfur hexafluoride conductance is a few percent lower. A third array with 5 holes has also been examined and shows similar structure although the conductance has exhibited instabilities on the order of 10%, possibly due to partial blockage of the holes. The new system has not yet been operated with water, but we anticipate comparing pressures generated by the different conductances to directly check viscosity effects for water at higher pressures and surface adsorption effects at lower pressures.

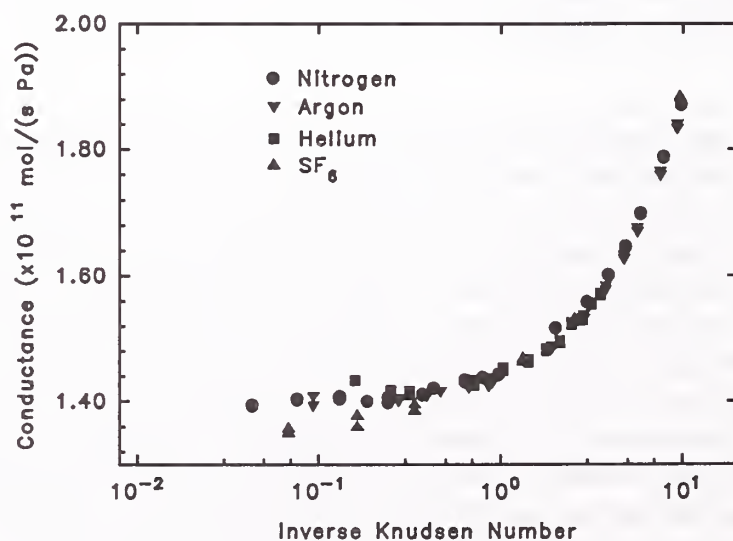


Figure 4: Nitrogen equivalent conductance of an array of 50 laser-drilled holes with nominal 5 μm diameters.

2.3 System Performance

The pressure generated in an orifice-flow system is directly proportional to the flow passing through the orifice. For inert gases the pressure reaches an equilibrium value within a time determined primarily by the volume of the system; for our system the observed time is less than a minute. However for water, equilibrium will be limited by surface adsorption-desorption effects. Our calibration chamber typically takes about 1 hour after the initiation of water flow to attain 95% of the equilibrium pressure and the pressure asymptotically approaches to within 99% of the equilibrium value in 2-3 hours. Temperature control of the water source maintains the supply pressure constant to better than 0.1%. Once established, indicated variations of the pressure in the calibration chamber are typically 0.1-0.3% over periods of days. Changing the temperature of the water supply allows the calibration pressure to be increased to a new equilibrium value in about an hour. The uncertainty of the generated pressure is currently being evaluated. We expect that it will be of the order of 5%.

3. INSTRUMENT RESPONSE

In general, vacuum instrument performance is complicated by interactions between the instruments and system gases. This is of particular concern with water, a substance noted for its strong surface adherence and chemical reactivity. As reported below, we have examined the performance of several different types of vacuum instruments when operated with water. We have also found that operation of vacuum gages with water can cause significant alterations in the composition of system gases, which can lead to serious errors in some situations.

3.1 Gas-Alteration Effects

Interactions between ion sources and chemically-active gases can generate significant quantities of different molecular species. In particular, we have found that operation with water will cause PPAs and both hot- and cold-cathode ion gages to generate significant quantities of H_2 , CO , CO_2 , and O_2 . The relative magnitudes of the gases produced will depend on the water pressure, type of ion source, and history. We have conducted a series of experiments in which a stable water pressure was established, and then cold- and hot-cathode gages were individually turned on for periods of about one hour each. The hot-cathode gages included both tungsten and thoria-coated filaments, which were operated at 1 mA emission. A quadrupole PPA, with a tungsten filament operating at 0.1 mA

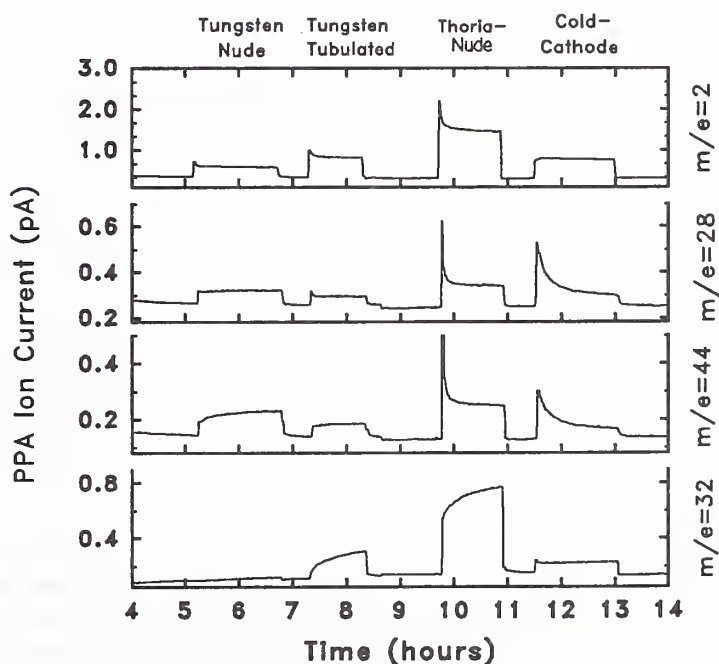


Figure 5: Ion currents generated by operating two tungsten-filament, a thoria-coated-filament, and a cold-cathode ion gage in a water pressure of 3×10^{-4} Pa.

emission current, was used to monitor a number of different partial pressures throughout the experiment. The results of one such experiment, conducted with a water pressure of 3.0×10^{-4} Pa, are illustrated in figure 5. Before water was deliberately introduced into the system at 1.8 hours the PPA signals were several orders of magnitude below the levels seen in the figure. Even the signal at $m/e=18$, the largest signal, presumably due to residual water, was not greater than 0.02 pA. After establishment of the equilibrium water pressure the $m/e=18$ signal increased to 43 pA and the signals at $m/e=2, 28, 32$ and 44 increased to the baseline levels seen in the figure. These baseline levels were presumably due to reactions in the PPA analyzer. As can be seen, turning the gages on generated a significant increase in these peaks.

From examination of signals at other mass-to-charge ratios we are confident that the signals at $m/e=2, 28, 32,$ and 44 are primarily due to $H_2, CO, O_2,$ and CO_2 . Depending on the gage that was operated, we estimate that as much as 4% of the incoming flow, or 0.5 l/s of the water is converted to other gases by single gage operation. For a given pressure and gage the magnitude and time dependence of the H_2, CO and CO_2 signals are repeatable; however, for this experiment the O_2 signal was very time dependent. In another experiment conducted with a water pressure an order of magnitude greater, the O_2 pressures are relatively higher, compared to the other gases, and much more constant, although still highly correlated with gage operation. This tends to indicate that at lower pressure the time dependence of the O_2 signal is due to some equilibration process that has not yet reached saturation. It is not too surprising to find oxygen and hydrogen generated from water in the presence of a hot filament, and carbon compounds are generally believed to be formed by reactions with carbon impurities on the surface of hot filaments. However, the large effect of the cold-cathode gage is somewhat surprising.

Other gases are generated in smaller quantities; although not shown in figure 5, a 0.5 pA signal was generated at $m/e=16$. The magnitude of this peak was relatively insensitive to the operation of the ion gages and we believe it is primarily due to atomic oxygen generated in the PPA ion source, with a small fraction due to methane. We also found a signal at $m/e=19$ (about 0.27 pA) which was highly correlated with the presence of water but relatively independent of gage operation. This may be due to H_3O generated in the PPA ion source.

This alteration of the vacuum environment can cause several problems. In our dynamic calibration system, which has a continual flow of water through the orifice of 14 l/s, the water partial pressure is reduced by several percent when a gage is on, which necessitated operating only one gage at a time during calibrations. For smaller conductances or static systems (e.g., sampling systems for the residual gases in an integrated circuit package), the water signal can be reduced by much larger factors, with corresponding errors in the indicated water pressure. The product gases can also lead to erroneous conclusions about system diagnostics. A signal at $m/e=28$ can also be due to N_2 , so the signals generated at 28 and 32 by reactions with water could be misinterpreted as an air leak. The signal generated at $m/e=19$ can be misinterpreted as fluorine from residual halogenated cleaning compounds.

3.2 Ion Gage Response

Ionization gages are the most common vacuum instruments. We examined several performance factors for these gages: response time, relative sensitivity and stability. Response times varied for the different calibration chambers. In the best case, with a stable water pressure established in the calibration chamber, the cold-cathode gage reading reached within 1% of the equilibrium reading in less than one minute after being turned on. One would expect that the response time of a hot-cathode gage would be

much longer because of the large changes in temperature when they are turned on. However, while the responses were somewhat more complicated, they were still relatively prompt, particularly for tungsten filaments. The tungsten-filament gages reached within 2% of their equilibrium readings within one or two minutes after being turned on. The thoria-coated-filament gages were slower, exhibiting an initial 100% overshoot, followed by a decay to an equilibrium value. Five to ten minutes were required to reach within 2% of equilibrium values. In other cases response times approached an hour.

Once the hot-cathode ion gages reached their equilibrium readings they exhibited a water sensitivity between 90 and 95% of their nitrogen sensitivity. For pressures in the 10^{-4} to low 10^{-3} Pa range instabilities were typically no more than 0.2-0.3% over periods of a day. Direct tests of stability at higher pressures were not conducted, however; other evidence indicates that operation with water in the 10^{-2} Pa range for periods of days will cause decreases in gage sensitivity as large as 10-15%. We also obtained a limited amount of data indicating changes in the sensitivity of cold-cathode gages at low pressures that became progressively larger with continued water operation. The cold cathode gages maintained a stable calibration at higher pressures, but after water operation for about one month at pressures in the 10^{-4} Pa range they showed significant deviations for pressures below 10^{-6} Pa; gage readings were one to two orders of magnitude low at a pressure of 10^{-7} Pa. After several more months of operation at water pressures in the 10^{-6} to 10^{-3} Pa range significant deviations were evident at pressures as high as 10^{-5} Pa. In all cases, the cold-cathode gages read low, with the deviations increasing with decreasing pressure. This effect was greatly reduced after baking overnight at 250°C.

3.3 Spinning Rotor Gages

The Spinning Rotor Gage (SRG) determines pressures from the change of rotation rate of a magnetically-levitated, spinning steel ball [10]. Since it does not employ a hot filament or high-voltage discharge it should be largely free of the gas-interaction effects attendant on the operation of ion gages or PPAs. However, the SRG sensitivity depends directly on the interactions between gas molecules and the ball's surface, which will surely be different with water than with inert gases. We examined two different SRGs and found the effective accommodation coefficient (calibration factor) for water to be about 6% larger than for nitrogen. This is an exceptionally large change for an SRG, but is consistent with the near-perfect tangential momentum accommodation one would expect for water.

3.4 Partial Pressure or Residual Gas Analyzers

Partial Pressure Analyzers are mass-spectrometer type instruments designed to measure the partial pressures of different molecular species. Most users implicitly assume that the partial pressure sensitivities are constant, independent of the pressures of other gases. However, previous studies [11] of these instruments have found that the sensitivities for specific gases can depend on the pressure of other gases, and that operation with active gases can cause time-dependent sensitivities. We have examined these effects with water for five different PPAs [12]: four quadrupoles and one magnetic-sector. The four quadrupole instruments are of the same types as used in our earlier experiment [11] and we have retained the same alphabetical designation; the instruments in the present test are designated A-2, C-3, C-4, and D-4. A-2 and D-4 were equipped with tungsten filaments operated at 1 mA emission, C-3 and C-4 had thoria-coated filaments operated at 0.1 mA emission. The magnetic-sector instrument, with a 60 degree, 80 mm radius magnetic sector, is designated F. Its tungsten filament was operated with a total emission current of 240 μ A and a trap (ionizing) current of 60 μ A.

The calibration system used for the PPA study is similar to the one used for the previous study in that it includes, in addition to the water source, auxiliary gas systems that allow for the independently controlled introduction of two additional gases. These systems are basically a gas reservoir and UHV leak valve and they allow the maintenance of a gas pressure in the calibration chamber that typically will decay between 0.1 and 1% an hour, depending on operating conditions. These gas sources can also be valved in or out, and the chamber is equipped with spinning rotor gages that can be used to measure the pressure of these additional test gases.

The primary purpose of the most recent tests was to further investigate the dependence of partial pressure sensitivities on the pressure of other gases by including water as one of the test gases, and to determine if operation with water causes time-dependent sensitivity changes, as had been observed earlier for other active gases. In preparation for tests the vacuum chamber was moderately baked with internal infrared lamps, yielding a base pressure of about 10^{-7} Pa. Following bakeout and initial adjustments, a series of experiments were conducted, typically of one to three days duration, with the following scenario: Before introduction of water, constant argon and helium pressures were established in the calibration chamber. During this initial period the argon and helium flows were independently interrupted for periods of 15 to 60 minutes to evaluate the dependence of the helium sensitivity on the argon pressure, and vice versa. Following this initial phase the water source was valved into the calibration chamber for a period of two to three hours, and then valved out. Generally, while the water was "on", the argon and helium were again separately valved out of the calibration chamber for periods of 15 to 30 minutes each to test the dependence of the water sensitivity on helium and argon pressures. Following removal of the water, the argon and helium pressures were maintained for 12 to 24 hours. The He, H₂O, and Ar ion currents were monitored during the entire experiment for all five instruments.

Four different combinations of partial pressures were used with water, helium and argon partial pressures between 2×10^{-5} and 1.1×10^{-3} Pa. Typically, the helium pressures decayed by about 0.1%/hour due to depletion of the helium reservoir. The argon system has a smaller reservoir and, depending on operating conditions, decay rates were between 0.1 and 1%/hour. Typically, the water pressure in the calibration chamber approached to within 2-5% of its equilibrium value one hour after valving in the source.

The results for different instruments can be quite different, as illustrated in figure 6. In this experiment, after the argon and helium pressures were established in the calibration chamber, the water source was "turned on" at 0 hours, then turned off about 2.2 hours later. While the water was on, the helium and argon were separately turned off; as indicated by the bars in the figure, the helium was turned off at about 1.1 hours for about 15 minutes, the argon was turned off at 1.75

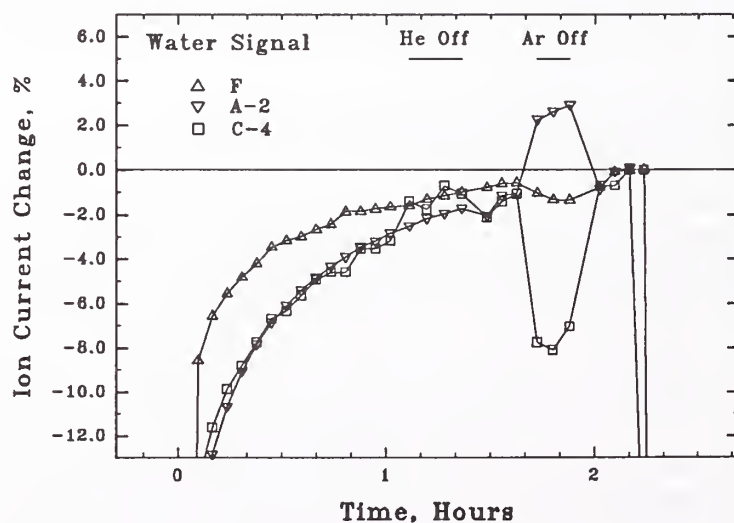


Figure 6: Normalized water partial pressure signal changes for three different PPAs, as a function of time and helium and argon background pressures.

hours for about the same period. The figure includes the $m/e=18$ signal for three of the gas analyzers, each normalized to their maximum signal. As can be seen, reducing the helium pressure to "zero" caused little or no change in the PPA signals outside of a possible 1% rise in the signal for C-4. This is typical; changes in helium pressure were never observed to cause more than a 2-3% change in the signals for water or argon. However, when the argon was removed, the signal from quadrupole C-4 dropped by about 7%, while the signal for quadrupole A-2 increased by about 3%. The magnetic-sector instrument, F, was little affected, as were quadrupoles D-4 and C-3 (data not shown). Also seen in figure 6 are different time responses to the water for the three instruments, even though they were all monitoring the same pressure.

Our earlier study [11] had shown longer-term changes in sensitivity for some PPAs when operated with O_2 and CO . Figure 7 shows the response of the argon signal of three PPAs to operation with 4.4×10^{-4} Pa of water. Again, the argon partial pressure (1.3×10^{-4} Pa) was established and stabilized, and the water was turned on at 0 hours, and turned off at about 2.2 hours. PPA F experienced a reasonably prompt drop of 8% in the argon signal upon introduction of the water, and a prompt recovery with removal of the water, behavior that is similar to that observed with changing pressures of inert gases. (The periodic noise in the F signal is due to interfering electrical signals broadcast by the type-C instruments.) PPA D-4 exhibited a time-dependent decrease of about 6%, followed by a relatively prompt recovery, and a stable long-term continuation. In general, D-4 exhibited the best long-term stability, the change in its signal between 4 and 14 hours rather accurately tracks the measured decline in the argon pressure. However, it generally exhibited transient responses to changes in either water, argon, or helium pressures, typically with a time constant of about 30-60 minutes. Instrument A-2 in general exhibited the most complex behavior with the largest changes, as illustrated in the figure. The initial prompt increase of 6% was a response to the increased water pressure. This was followed by a time dependent decrease of 10%. Removal of the water prompts a prompt decrease of 8% in the argon signal, followed by a long-term asymptotic recovery. In this case it appears that the longer-term change in PPA sensitivity must be due to a reversible chemical reaction. At higher water pressures, 1.1×10^{-3} Pa, the changes in the argon signal for this instrument were as large as 28% over a 2.7 hour period. Similar but somewhat smaller changes occurred in the helium signal.

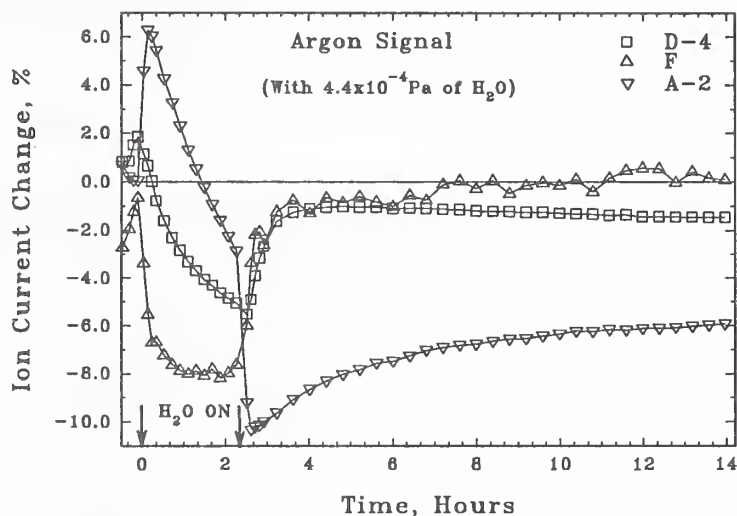


Figure 7: Normalized ion current changes for three different PPAs. The argon pressure is constant at 1.3×10^{-4} Pa, the water is present for first 2.2 hours.

In general, the magnitude of these effects decreased with the water pressure, but we have observed them even at very low pressures. In a separate experiment, a different PPA used to make high-precision measurements of helium partial pressures in the 10^{-8} Pa range repeatedly exhibited changes in its helium sensitivity of the order of 1% over periods of hours when exposed to water pressures in the 10^{-8} Pa range.

The sensitivities of ionization gages for different gases are known to roughly scale with the electron-collision ionization cross sections for the different gases. However, for PPAs, the sensitivities for different gases relative to a reference gas (typically nitrogen or argon) will depend not only on ionization cross sections, but also on the transmission probability of the mass filter, including the probability of coupling ions extracted from the source into the acceptance angle of the mass filter. While the relative sensitivities for different types of ion gages will typically vary by no more than about 20% from mean values, our earlier study [11] found that relative sensitivities for PPAs can differ, in the extreme, by an order of magnitude from the relative sensitivities generally observed for ionization gages. In the most recent experiments the sensitivity for He relative to Ar varied from 0.12 to 0.43 for the five PPAs, while the sensitivity for H₂O relative to Ar varied from 0.54 to 0.93. It is clear that very large errors can be incurred by the many users and manufacturers who assume that relative sensitivities published for ion gages can be used for PPAs as well. Elimination of this additional source of error requires calibration of each instrument with the gases to be used.

4. SUMMARY

A Knudsen water effusion source has been constructed utilizing three conductances composed of arrays of 5 micrometer holes. The conductances of these arrays were measured with nitrogen, argon, helium, and sulfur hexafluoride and were modeled to account for deviations from molecular flow. Although we can not measure the water conductance directly, we employ both kinetic theory and slip-flow models to predict the conductance of the arrays for water based upon the measured conductance with other "permanent" gases. Using these arrays to generate known flow rates of water in conjunction with our primary vacuum standards, we are able to generate known water pressures from 10⁻⁵ to 10⁻² Pa.

Using a prototype Knudsen water effusion source with a 100-hole array we investigated the water sensitivity and gage interactions of various types of vacuum instrumentation. Hot-cathode ionization gages were determined to have water sensitivities of 0.90 to 0.95 times their nitrogen sensitivity. The equilibration time when measuring water vapor was on the order of a minutes for gages with tungsten filaments and slightly longer for thoria-coated filaments. A variety of partial pressure analyzers were examined to determine the effect of water vapor upon the sensitivity for other gases. The results of these tests were very instrument dependent, but for all of the PPAs the presence of water vapor introduced transient and/or permanent changes in the sensitivities for other gases. The results also showed appreciable generation of gases, notably H₂, CO, CO₂, and O₂, due to filament-water vapor interactions that were gage and filament material dependent. The PPA data point out a great number of problems associated with their use to monitor contaminant gases in vacuum systems, particularly with small-volume/small-conductance systems.

The Spinning Rotor Gage is an attractive alternative for active-gas pressure measurements, but its use is limited to pressures above about 10⁻⁴ Pa, and it is not useful for partial pressure analysis. The effective accommodation coefficients for the two SRGs examined were determined to be 6% larger than their nitrogen values. Although this is a large change, it is consistent with the near-perfect tangential momentum accommodation one would expect with perfectly adsorbing gases such as water.

5. ACKNOWLEDGMENTS

The assistance of Donald Martin in assembling the primary water standard, and that of Albert Filippelli in analyzing data, are gratefully acknowledged. This work was supported in part by the Johns Hopkins University Applied Physics Laboratory.

6. REFERENCES

- [1] Tilford, C.R., Dittmann, S., and McCulloh, K.E., "The National Bureau of Standards primary high vacuum standard", *J. Vac. Sci. Technol. A* 6 (5), pp. 2853-2859 (1988).
- [2] McCulloh, K.E., Tilford, C.R., Ehrlich, C.D., and Long, F.G., "Low-range flowmeters for use with vacuum and leak standards," *J. Vac. Sci. Technol. A* 5 (3), pp. 376-381 (1987).
- [3] Tison, S.A., "Experimental Data and Theoretical Modeling of Gas Flows Through Metal Capillary Leaks", *Vacuum*, In Press (1993).
- [4] Jones, R.H., Kruger, V.R., and Olander, D.R., "Characterization of Multichannel Sources and Design of Molecular Beam Systems for Their Utilization", USAEC Rept. UCRL-17859, 1968.
- [5] Steckelmacher, W., "Knudsen flow 75 years on; the current state of the art", *Rep. Prog. Phys.* **49**, 1083-1107 (1986).
- [6] Barrer, R.M. and Nicholson, D., "Slip flow in long single capillaries", *Canadian Journal of Chemistry* **43**, pp. 896-908 (1965).
- [7] Scott, D.S., and Dullien, A.L., "The Flow of Rarefied Gases", *A.I.C.H.E J.*, **8** (3), pp. 293-297 (1962).
- [8] Clausing, P., "On the molecular flow with Langmuirian adsorption of the molecules on the wall of the tube; a correction", *Physica* **28**, pp. 298-302 (1962).
- [9] de Boer, J.H., *The Dynamical Character of Adsorption* (Clarendon, Oxford, 1953).
- [10] Dittmann, S., Lindenau, B.E., and Tilford, C.R., "The molecular drag gauge as a calibration standard," *J. Vac. Sci. Technol. A* 7 (6), pp. 3356-3360 (1989).
- [11] Lieszkovszky, L., Filippelli, A.R., and Tilford, C.R., "Metrological characteristics of a group of quadrupole partial pressure analyzers," *J. Vac. Sci. Technol. A* 8 (5), pp. 3838-3854 (1990).
- [12] Tilford, C.R., "Characteristics of partial pressure analyzers", *Proceedings of the Society of Photo-Optical Instrumentation Engineers*, vol. 1761, pgs. 119-129 (1993).

USING PERMEATION TUBES TO CALIBRATE TRACE MOISTURE ANALYZERS

James J. McKinley
Kin-Tek Laboratories, Inc.
504 Laurel St., LaMarque, TX 77568

ABSTRACT

The determination of trace moisture concentration is a common and very important measurement in a wide variety of process gas streams. Calibration of moisture analyzers poses special problems which have not generally been addressed at the user level. This paper describes techniques for the effective use of permeation tubes for calibrating a wide variety of trace moisture analyzers. The operating characteristics of permeation tubes, suitable operating procedures, and the appropriate interfacing techniques are described.

Using current technology, the permeation method is useful over the concentration range from about 0.5% to less than 0.01 ppm. The method is useful for a broad variety of gases, and can even be extended to some liquid streams.

INTRODUCTION

The need to monitor trace concentrations of moisture in a wide variety of gases is rapidly growing. Varying concentrations of water vapor in process gases affects the product quality and/or yield in many processes. Examples range from the production of micro electronic devices to high grade polymers and other chemical products, to the welding and heat treating of components subject to extreme stresses such as those found in jet engines.

Unfortunately, there are no true absolute analytical systems for moisture which can be applied to this variety of applications. In most cases the response is affected by the background gas, and all are subject to poisoning by certain contaminants. This is especially true as the concentrations to be measured go to sub ppm levels. The problem is further aggravated by the tendency of analytical systems to behave nonlinearly at the lowest concentrations. For example, it is frequently true that at the lowest concentration levels a system may cease to respond to changes. Thus, there is a critical need for a generally applicable method of preparing calibration standards for moisture analyzers under field conditions. These standards need to be at actual working concentration levels to reflect the full operating characteristics of the system in use.

The problems encountered in preparing moisture standards are formidable. First, the conventional static blend method does not work for moisture standards. Because of the pervasiveness of environmental moisture there is no effective way to predetermine the concentration of the mixture. The problem is the storage container itself. While it might be possible to add a known concentration of moisture to the container, the contribution of the container to the final concentration is not known. It may add moisture to the mixture, or moisture may be removed. Furthermore, the concentration may vary over the life of the mixture due to variations in temperature and pressure of the contents.

A second key problem is that there is no actual zero reference available. For higher level measurements dessicants will produce a reference stream of much lower concentration than that which is to be measured. At the 1000 ppm level one might easily expect to produce a 1 ppm zero reference. The 0.1% zero error would usually be trivial and the 1 ppm background could effectively be called zero. However, it is unlikely that one could routinely expect to obtain a zero reference of less than 1 ppb. One ppb is a zero error of 1% at the 100 ppb level, or 5% for a 20 ppb measurement.

The problem is further complicated by the need for standards in a variety of matrix gases. While there are very elegant methods for generating standards in well behaved gases such as nitrogen, they are not useful for making mixtures in acid gases, such as HCl, or a condensable hydrocarbon like propylene. Several methods have been used for generating trace moisture standards. In the most absolute method a gas stream is saturated under cryogenic conditions at carefully known temperature and pressure. This method

establishes an absolute reference point. However, this method is relatively cumbersome to use and is not well suited for field applications. It is also limited to gases which will not condense at the temperatures required to obtain very low concentrations. Standard addition methods add a known amount of moisture to an unknown background. While they do not establish an absolute reference point, they offer the advantage that they can be used under field conditions, and can be applied to a wide variety of background gases. Examples of this method include sequential dilution of a stream saturated to a known concentration, the addition of moisture from a permeation tube, and the addition of moisture by catalytically combining oxygen and hydrogen. The last method suffers from many limitations. In this paper we are addressing the use of permeation tubes as the element for providing the known concentration change.

THE PERMEATION TUBE METHOD .

Permeation tubes are devices using the permeation of vapors through a membrane, in this case Teflon, to produce a very stable, very low gas flow source. Figure 1 shows a diagram of a basic permeation tube device. Essentially it is a length of Teflon tubing with water sealed inside. Water vapor passes slowly through the tube wall and into the surrounding atmosphere. If we then maintain a flow of clean dry gas over the tube, we add a known amount of moisture to that flow. The rate of flow of moisture emitted from the tube is measured by holding the tube at constant temperature in a stream of dry gas for an extended period of time and periodically weighing the tube to measure the rate of weight loss. Figure 2 shows the basic concept of generating a calibration mixture using permeation tubes. The permeation tube is immersed in the flow of clean dry gas. The permeate and dilution flows combine to form a mixture to which a known amount of moisture has been added. The concentration of this added moisture is given by

$$C = \frac{f}{f + F} 10^6 \quad \text{Eq. 1}$$

where

C is the concentration in ppm.

f is the permeation flow of moisture

F is the flow of dilution gas.

Recall that the flow of moisture from the permeation tube is extremely small, (nanoliters per minute) and the dilution flow is substantially larger, (typically liters per minute). Hence, Eq. 1 reduces to:

$$C = \frac{f}{F} 10^6 \quad \text{Eq. 2}$$

The flow of moisture from the tube is described by the equation

$$f = \frac{k A \Delta p}{t} \quad \text{Eq. 3}$$

where

f is the permeation flow

k is the permeability of the membrane to water

A is the surface area of permeation

Δp is the partial pressure difference of water across the membrane

t is the thickness of the membrane

Operating at a fixed temperature the rate of addition of moisture to the stream can be set by choosing permeation tubes with different areas or different membrane thicknesses.

Additionally, the emission rate of any tube can be varied by changing the operating temperature of the tube. Two factors affect the temperature dependence of permeation. First, the vapor pressure of water varies as the temperature is varied, so the partial pressure difference of moisture across the membrane, Δp , will vary

exponentially with inverse temperature. The permeability of the membrane also varies exponentially with inverse temperature.

$$k = k_0 \text{Exp}(- B/T) \quad \text{Eq. 4}$$

where

k_0 , B are equal constants
T is the absolute temperature

The flow of moisture from a permeation tube is strongly dependent on the temperature of the tube, so temperature must be carefully controlled to make accurately known standards.

Permeation tubes can be built in a variety of configurations to give a wide range of concentrations. The photo in Figure 3 shows several designs. These range from a very short length of membrane tubing attached to a non-permeable reservoir to large refillable canisters containing many meters of permeation membrane. The very small tubes are used to make low ppb additions. The large canisters can be used to add hundreds or even thousands of ppm to a stream. Figure 4 shows schematically the structure of such a high emission rate tube. In this design, water is on the outside of the permeation membrane and the dilution gas flows concentrically down through the permeation tube. Water flowing into the tube is picked up by the dilution gas and carried to the analytical device.

Figure 5 shows a typical flow diagram for an instrument used to generate trace concentrations of moisture. The dry dilution gas enters at the lower left of the schematic. This dilution gas is pressure regulated to form a stable reference point for flow control. The dilution flow passes through, a mass flowmeter, and then divides into two streams. One stream, controlled at a constant flow rate, passes continuously over the permeation tube and mixes with the moisture emitted by the tube. This stream is kept flowing constantly to keep the emitted moisture purged from the permeation chamber. The second flow will normally be the larger portion of the total dilution flow and can be switched off to save use of extremely dry dilution gas.

In use, the main dilution flow is first switched on and the system allowed to reach equilibrium with the moisture in the dilution gas to obtain a "zero" response. Then, the span solenoid is switched to introduce moisture from the permeation tube to the dilution gas. Flowing this mixture to the analyzer introduces a known level of concentration change. By varying the dilution flow a variety of concentrations changes can be generated.

CALIBRATION BY STANDARD ADDITION

One of the key problems in the calibration of moisture analyzers is the absence of a true zero. The moisture concentration in the dilution stream may be very significant compared to the calibration level desired. Additionally, the calibration system itself may contribute to the background moisture either through outgassing, or from leaks in the system. To compensate for this unknown background we use the method of standard additions.

To use this method, first obtain a response from the analyzer due to the dilution gas alone, i.e., the "zero addition response". Then add the permeated moisture flow to this stream and obtain a response due to the known concentration change. Since the dilution gas concentration is constant, several known addition responses can be obtained by changing the dilution gas flow rate. Using the difference between two known addition responses, calculate the sensitivity S of the system to the known addition.

$$S = \frac{\Delta R}{\Delta C} \quad \text{Eq.5}$$

where

ΔR is the change in response of the analyzer
 ΔC is the change in concentration introduced

Apply this response factor S to the observed response to zero to estimate the original background concentration.

$$C_0 = \frac{R_0}{S} \quad \text{Eq. 6}$$

Using this estimate for the background concentration, C_0 , the calibration curve can be adjusted to more accurately reflect true concentration. Figure 6 shows this graphical estimation of concentration from standard additions.

If only one standard addition is used to estimate the background concentration, the method would obviously assume the linearity of the response curve through zero. Generally, the error introduced by this assumption is small. Multiple additions can be used to estimate response linearity or define nonlinear response curves. For best accuracy, standard addition concentrations should be large compared to the background concentration.

SPECIAL PROBLEMS IN CALIBRATING MOISTURE ANALYZERS

There are several special problems associated with calibrating trace moisture monitors. Of particular significance are (a) generating zero gas, (b) excluding all external moisture, (c) obtaining adequate dry-down of the system, (d) transmitting concentration changes to the analyzer.

If the matrix gas to be tested is nitrogen or some other relatively inert material, a variety of methods maybe used for reducing the background concentration in the zero gas. Table 1 shows several options for obtaining very dry streams. Experience has shown that values in Table 1 are conservative, and concentrations lower than those shown are often obtained. When the background (diluent) gas is reactive, however, the choices are much more limited. Usually, molecular sieves are the only effective option for drying these gases.

The exclusion of atmospheric contamination from the mixture is also a very significant problem. If one considers a dry background stream as having one ppb moisture, the contamination potential from air saturated at 20 degrees C is approximately $2.5 \times 10^7 : 1$. The leakage specification for high quality tube fittings is typically 4×10^{-9} cc / sec per fitting. This translates to a contamination potential in 1 l/min. of 0.24 ppb from each tube fitting. We have found, however, that for carefully made tube connections the actual contamination tends to be much lower than that value. Also, we have found no significant leakage difference between Swagelock compression ferrule fittings and VCR face seal fittings. The VCR fittings, however, do offer advantages in that there are no spaces where moisture can be trapped and released slowly over a long period. Additional improvement can be made by immersing the entire system in dry gas.

To obtain good dry-down characteristics the choice of components and materials is of extreme importance. We have found that the materials used in all components must be of high quality, surface area should be minimized, and all components must be thoroughly cleaned of any possible impurities. Tubing used in the system should be internally electropolished. Tubing can be somewhat passivated to moisture adsorption by heating in the presence of high purity nitrogen.

In our work we have found that a key element in obtaining adequate dry-down is knowing what to expect. Figure 7 is a simulation of a typical dry-down curve. In the initial dry-down phase, the reduction of moisture in the system is exponential as would be expected. However, this initial dry-down will often asymptotically approach some unexpectedly high value. Applying heat to the various components in the system will evolve moisture, but when the heat is removed and the temperature of the component returns to ambient, the resulting moisture level will often be unchanged. After an extended period at this level the moisture content in the system may drop rather suddenly, almost step-wise, to a new lower value. This new level will persist for a time and then drop again. Each succeeding step is generally smaller in size than the previous step. The cleaner the system is initially the fewer steps observed. Also, the higher the temperature of the system during dry-down, the shorter time between steps. In drying down moisture generating systems we have found two things that always help: (1) use heat, and (2) be patient. Once a system has gone through an initial dry-down, we find that it is usually much easier to dry the system down thereafter.

Once a system has reached dry-down it is also important to test the system to be sure that it will transmit changes in moisture concentration. Moisture should be sequentially added to and removed from the system to insure that

the overall system will respond rapidly to changes in moisture concentration. High quality stainless steel components, if they are clean, will transmit adequately. If a sluggish response is observed, it should be assumed that there is some area in the system that has not been adequately cleaned, or that some undesirable material has been inadvertently included in the system.

APPLICATION DETAILS

Several factors must be considered for the proper use of a standards generating system to calibrate trace moisture monitors. First the requirements of the specific type of analyzer to be calibrated should be considered. Some analyzers, for example, are particularly sensitive to flow. These devices will generally feature internal flow control. But, some provision must be made in the interface to allow excess of calibration mixture to bypass the analyzer itself. Other systems, such as FTIRs, are insensitive to flow changes but have strong sensitivity to changes in pressure. Figure 8 shows an interface system which can be used with most moisture monitors. With this arrangement the flow of dilution gas through the calibration unit can be adjusted over a wide range to vary the mixture concentrations. A back pressure regulating device holds a constant pressure on the sample line and allows the flow to the analyzer to remain constant regardless of the flow coming from the calibration unit.

Maintaining a constant back pressure on the sample line has a second desirable effect. When pressure in the sample line rises, more moisture is adsorbed by the tubing. This causes a temporary reduction in concentration delivered to the analyzer. Conversely, when the pressure is lowered the sample line releases moisture and causes a temporary elevation in the moisture delivered to the analyzer. Thus, simply changing back pressure on the sample lines can give the appearance of changing moisture concentrations even when the moisture level is constant. Back pressure control eliminates this error source. Similar effects can be caused by changes in the temperature of the sample line. Thus, it is desirable to heat, or at least insulate the sample line so as to minimize changes in temperature.

Some basic guidelines for proper interfacing of the calibration instrument to the moisture analyzer are (a) match the calibration conditions to the sample input conditions, (b) make the calibration gas flow and the analyzer input flow independent, (c) arrange the system so that calibration gas flow is never blocked, (d) use clean, inert tubing and other components in the interface, (e) set up the system so that zero integrity can be assured, (f) run the system under constant back pressure, and (g) keep interconnecting lines at constant temperature.

Some consideration should also be given to the quantity of calibration gas to be delivered. We have found that for most applications delivering a quantity in the range of .5 to 5 l/min. is optimal. At low concentrations there are advantages to using higher flow rates. For example, the contamination concentration caused by any stray leakage is reduced at higher flow rates. Permeation tubes in general can be certified more quickly and more accurately for higher emission rates. High flow rates also tend to speed response of the overall system and shorten the dry-down time. The down side of using high flow rates is that the demand for zero gas is increased.

BACKGROUND GAS CONSIDERATIONS

The emission rate of water from permeation tubes has been found to be essentially independent of the background gas for most gases. With some gases, however, there are interactions between the moisture molecule and the background gas molecules which make it difficult to deliver the standard to the analyzer. In some gases the moisture reacts rapidly with the background gas to form some other compound. An example of this situation occurs with moisture in WF_6 . In other cases the moisture and background gas do not actually react but rather associate to form an aerosol, or some other particle-like entity. These pseudo particles tend to stick to the walls of the sample transmission tubing much more aggressively than moisture would in its free form. For these interactive mixtures it is sometimes desirable to set up the system so that the moisture is actually added to a small flow of inert carrier gas and transported in that gas to a junction point right at the analyzer. The reactive dilution gas can then be mixed with the moisture-containing carrier just before the mixture enters the analyzer. Thus, the effects of reaction or association of the water and the background gas are minimized.

SUMMARY

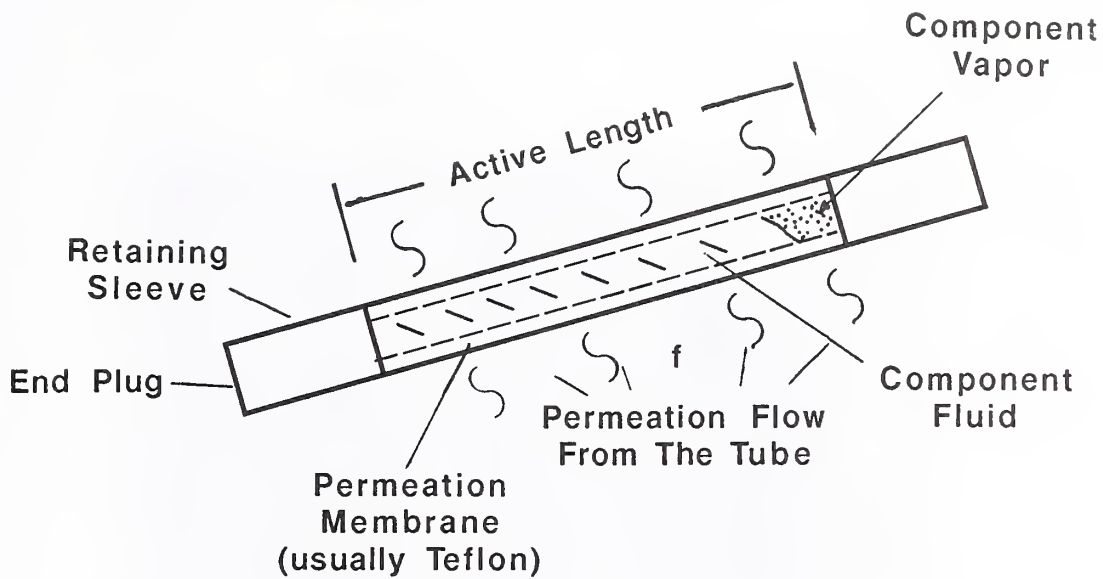
Trace moisture systems need frequent calibration checks to insure their proper operation. Many of these systems tend to drift to zero under very low moisture conditions, i.e., they die of starvation. Because there is no available absolute zero reference for most gases, the method of standard additions is the most practical one to use for moisture calibration. Permeation tubes are a good, convenient source for making known additions to a flowing gas stream. The method can be used over a wide concentration range and with a variety of background gases. Standard addition methods, while they do not establish an absolute reference point, offer the advantage that they are simple to use under field conditions, and can be applied to a wide variety of background gases. The key to this method is that it must provide a means of adding an accurately known change in concentration to a relatively dry background stream.

REFERENCES

[1] Zatco, Dr. David, and Daniel J. Ragsdale, 1988. Determination of H₂O. In The Part Per Billion Region In High Purity Gases. Paper No. 10249. Presented at the 39th Pittsburgh Conference on Analytical Chemistry and Applied Spectroscopy.

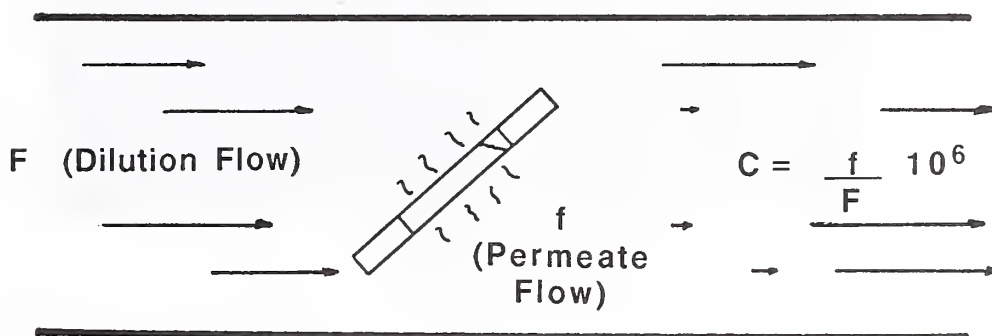
METHOD	MINIMUM CONCENTRATION [1]
NEW MOLECULAR SIEVES	5 - 7 (ppb)
USED MOLECULAR SIEVES	20 - 40
METAL GETTERS	3
ORGANO - LITHIUM GETTERS	6
CRYOGENIC DRYERS	Very Low

TABLE 1
GENERATING ZERO GAS



BASIC PERMEATION TUBE

Figure 1



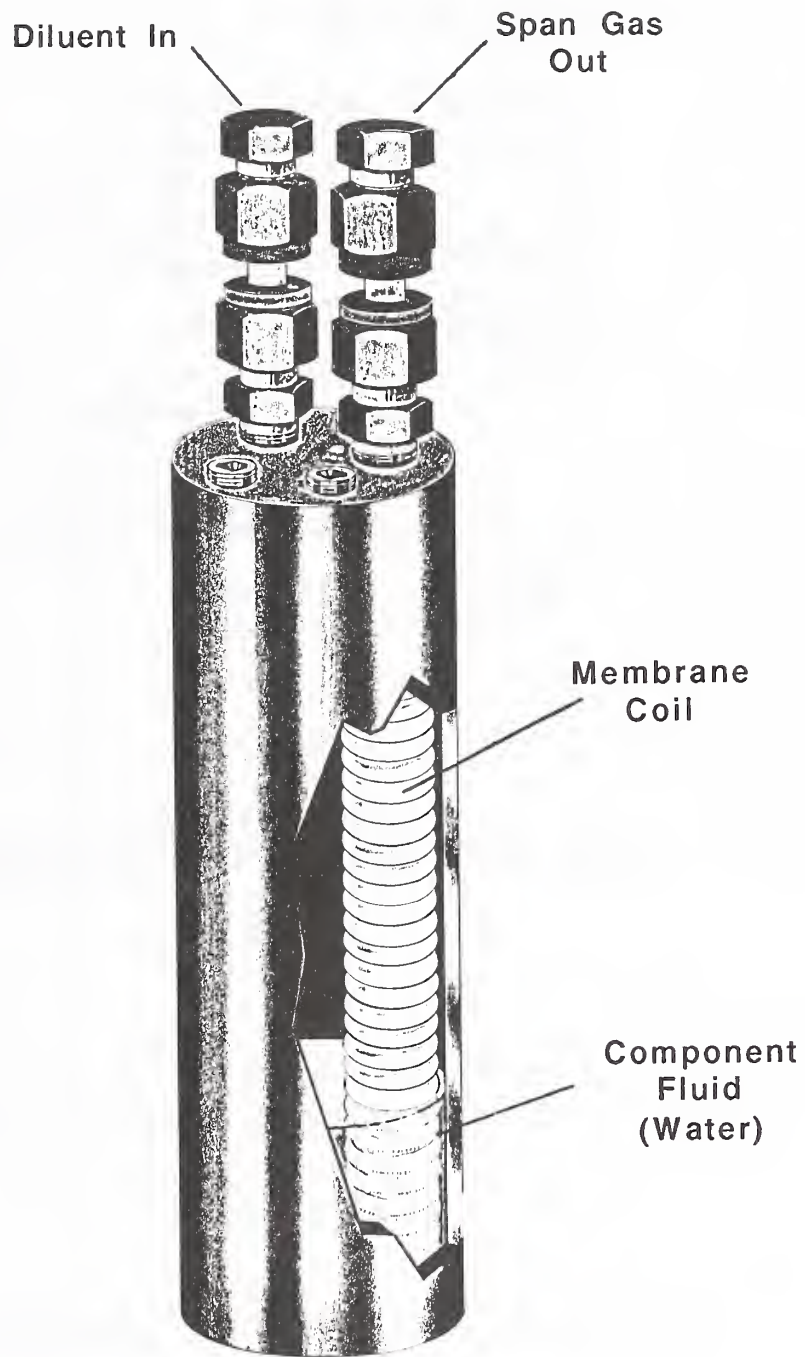
USING PERMEATION TUBES TO GENERATE TRACE CONCENTRATION MIXTURES

Figure 2



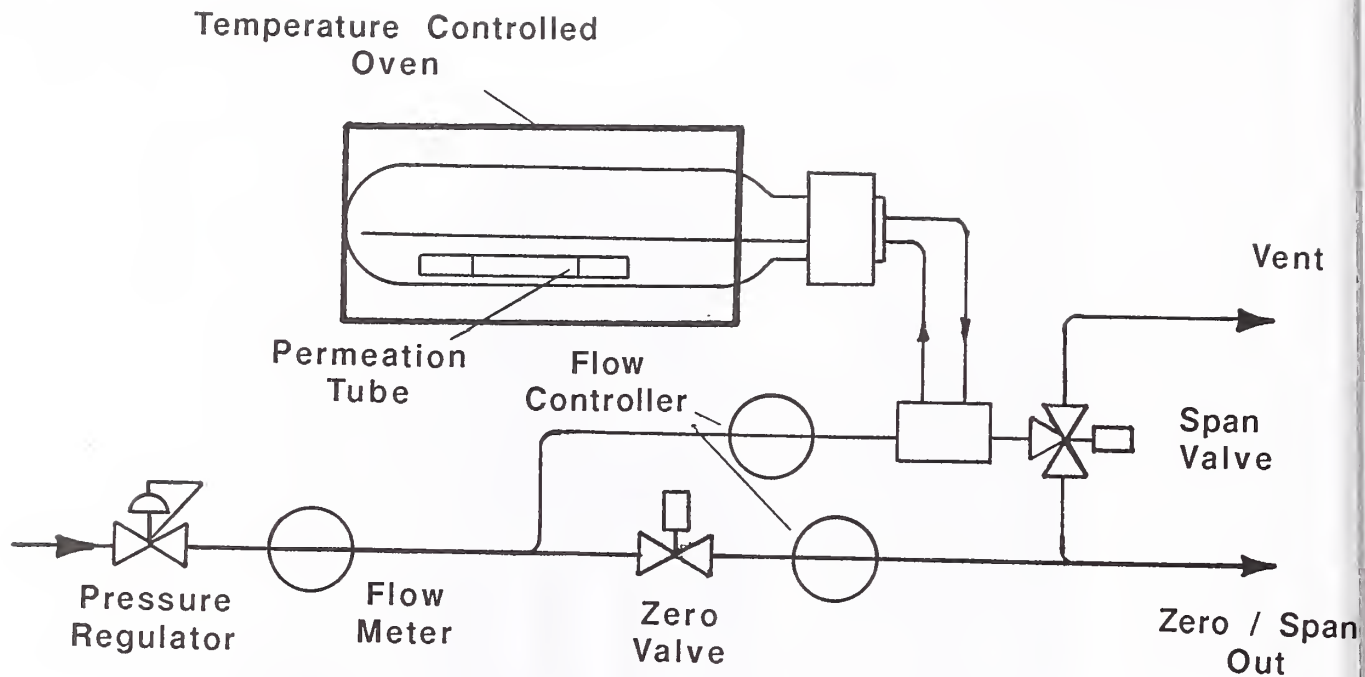
PERMEATION TUBES

Figure 3



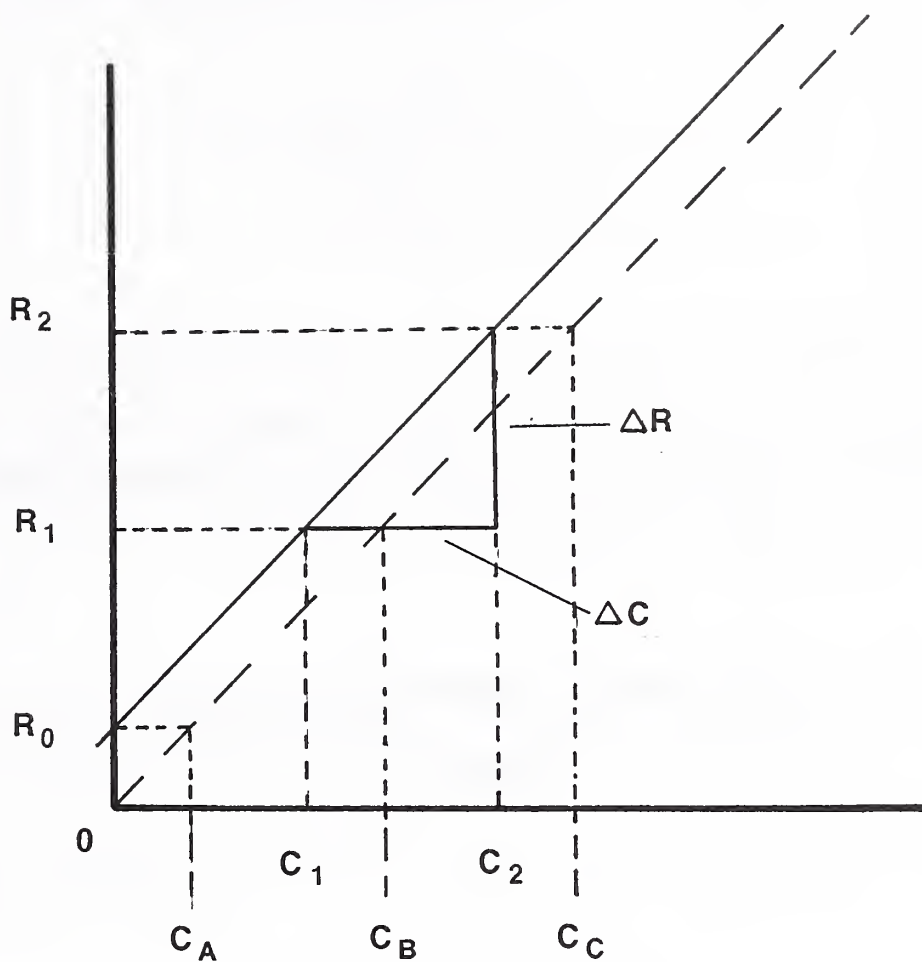
**HIGH EMISSION
PERMEATION TUBE**

Figure 4



FLOW DIAGRAM
MOISTURE STANDARDS GENERATOR

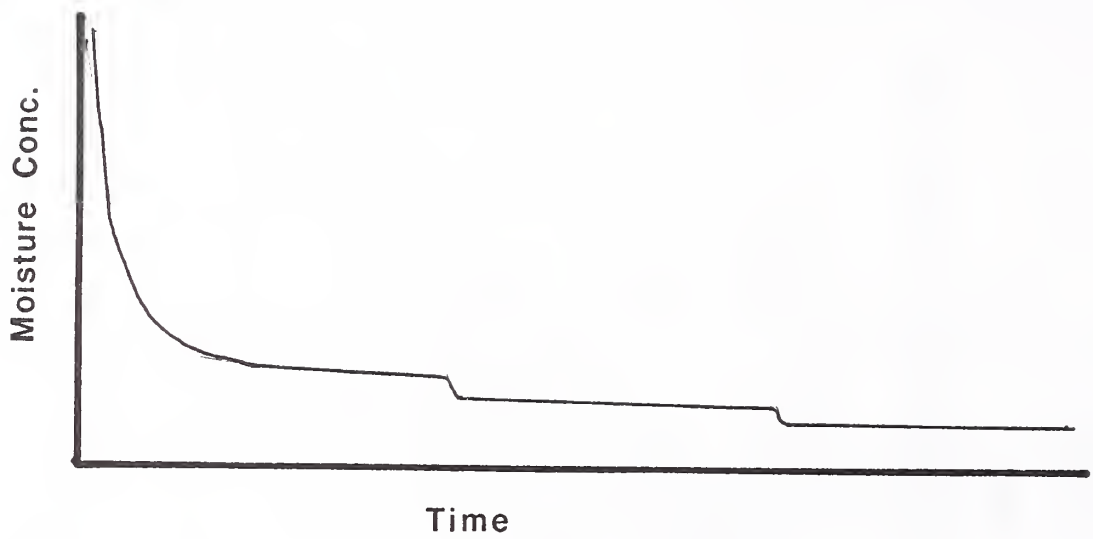
Figure 5



C_1, C_2 Are Standard Additions
 $C_A =$ Estimated Background Gas Conc.
 $C_B = C_A + C_1$ $C_C = C_A + C_2$

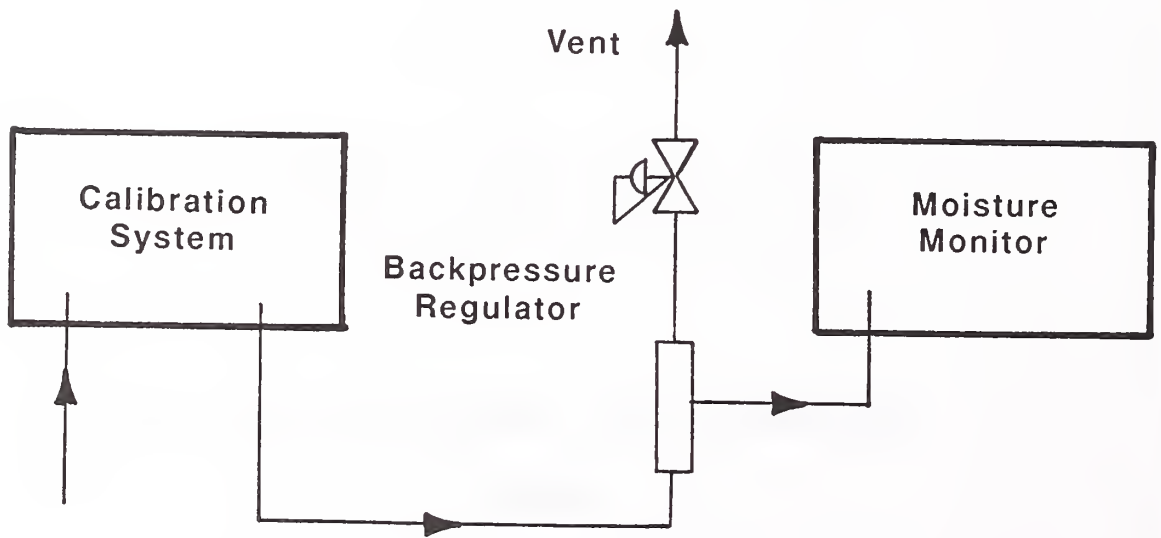
CALIBRATION BY STANDARD ADDITIONS

Figure 6



SIMULATED DRY-DOWN CURVE

Figure 7



INTERFACE SYSTEM

Figure 8

THERMODYNAMIC PROPERTIES OF MOIST AIR CONTAINING 1000 TO 5000 PPM_v OF WATER VAPOR

Peter H. Huang
National Institute of Standards and Technology
Process Measurements Division
Bldg. 221, Rm. B314
Gaithersburg, MD 20899
(301) 975-2621

Abstract: This paper provides calculated values of water vapor density, enthalpy, entropy, and Gibbs free energy associated with moist air. They cover the range of interest in moisture control and measurement methods for microelectronic packages from water vapor concentration of 1000 to 5000 PPM_v. These values are essential for establishing moisture standards for IC package gas analysis, for developing new measurement techniques for accurate determination of a known water vapor content, and for improving the understanding of moisture absorption/desorption phenomena in small or large chip packages. All values are referred to the recent realization of the International Temperature Scale of 1990 (ITS-90).

Molar enthalpy, molar entropy, and molar Gibbs free energy of moist air are expressed explicitly in terms of the associated water vapor density. The values of the molar quantities are the sum of three parts due to: (1) the mole fraction of water vapor, (2) the mole fraction of dry air, and (3) the effects of interaction between air molecules and water molecules.

Key Words: Microelectronic package; mixture; moisture standards; molecular interaction; thermodynamics; water vapor.

1. INTRODUCTION

Moisture measurement and control for microelectronics requires accurate and reproducible determination of water vapor concentration in moist air. The current Method 1018 has been implemented by both commercial and semiconductor manufacturers' analytical facilities as part of MIL-STD-883 for measuring water vapor content within a microelectronic package. In several correlation experiments, the participating laboratories performed mass spectrometric measurements of various moisture levels [1]. Devices were designed and packaged with three different cavity volumes and two different sealing technologies to contain moisture in the range of 2000 to 5000 PPM_v. Moist air can be treated as a mixture of the two real gases, water vapor and dry air. A unit of PPM_v is defined as the ratio of volume of water vapor to that of dry air. Moist air containing water vapor concentrations in the range of 1000 to 5000 PPM_v is equivalent to the saturation temperature in the range of approximately -20 °C to -2 °C at 101325 Pa (1 atm). The correlation of moisture measurements indicated a deviation of approximately $\pm 20\%$ from the overall mean moisture value in this range [1]. However, the existing correlation data and test methods are not sufficient to assure accurate and reliable analyses of moisture content in small packages with volumes on the order of 0.01 cm³ or less. The recent trend towards manufacture of smaller plastic packages for almost every type of integrated circuit housing implies that the following areas are the most important for research: (1) establishment of a suitable moisture standard in the range 1000 to 5000 PPM_v; (2) determination of the upper limit for acceptable moisture level in plastic packages from extensive laboratory correlation experiments; (3) effects of moisture absorption/desorption phenomena associated with mechanical, electrical, and thermal properties of

thermosets for packaging materials; (4) new techniques for measurement and control of moisture in microelectronic packages.

All of the above mentioned research areas involve studies of the thermodynamic properties of moist air. The purpose of this work is, therefore, to provide thermodynamic property values for water vapor density, enthalpy, entropy, and Gibbs free energy associated with moist air in a saturated state containing 1000 to 5000 PPM_v of water vapor. The virial equation state of moist air [2,3,4] is solved to determine water vapor density. Thermodynamic functions of molar enthalpy and entropy are derived in terms of water vapor density, mole fraction of water vapor, mole fraction of dry air, the second virial coefficient, saturation temperature and total pressure. The Gibbs free energy is then calculated from the temperature, enthalpy, and entropy.

2. THE VIRIAL EQUATION OF STATE

One of the most commonly used equations of state for moist air is a power series expression in terms of molar volume V_m of the mixture, as follows:

$$\frac{PV_m}{RT} = 1 + \frac{B_m(T)}{V_m} + \frac{C_m(T)}{V_m^2} + \dots \quad (1)$$

where P is the total pressure, R is the universal gas constant, T is the absolute thermodynamic temperature, $B_m(T)$ is the second virial coefficient of the mixture, and $C_m(T)$ is the third virial coefficient of the mixture. The terms involving the third virial coefficient are negligible in comparison with the terms containing the second virial coefficient in the range of pressures from 0 to about one atmosphere and temperatures from about -100 °C to about 60 °C [2,3,4]. According to thermodynamics [5] and statistical mechanics [6], the appropriate functional equation relating the interactions of the molecules of dry air and water vapor can be defined as follows:

$$B_m(T) = X_{as}^2 B_{aa} + 2X_{as}X_{ws} B_{aw} + X_{ws}^2 B_{ww} \quad (2)$$

where

- X_{as} = the mole fraction of dry air in the saturated moist air
- X_{ws} = the mole fraction of water vapor in the saturated moist air
- B_{aa} = the second virial coefficient pertaining to interactions between two dry air molecules
- B_{ww} = the second virial coefficient pertaining to interactions between two water molecules
- B_{aw} = the second cross-virial coefficient pertaining to interactions between one dry air and one water molecule

The coefficients B_{aa} , B_{aw} , and B_{ww} are given by the following expressions [4]:

$$B_{aa}(T) = 0.349568 \times 10^2 - 0.668772 \times 10^4/T - 0.210141 \times 10^7/T^2 + 0.924746 \times 10^8/T^3, \text{ cm}^3/\text{mol} \quad (3)$$

$$B_{aw}(T) = 0.32366097 \times 10^2 - 0.141138 \times 10^5/T - 0.1244535 \times 10^7/T^2 - 0.2348789 \times 10^{10}/T^4, \text{ cm}^3/\text{mol} \quad (4)$$

$$B_{ww}(T) = RT(0.70 \times 10^{-8} - 0.147184 \times 10^{-8} e^{1734.29/T}), \text{ cm}^3/\text{mol} \quad (5)$$

The mole fraction of water vapor X_{ws} and of dry air X_{as} for moist air at a given pressure P and temperature T are given by the equations, as follows:

$$X_{ws} = f(P,T) e_s(T)/P \quad (6)$$

$$X_{as} = 1 - X_{ws} = \frac{P - f(P,T) e_s(T)}{P} \quad (7)$$

where $f(P,T)$ is the enhancement factor [7,8] and $e_s(T)$ is the saturation water vapor pressure either with respect to water or ice [9,10]. The values of saturation water vapor pressure given by the formulation in [9] agree with those in steam tables [11]. In this work functional equations for $f(P,T)$ and $e_s(T)$ in references [8,10] are used for calculations in Eqs. (6) and (7).

The current NIST humidity calibration standard employs functional equations of enhancement factor and saturation water vapor pressure to calculate values of humidity units such as dew/frost-point and relative humidity in the NIST two-pressure humidity generator [12]. However, the temperature dependence of the enhancement factor is expressed in terms of the International Practical Temperature Scale of 1968 (IPTS-68), as indicated below [8]:

$$f(P, t_{68}) = \exp \left\{ \alpha(t_{68}) \left[1 - \frac{e_s(t_{68})}{P} \right] + \beta(t_{68}) \left[\frac{P}{e_s(t_{68})} - 1 \right] \right\} \quad (8)$$

where $\alpha(t_{68})$, $\beta(t_{68})$, and $e_s(t_{68})$ are functions of temperature on IPTS-68 and t_{68} is in degrees Celsius. To obtain $f(P, t_{90})$ based on the International Temperature Scale of 1990 (ITS-90) using Equation (8), we need to convert $\alpha(t_{68})$, $\beta(t_{68})$, and $e_s(t_{68})$ to $\alpha(t_{90})$, $\beta(t_{90})$, and $e_s(t_{90})$, respectively. Since the constant coefficients [8,10] associated with $\alpha(t_{68})$, $\beta(t_{68})$, and $e_s(t_{68})$ are based on IPTS-68, one can not merely replace t_{68} by t_{90} for calculating these functional values using the same constant coefficients. The functions $\alpha(t_{90})$, $\beta(t_{90})$, and $e_s(t_{90})$ can be expressed as a function of t_{68} using a Taylor's series expansion truncated after the second order term. We obtain the following equations:

$$\alpha(t_{90}) = \alpha(t_{68}) + \frac{\partial \alpha}{\partial t} \Big|_{t_{68}} (t_{90} - t_{68}) + \frac{1}{2} \frac{\partial^2 \alpha}{\partial t^2} \Big|_{t_{68}} (t_{90} - t_{68})^2 \quad (9)$$

$$\beta(t_{90}) = \beta(t_{68}) (1 + \eta) \quad (10)$$

in which

$$\eta \equiv \frac{1}{\beta(t_{68})} \frac{\partial \beta}{\partial t} \Big|_{t_{68}} (t_{90} - t_{68}) + \frac{1}{2} \frac{1}{\beta(t_{68})} \frac{\partial^2 \beta}{\partial t^2} \Big|_{t_{68}} (t_{90} - t_{68})^2 \quad (11)$$

and

$$e_s(t_{90}) = e_s(t_{68}) (1 + \xi) \quad (12)$$

in which

$$\xi \equiv \frac{1}{e_s(t_{68})} \frac{\partial e_s}{\partial t} \Big|_{t_{68}} (t_{90} - t_{68}) + \frac{1}{2} \frac{1}{e_s(t_{68})} \frac{\partial^2 e_s}{\partial t^2} \Big|_{t_{68}} (t_{90} - t_{68})^2 \quad (13)$$

The equivalent temperatures on IPTS-68 for a given temperature measurement based on ITS-90 are documented in [13].

In order to compute the thermodynamic properties associated with moist air, it is necessary to make use of the Eqs. (6) and (7). The values of the mole fraction of water vapor and of dry air in moist air can

be calculated when the pressure P and the temperature t_{90} of the moist air are given, provided that the corresponding values of the function $f(P, t_{90})$ are known. Since ITS-90 was designed to accurately represent the Thermodynamic Temperature Scale (TTS), the ITS-90 temperature is a close approximation of the TTS with no more than 4 mK deviation in the range of interest from -100 to 100 °C for humidity measurements [14]. The water vapor density in saturated moist air is:

$$\rho_w = \frac{18.0152 X_{ws}}{V_m} \times 10^6 \text{ g/m}^3 \quad (14)$$

where V_m is obtained from Equation (1) and X_{ws} is obtained from Equation (6).

Equation (14) is then used with other parameters in the calculations of enthalpy, entropy, and Gibbs free energy associated with moist air.

3. THERMODYNAMIC FUNCTIONS

Letting H and S denote molar enthalpy and molar entropy, respectively, at a given pressure P and temperature T , one can write $H = H(S,P)$, where S and P are independent variables, and the thermodynamic relation:

$$dH = TdS + VdP \quad (15)$$

When the Maxwell's relation

$$\left(\frac{\partial S}{\partial V} \right)_T = \left(\frac{\partial P}{\partial T} \right)_V \quad (16)$$

is substituted in Equation (15), the molar enthalpy of moist air representing the effects of interactions due to dry air and water molecules is given by [15,16]:

$$H'_m(V_m, T) = PV_m - RT + \int_{\infty}^{V_m} \left[T \left(\frac{\partial P}{\partial T} \right)_{V_m} - P \right] dV_m \quad (17)$$

On combining Eqs. (1), (2), (14), and (17), the molar enthalpy of moist air in a saturated state H_m can be expressed explicitly in terms of water vapor density ρ_w . In the earlier work [3,4,15,17], the enthalpy was expressed in terms of molar volume. Using Equation (1) truncated after the second term, we obtain

$$H_m = X_{as} \left(\sum_{i=0}^5 a_i T^i + H'_a \right) + X_{ws} \left(\sum_{i=0}^5 b_i T^i + H'_w \right) + RT \left[\frac{\rho_w \left(B_m - T \frac{dB_m}{dT} \right)}{18.0152 X_{ws}} \right], \text{ J/mol} \quad (18)$$

where $H'_a = -7914.1982 \text{ J/mol}$, $H'_w = 35994.17 \text{ J/mol}$, the first summation is the ideal gas (zero-pressure) molar enthalpy of dry air, and the second summation is that of water vapor. The constant coefficients a_i 's and b_i 's are available in [6]. The constant H'_a makes the molar enthalpy of dry air consistent with the assigned value zero at the reference state $T = 273.15 \text{ K}$ and $P = 101325 \text{ Pa}$ (1 atm). The constant H'_w makes the molar enthalpy of saturated liquid water consistent with the assigned value zero at the reference state $T = 273.16 \text{ K}$, the triple-point temperature for the pure water substance.

The enthalpy of moist air is equivalent to its total energy. Equation (18) shows that the molar enthalpy of moist air is a function of its temperature; the absolute amount of moisture it contains, namely, water vapor density, and its total pressure. The last term of Equation (18) containing the second virial coefficient and its derivative, at a given temperature, account for the deviation of the moist air from ideal gas enthalpies of water vapor and dry air.

The ideal gas molar entropy of dry air S_a° and of water vapor S_w° at $P = 101325$ Pa (1 atm) are given by [3,4,15,17]:

$$S_a^\circ = R \ln 101325 + \sum_{i=0}^4 c_i T^i + c_5 \ln T, \text{ J/(mol} \cdot \text{K)} \quad (19)$$

$$S_w^\circ = R \ln 101325 + \sum_{i=0}^5 d_i T^i + d_6 \ln T, \text{ J/(mol} \cdot \text{K)} \quad (20)$$

where the constant coefficients c_i 's and d_i 's are available in [6].

By virtue of Equation (16), it can be shown that the equation for the molar entropy of moist air S_m in a saturated state is given by [14]:

$$S_m = X_{as} S_a + X_{ws} S_w + X_{as} R \ln \left(\frac{V_m}{X_{as} RT} \right) + X_{ws} R \ln \left(\frac{V_m}{X_{ws} RT} \right) + \int_{\infty}^{V_m} \left[\left(\frac{\partial P}{\partial T} \right)_{V_m} - \frac{R}{V_m} \right] dV_m \quad (21)$$

where S_a and S_w are molar entropy of dry air and of water vapor, respectively. On combining Eqs. (1), (2), (14), and (21), the molar entropy of moist air can be expressed explicitly in terms of water vapor density ρ_w , as follows:

$$S_m = X_{as} (S_a^\circ + S'_a) + X_{ws} (S_w^\circ + S'_w) - R \ln(P/101325) + X_{as} R \ln \left(\frac{18.0152 P X_{ws}}{\rho_w R T X_{as}} \right) + X_{ws} R \ln \left(\frac{18.0152 P}{\rho_w R T} \right) - R \left[\rho_w \left(B_m + T \frac{dB_m}{dT} \right) / 18.0152 X_{ws} \right], \text{ J/(mol} \cdot \text{K)} \quad (22)$$

where $S'_a = -196.125454$ J/(mol · K) and $S'_w = -63.31449$ J/(mol · K). The constant S'_a makes the molar entropy of dry air consistent with the assigned value zero at the reference state, $T = 273.15$ K and $P = 101325$ Pa (1 atm). The constant S'_w makes the molar entropy of saturated liquid water consistent with the assigned value zero at the reference state $T = 273.16$ K, the triple-point temperature for the pure water substance.

The molar Gibbs energy, G_m , at a given temperature, T , associated with the moist air in a saturated state can be calculated by the following thermodynamic relation:

$$G_m = H_m - T S_m \quad (23)$$

in which H_m and S_m are obtained by Eqs. (18) and (21), respectively.

4. RESULTS

Table 1 lists values for ρ_w , H_m , S_m , and G_m calculated at eleven water vapor concentration values. The results quoted in Table 1 were obtained with the aid of a personal computer.

Figures 1 and 2 show that at ambient pressure, 101325 Pa (1 atm), ρ_w , H_m , S_m , and G_m increase in magnitude as the water vapor concentration increases. G_m , however, reaches a maximum value of approximately -6.0 J/mol at approximately 3700 PPM_v. It then decreases as the water vapor concentration increases to above 5000 PPM_v. A linear relationship is obtained for water vapor density and water vapor concentration as expected.

5. ESTIMATES OF UNCERTAINTY

The estimated uncertainties in the water vapor densities, molar enthalpies, and molar entropies are identical to the those in [4] for the specific enthalpies and specific entropies of moist air per unit mass of dry air. In the range 1000 to 5000 PPM_v water vapor concentration, the estimated maximum relative uncertainties are 0.6 percent for molar enthalpy and 0.1 percent for molar entropy, respectively. The estimated relative uncertainty of G_m is 0.7 percent based on Equation (23).

Since mole fraction of water vapor is related to saturation water vapor pressure through Equation (6), the uncertainty in ρ_w can be estimated to be

$$\frac{\Delta \rho_w}{\rho_w} \approx \frac{\Delta e_s}{e_s} \quad (24)$$

The relative uncertainty in the saturation water vapor pressure is small, less than 0.1 percent [10], over the saturation temperature range in this work.

6. REFERENCES

- [1] Moore, B.A., and Kane, D., Laboratory Correlation and Survey Experiment: A Status Report, NBSIR 87-3588 (June 1987).
- [2] Goff, J.A., and Gratch, S., Thermodynamic Properties of Moist Air, Trans. Am. Soc. Heating Ventilating Engineers, 51, 125 (1945).
- [3] Goff, J.A., Standardization of Thermodynamic Properties of Moist Air - Final Report of Working Subcommittee, International Joint Committee on Psychrometric Data, ASHVE J. Section, Heating, Piping, Air Conditioning, 55, 118 (1949).
- [4] Hyland, R.W., and Wexler, A., Formulations for the Thermodynamic Properties of Dry Air from 173.15 K to 473.15 K and of Saturated Moist Air from 173.15 K to 473.15 K, at pressures to 5 MPa, ASHRAE Transactions 89 (2A), 520 (1983); Formulations of the Thermodynamic Properties of the Saturated Phases of H₂O from 173.15 K to 473.15 K, ASHRAE Transactions 89 (2A), 500 (1983).
- [5] Fowler, R.H., and Guggenheim, E.A., Statistical Thermodynamics, pp. 693 (Cambridge, University Press, 1939).

- [6] Hirschfelder, J.O., Curtiss, C.F., and Bird, R.B., *Molecular Theory of Gases and Liquids*, pp. 1219 (New York, John Wiley & Sons, 1954).
- [7] Hyland, R.W., *Correlation for the Second Interaction Virial Coefficients and Enhancement Factors for Moist Air*, J. Res. NBS 79A, 551 (1975).
- [8] Greenspan, L., *Functional Equations for the Enhancement Factors for CO₂-free Moist Air*, J. Res. NBS 80A, 41 (1976).
- [9] Wexler, A., *Vapor Pressure Formulation for Water in the Range 0 to 100 °C, A Revision*, J. Res. NBS 80A, 775 (1975).
- [10] Wexler, A., *Vapor Pressure Formulation for Ice*, J. Res. NBS 81A, 5 (1976).
- [11] Haar, L., Gallagher, J.S., and Kell, G.S., *NBS/NRC Steam Tables: Thermodynamic and Transport Properties and Computer Programs for Vapor and Liquid States of Water in SI Units*, Hemisphere Publishing Corp., New York (1984).
- [12] Hasegawa, S., and Little, J.W., *The NBS Two-Pressure Humidity Generator, Mark 2*, J. Res. NBS 81A, 81 (1976).
- [13] Mangum, B.W., and Furukawa, G.T., *Guideline for Realizing the International Temperature Scale of 1990 (ITS-90)*. NIST Tech. Note 1265 (1990).
- [14] Furukawa, G.T., *Private Communication*.
- [15] Beattie, J.A., *The Computation of the Thermodynamic Properties of Real Gases and Mixtures of Real Gases*, Chem. Rev. 44, 141, (1949).
- [16] Crawford, F.W., Harris, E.J.R., and Smith, E.B., *Molec. Phys.* 37, 1323 (1979).
- [17] Vukalovich, M.P., Zubarev, V.N., Aleksandrov, A.A., and Kozlov, A.D., *Thermophysical Properties of Air*, Heat Transfer-Soviet Res., 6, 152 (1974).

Table 1. Thermodynamic Property Values Calculated at Eleven Selected Water Vapor Concentrations in PPM_v for Moist Air in a Saturated State at 101.325 KPa

t_{90} (°C)	PPM _v	H_m J/mol	S_m J/(mol•K)	ρ_w g/m ³	G_m J/mol
-2	5156	172.6876	0.6654	4.16	-7.7356
-4	4354	78.5931	0.3164	3.55	-6.5660
-6	3667	-10.3605	-0.01629	3.01	-6.0086
-8	3081	-94.8460	-0.3347	2.55	-6.1003
-10	2582	-175.4575	-0.6410	2.16	-6.7784
-12	2158	-252.7181	-0.9368	1.82	-8.0728
-14	1799	-327.0879	-1.2238	1.53	-9.9401
-16	1495	-398.9698	-1.5034	1.28	-12.3705
-18	1240	-468.7166	-1.7769	1.07	-15.3406
-20	1025	-536.6356	-2.0454	0.891	-18.8426
-22	844.3	-602.9944	-2.3098	0.740	-22.8881

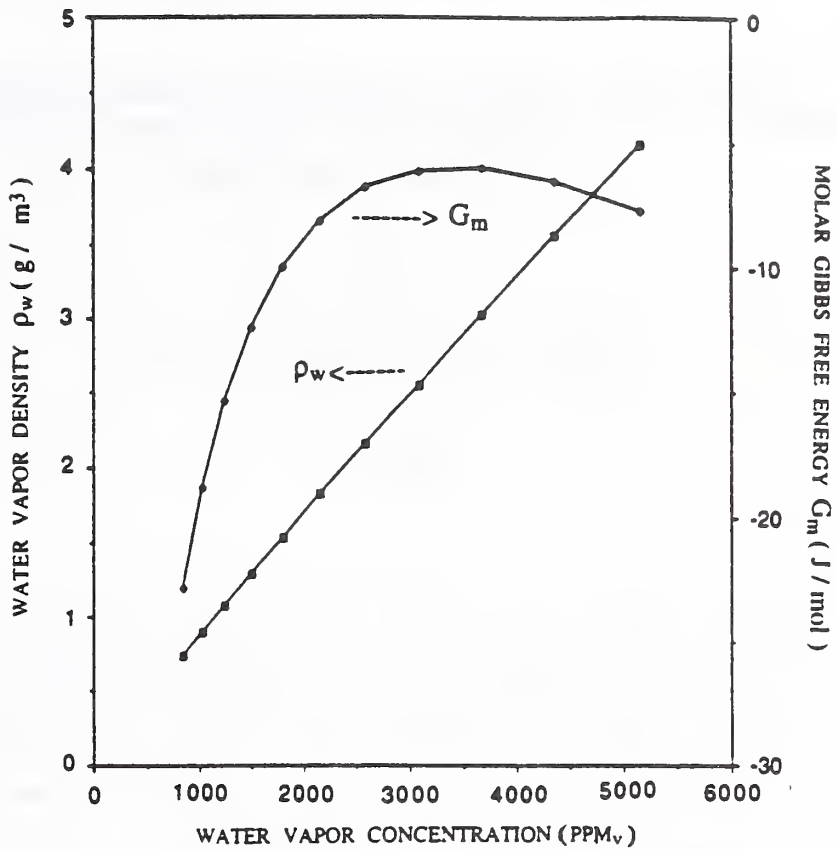


Figure 1. Molar Gibbs free energy G_m and water vapor density ρ_w of moist air in a saturated state at $P=101325$ Pa (1 atm) as a function of water vapor concentration.

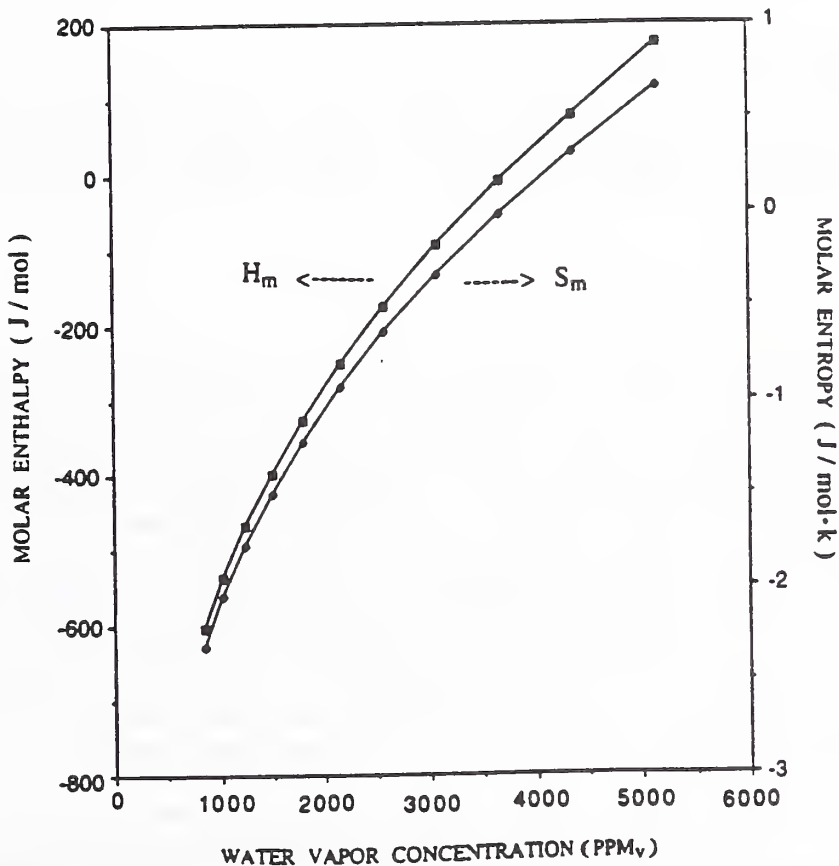


Figure 2. Molar enthalpy H_m and molar entropy S_m of moist air in a saturated state at $P=101325$ Pa (1 atm) as a function of water vapor concentration.

STUDIES ON A SOLVENT RESISTANT HUMIDITY SENSOR WITH HIGH WATER VAPOR AFFINITY: IMPORTANT IMPLICATIONS FOR MICROELECTRONICS

by

Gerald Schultz and Christopher Polla
Phys-Chem Scientific Corporation
New York, NY

ABSTRACT

ABSTRACT

A new humidity sensor based on impedance changes in an ionically conducting polymer is subjected to common volatile organic compounds (VOC) of widely varying dipole moments, hydrogen bond strengths, and boiling points. Sensors were tested under dynamic conditions i.e., exposed to VOC at known relative humidities, concentration of VOC ranging from 1000 to 100,000 ppm by volume. Shifts from sensor's standard response curve were reversible and followed VOC/water vapor volume ratio, miscibility of VOC in water, and boiling point of VOC. Under static conditions, where the sensor was exposed to the saturated vapors of VOC and totally immersed in the VOC, changes were reversible as well.

KEY WORDS

Bound water, enthalpy of absorption, free water, humidity generator, humidity sensor, hydration shells, polyelectrolyte, volatile organic compound.

INTRODUCTION

In this article we determine the specificity of a polyelectrolyte based humidity sensor[1] to water vapor in the presence of a broad range of volatile organic compounds (VOC's). Although the literature presents data for polymer type humidity sensors under static conditions where sensor is first immersed in VOC and then tested under known RH conditions after the VOC has been evaporated, in only one instance[2] have we found studies where testing is done dynamically i.e., sensor response is noted at various known relative humidities in the presence of a known concentration of VOC. For this reason our studies are done under dynamic as well as static conditions. There are obvious implications to studies of this kind; the measurement of the water content in encapsulated microelectronic packages where VOC's may be present is just one example.

VOC's were chosen over a wide range of dipole moments, hydrogen bond strengths, and boiling points. Having noted the effects of VOC on sensor response, an attempt is made to rationalize the results with

respect to thermodynamic and kinetic arguments.

The use of polyelectrolytes as the active principle in humidity sensors goes back at least to 1951[3]. These materials display a high negative free energy of absorption, gaining a significant portion of their weight in water. The process is driven by a large negative change in enthalpy which far outweighs an unfavorable negative change in entropy[4]. The polymer hydrates in the presence of water vapor, increasing the mobility of the counter-ion which is reflected in an increase in conductivity of five orders of magnitude over the 10 to 90 %RH interval. The standard response curve of the sensor in AC resistance vs %RH is given in figure 1.

The polyelectrolyte sensor discussed in this article was originally developed for use in Heating Ventilating and Air Conditioning (HVAC) applications where the RH range of interest is 20 %RH to 70 %RH. The sensor can withstand temperatures in excess of 140°C for 6 hrs with a 1%RH shift from standard response curve (figure 2). At 25°C and 5000 ppm water vapor the sensor has an AC resistance at 5 kHz of 6 million ohms. Figure 3 shows the stability of the sensor over 17 months, at 53 %RH, 71 %RH, and 93 %RH as measured by the saturated salt technique.

EXPERIMENTAL

Dynamic Testing

A divided flow vapor generator (figure 4) is constructed for the purpose of creating known relative humidities[5] at varying vapor concentrations of volatile organic compounds. The generator was calibrated against a NIST traceable dew point measuring system manufactured by EG&G with the results listed in table 1. These results indicate that in the 15-70 %RH range there is agreement to 1.6%RH or better. The repeatability of the generator is 1%RH.

The operating principle of the generator is as follows. Two metered independent dry nitrogen streams are saturated with respect to water vapor and solvent vapor at 25°C respectfully and mixed in varying proportions with a stream of dry nitrogen. Flow meters for the wet and dry streams are matched to within two percent. The solvent vapor flow meter is matched within 10 percent or better of the other two. Valves 1 and 2 are adjusted so that no pressure differential exists among the three streams as measured by means of a differential manometer. Each of the streams are therefore at the same pressure (being slightly above 1A) and are allowed to expand to 1A in a sampling chamber where the RH sensor is placed.

The %RH, VOC, and water vapor concentrations (in ppm) at 1A are computed in the following manner.

$$\%RH = \frac{V}{\frac{V}{w} + \frac{V}{d} + \frac{V}{s}} \times 100$$

$$\text{ppm H}_2\text{O} = \frac{(RH/100) (P_w)}{1 - ((RH/100) (P_w))} \times 10^6$$

$$\text{ppm VOC} = \frac{(f) (P_s)}{1 - ((f) (P_s))} \times 10^6$$

where V_w = flow rate of water saturated stream

V_d = flow rate of dry nitrogen

V_s = flow rate of solvent saturated stream

P_w = saturated vapor pressure of water in atmospheres

P_s = saturated vapor pressure of solvent in atmospheres

$f =$ solvent volume fraction, $\frac{V_s}{V_d + V_s + V_w}$

Three underlying assumptions are made. During the course of the experiments the total pressure is constant. Water vapor, VOC, and nitrogen taken together behave as ideal gases. Water vapor and solvent vapor streams are saturated at 25°C (or very nearly so).

The humidity sensor is instrumented with an analog transmitter[1] of sufficient resolving power to detect shifts from standard response curve due to the presence of VOC. The transmitter measures the total current through the humidity sensor which is a function of relative humidity at constant temperature. The output of the transmitter is a linear function of %RH at 25°C.

VOC's are run in the 15% to 67%RH range at varying ppm levels depending on the flow rates of the VOC stream, humid and dry streams, and the saturated vapor pressures of solvent and water. The sensor is initially allowed to equilibrate at either 31%RH or 68%RH, depending on the RH range of study, before metering in the VOC vapor. The concentration of vapor is raised in 3 increments by increasing the flow rate of the solvent vapor stream. Each increment lowers the RH by dilution. Enough time is given for the sensor to reach equilibrium after each increment. The shift in RH due to the effects of VOC is computed as follows.

$$\text{RH shift} = (RH_f - RH_i)_{\text{observed}} - (\text{delta RH})_{\text{dilution}}$$

where $(RH_f - RH_i)_{\text{observed}}$ is defined as the difference between the initial RH (RH_f) and the RH as read after i each VOC increment (RH_i).

and (ΔRH) is the difference in RH
dilution due to dilution:

$$\frac{V(100)}{V + \frac{w}{d} + \frac{w}{s}} - \frac{V(100)}{V + \frac{w}{d}}$$

Following the last VOC increment, the flowmeter is turned off and the sensor is allowed to settle back to its original reading. Any discrepancies between the initial reading of the transmitter (before the VOC was metered in) and this final reading is regarded as offset and is used in calculating the maximum uncertainty of the data. It is felt that offset is not due to irreversible interactions between solvent and sensor (see static studies below). The offset was typically less than 1%RH. However, in those cases where the offset was greater, as much as 3%RH, the run was repeated until lower offsets were achieved. Total uncertainties due to offset and scatter of data, expressed as the difference between the lowest and highest %RH shift, ranged from 1% to 4%RH. Graphs were constructed from the means of the data. Anywhere from 6 to 21 runs were done for each VOC.

Static Studies

The purpose of this study is to measure reversibility of VOC effects. A group of 45 sensors, five for each VOC, were immersed for 24 hours and then air dried at room temperature. Sensors were retested and the shifts from standard response curve were noted.

In another group, 45 sensors, five for each VOC, were exposed to saturated vapors for 66 hours at room temperature. Sensors were retested after dissipation of vapors and shifts from standard response curve were noted.

RESULTS AND DISCUSSION

Figures 5 and 6 display shifts in %RH vs VOC/water vapor ratio from standard response curve under dynamic conditions for two regions, at low RH(15-30%RH) and high RH(45-70%RH), for each of the nine VOC's. The physical properties of these compounds are given in table 2. Figures 7 and 8 display shifts as a function of ppm on a volume basis at 20% and 70%RH respectfully. Shifts were reversible under dynamic conditions.

Table 3 lists the results of exposure to VOC under static conditions where sensors were first immersed in VOC for 24 hrs or exposed to saturated vapors for 66 hrs and then retested under known RH conditions after removal of VOC. As can be seen from the data, there are no significant shifts from standard response curve. This indicates that the interactions between humidity sensitive polyelectrolyte and VOC are physical in nature and completely reversible.

Figures 5-8 show some important trends for the entire group of 9 VOC's. For example VOC's that are immiscible in water show positive deflections from sensor standard curve i.e., more conductive. These deflections become more positive for the same VOC/Water Vapor Ratio as the RH increases. Evidently the enthalpy of absorption is increased and/or the activation energy for conduction[7] is decreased by the introduction of hydrophobic VOC. Others have observed[4] that the enthalpy of absorption of polyelectrolytes, particularly at low RH, is influenced by the electrostatic interactions of the salt groups. It is reasonable to propose that hydrophobic VOC's alter these interactions causing greater water absorption.

Water miscible solvents show negative deflections in the low RH region i.e., decreased conductivity. In this case, the enthalpy of water vapor absorption is decreased and/or the activation energy for conduction is increased. Miscibility would lower the activity of water thus causing less interaction between the counter-ion and water. These deflections become less negative for the same VOC/Water Vapor ratio as the RH increases.

Figures 9 and 10 show another important trend in that shifts from standard response curve of the sensor, in either the water miscible or immiscible groups, increase with increasing boiling point of VOC. Evidently, as the VOC approaches its saturated vapor pressure (higher activity) it has a greater tendency to change phase and alter the electrical properties of the polyelectrolyte. Acetone has an anomalously large deflection which may be due to its large dipole moment.

Figure 11 shows the standard response curve of the sensor in the presence of 1000 ppm of isopropanol, amyl acetate, and cellosolve taken individually at 25°C. The curve undergoes a slight change in shape with higher deflections occurring at 20%RH than 70 %RH for isopropanol and cellosolve . This is not an unexpected result since the water absorbed at low RH is bound in the hydration shells of the polyanion and counter-ion whereas at higher RH the water is free[8]. The deflection from the standard response curve at 20 %RH and 1000 ppm VOC, even for higher boiling solvents like amyl acetate and cellosolve is only 2% RH. Undoubtedly, the high specificity for water vapor of the above mentioned humidity sensor in the presence of VOC's is due to the high water vapor affinity of polyelectrolytes.

Table 1.

Generator RH @25°C	Standard RH @25°C
13.9	14.0
48.8	50.0
67.2	68.8
79.0	81.0

Table 2.

VOC	Boiling Point	Dipole Moment	Hydrogen[6] Bond Strength	Water Miscibility
acetone	56.2	2.88	10	misc.
isopropanol	82.1	1.66	approx. 19	misc.
methanol	65.0	1.70	18.5	misc.
cellosolve	135.0	-	13.0	misc.
carbon tetrachloride	76.5	0.0	-	immisc.
toluene	110.6	0.36	4.5	immisc.
hexane	69.0	0.0	approx. 0	immisc.
trichloroethane	76.0	1.79	3.5	immisc.
amyl acetate	149.0	1.75	approx. 9	immisc.
water	100.0	1.85	39.0	-

Table 3.

Static Testing

<u>VOC</u>	<u>Saturated Vapors(66 hrs)</u>	<u>Liquid Immersion (24 hrs)</u>
acetone	-1%RH	1%RH
isopropanol	-1%RH	-1%RH
2methanol	1%RH	1%RH
cellosolve	-1%RH	1%RH
carbon tetrachloride	1%RH	1%RH
toluene	0%RH	-1%RH
hexane	-1%RH	1%RH
trichloroethane	1%RH	0%RH
amyl acetate	-1%RH	-3%RH
formalin	-2%RH	-2%RH

REFERENCES

1. Schultz, G., Relative Humidity Measurement With An Analog Transmitter, *Measurements & Control*, Issue 156, 96-99, (1992).
2. Sashida, T., Sakaino, Y., An Interchangeable Humidity Sensor For An Industrial Hygrometer, *Proc. of the 1985 International Symposium on Moisture and Humidity*, Washington D.C., April 15-18, 1985, pp. 525-534
3. Pope, M., *Electric Hygrometer*, U.S. Patent 2,728,831, Nov. 9, 1951.
4. Sundheim, B.R., Waxman, M.H., Gregor, H.P., *Studies On An Ion Exchange Resin VII*, *J. Phys. Chem.*, 57, 974-978.
5. Smith, P.R., A New Apparatus For The Study Of Moisture Sorption Humidity and Moisture, Arnold Wexler, and William A. Wildhack Eds., Vol. 3, pp. 487-494, (Reinhold, New York 1965).
6. Crowley, J.D., Lowe, Teague, *Journal of Paint Technology*, 38, No. 496, 269-80(1966).
7. Glastone, Laidler, Eyring, The Theory Of Rate Processes, Chapter XI, McGraw-Hill Book Co., Inc., N.Y., N.Y. 1941.
8. Helfferich, F., Ion Exchange, p. 106 (McGraw-Hill Book Co., Inc., N.Y., N.Y., 1962).
9. Waxman, M.H., Sundheim, B.R., Gregor, H.P., *Studies on Ion Exchange Resins VI*, *J. Phys. Chem.*, 57, 969-973.
10. Barrer, R.M., Zeolites and Clay Minerals as Sorbents and Molecular Sieves, Academic Press, London, 1978.

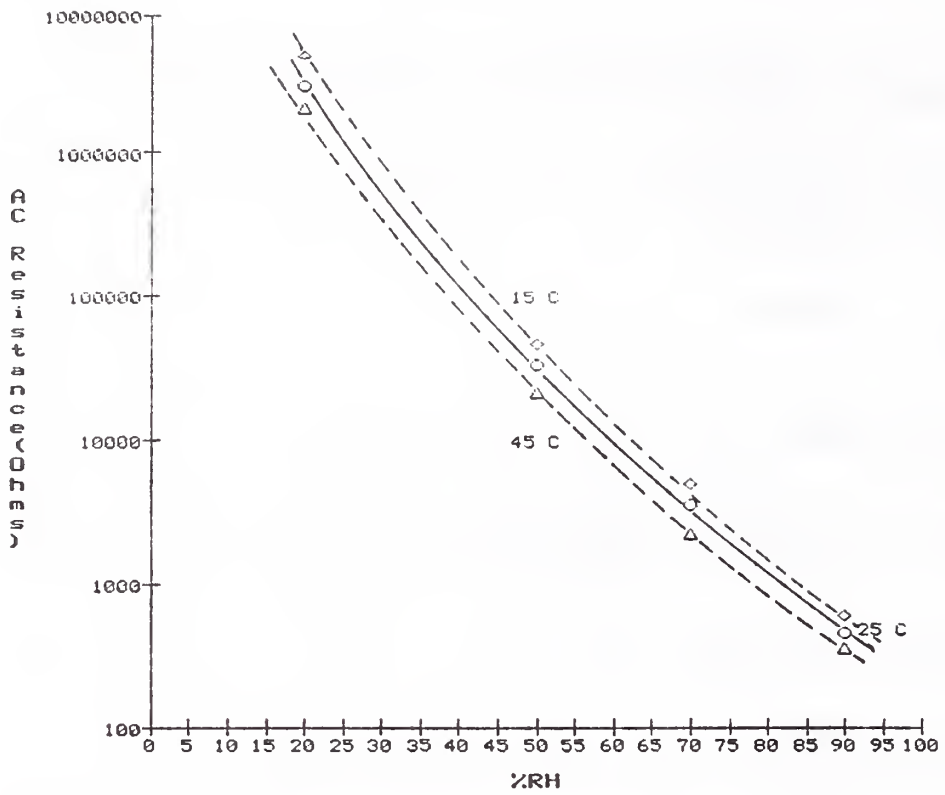


Figure 1. Standard response curve as a function of temperature measured at 5 kHz/1 Volt in GenRad 1689 RLC Digibridge.

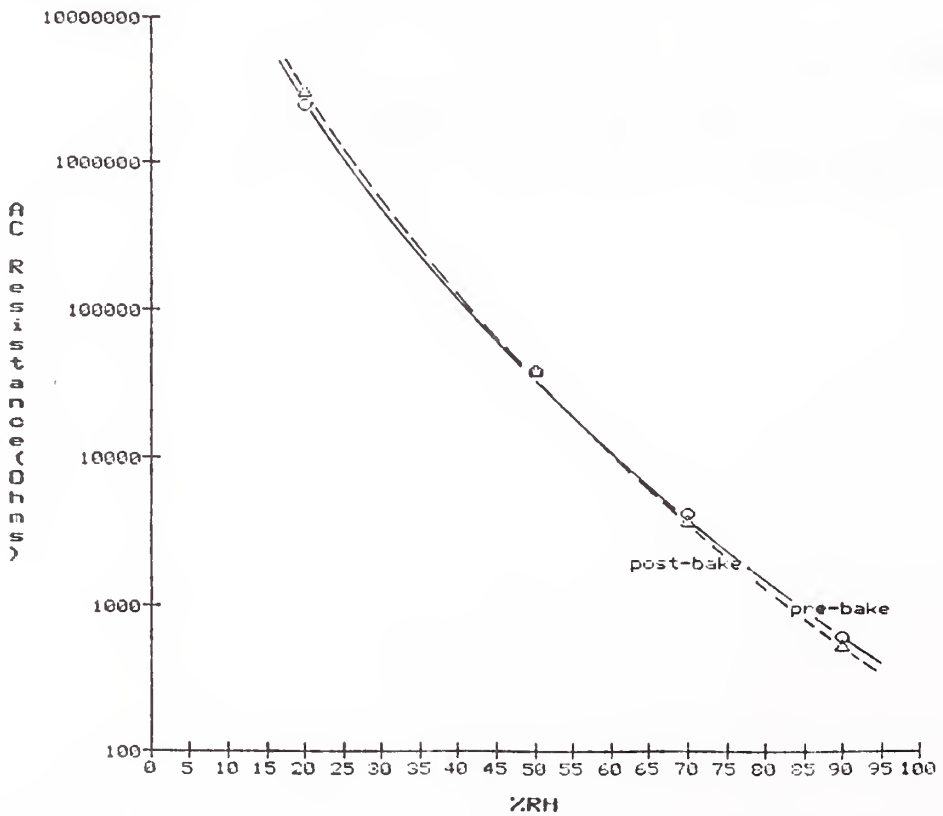


Figure 2. Shift in standard response curve upon exposure to 140 C/6 hrs.

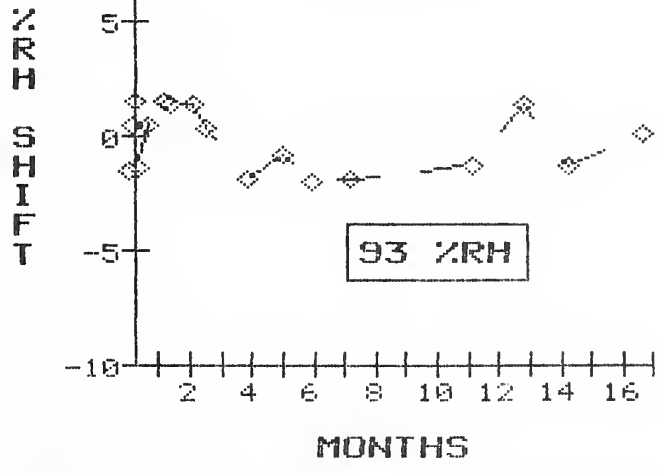
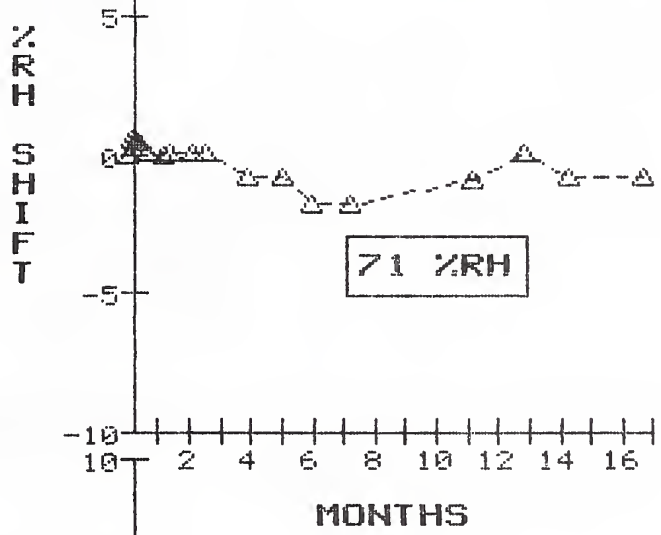
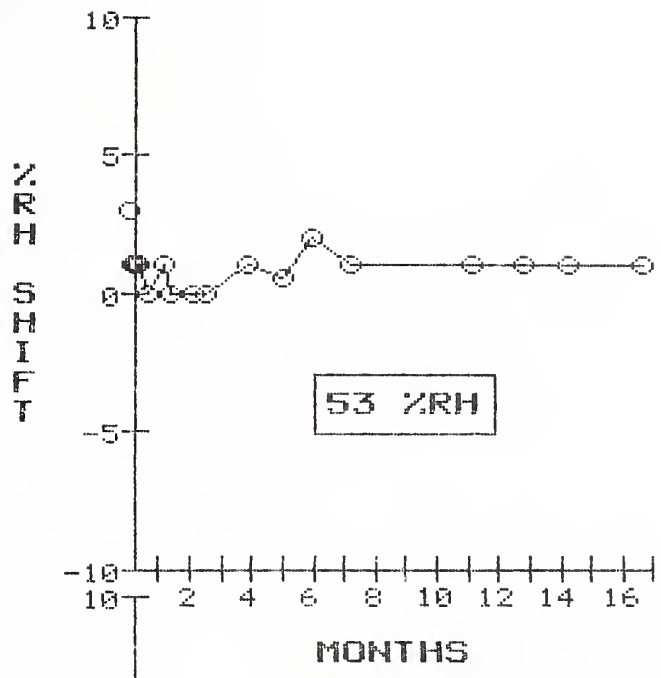


Figure 3. Sensor stability by saturated salt technique

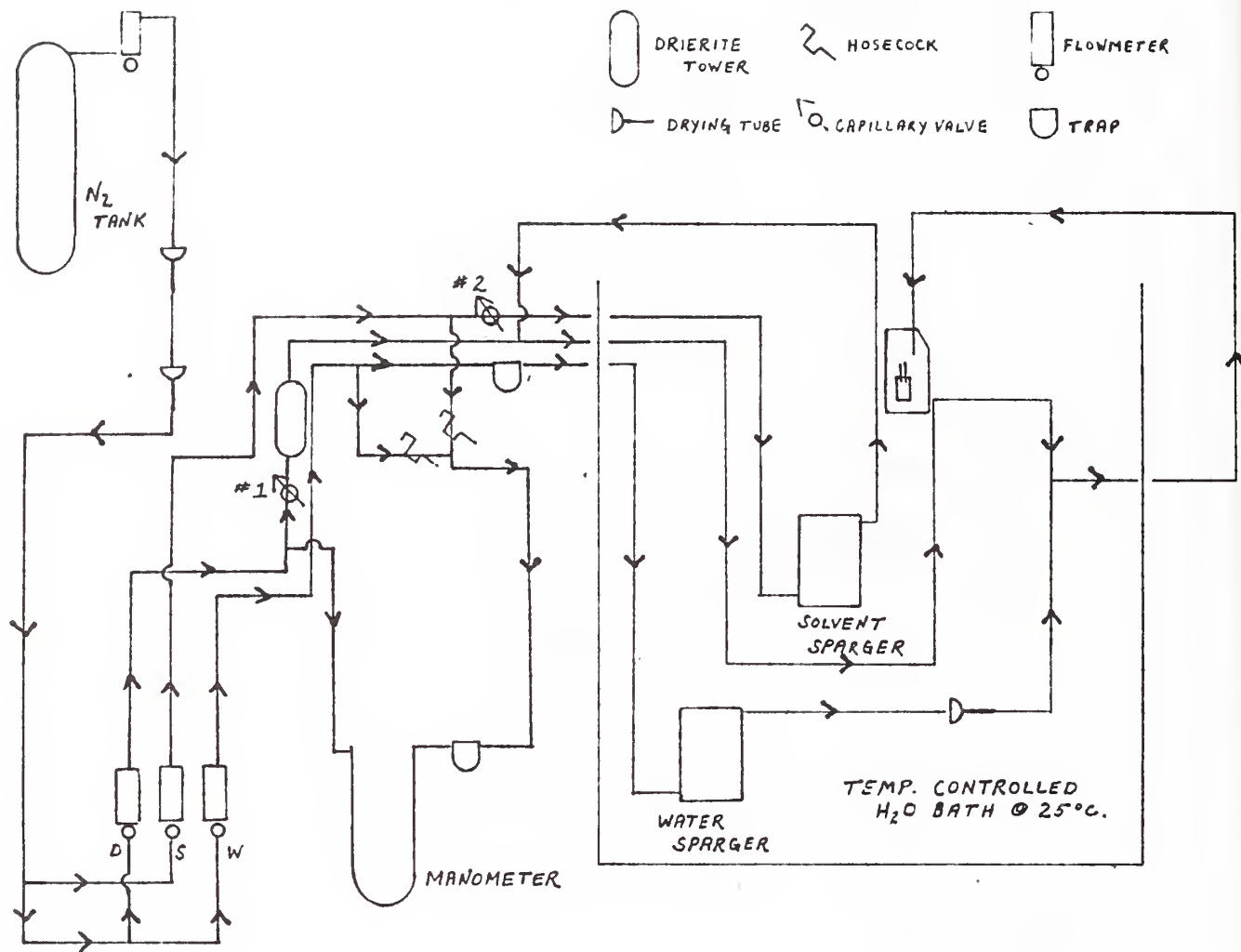


Figure 4. RH/VOC Generator schematic diagram

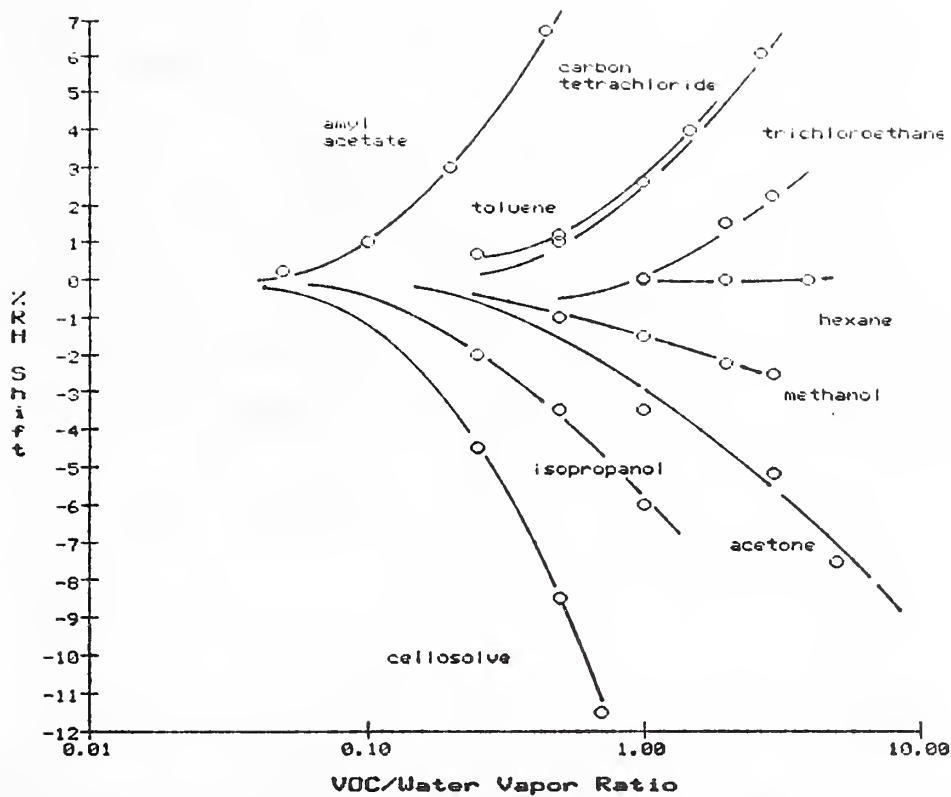


Figure 5. Shifts in %RH from standard response curve as a function of VOC/Water Vapor Ratio at 25 C in the low RH region.

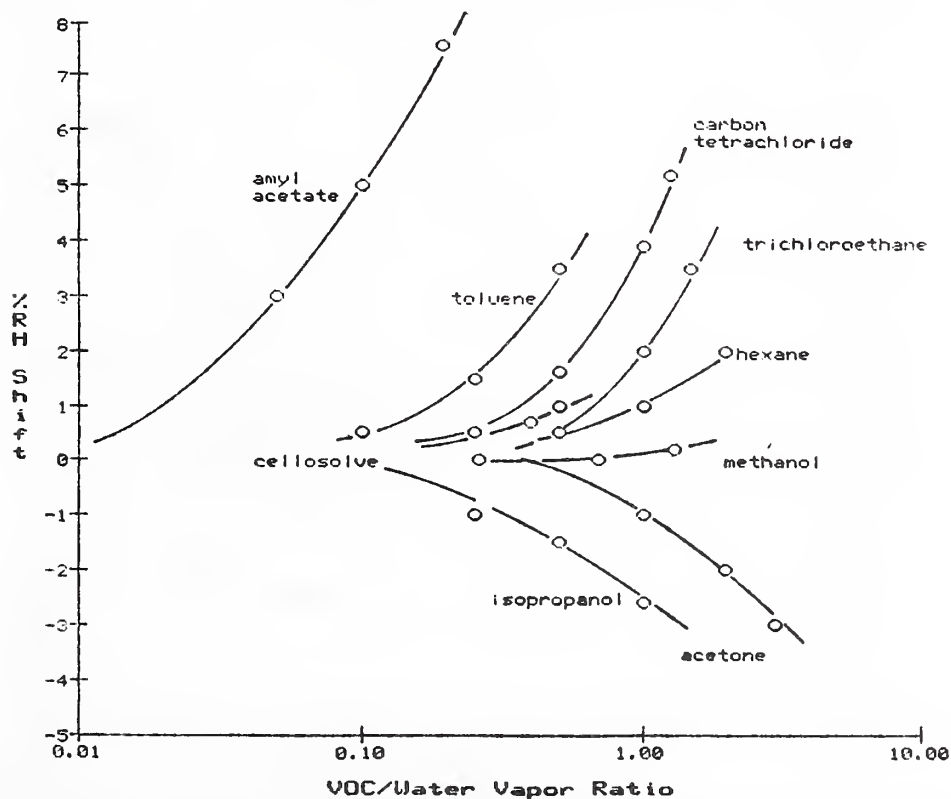


Figure 6. Shifts in %RH from standard response curve as a function of VOC/Water Vapor Ratio at 25 C in the high RH region.

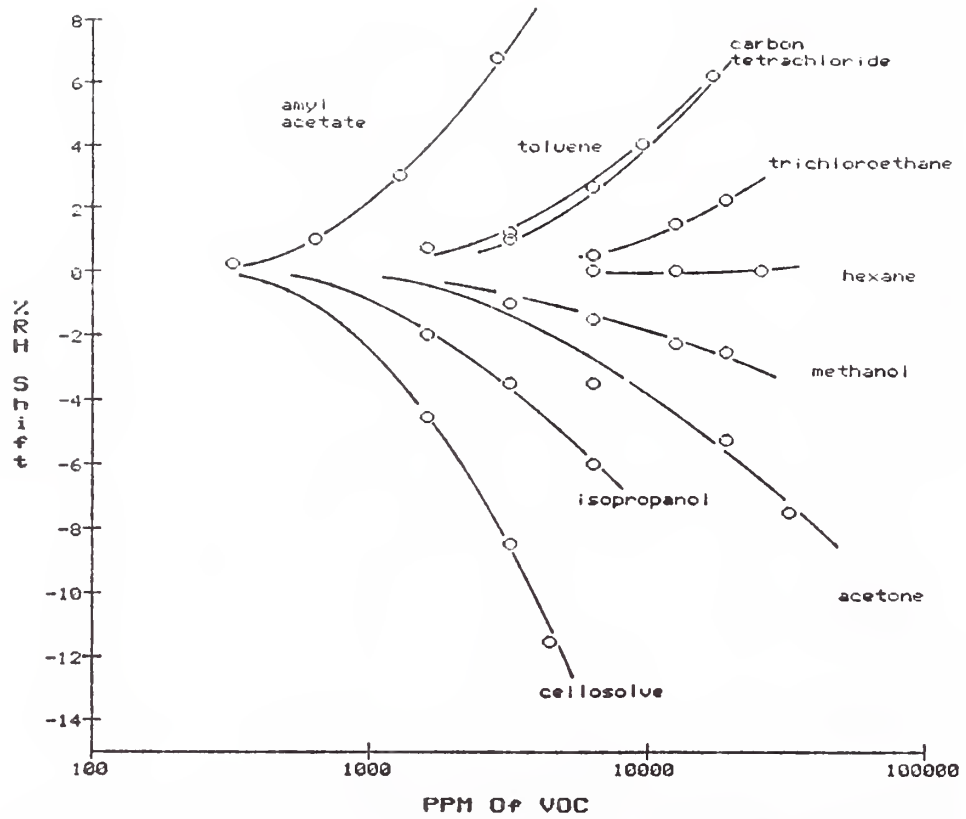


Figure 7. Shifts in %RH from standard response curve as a function of ppm VOC at 25 C at 20%RH.

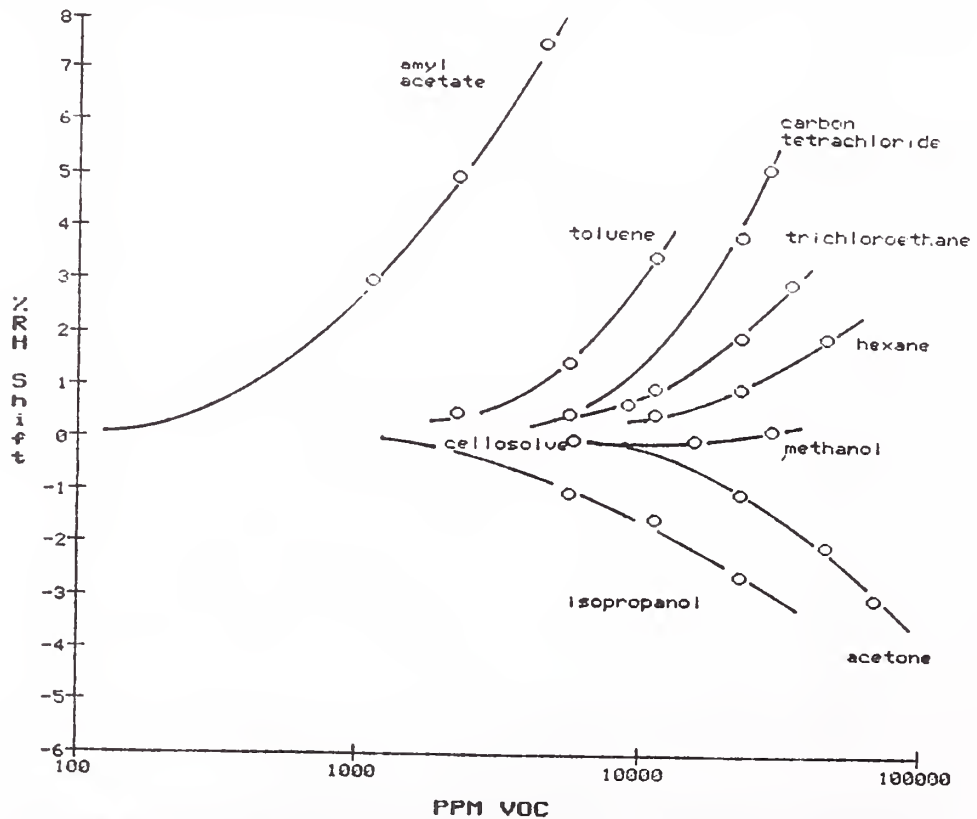


Figure 8. Shifts in %RH from standard response curve as a function of ppm VOC at 25 C at 70%RH.

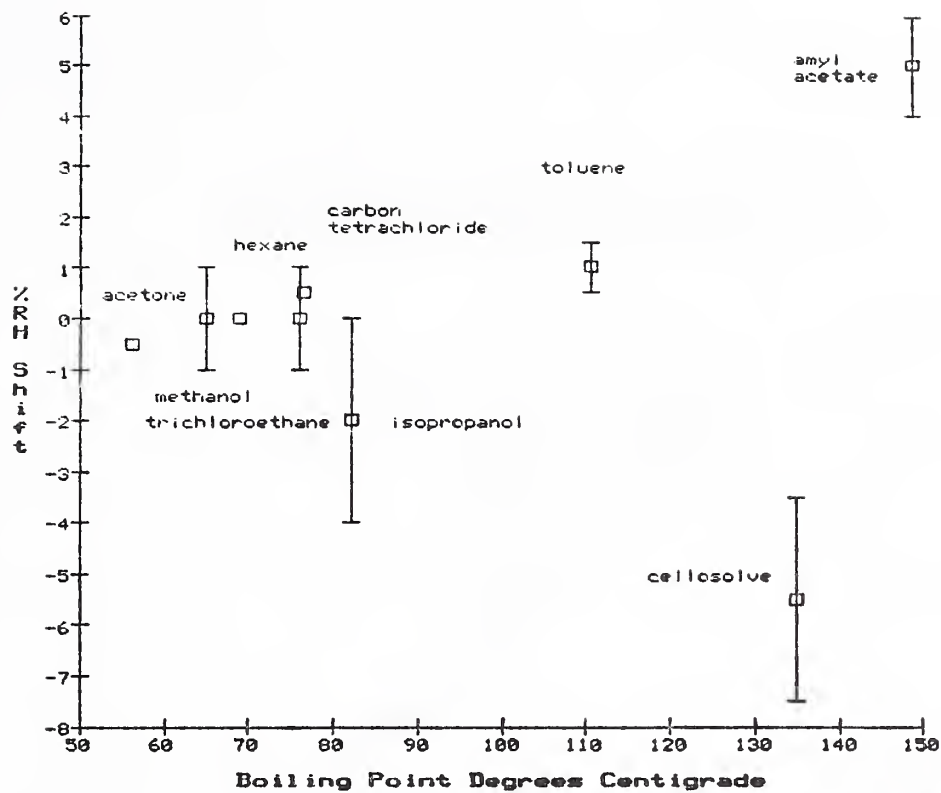


Figure 9. Shifts in %RH from standard response curve as a function of boiling point of VOC at 2000 ppm at 25 C and 20%RH.

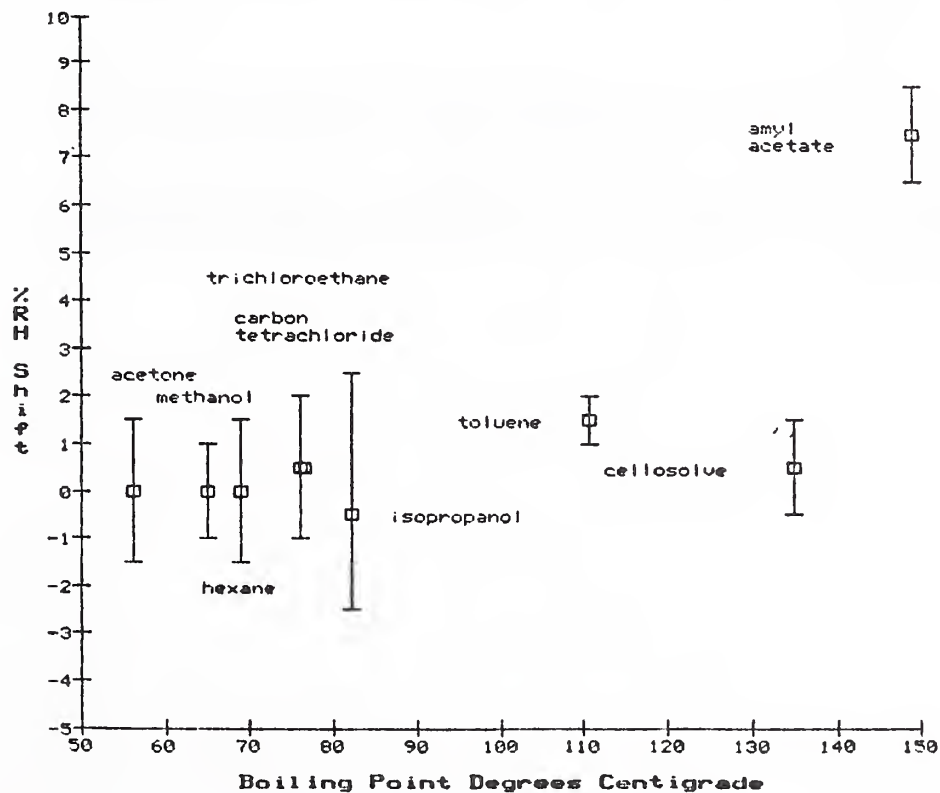


Figure 10. Shifts in %RH from standard response curve as a function of boiling point of VOC at 4000 ppm at 25 C and 70%RH.

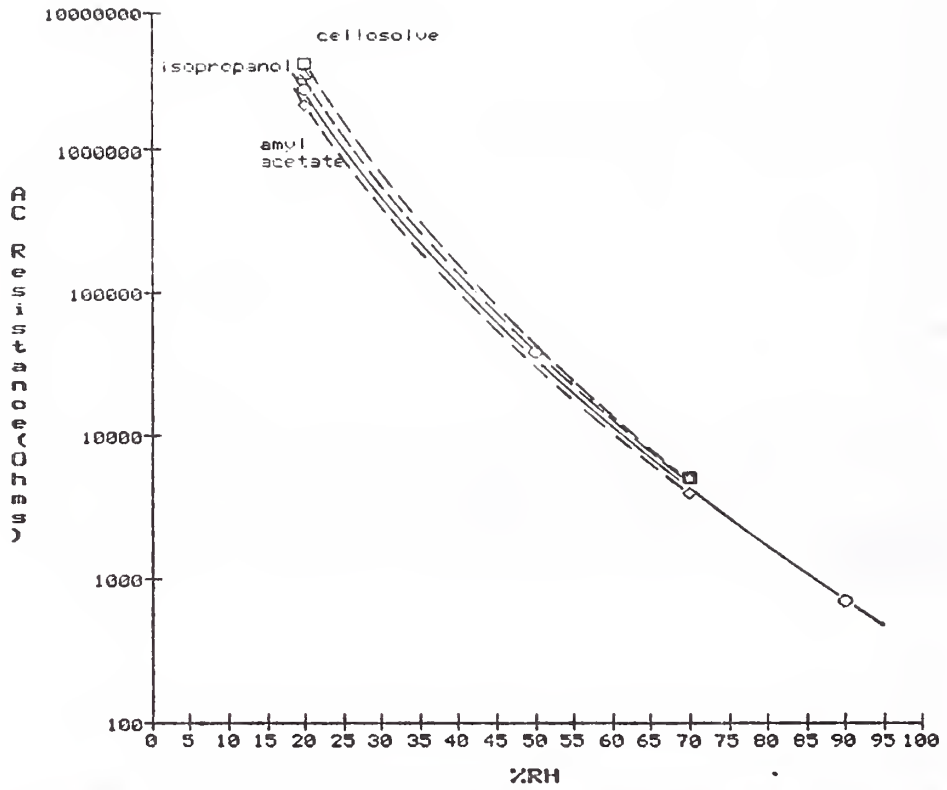


Figure 11. Shift in %RH from standard response curve due to exposure to cellosolve, amyl acetate, and isopropanol at 1000 ppm.

**HYDROGEN DESORPTION FROM BASE
AND PROCESSED PACKAGING ALLOY**

by

Philipp wh Schuessler
Stephen G. Gonya
IBM/FSC
Owego, NY

ABSTRACT

By the late '80's various microelectronic device manufacturers had experienced the "Hydrogen Phenomenon" knowingly and unknowingly. This phenomenon occurs when residual or absorbed hydrogen has remained within microstructure trap sites of the ferrous alloy packaging materials that they had selected. But as a function of burn-in or other thermal stresses, the hydrogen is desorbed into the cavity of the device. A variety of chemical reactions are then potentially available by which the desorbing hydrogen gas can destroy device integrity and product reliability. To date, a multitude of subsequent chemical reactions have been identified which can be cause for the failure of the product. This paper identifies an in depth analytical routine which has allowed the supplier community to provide the user community with hydrogen free packages. Potential sources or traps for absorbed hydrogen have been theoretically identified. "Bake out" procedures, and the affects of annealing and plating are also reviewed, all of which have been found to ultimately impact device reliability, i.e., should product design, and process variables all align contrarily to the needs of the product type in question.

INTRODUCTION:

The phenomenon of Hydrogen Desorption was first observed on captive microwave devices made with Gallium Arsenide die. Titanium adhesion metallurgy also used as in-line resistors were noted to become bumpy and even lose adhesion. Meanwhile the circuits were noted to electrically drift. Residual Gas Analysis (RGA) of this device showed increasing concentrations of hydrogen as a result of thermal stress, e.g., burn-in.

Other device technologies were noted to acquire increasing concentrations of moisture such that in several cases Quality Conformance Inspection (QCI) criteria of Mil-Std-888 Test Method 5008 could not be met. Concurrent with the increase in moisture was the noted increase in hydrogen concentrations. In some cases residual traces of normal air were also noted to change as Argon concentrations remained low, e.g., 100 ppm, but the expected oxygen level at circa 2000 ppm was totally absent.

These incidents all drew their origin from the absorbed hydrogen slowly desorbing into the cavity of the respective devices. Hydride formation with metal systems, such as titanium, and metal oxide reduction, such as the reduction of silver solder glass die attach materials, are now understood to be the root cause for these problems.

IBM personnel set in place a team of industrial participants to help in clarifying the problem. A base metal supplier, packaging houses and an independent analytical facility participated in the study which is detailed in the following paragraphs.

EXPERIMENTAL:

It was deemed imperative that the studies on desorption of hydrogen should have at least two primary factors. First, the study was to be based on alloys and subsequent processes with known, identifiable histories. Secondly, the study was to be statistically significant, in other words, single point occurrences and analysis were not acceptable as credible evidence or data. For this reason often times three to five analyses were prepared from the same sample. With that thought in mind, the reader should be aware, that every "data point" provided in this report is in reality an average of at least three readings or samples.

Base alloys were submitted for analyses in three different thicknesses, 10, 40, and 60 mil. These were selected from U.S. and foreign sources, but their exact identity remained as a blind parameter to the IBM study. The sources of these alloys remained known only to the base alloy supply house.

The procedure for hydrogen desorption and subsequent analysis has been reported earlier in literature and will not be presented in great detail here. Basically, the procedure consisted of sealing known weights of Kovar alloy in pyrex glass ampules in an inert atmosphere of high purity nitrogen. These ampules were then subjected to the desired thermal stress for a given period of time, usually in 200 hour intervals. After which the ampules were submitted for Residual Gas Analyses via the

methods and instrumentation qualified for test method 1018 analyses of Mil-Std-883. After their respective analyses, the samples were then resealed under previously established, controlled conditions into pyrex ampules for the next 200 hour interval of thermal stress. Absolute hydrogen concentrations were verified by the fabrication and testing of ampules with known hydrogen-nitrogen levels as supplied by an independent gas supply facility. A maximum of 2.5% hydrogen in nitrogen was used as a standard. This standard was verified at the beginning of the study and again eighteen months later where the mass spectrometer was found to be able to maintain the quantification of hydrogen in nitrogen to $\pm 5\%$ of the original value.

TASK I. HYDROGEN DESORPTION FROM BASE METAL

Mono atomic hydrogen is the only hydrogen gas species capable of diffusing through metals as an interstitial solute. Hydrogen can be "trapped" in the metal at structural imperfections and incoherent boundaries such as grain boundaries, dislocations, vacancies, micropores, precipitate interfaces, inclusion and particle boundaries. Absorbed hydrogen in excess of the lattice solubility will segregate to trap sites within the metal and increase the total hydrogen solubility by orders of magnitude. Trap site hydrogen can then be desorbed from the metal by thermal aging. Each type of reversible trap site has an associated activation energy for hydrogen diffusion out of the metal and gives rise to strong and weak trap sites. Sources of absorbed hydrogen include; melting processes, acid cleaning, electroplating and electrocleaning, corrosion, hydrogen brazing and annealing, air annealing in humid atmospheres.

The first task measured the quantity of desorbed hydrogen from Kovar sheet stock as a function of time, temperature, and sheet thickness. The tests included several lots from 10, 40, and 60 mil sheet thicknesses. Test coupons were hermetically sealed in pyrex ampules with dry nitrogen and thermally aged as part of a time/temperature matrix. All RGA data was normalized to percent H₂ evolved in a 1.0 cc volume from a 1.0 gram sample.

The majority of hydrogen was desorbed in the first 200 hours at temperature with the thicker sheet samples desorbing the greatest amount. Mean percentage values of desorbed hydrogen after 200 hours at 150°C were 4.0%, 2.0%, and <0.02% for 60, 40, and 10 mil thick Kovar respectively. Sheet thickness is a dominant factor in the levels of desorbed hydrogen and this may be related to fabrication of the different sheet thicknesses with the 10 mil stock requiring more thermal-mechanical processing, i.e., the fabrication process itself may desorb some hydrogen.

The microstructure of the different Kovar stock thicknesses showed a trend of increasing inclusion density with decreasing sheet thickness. The 10 mil stock has the highest inclusion density and also a finer grain size compared to either the 60 or 40 mil stock. The microstructure may influence the quantity and rate of desorbed hydrogen with higher inclusion and grain boundary densities providing weak trap sites and increased hydrogen flux out of the metal. The cleaner microstructure of the 60 mil and some of the 40 mil stock show the highest desorbed hydrogen levels which may be related to strong trap sites within the grains. There appears to be higher desorption peaks at 150°C and 300°C for all three thicknesses. These peaks may be due to the type of hydrogen trap sites within the material and their associated activation energies.

There was a slight tarnishing of coupons exposed to 300°C which is probably due to oxidation of the Kovar by moisture present in the ampule and may partly account for increased hydrogen levels at that temperature. Water content within the ampules was minimized but difficult to control and no quantitative evaluation of moisture level changes was attempted. For the Kovar alloy (Ni29-Co17-Fe54) at 150°C and an assumed water to hydrogen ratio of 50 the oxidation reaction by water is possible. However, this effect is not believed to be dominant since the study showed no correlation with coupon surface area as would be expected if surface oxidation were generating the hydrogen.

Also, it is not thermodynamically possible to directly reduce water to hydrogen and oxygen under the operating test conditions. However, the reverse reaction to form water can take place and it is catalyzed by gas absorption on the metal surfaces.

TASK II. OXIDE REDUCTION BY DESORBED HYDROGEN

To demonstrate the mechanism of hydrogen desorption and oxide reduction a matrix was run using copper coupons oxidized to a dark blue-purple appearance. The oxidized copper coupons were sealed in ampules with 60 mil Kovar coupons known to desorb hydrogen. Other test groups were run in parallel to baseline the amount of water initially present and the total amount of desorbed hydrogen from the Kovar coupons. Blank coupons that did not desorb hydrogen were used in the matrix to account for any absorbed water on the coupon surface. After 200 hours at 150°C the following mean value results were obtained for water and hydrogen.

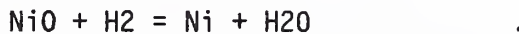
	<u>SAMPLE</u>	<u>ppm H2</u>	<u>ppm H2O</u>	<u>COMMENTS</u>
A.	Kovar Coupon Blank Coupon	6232	2899	Baseline Hydrogen
B.	Kovar Coupon Oxidized Cu Coupon	5164	4353	Oxide Reduction
C.	Blank Coupon Blank Coupon	ND	2959	Baseline Water
D.	Blank Coupon Oxidized Cu Coupon	ND	3559	No Oxide Reduction

Ampules with the oxidized copper and Kovar coupons visibly showed reduction of the copper oxide layer and after 200 hours the copper was clean. Quantitative RGA data showed that hydrogen levels had decreased and the water levels increased in roughly the same amount which would be consistent with the hydrogen reduction reaction:



Ampules with the oxidized copper and blank coupons showed no visible oxide reduction and no desorbed hydrogen. This test demonstrates that the sequence of hydrogen desorbing from base metal and subsequent oxide reduction will take place at 150°C. Using the above data for calculations, about 300 anstroms of copper oxide were reduced to produce the observed rise in moisture level.

Other metals whose oxides are able to be reduced by hydrogen include silver, lead, cobalt, nickel, tin, iron, and tungsten. Hydrogen can reduce any available oxide to generate water if it is thermodynamically favorable under the operating conditions. Use of the Gibbs free energy change and the Van't Hoff isotherm will determine the potential for oxide reduction and the equilibrium partial pressure ratio of water and hydrogen. Graphical representation of these reactions with quantitative thermodynamic data are presented in the Ellingham diagram for metal oxides. Using nickel at 150°C as an example, the following equations demonstrate the use of the thermodynamic factors involved.



$$\Delta G^\circ (150\text{C}) = -19935 \text{ Joules} = -RT \ln P(\text{H}_2\text{O})/P(\text{H}_2)$$

$$P(\text{H}_2\text{O})/P(\text{H}_2) = 290 \text{ at Equilibrium; } <290 \text{ NiO Reduction} \\ >290 \text{ Ni Oxidation}$$

AMPULE EXAMPLE: Total Pressure = 1.0 atm
 99.49% N₂
 0.5% H₂O
 100 ppm H₂

$$P(\text{H}_2\text{O})/P(\text{H}_2) = 50 < 290 \rightarrow \text{NiO Reduction}$$

$$\Delta G (150\text{C}) = \Delta G^\circ (150\text{C}) + RT \ln P(\text{H}_2\text{O})/P(\text{H}_2) = -6177 \text{ Joules}$$

Studies with gold over nickel plating showed nickel can diffuse through the gold layer, primarily along grain boundaries, and then spread over the gold surface forming a thin layer of nickel oxide capable of being reduced by hydrogen. Auger surface analysis of plated device packages after burn-in show both nickel and oxygen on the gold surface. Metal hydroxides on surfaces can also react with hydrogen gas to release water and reduce the hydroxide to an oxide. The latter reaction occurs very rapidly and at low temperatures.

TASK III. SURFACE FINISH AND TREATMENT EFFECT

To investigate surface treatment effects used on microelectronic packages a series of Kovar coupons were sent to two different package supply houses for various package treatments and surface finishing. The returned coupons were then sealed in ampules and thermally aged at 150°C. The test matrix included both virgin and hydrogen free coupons prepared by the following supplier treatments.

1. Hydrogen Braze
2. Hydrogen Anneal
3. Wet Hydrogen Glass Seal
4. Hydrogen Bake Out
5. Au Over Ni Plate by Supplier A
6. Au Over Ni Plate by Supplier B
7. Supplier A Process:
 - i) glass seal
 - ii) Au/Ni plate
8. Supplier B Process:
 - i) hydrogen anneal
 - ii) hydrogen bake out
 - iii) Au/Ni plate

High temperature brazing in a high concentration H₂ forming gas increased the subsequent desorbed hydrogen content of the metal compared to virgin levels, contrarily, low temperature hydrogen annealing in a low concentration H₂ atmosphere reduced the desorbed hydrogen content. The glass sealing process in wet hydrogen gas also reduced the desorbed hydrogen content. The hydrogen bake-out process performed by one

supplier reduced hydrogen desorption below detectable levels on all samples processed. Although the bake-out appeared to be effective in reducing hydrogen levels, it is a high temperature process and cannot be used as a final operation after plating because of nickel diffusion to the gold surface causing various attachment problems.

Gold over nickel electroplating and the supplier processes with final electroplating showed inconsistent results. The plating appears to absorb hydrogen into the metal or the plating itself was a source of hydrogen. The plating may also act as a temporary barrier to hydrogen diffusing out of the metal or that hydrogen diffusing from the plating will increase its flux level with longer times at temperature. Further study is required to determine which phenomena are actually occurring and what levels of hydrogen are involved.

CONCLUSIONS:

Microelectronic manufacturers have experienced various device problems related to hydrogen inside the package cavity. This phenomenon occurs when residual or absorbed hydrogen remains within the ferrous alloy packaging materials. As a function of burn-in or other thermal stresses the hydrogen is desorbed into the cavity of the device. A variety of chemical reactions are then potentially available by which the desorbing hydrogen gas can destroy device integrity and product reliability.

The majority of hydrogen was desorbed from Kovar alloy samples in the first 200 hours at temperature with the thicker sheet stock desorbing the greatest amount. Mean percentage values of desorbed hydrogen after 200 hours at 150°C were 4.0%, 2.0%, and <0.02% for 60, 40, and 10 mil thick Kovar respectively.

Hydrogen can reduce any available oxide to generate water if it is thermodynamically favorable under the operating conditions. Tests using oxidized copper coupons sealed in ampules with Kovar known to desorb hydrogen showed complete reduction of the oxide layer after 200 hours at 150°C. Quantitative RGA data showed that hydrogen levels had decreased

and water levels had increased during oxide reduction which is consistent with the hydrogen reduction reaction. This test demonstrates that the sequence of hydrogen desorbing from base metal and subsequent oxide reduction will take place at 150°C burn-in temperature. Studies with gold over nickel plating showed nickel can diffuse through the gold layer and spread over the gold surface forming a thin layer of nickel oxide which is also capable of being reduced by hydrogen.

Kovar samples exposed to high temperature H₂ brazing increased the subsequent desorbed hydrogen content of the metal, whereas, low temperature H₂ annealing reduced the hydrogen content. A hydrogen bake-out process reduced hydrogen desorption below detectable levels and appeared to be very effective in reducing hydrogen levels in the metal.

Electroplated samples showed inconsistent results. The plating process appeared to absorb hydrogen into the metal or the plating itself was a source of hydrogen.

DATA MATRIX OF BASE KOVAR HYDROGEN DESORPTION

DATA IN % H₂ CC/G BY VOLUME

ND = NONE DETECTED; <0.02 % H₂

I. 60 MIL STOCK

<u>LOT</u>	<u>TIME</u>	<u>100°C</u>	<u>150°C</u>	<u>200°C</u>	<u>250°C</u>	<u>300°C</u>
510	50 HRS	0.94	2.96			
	100	0.43	0.03			
	150	0.22	0.54			
	200	0.39				
510	200 HRS		3.90	2.99	2.74	3.07
	400		0.13			
	600		ND			
	1000		ND			
823	200 HRS		3.59			
	400		0.03			
120	200 HRS		6.48	2.87	2.77	2.62
	400		0.07	0.10	0.13	0.47
	600		ND			
606	200 HRS		3.38			
	400		0.02			
602	200 HRS		3.16			
	400		0.03			

II. 40 MIL STOCK

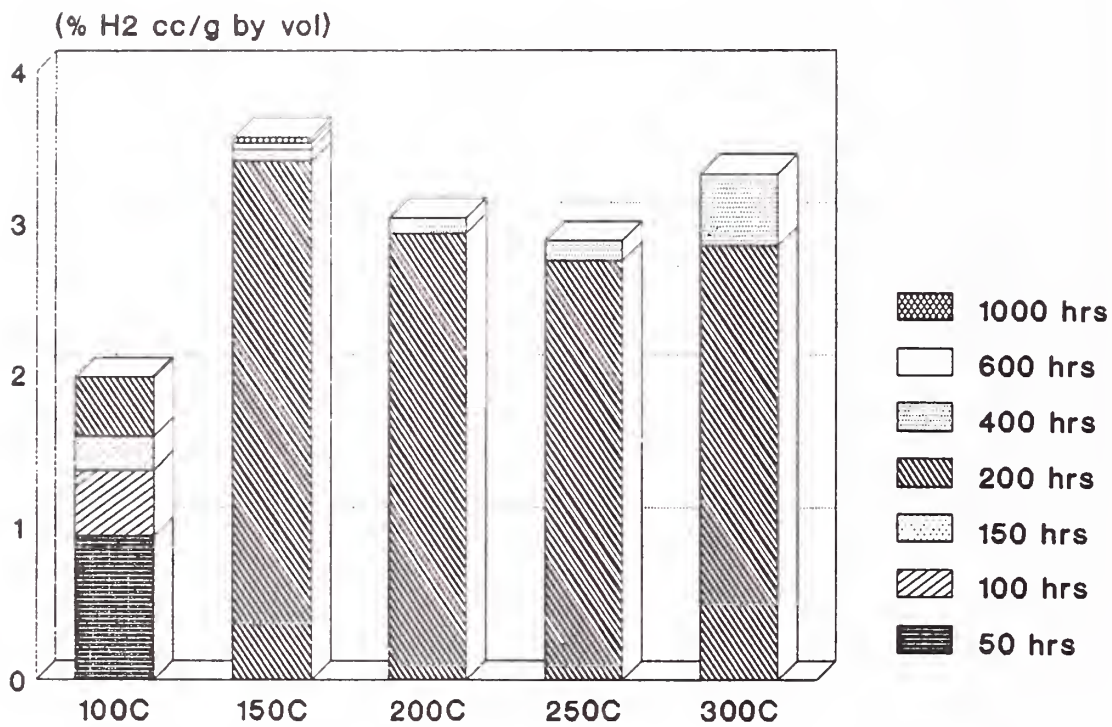
<u>LOT</u>	<u>TIME</u>	<u>100°C</u>	<u>150°C</u>	<u>200°C</u>	<u>250°C</u>	<u>300°C</u>
26828	50 HRS	1.35				
	100	0.18				
	150	ND				
	200	0.13				
26828	200 HRS		3.70	3.62	3.73	4.15
	400		ND	ND	0.07	0.56
	600		ND			0.33
	800		-			0.33
	1000		ND			0.24
26820	200 HRS		1.68	1.43	1.53	1.82
	400		ND	ND	ND	0.32
	600		ND			0.28
	800		-			0.26
	1000		ND			0.25
27347	200 HRS		2.13	1.96	1.89	2.09
	400		ND	ND	0.02	0.65
	600		ND			0.28
	800		-			0.25
	1000		ND			0.20
24196	200 HRS		ND	ND	ND	0.37
	400		ND	ND	ND	0.25
	600		ND			0.23
	800		-			0.27
	1000		ND			0.20
27770	200 HRS		2.10	2.01	1.76	2.10
	400		ND	ND	ND	0.31
	600		ND	ND	ND	0.40
	800		-			0.09
	1000		ND			0.14
801	200 HRS		1.93	0.69	0.72	1.36
	400		ND	0.04	0.06	0.45
905	200 HRS		0.56			
	400		ND			
003	200 HRS		2.69			1.51
	400		ND			

III. 10 MIL STOCK

<u>LOT</u>	<u>TIME</u>	<u>100°C</u>	<u>150°C</u>	<u>200°C</u>	<u>250°C</u>	<u>300°C</u>
334	200 HRS		ND			1.75
460	200 HRS		ND			0.87
860	200 HRS		ND			1.74
144	200 HRS		ND	ND	ND	1.72
	400		ND	-	-	0.57
	600		-	-	-	0.71
	800		-	-	-	
	1000		ND	ND	0.08	
259	200 HRS		ND			1.05
679	200 HRS		ND			1.17

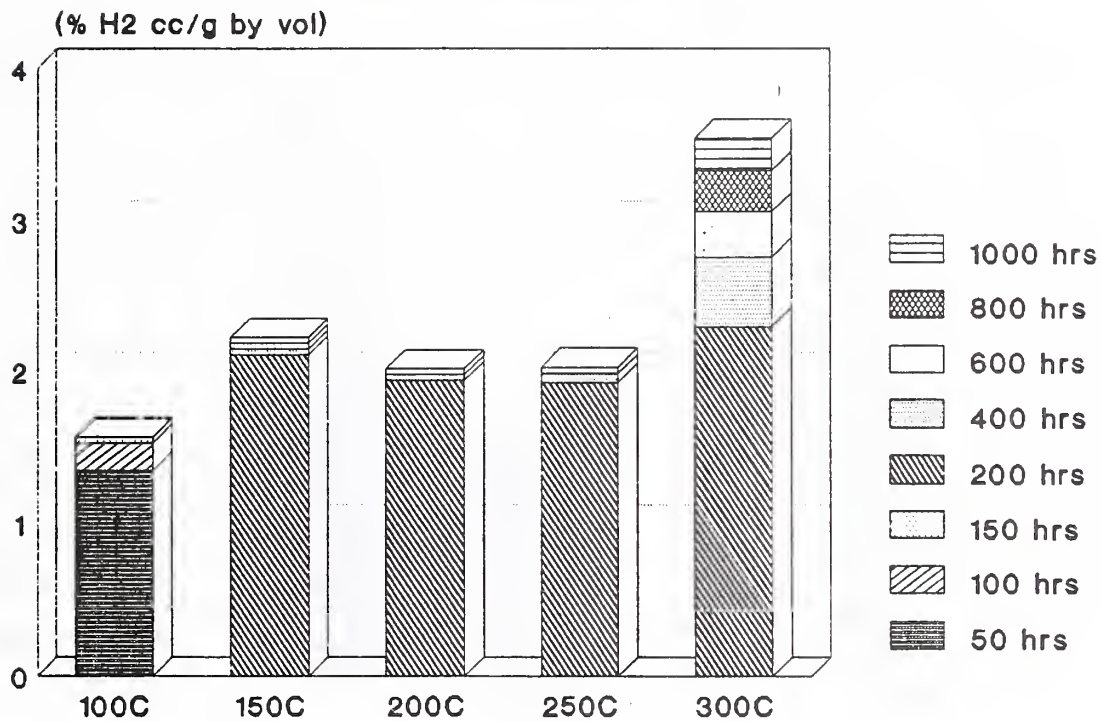
TIME/TEMP HYDROGEN DESORPTION

60 mil Kovar Stock



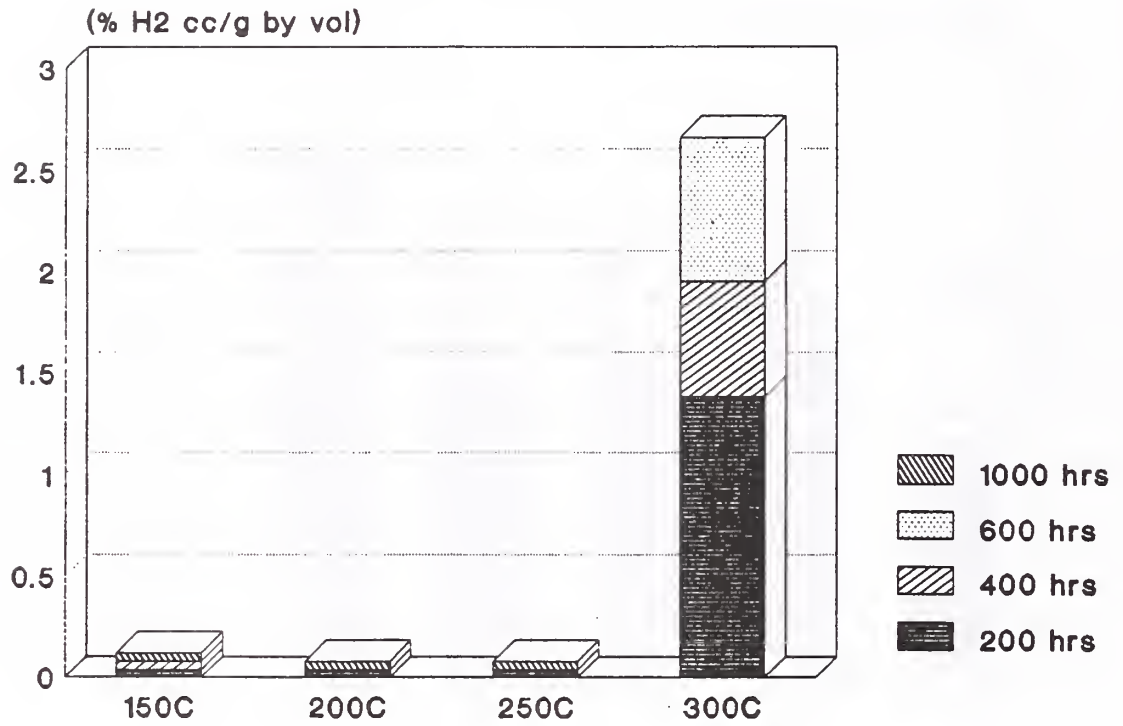
TIME/TEMP HYDROGEN DESORPTION

40 mil Kovar Stock

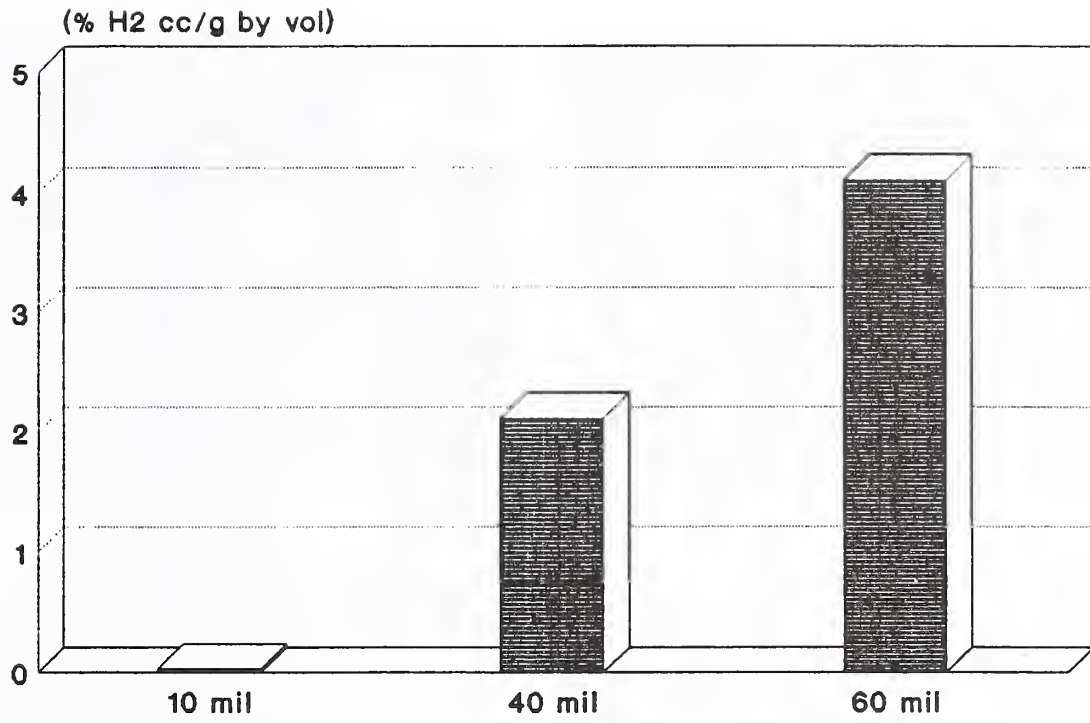


TIME/TEMP HYDROGEN DESORPTION

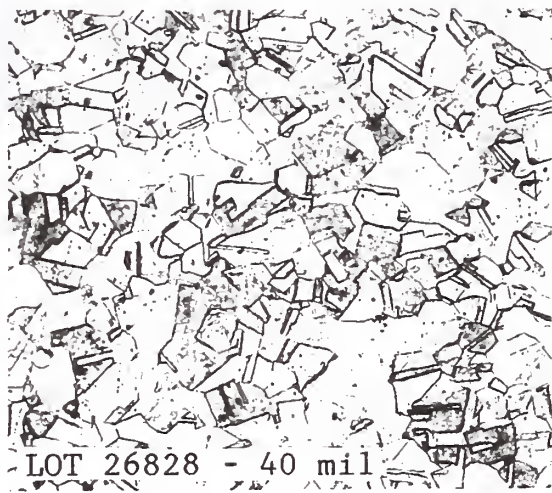
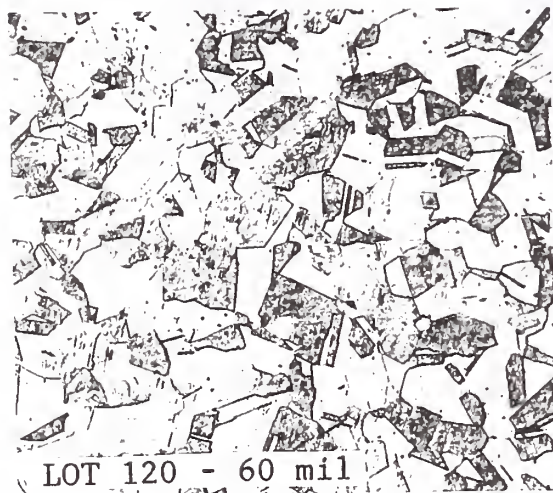
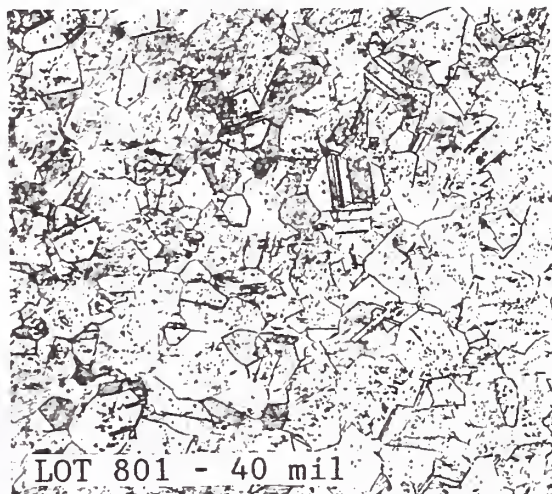
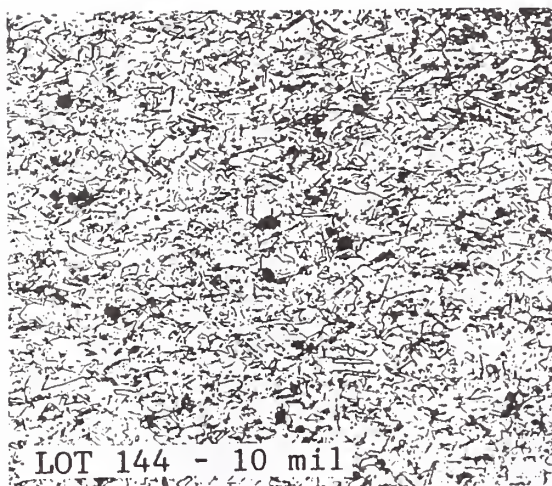
10 mil Kovar Stock



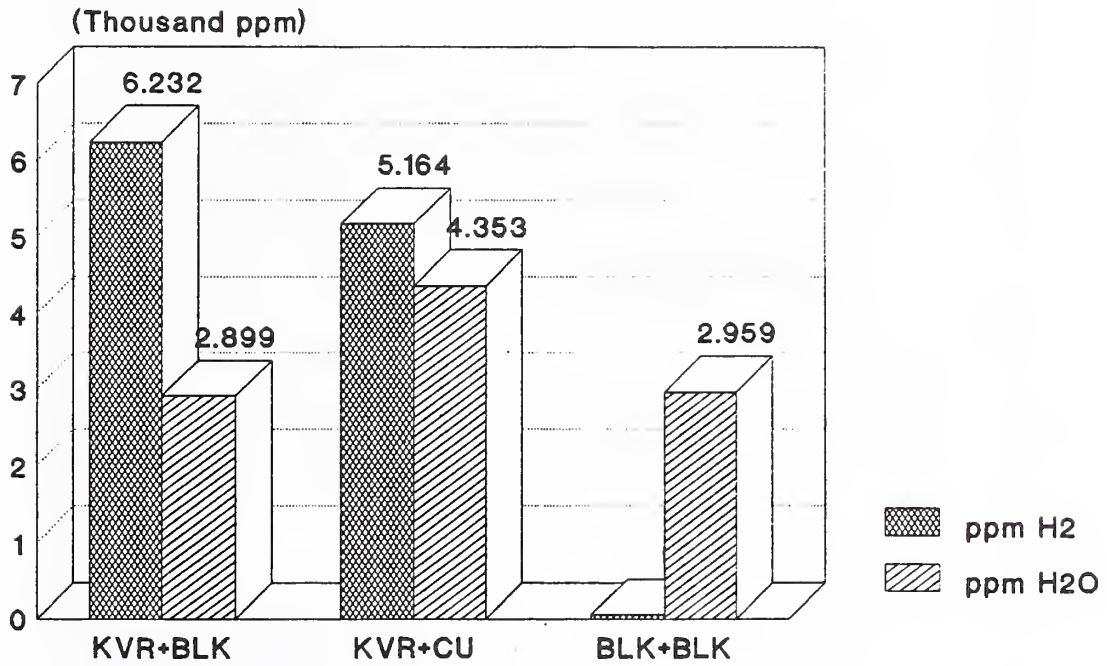
COUPON THICKNESS 150C/200HR



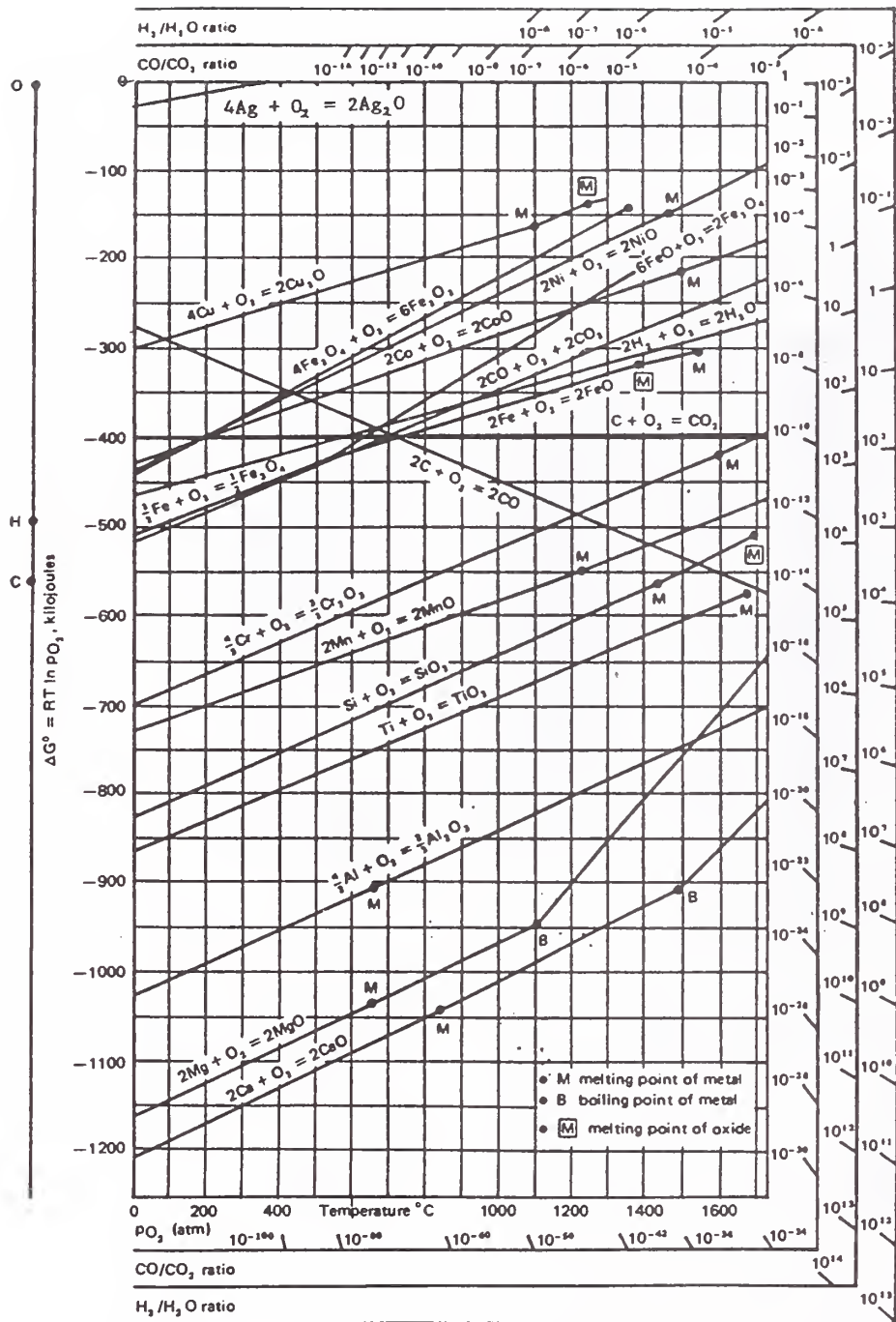
KOVAR MICROSTRUCTURES, 320x



Cu OXIDE REDUCTION STUDY by Kovar Hydrogen Outgassing



KVR - Kovar Coupon
BLK - Blank Coupon
CU - Oxidized Cu Coupon



The Ellingham diagram for metallurgically important oxides.

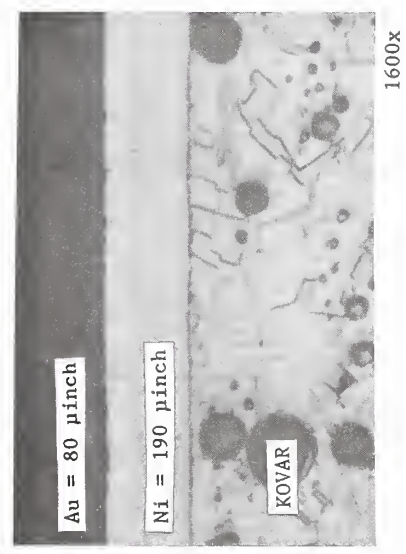
Gaskell, D.R. "Introduction to Metallurgical Thermodynamics" Hemisphere Publishing, NY 1981 2nd Edition.

AES PROFILE
 5.00KV, .000UA
 FILE: 200CS

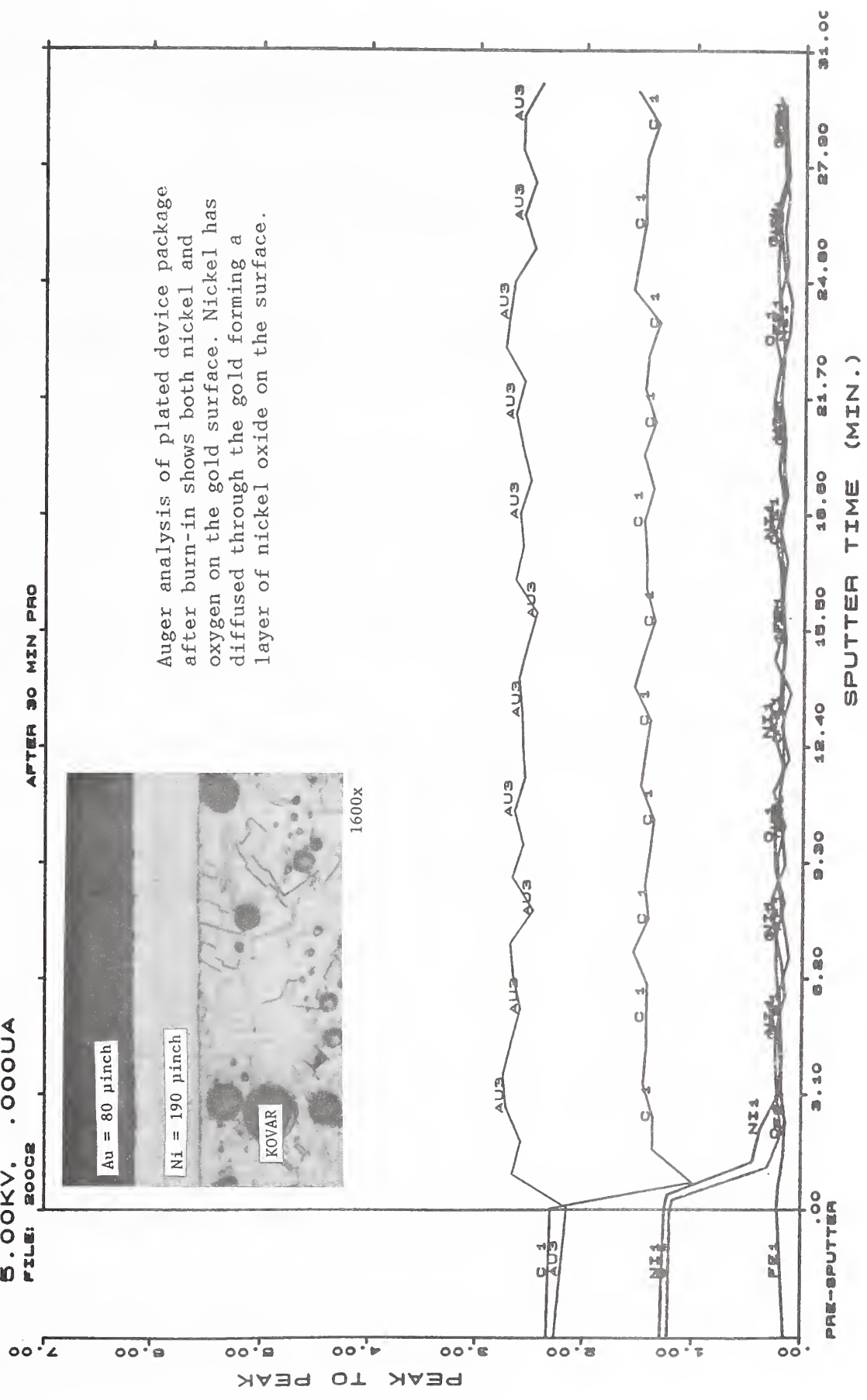
XR= 1.5, YR= 1.5
 CND= 450

07/26/91
 5.0KV, 2.500MA

AFTER 30 MIN PRO



Auger analysis of plated device package after burn-in shows both nickel and oxygen on the gold surface. Nickel has diffused through the gold forming a layer of nickel oxide on the surface.



DATA MATRIX OF PREPARED KOVAR COUPONS
HYDROGEN DESORPTION AT 150°C

DATA IN % H₂ CC/G BY VOLUME

ND = NONE DETECTED; <0.02% H₂

<u>CONDITION</u>	<u>HOURS</u>	<u>KOVAR COUPON LOTS</u>			
		<u>60 MIL</u>		<u>40 MIL</u>	<u>10 MIL</u>
		<u>510</u>	<u>120</u>	<u>905</u>	<u>144</u>
VIRGIN STOCK	0	2.12	1.64	0.56	ND
HYDROGEN BRAZE	200	2.61	2.65	1.71	ND
	400	0.04	-	-	ND
HYDROGEN ANNEAL	200	0.76	0.74	0.65	ND
	400	-	ND	-	ND
WET H ₂ GLASS SEAL	200	0.25	0.26	0.20	ND
HYDROGEN BAKE OUT	200	ND	ND	ND	ND
	400	ND	ND	-	-
SUPPLIER A Au/Ni PLATE	200	0.06	ND	ND	ND
	400	0.03	0.07	-	0.09
	600	0.09	-	-	-
SUPPLIER B Au/Ni PLATE	200	0.06	0.07	ND	ND
	400	0.13	0.29	-	ND
	600	-	0.16	-	-
SUPPLIER A PROCESS	200	ND	ND	-	0.22
SUPPLIER B PROCESS	200	ND	0.02	-	0.21
<hr/>					
H ₂ FREE STOCK	0	ND	ND	-	ND
SUPPLIER A PROCESS	200	0.04	ND	-	-
SUPPLIER B PROCESS	200	0.10	0.05	-	-

LITERATURE REFERENCE

Y. DAPING AND C. WENXIU, "INVESTIGATION OF TRAPPED HYDROGEN IN 18 Ni MARAGING STEEL BY USING THERMAL HYDROGEN EVOLUTION TECHNIQUE," INSTITUTE OF METAL RESEARCH, ACADEMIA SINICA, SHENYANG, 1987.

W. E. SWARTZ JR. AND J. H. LINN, "AN X-RAY PHOTOELECTRON SPECTROSCOPY STUDY OF THE DIFFUSION OF IRON, NICKEL AND COBALT THROUGH GOLD FILMS," THIN SOLID FILMS, 114 (1984).

T. RAMSEY AND G. HEINEN, "CONTROLLING MOISTURE IN CERAMIC PACKAGES," SEMICONDUCTOR INTERNATIONAL, AUGUST 1988.

A. TURNBULL, M. W. CARROLL AND D. H. FERRISS, "ANALYSIS OF HYDROGEN DIFFUSION AND TRAPPING IN A 13% CHROMIUM MARTENSITIC STAINLESS STEEL," ACTA METALL. 37, 2039 (1989).

R. SONG AND S. PYUN, "HYDROGEN PERMEATION THROUGH A BILAYER OF FE/ELECTRODEPOSITED Ni," J. ELECTROCHEM SOC, 137, 1051 (1990).

T. M. HARRIS AND R. M. LATANISION, "GRAIN BOUNDARY DIFFUSION OF HYDROGEN IN NICKEL," METALL TRANS A, 22A, 351, FEBRUARY 1991.

S. LINDEROTH, "HYDROGEN DIFFUSIVITY IN ALUMINUM," PHILOSOPHICAL MAGAZINE LETTERS, 57, 229, (1988).

P. SCHUESSLER AND D. FELICIANO-WELPE, "THE EFFECTS OF HYDROGEN ON DEVICE RELIABILITY," HYBRID CIRCUIT TECHNOLOGY, JANUARY 1991.

K. SATO, ET AL, "INVESTIGATION OF SHORT CIRCUIT CAUSED BY REDUCTION OF PbO SEALING GLASS USED FOR VLSI PACKAGE," HITACHI VLSI ENGINEERING CORP.

W. O. CAMP, ET AL, "HYDROGEN EFFECTS ON RELIABILITY OF GaAs MMIC'S," GaAs-IC SYMPOSIUM TECHNICAL DIGEST, 1989.

Session II

Moisture Effects

Degreaser Fluid Induced Electrical Assembly Corrosion; Failure Analysis of a Moisture Limited Mechanism

**David O. Ross
Rome Laboratory
525 Brooks Road, ERDR
Griffiss AFB, NY 13441-4505**

1.0 ABSTRACT

This paper describes the analysis of a major electronic system's corrosion problem. The corrosion source was traced to the cleaning system utilized by the OEM (Original Equipment Manufacturer). The failure analysis was complicated by many factors, including the delayed onset of corrosion imposed by the moisture dependent breakdown of the cleaning solvent that created the corrosive catalyst.

2.0 BACKGROUND AND INTRODUCTION

This failure analysis was initiated at Rome Laboratory for a Program Management Office (PMO) to identify the cause of the severe corrosion experienced by specific units deployed in West Germany. Since the corroded assemblies had previously been repaired, the PMO and the original equipment manufacturer (OEM) sent identical assemblies that had been exposed to a similar West German environment. Additional assemblies were supplied which had only been exposed to the dry environment of Fort Bliss (El Paso), Texas, as well as some assemblies which came directly from the OEM's facility.

The initial visual inspections yielded surprising results, which quickly led to redirection of the effort. All assemblies were corroded, including those from Fort Bliss and the OEM. This widespread corrosion was particularly disturbing due to the planned deployment of this system in Operation Desert Shield near the highly corrosive (salt atmosphere, high humidity, and high ambient temperature) coastal areas of the Persian Gulf.

3.0 SAMPLE DESCRIPTION

Assemblies R1 through R4 were from the Radar Set, while all others were from the Engagement Control Station (ECS). Assemblies W1 through W3 and R1 through R4 had experienced the West German environment, assemblies T1 through T3 were from the dry Fort Bliss, Texas environment, while assemblies M1 and M2 were from the OEM

environment (see Table 1). All West German assemblies had also experienced the Fort Bliss environment for some undefined period of time. These assemblies were from the electronics box first exposed to the incoming (external environment) cooling-air for their shelter (ECS or radar). No other electronics boxes in those shelters were experiencing corrosion problems. The Radar Set, which had a lower cooling-air flow rate, also had a significantly weaker corrosion problem.

4.0 RESULTS AND DISCUSSION

4.1 CONFORMAL COATING BREAKDOWN

4.1.1 ULTRAVIOLET LIGHT ANALYSIS

Two West German environment assemblies (W2 and W3) were examined under ultraviolet (UV) light to evaluate the conformal coating's coverage and condition. The UV dye in the conformal coating of W2 was inexplicably destroyed in areas where the conformal coating appeared intact, while the conformal coating and UV dye on W3 were normal. See Figure 1. In the following process review, the OEM process personnel stated that the phenomenon was caused by cleaning a conformally coated assembly with 1,1,1-trichloroethane (also known as TCA or methylchloroform).

4.1.2 ABRASIVE DAMAGE

Noting that an air flow rate correlation, abundant particulates, and damaged conformal coating were all present on the assemblies, a conformal coating abrasion mechanism was investigated. A Scanning Electron Microscope (SEM) investigation found no abrasive damage.

4.1.3 CORRELATION WITH CORROSION

The conformal coating on all assemblies was breaking down in a similar pattern to the general corrosion pattern described in 4.2.1, below. See Figure 2. Although the corrosion and conformal coating breakdown most often occurred together, one would be found occasionally in the absence of the other. See Figures 3 and 4. This evidence lead to the hypothesis that neither corrosion nor breakdown caused the other to occur, but might instead have a related cause.

4.2 GENERAL CORROSION DISTRIBUTION

4.2.1 CORROSION LOCATIONS

The corrosion on all sample assemblies was greatest on the metal closest to the cooling-air inlet, with the corrosion decreasing with increasing distance from the inlet. Starting abruptly and intensively about 1.5 cm above the connector, the corrosion decreased with increasing distance from the connector. This variation along the inlet edge would be consistent with air flow rate since the

air duct design produces a higher flow rate nearer the connector (the air flow path parallels the card edge, and then makes a right angle turn at that point). This distribution indicates that something is being scavenged from the inlet air flow that is related to the general corrosion. It was noted that the ECS and Radar Set both used a convection cooling method, common in commercial electronics and manpacked military electronics, but unusual for other military systems. Most non-manpacked military electronics use conduction cooling methods, so that external air does not contact the electronics.

An air flow rate correlation is also evident with the reduced corrosion of R2 and R3 from the Radar Set. Assemblies W2, and W3 from the ECS both showed substantially heavier corrosion than R2 and R3, and yet were approximately the same ages as and from the same general environment as R2 and R3. See Table 1.

4.2.2 PART SUSCEPTIBILITY

Three specific part types were noted as being particularly prone to corrosion. The first type was resistor packs with gold plated leads that were not fully pre-tinned. See Figure 5. Gold plated leads that have not been fully pre-tinned are normally very sensitive to corrosion [1-10], so this was no surprise. The second "part" type consisted of inductors assembled from copper wire inserted through hollow ferrite cylinders. The gap between the copper wire and the ferrite developed a green halo of corrosion product. See Figure 6. The third part type was a hybrid, which was corroding at the weld line and at lid bends. See Figure 7.

4.2.3 MOISTURE SENSITIVITY

When two assemblies (T2 and T3), with the same part number (11437158) and same environment (Fort Bliss), had significantly different levels of corrosion, a direct correlation was established between water in the incoming air and the general corrosion levels. The OLDER board (T2) had a significantly higher level of particulates, and a significantly LOWER level of corrosion. See Figures 8 and 9. The PMO stated that the only identifiable historical difference between these two assemblies was the failure of a refrigeration condensation drain line on the younger assembly's shelter (T3). The drain line had dripped water into the shelter's incoming cooling-air for an undetermined period of time prior to the removal of the subject assembly. The gross differences in corrosion levels between the two assemblies (which normally would be minor and reversed in magnitude) force the conclusion that water must be a major corrosion contributor.

4.3 CORROSIVE SOURCES

4.3.1 SCANNING ELECTRON MICROSCOPE ANALYSIS

SEM-EDX (Energy Dispersive X-ray) examination of the active corrosion zones found only one anomaly, chlorine. See Figures 10 and 11. Finding the source of this chlorine could lead to finding a cure for the corrosion problem. Since swimming pools or other common sources were not normally located near this equipment, chlorine gas was ruled out as a source of chlorine. Some other element(s) had to be associated with the chlorine source; for example, alkali or alkaline earth metals (whose chlorides are common sources of chlorine contamination) were not detected with the chlorine in the active corrosion zones. The only elements detected were: the metals being corroded, chlorine, and the gold sputter coat. Elements not normally detectable by SEM-EDX were those with atomic numbers lower than neon. By eliminating lithium, beryllium, boron, and fluorine as extremely unlikely, only hydrogen, carbon, nitrogen, and oxygen remained. Some form of an organic chloride was therefore assumed as the source of the chlorine. The presence of bubbles in several corrosion zones with strong chlorine peaks also indicated that the chlorine source or its by-products might be volatile. See Figures 12 and 13.

4.3.2 HUNTING THE CHLORINE SOURCE

The fluxes used by the OEM had both chlorine and bromine [11], but bromine was never found in an active corrosion zone. Therefore, flux residue was eliminated as a potential source of the general corrosion problem.

The two common organics of the assemblies, the circuit board matrix (epoxy) and the conformal coating (polyurethane) were investigated as potential sources of the chlorine. Although occasional traces of chlorine were found in them, these organics could not account for the levels of chlorine observed.

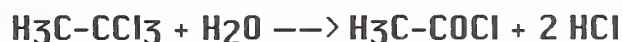
One major organic in the production process remained to be investigated. It was an organic chloride that formed a major component of the cleaning solvent, but was followed by a water wash and a bakeout prior to the conformal coating operation. However, some assemblies would encounter the organic chloride (1,1,1-trichloroethane) after the conformal coating operation as evidenced by assembly W2 during its UV exam, and the awareness of the OEM production line personnel of the UV dye phenomenon (see 4.1.1).

A literature search found that the "pH insensitive" reaction rate (half-life) for the hydrolysis of trichloroethane (TCA) was

approximately a year at room temperature [12] (with a variance of a factor of two, depending on the researcher and test conditions). Using the common, but potentially hazardous assumption of a doubled reaction rate for every 10°C rise, an assembly operating at 55°C would accelerate the TCA half-life to about six weeks. This hydrolysis reaction rate was slow enough to be missed by the OEMs standard board cleanliness test, yet clearly fast enough to cause the corrosion problem. See Table I. Further literature searches noted that the TCA hydrolysis reaction could be catalyzed by iron, and other metals. The catalysis of TCA hydrolysis at an iron surface would explain the high level of chlorine on the surface of the component leads and in the bubbles located on the lead surfaces. See Figures 12 and 13. The inductor corrosion may also be attributable to this mechanism, depending on the porosity of the iron bearing ferrite.

4.3.3 HYDROLYSIS REACTION OF TCA

The hydrolysis reaction of TCA requires initially one water molecule for each TCA molecule (H₃C-CCl₃) consumed, and produces a molecule of acetyl chloride (H₃C-COCl) and two molecules of hydrochloric acid (HCl). This is the only slow reaction discussed in this paper, all other reactions discussed here are extremely rapid, if provided with sufficient water.



The acetyl chloride molecule is extremely reactive, and in the presence of excess water, reacts with a second water molecule to create a molecule of acetic acid (H₃C-CO₂H) and a third molecule of hydrochloric acid.



The hydrochloric acid, being a strong acid, would dissociate immediately in the presence of water into the hydrated hydrogen and chloride ions. Therefore both ions would need to compete for water molecules before they could start their destruction.



Thus for every molecule of TCA hydrolyzed, two water molecules would be consumed and one molecule of acetic acid and three molecules of hydrochloric acid would be produced.



However, without excess water, the corrosive effects of the hydrochloric acid would be extremely limited, and the acetyl chloride would attack the available unsaturated organics (the UU dye), and carbonyl organics (the polyurethane conformal coating), rather than form acetic acid. The acetyl chloride attack on other, less electron-rich organics (the epoxy resin system) is less likely.

It is evident that the competition for water in the corrosion zone would be extreme, if the source of water was at all restricted. Without water, all of these reactions would stop. Other than the TCA decomposition reactions, these reactions are catalytic but consume water, so in the presence of a steady source of water (the inlet air), a little TCA would cause significant amounts of damage [13].

At this point, the evidence starts to gel. First is the sensitivity of the general corrosion reaction to a water source (inlet air). Second is the acidic nature of the conformal coat reported by the OEM [14]. Third is that the ECS shelter exhaust had a 30 times higher acidity ($\Delta 1.5$ pH) as compared to the system's diesel engine exhaust pipe (where the acidic gases CO_2 , NO , NO_2 , and SO_2 are expected) [11]. Fourth is the breakdown of the conformal coating in the same general pattern as the corrosion.

4.3.4 MASS SPECTROMETER ANALYSIS

The mass spectrometer analysis used circuit boards that had passed through the OEM's production cleaning process, but were not conformal coated. After aging for six weeks at Rome Laboratory at room temperature (20°C nominal), the surface epoxy layer (butter coat) was removed and analyzed on a quadrupole mass spectrometer (QMS) optimized for residual gas analysis. The results clearly showed chloride ion (peaks 35 and 37 in a 3:1 ratio that matches the natural isotope ratio of chlorine), and hydrochloric acid (peaks 36 and 38 in the same 3:1 ratio). See Figure 14. The hydrochloric acid was generated by the catalytic decomposition of the TCA present in the sample by the stainless steel sample holders (iron catalysis). The results of the QMS analysis showed the presence of TCA in both the conformal coating and circuit board materials.

4.4 OUTSIDE LABORATORY ANALYSIS

4.4.1 IONIC ANALYSIS

The OEM requested that an outside laboratory (OL) analyze the ionic contamination levels of the OEM's as-cleaned circuit boards,

polyimide as-cleaned boards, and cleaned circuit boards after 10-12 weeks storage (one sample was stored in plastic wrapping and the other sample was wrapped in a paper towel). The test method used was from Method 5011 of MIL-STD-883 for determining the ionic contamination of organic adhesives. The results showed that the polyimide boards had no detectable chloride, while the paper stored board had a very high chloride content (144 ppm average). The remaining boards (including the one stored in plastic) had lower levels of chloride (20-77 ppm average).

4.4.2 MASS SPECTRAL ANALYSIS

The OEM also tasked the OL to determine the presence or absence of TCA in the same samples. A solids probe mass spectrometer was used for this analysis. The polyimide boards, and the paper towel stored board (with a high chloride content) showed no sign of TCA. The remaining boards all showed substantial quantities of TCA.

At the suggestion of Rome Laboratory, the OL ran a quantitative analysis for TCA content using a gas chromatography/ mass spectrometer (GC/MS) combination. The quantitative analysis results ranged from 611 ppm (0.06%) to 2940 ppm (0.3%) for the as-cleaned epoxy boards. These numbers are crude (since the calibration only ranged over 20-200 ppm, so most values are excessively extrapolated), but do provide a relative distribution of the TCA concentrations. The paper stored board with high chloride content showed 107 ppm TCA, while the plastic stored board showed 1210 ppm (0.1%) TCA. The polyimide boards had no detectable TCA.

From these results it appeared that the epoxy-glass boards preferentially retain TCA, which was consistent with Rome Laboratory analysis and supportive of Rome Laboratory conclusions. Driving off the TCA at 75°C for 40 minutes removed less than 4% of the measured TCA. The paper stored board apparently hydrolyzed its TCA and formed hydrochloric acid. The plastic storage of the other board appears to have sufficiently restricted that boards access to the water required for the hydrolysis reaction. It is interesting that polyimide boards (of the type used in this analysis) did not retain TCA in detectable quantities.

5.0 CONCLUSIONS

Corrosion was found on all examined assemblies. Examination of Fort Bliss, Texas assemblies highlighted a very strong correlation between corrosion and available moisture. Examination of active corrosion zones revealed the consistent presence of chlorine in

significant quantities. No extraneous metals were found in the presence of the chlorine, indicating that the chlorine source was an organic chloride. Flux residue was eliminated as a possible source of the corrosive chlorine since bromine was not found in active corrosion zones.

The cause of the general corrosion was found to be the hydrolysis reaction of the assembly cleaning solvent (1,1,1-trichloroethane), which generates both hydrochloric acid and acetyl chloride. Trichloroethane is known to have a half life in the presence of atmospheric water at room temperature of about one year. At an assembly operating temperature of 55°C, the half life should accelerate to about six weeks. This reaction would provide the quantities of chlorine found, in the locations where it was found. Mass spectra (QMS and GC/MS) analysis of conformal coating and circuit boards detected trichloroethane, and hydrochloric acid. Trichloroethane was positively identified in large quantities (0.3%) in as-cleaned assemblies, and lengthy bakeouts were shown to be ineffective in removing the solvent.

6.0 RECOMMENDED CORRECTIVE ACTIONS:

Long term:

- 1) Delete the use of 1,1,1-trichloroethane in all processes, or
- 2) Implement the use of polyimide circuit boards.

Short term:

1) Delete the use of 1,1,1-trichloroethane in the rework process.

- 2) Fully pretin all parts, and seal the inductor gaps.

Fielded units (during maintenance):

- 1) Inspect all incoming assemblies for corrosion.
- 2) When corrosion is found, strip off all possible conformal coat and reapply without using 1,1,1-trichloroethane.

Fielded units (field units, ASAP):

Reduce or eliminate the introduction of water into the electronics areas. Both the hydrolysis reaction, and subsequent corrosion reactions consume water. Use molecular sieves, dehumidifiers, refrigeration units, a combination, or any other reasonable process that would reduce moisture levels.

7.0 ACKNOWLEDGMENTS

The author wishes to acknowledge the active participation, assistance, and support of the following Rome Laboratory team members in the conduct of this analysis: Kim Berry, Don Calabrese, Edgar Doyle, Ivars Irbe, Ben Moore, and Patricia Speicher.

8.0 REFERENCES

1. K. Berry, "Corrosion Resistance of Military Microelectronic Packages at the Lead-Glass Interface", *Electronic Packaging and Corrosion in Microelectronics, Proceedings of ASM's Third Conference on Electronic Packaging: Materials and Processes and Corrosion in Microelectronics*, Minneapolis MN, pp. 55 - 61 (1987)
2. A. J. Raffalovich, "Corrosive Effects of Solder Flux on Printed Circuit Boards", *IEEE Transactions on Parts, Hybrids, and Packaging*, PHP-7 (4), pp. 155 - 162 (1971)
3. L. Zakraysek, "Microelectronic Component Lead Finishes", *Plating and Surface Finishing*, 68(9), pp. 72 - 76 (1981)
4. K. W. Rosengarth, Jr., "Corrosion Protection for Semiconductor Packaging", *Solid State Technology*, 27, pp. 191 - 196 (1984)
5. M. J. Elkind and H. E. Hughes, "Prevention of Stress-Corrosion Failure in Iron-Nickel-Cobalt Alloy Semiconductor Device Leads", *Physics of Failure Symposium Proceedings*, 5, pp. 478 - 495 (1966)
6. R. R. Sheppard, "Semiconductor Lead Corrosion Problems", Document Number H9-F-82-01, L. B. Johnson Space Center/H9 (January 1982)
7. J. D. Shea, "Circuit Malfunction Analysis", Document Number C2-F-78-42, *Integrated Circuit Engineering*, Santa Clara, CA (August 1977)
8. L. J. Welrick, "A Metallurgical Analysis of Stress-Corrosion Cracking of Kovar Package Leads," *Solid State Technology*, pp. 25 - 30 (March 1975)
9. B. Reich, "Stress Corrosion Cracking of Gold Plated Kovar Transistor Leads," *Solid State Technology*, pp. 36 - 38 (April 1969)
10. S. C. Kolesar, "Principles of Corrosion," *Proceedings of the 12th Annual Symposium on Reliability Physics*, pp. 155 - 159 (1974)
11. D. M. Fradette to U. O. Chance, "Minutes of Netherlands Corrosion Meeting, 13, 14 December 1989", OEM Document DMF:bb:7663:SD:89:6701, dated 19 December 1989
12. P. M. Jeffers, L. M. Ward, L. M. Woytowitch, and N. L. Wolfe, "Homogeneous Hydrolysis Rates for Selected Chlorinated Methanes, Ethanes, Ethenes, and Propanes," *Environmental Science and Technology*, 23 (8), pp. 965-969 (August 1989).
13. Kirk-Othmer, *Encyclopedia of Chemical Technology*, 3rd Edition, 5, Wiley - Interscience (1978)
14. Private communications, D. O. Ross with T. Chin, OEM.
15. *Electronic Materials Handbook*, 1, ASM INTERNATIONAL (1989).

Table I

Sample Descriptions

<u>ID</u>	<u>Mfr.</u>	<u>Field Location</u>	<u>Shelter</u>	<u>≈ Service Time</u>	<u>Failure Report</u>
M1	OEM	OEM	ECS	10 years	*
M2	OEM	OEM	ECS	9.5 years	**
T1	OEM	Ft. Bliss, Texas	ECS	8 years	"Broken Lead"
T2	OEM	Ft. Bliss, Texas	ECS	6.5 years	"Broken"
T3	OEM	Ft. Bliss, Texas	ECS	5 years	"Inoperative"
W1	OEM	West Germany	ECS	7.5 years	Not Available
W2	OEM	West Germany	ECS	4 years	Not Available
W3	2nd	West Germany	ECS	2.5 years	Not Available
R1	OEM	West Germany	Radar	3 years	Not Available
R2	OEM	West Germany	Radar	3 years	Not Available
R3	OEM	West Germany	Radar	3 years	Not Available
R4	2nd	West Germany	Radar	2.5 years	Not Available

Mfr. = Manufacturer

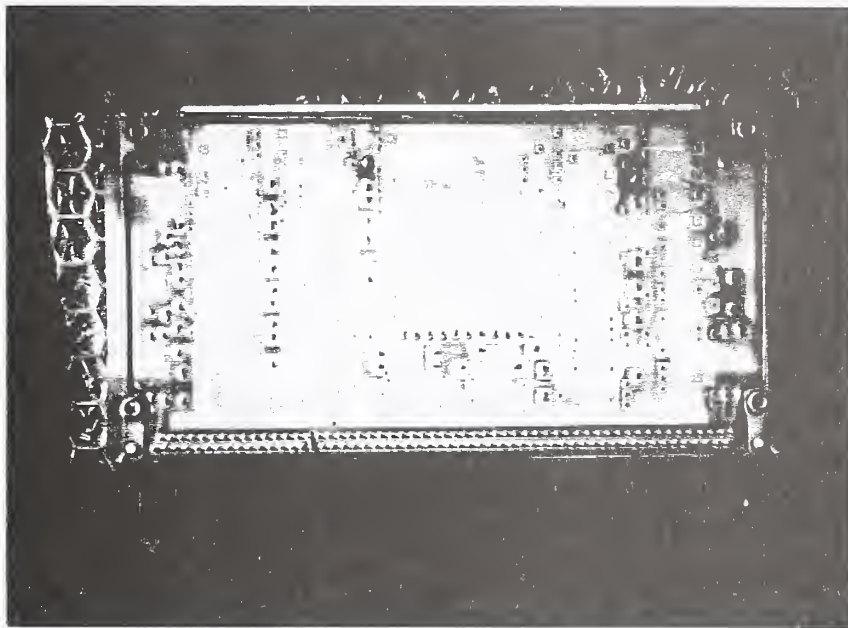
ECS = Engagement Control Station

OEM = Original Equipment Manufacturer

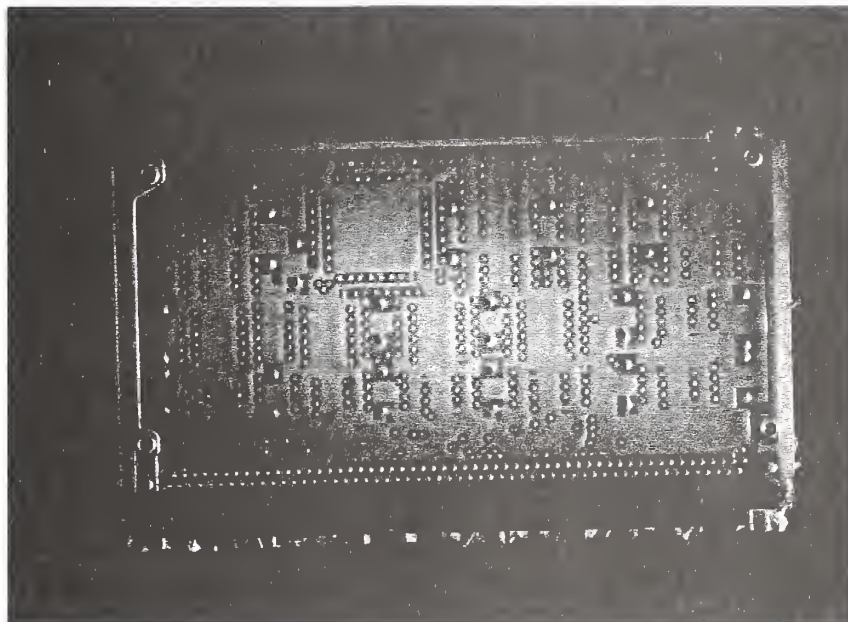
2nd = Second Source

* = "P&S Outdata Light On"

** = "Y Character Positioning Off"



a. (W2) Dark areas around vias indicate UV dye degradation.



b. (W3) No UV dye degradation; conformal coating in good condition.

Figure 1. (W2 and W3) Optical photographs of the solder side of the assemblies in ultraviolet (UV) light. 0.5X

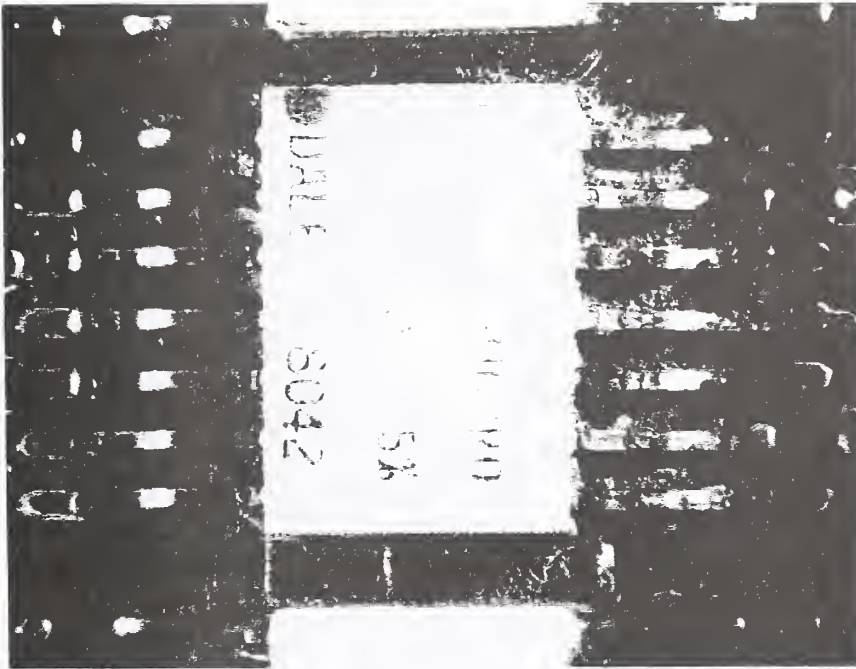


a. Low magnification view. 6X

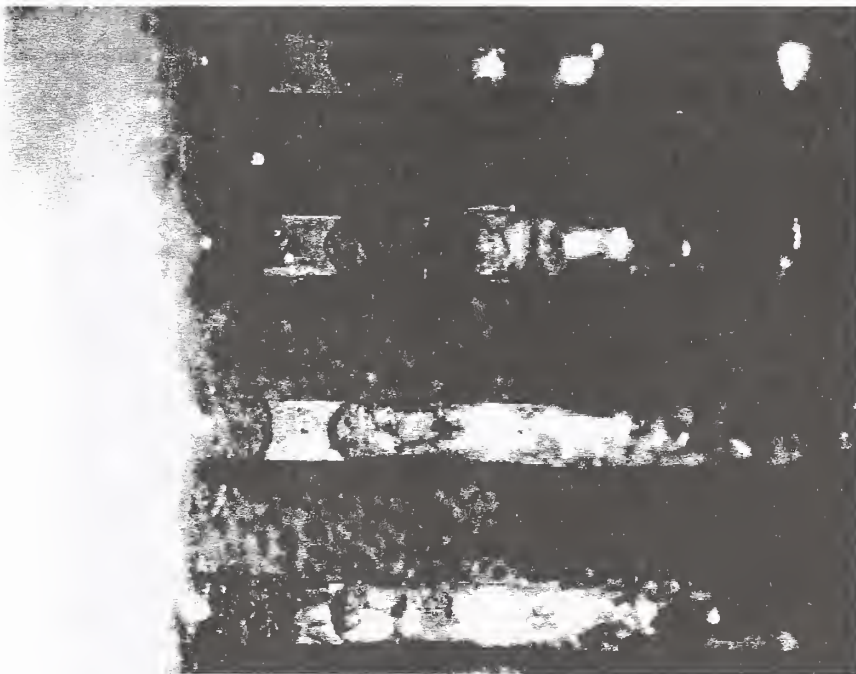


b. Magnified view of the area in the upper right corner of (a). 18X

Figure 2. (M1) Peeling conformal coating and corrosion on circuit traces, vias, flatpack leads, and an inductor near the inlet.

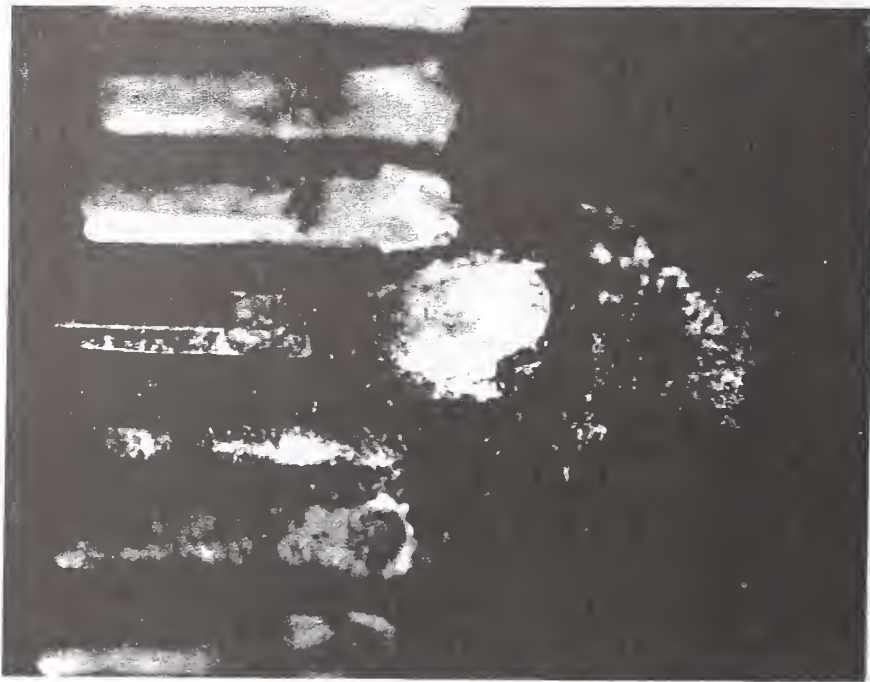


a. Overall view. 6X

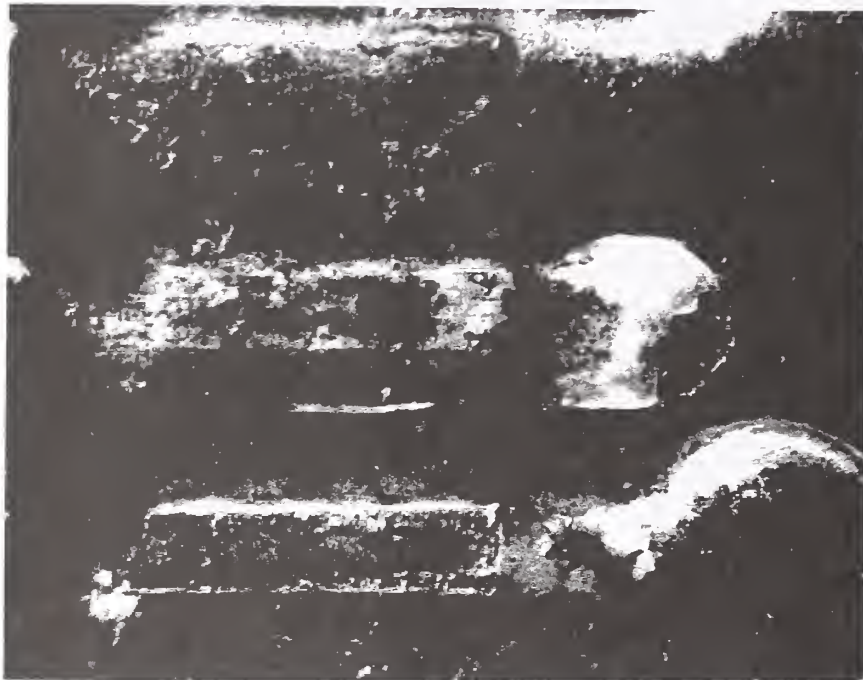


b. Magnified view of leads on the inlet side. 18X

Figure 3. (M1) Corrosion concentrated on the inlet side of a Dale resistor pack, with no apparent conformal coating breakdown. Note exposed gold plating on pre-tinned leads.

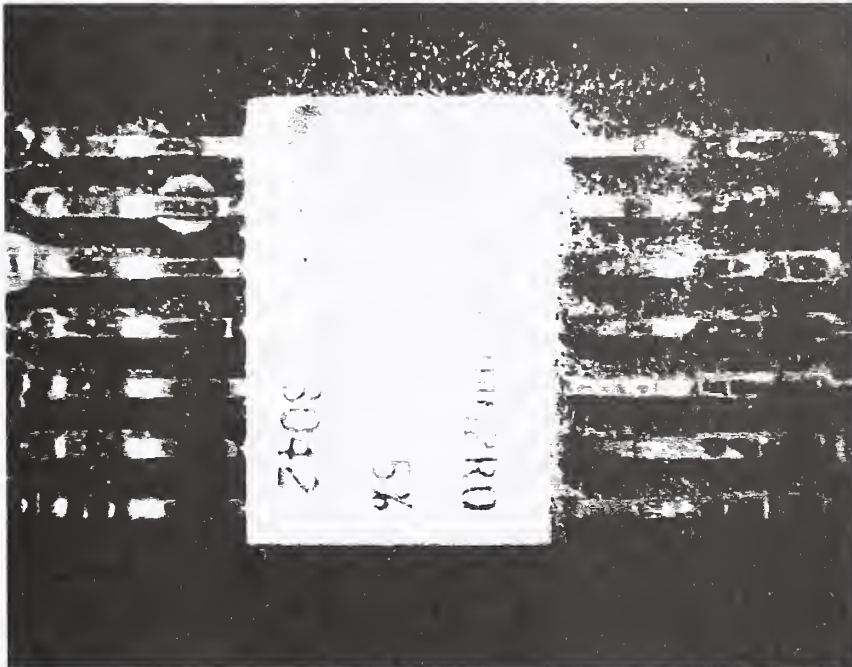


a. Copper corrosion products under lifted conformal coating. 15X



b. Peeling conformal coating only. 25X

Figure 4. (T3) Peeling conformal coating on vias, with and without corrosion.



a. Overall view. 6X



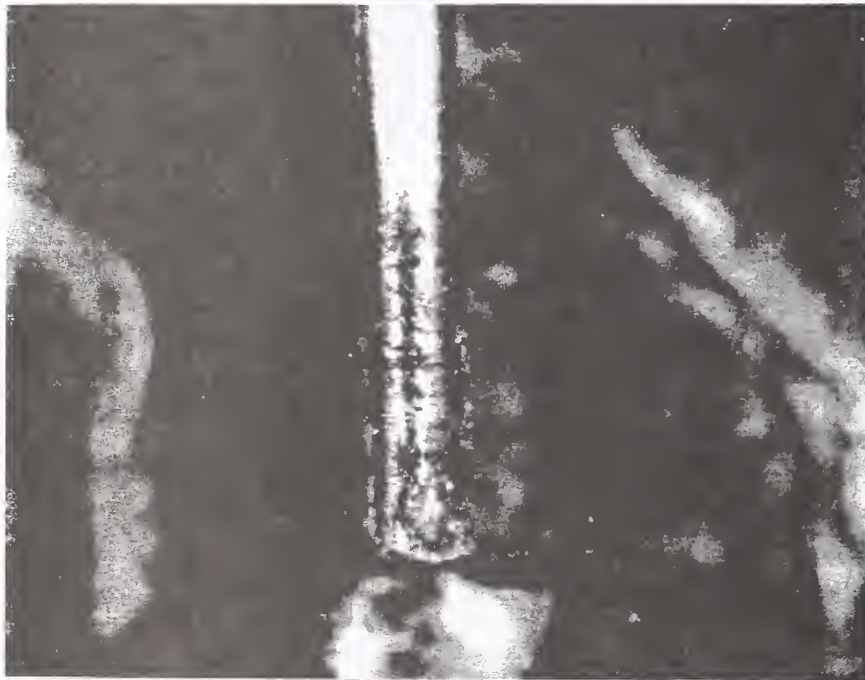
b. Magnified view of leads on the inlet side. 18X

Figure 5. (M1) Corrosion concentrated on the inlet side of a Dale resistor pack.

Figure 6. (T3, M1, W1) Inductor
lead corrosion (green corrosion
product, usually containing
chloride) concentrated at the
inductor/lead interface.



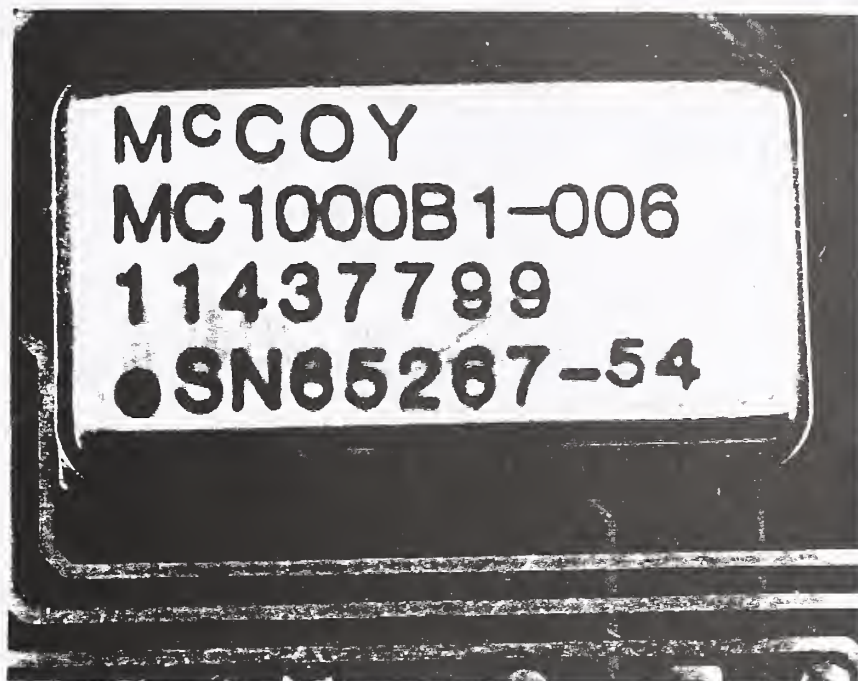
a. (T3) 25X



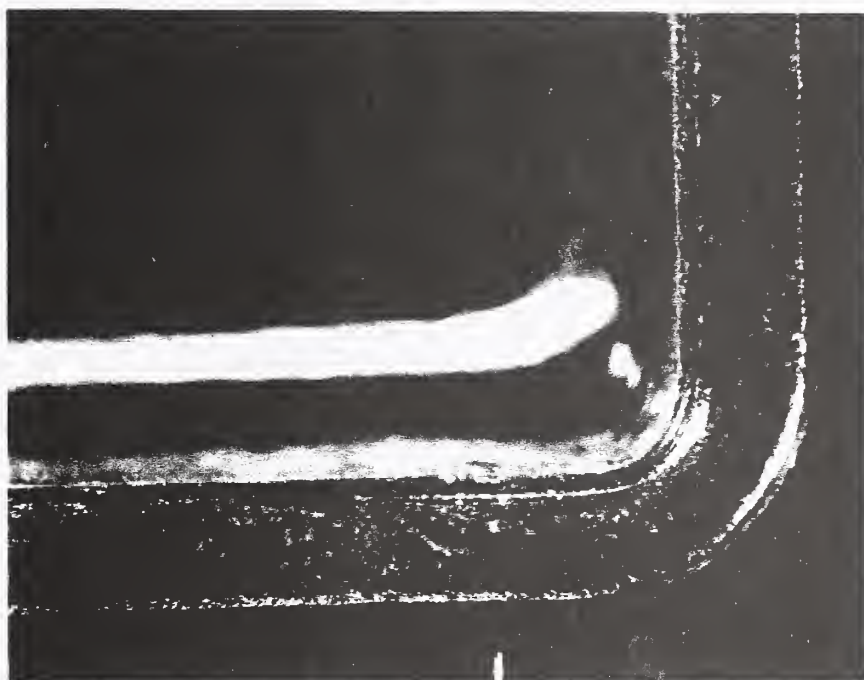
b. (M1) Note also the brown
corrosion products (usually
a copper oxide).



c. (W1) 12X

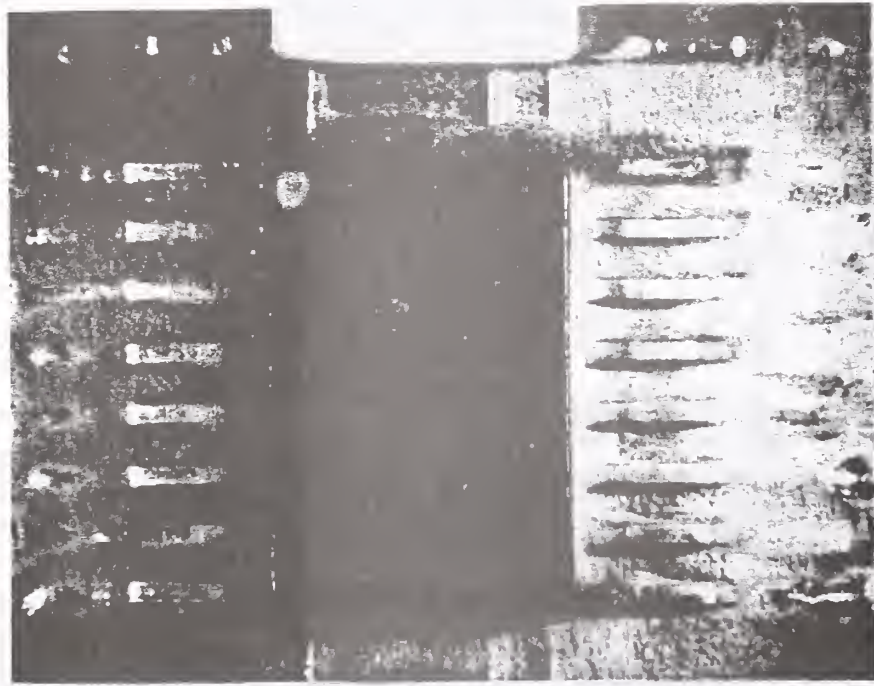


a. Overall view. 4X



b. Magnified view of the flange area. 18X

Figure 7. (T3) Corrosion on the metal can flange.



a. Overall view. 6X



b. Magnified view of leads on the inlet side, showing minor corrosion at lead edges. The onset of conformal coating breakdown at lead edges was also observed (see arrows). Compare with Figure 9. 25X

Figure 8. (T2) Sand deposits and corrosion concentrated on the inlet side of the device nearest the inlet (worst-case corrosion on T2).

Figure 9. (T3) Corrosion and peeling conformal coating concentrated on the inlet side of the device nearest the inlet (worst-case corrosion on T3). This is the same part location as shown in Figure 8.

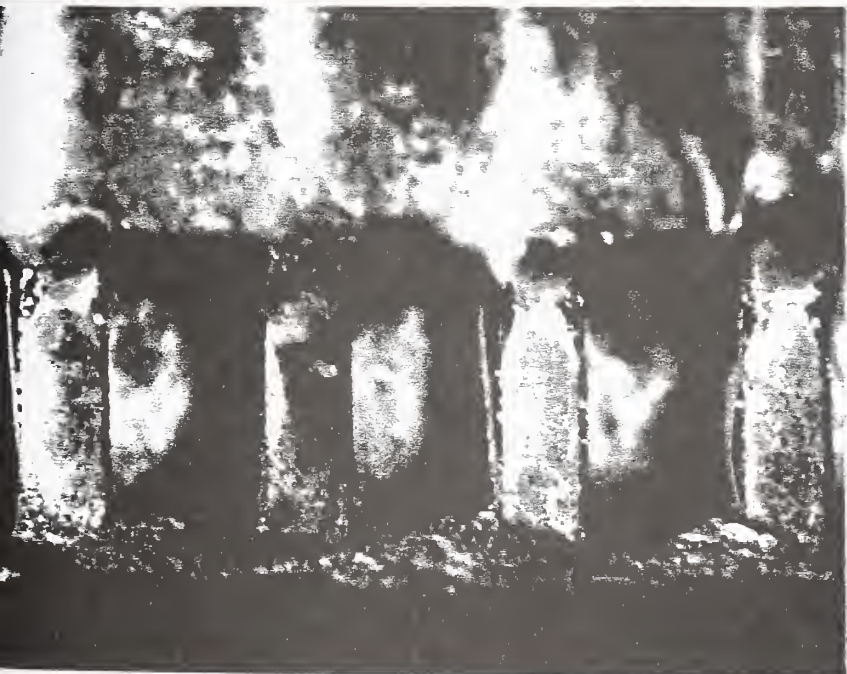


JM38510/
014038FA
USA 07263
AF 8507

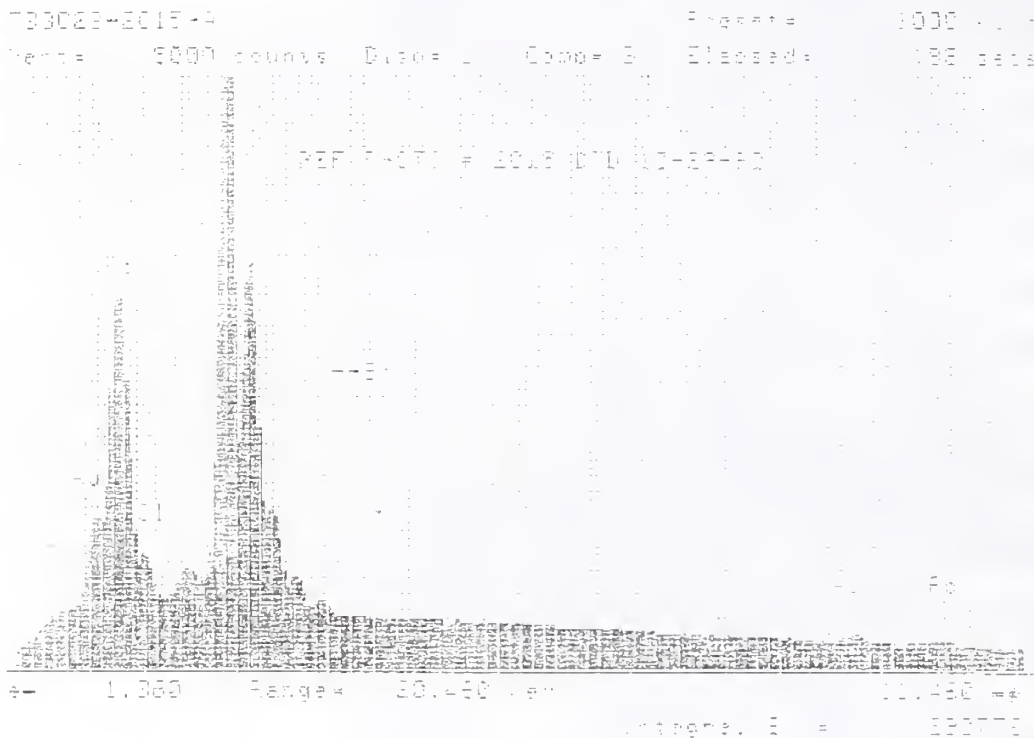
a. Overall view. 6X



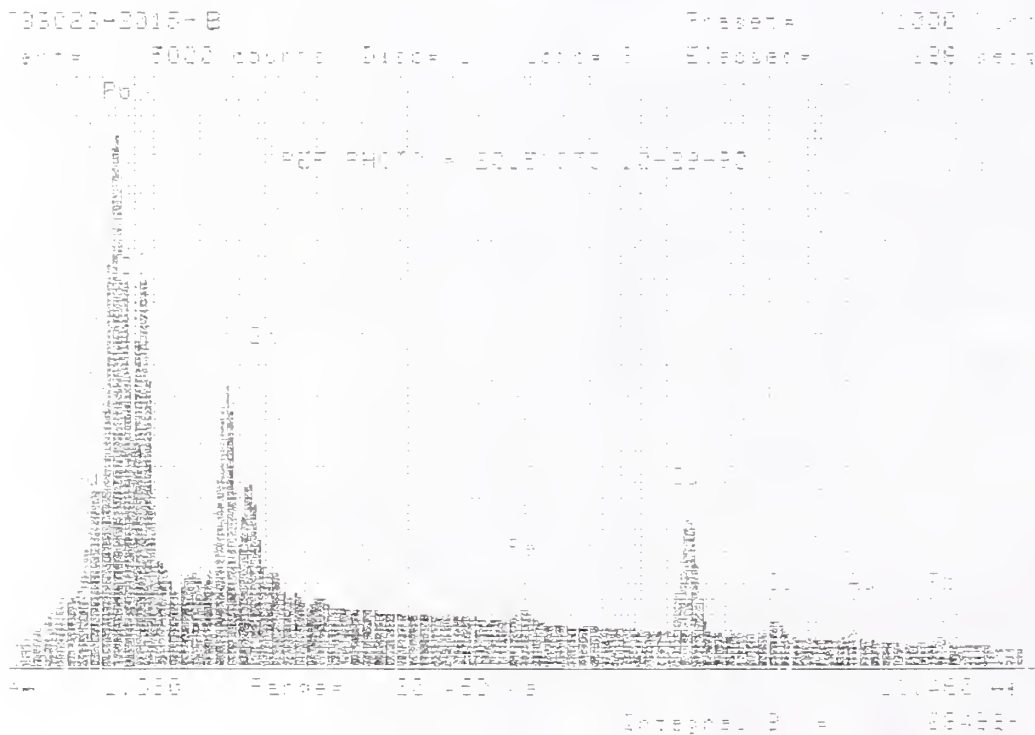
b. End view of leads on the inlet side. 17X



c. Top view of the leads in (b). Compare with Figure 8. 25X

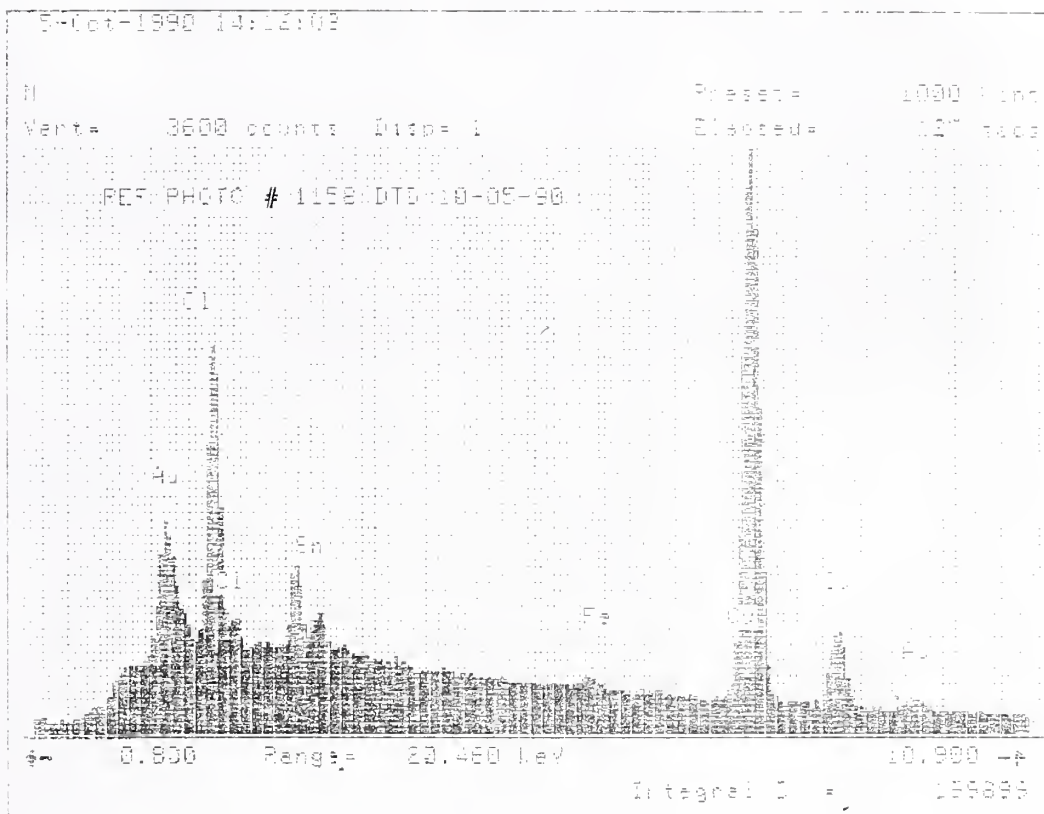


a. Center of via, showing tin and tin lead oxides with a small (catalytic) amount of chlorine.



b. Outer area of corrosion. Note the strong presence of chlorine, as well as the presence of lead, tin, and copper.

Figure 10. (W3); continued. Note that chlorine is the only element not accounted for in the via construction.

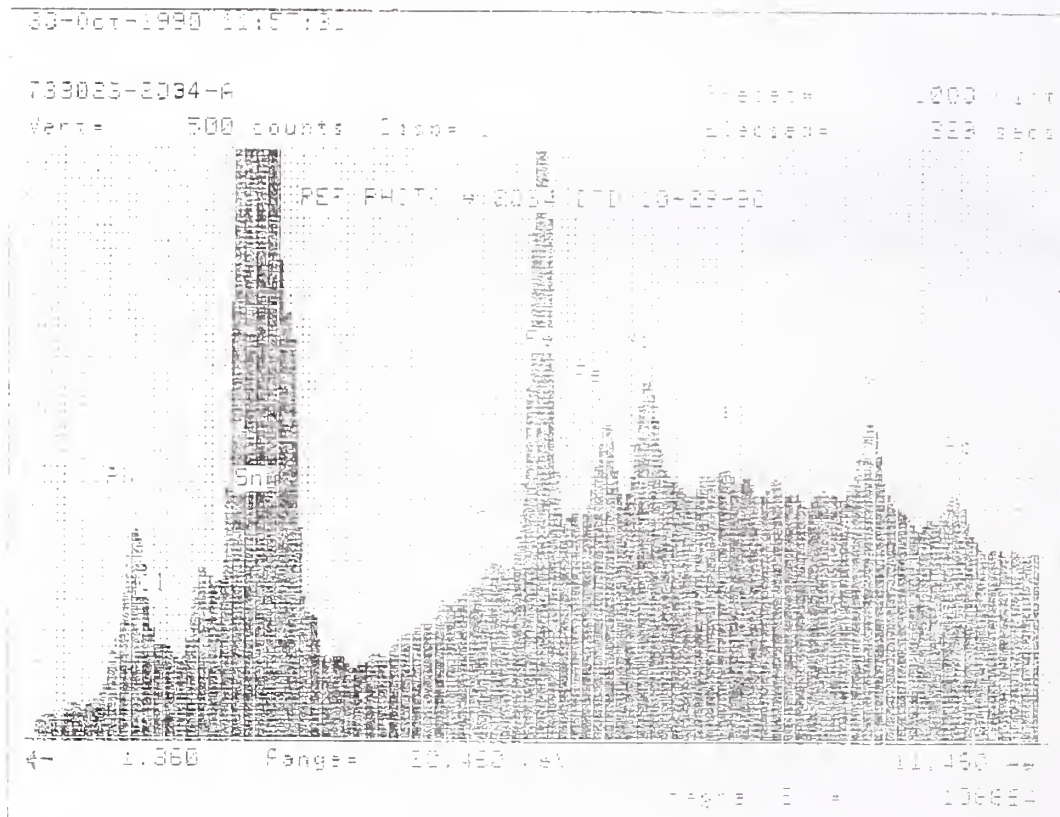


Corroded area of the inductor lead.

Figure 11. (W2)



a. Area of EDS analysis in (b).



b. EDS spectrum of corrosion area.

Figure 12. (W3) SEM/EDS analysis of the corroded area on the lead shown above.

182X 4KV WD:15MM S:00000 P:02163
200UM



Figure 13. (W3) Bubbles located in the corroded area of the lead shown in previous figure.

1-16-91 733023 ROME LABORATORY

a. General area of bubble formation.

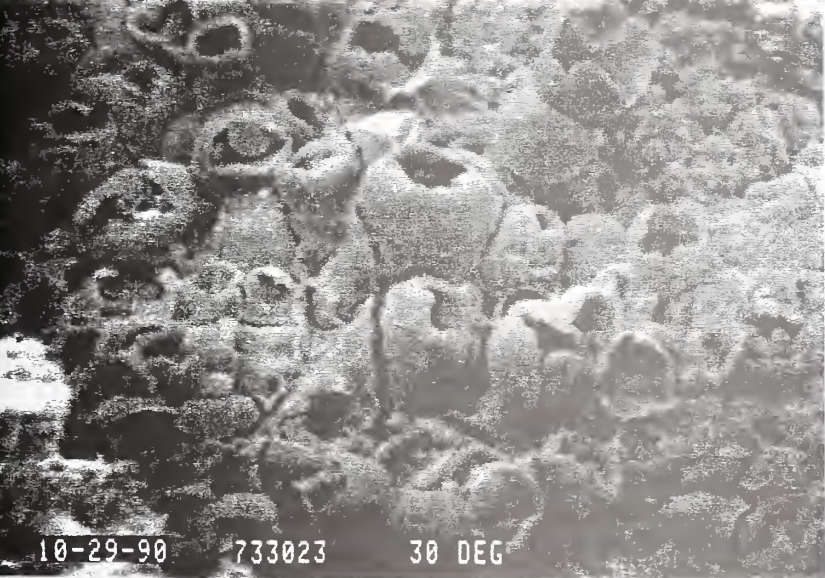
1,25KX 4KV WD:20MM S:00000 P:02152
20UM



1-16-91 733023 ROME LABORATORY

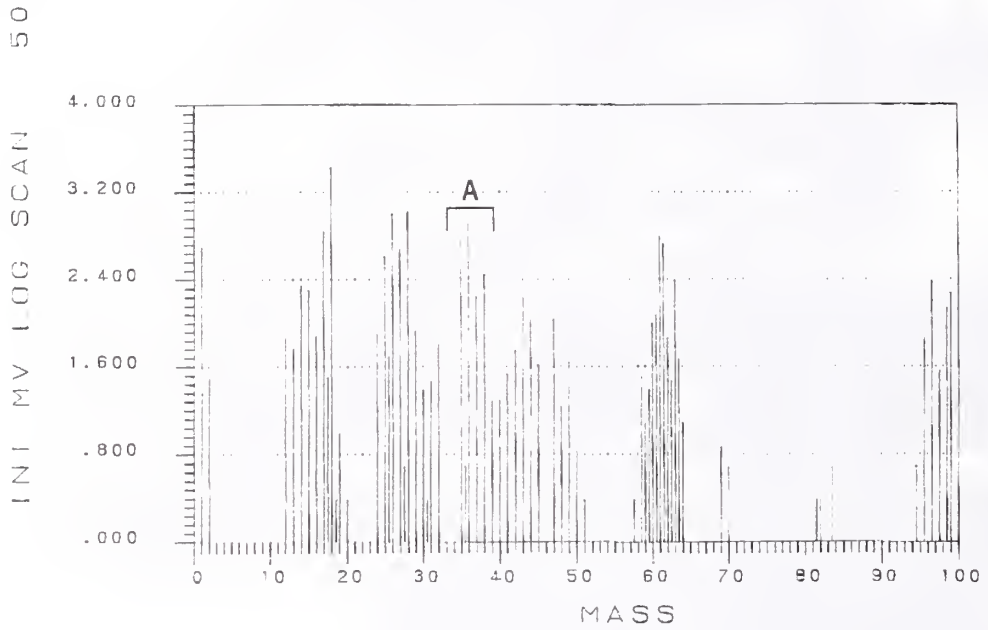
b. Magnified view of bubbles.

1,42KX 10KV WD:27MM S:00000 P:02032
20UM

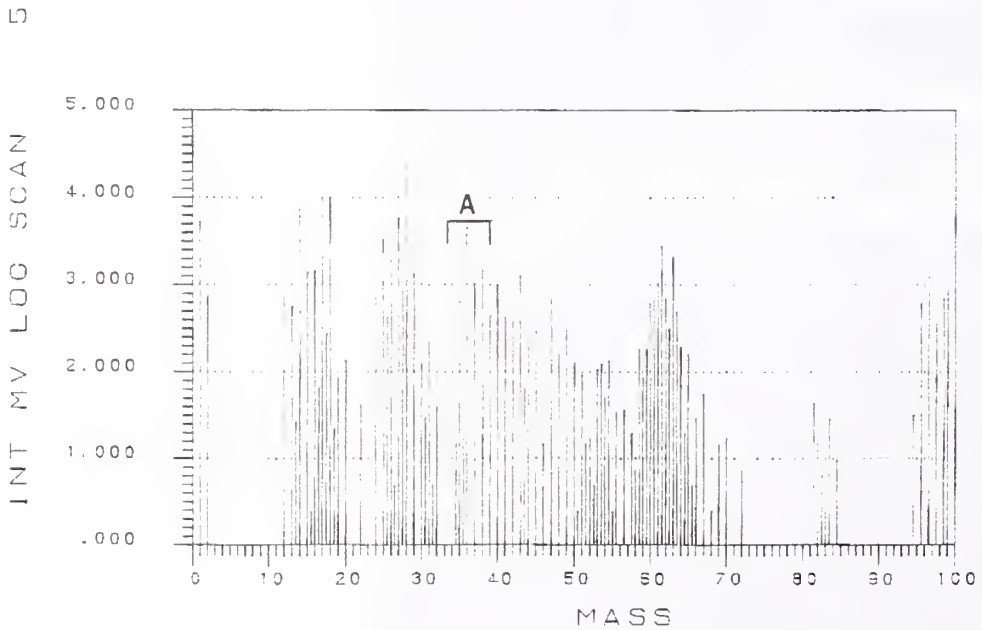


10-29-90 733023 30 DEG

c. Same as (b), different area.



a. As-soldered (sample S1).



b. As-reworked (sample R1).

Figure 14. Mass spectra of top coating from circuit board. Hydrochloric acid peaks are located at A.

MOISTURE EFFECTS ON INTERPHASE CONDUCTIVITY

J.E. Anderson and K.M. Adams
Research Laboratory, Ford Motor Company, Dearborn, MI

P.R. Troyk
Pritzker Institute for Medical Engineering,
Illinois Institute of Technology, Chicago, IL

Electrical impedance is a useful reliability predictor for encapsulated microelectronics. Experiments use test specimens with surface electrodes deposited on insulator substrates such as quartz or alumina. Specimens are cleaned, then coated with polymer encapsulants. Impedance measurements are made under high temperature, high humidity conditions that simulate worst-case operating environments.

Conventional tests rank-order encapsulant materials by their ability to maximize impedance. These are *relative* measurements where one material is compared with others. The present *unconventional* research approaches encapsulated microelectronics on an *absolute* basis. Given a known test specimen geometry and electrical parameters for the bulk encapsulant, what impedance should be measured?

This approach derives from Curtis, who showed that a conformal mathematical transformation links bulk conductivity measured between parallel plate electrodes to *interphase conductivity* of the same material when it covers surface electrodes. [In recent work, IEEE Trans. Comp. Hybrids & Manuf. Techn. 11, 420 (1991), we suggest the term *interphase conductivity* describes the situation where electrodes are located at an interphase boundary between two dissimilar materials; e.g., surface conductivity measurements beneath a surface coating.]

We performed impedance measurements on various polysiloxane encapsulants. Experiments were performed on dry materials, and on polysiloxanes equilibrated with water, methanol, ethanol and isopropanol. Bulk measurements were made on polysiloxane sheets; interphase measurements, on encapsulated aluminum comb-electrodes deposited on quartz. Surface impedance measurements were made on clean, uncoated specimens.

Interphase conductivities of dry materials are consistent with predictions derived from corresponding bulk conductivities. In contrast, solvent-equilibrated samples showed large discrepancies with bulk conductivity predictions. Under high humidity conditions, interphase conductivities of encapsulated specimens were substantially smaller than corresponding surface conductivities measured on uncoated (bare) samples. However, interphase conductivities of these water-equilibrated samples were some 1000X larger than bulk conductivity predictions.

Reasons for these large discrepancies remain unclear. The talk will consider alternative explanations, along with impedance results on model water-organic systems that eliminate some of them.

I. INTRODUCTION

At ambient temperature and 0% relative humidity [RH], surface conductivities of insulators are typically 10^{-14} - 10^{-16} mho. These values correspond to current flow in near-surface regions of the insulator substrate. Surface conductivities increase to 10^{-8} - 10^{-10} mho at 100% RH and ambient temperature. This 10^4 - 10^6 X increase is caused by a thin layer of sorbed water that is in parallel electrically with the near-surface region. The enormous difference between the bulk conductivities of the solid insulator, $\sim 10^{-14}$ mho/cm, and the conductivity of bulk water, $\sim 10^{-6}$ mho/cm, causes thin water films to dominate surface conductivity at high RH.

Unencapsulated microelectronic devices represent similar conditions. At high RH, thin aqueous films form on device surfaces. These surface films provide high conductivity pathways which, in turn, promote electrochemical attack and increase device failure rates.

Polymer coatings, or encapsulants, reduce surface conductivity. One widely accepted mechanism of encapsulation function envisions competition between water molecules and polymer segments for surface sites. [1] Water films cannot form on surfaces with favorable polymer-substrate interactions. Encapsulation lowers *interphase* conductivity thus reducing electrochemical attack and failure rates.

Using methods described in the next section, one can predict interphase conductivity from surface electrode geometry and encapsulant bulk conductivity. The present research compared these predictions with experiments performed under variable RH conditions.

II. ELECTROSTATIC CALCULATIONS OF INTERPHASE CONDUCTIVITY

Comb test specimens are shown schematically in Fig. 1. Except for end effects, the specimens are the electrical equivalent of two infinitely-long parallel electrodes on a insulator surface. Using a conformal transformation, Curtis developed a closed-form solution for the conductivity of this system. [2] He assumed two infinitely-long electrodes, each of width w , separated by a distance d on the surface of a medium having bulk conductivity σ_a [mho/cm]. Interphase conductivity, σ_i , is given by

$$\sigma_i = 0.5 (K'/K) \sigma_a , \quad [1]$$

where K , K' are complete elliptic integrals of the first kind for modulus $k = d/(d + 2w)$ and $k' = (1-k)^{1/2}$, respectively. For $(d/w) = 1$, corresponding to our test specimens, $0.5 (K'/K) = 0.78$.

Results obtained from Eq[1] agree with earlier electrostatic finite element calculations. [3] Both show that changing pattern size while keeping (w/d) fixed has no effect on σ_i .

III. EXPERIMENTAL METHODS

Surface and interphase conductivity measurements were made on interdigitated comb structures consisting of 20 aluminum stripes on quartz substrates. They were fabricated at the Ford Research IC Facility. Each stripe was 6600 μm long by 140 μm wide by 1 μm

thick. Comb specimens were attached to Kyocera SBO-/64N665 DIL chip carriers with electronic grade epoxy. Electrical connections between comb and carrier were made with 25- μm gold wire. Specimens were cleaned with Freon/TMS and argon-ion etching prior to encapsulation. They were housed in micro-environmental chambers during electrical tests.

Bulk conductivity measurements were made on cast films of silicone rubber (Dow Corning Sylgard 184). The films were approximately 0.05 cm thick. Thicker films approach the detection limits of our electrical test equipment. Thinner films exhibit pinholes and tear easily. Samples were equilibrated with liquid water, methanol, ethanol and isopropanol. Samples were blotted dry to remove excess liquid before conductivity measurements were made. Electrical measurements were made in a Keithley Model 6105 Resistivity Chamber. A Keithley Model 617 Electrometer served as both a dc voltage source and as a current detector. Bulk, surface and interphase conductivities were determined from least-squares analysis of current-voltage data taken at 21 voltage increments between -20 and +20 Vdc. A 60-sec electrical equilibration time was used between the start of the voltage-step and the actual current measurement.

IV. EXPERIMENTAL RESULTS

Table I shows bulk conductivity data on polysiloxane. Both dry polysiloxane and solvent-equilibrated specimens are included. Results on water-equilibrated samples match results on other water-elastomer systems.[2] Samples equilibrated at 0% and 100% RH show indistinguishable conductivities of $\sim 10^{-16}$ mho/cm. The experimental conductivity at 100% RH lies far below additivity predictions. For example, polysiloxane sorbs ~ 0.1 (w/w) % water. Bulk water has a conductivity of $\sim 10^{-6}$ mho/cm. Using (weight fraction water) X (bulk conductivity of water), additivity predicts a conductivity of $\sim 10^{-9}$ mho/cm. In contrast to the water data, bulk polysiloxanes equilibrated with methanol, ethanol and isopropanol have significantly larger conductivities than the dry polymer. Experimental values lie below additivity predictions, but approach additivity in the case of isopropanol. We attribute this behavior to higher polysiloxane sorption of the alcohols relative to water. The data cannot be explained on the basis of liquid conductivities since the alcohols have smaller conductivities than bulk water.

Table II shows (bare) surface conductivities and (encapsulated) interphase conductivities of comb test samples. Interphase conductivities of water-equilibrated polysiloxanes are some 1000X smaller than corresponding bare (surface) conductivities. Curiously, the decrease matches the equilibrium water content of the bulk polymer, 0.001 - 0.002 weight fraction (cf. Table I). On the other hand, interphase conductivities increase by 100-1000X larger going from 0% to 100% RH. Using the RH insensitivity of bulk conductivity, electrostatic calculations predict interphase conductivities at 0% and 100% should be indistinguishable from one another. This prediction is *not* realized.

Methanol, ethanol and isopropanol represent a series of simple polar chemicals having progressively more organic character than water. This is reflected in their greater sorption in hydrophobic polysiloxane. Greater solubility (Table I) translates into higher conductivity in solvent-equilibrated polysiloxane. Perhaps fortuitously, increasing organic character and solvent sorption correlates with interphase conductivities that approach values predicted by electrostatic calculations.

V. DISCUSSION

Interphase conductivities of polysiloxane encapsulated specimens equilibrated with methanol, ethanol and isopropanol agree with electrostatic predictions to an order of magnitude. In light of considerable experimental uncertainties associated with both bulk and interphase conductivity measurements, this represent *satisfactory* (but not *great*) agreement.

Water-equilibrated samples provide a major discrepancy with electrostatic predictions. Using the bulk conductivity of water-equilibrated polysiloxane, Eq[1] predicts an interphase conductivity below the resolution limits of our instrumentation. Experimental values for samples equilibrated at 100% RH cluster around $1-5 \times 10^{-12}$ mho, well above instrumental noise and some 1000X larger than calculated values. This large discrepancy reflects an interphase conduction process. Small quantities of residual hygroscopic contamination on at the *interphase* provide a reasonable -- if unsatisfying -- explanation. This implies that severe cleaning protocols, such as those used in current sample preparation, cannot reduce surface contamination to 'undetectable levels'.

As noted earlier, it is somewhat surprising that bulk polysiloxane conductivities show no variation with sorbed water. Samples equilibrated at 0% and 100% RH give values close to 10^{-16} mho/cm. [Note that our detection limit is approximately 10^{-17} mho/cm for *bulk* samples.] We attribute this to dielectric constant (ϵ) effects on dissociation of H_2O molecules into H^+ and OH^- ions. In bulk water, $\epsilon_w = 78$, this dissociation is characterized by an equilibrium constant $K_w = 10^{-14}$. The equilibrium constant decreases by $\sim 10^{16}X$ in media with $\epsilon_p = 2-3$ (like polysiloxane): There are many fewer H^+ , OH^- charge-carriers. Dielectric constant variations with composition, and the accompanying variations of dissociation constants with ϵ , can produce large percolation-like conductivity behavior in binary liquid systems.[4]

VI. REFERENCES

1. White, M.L., Encapsulation of Integrated Circuits, *Proc. IEEE*, 57, 1610 (1969).
2. Curtis, H.L., *Insulating Properties of Solid Dielectrics*, U.S. Bureau of Standards Paper Number 234 (1915).
3. Troyk, P.R.; Anderson, J.E.; Conroy, D., Modeling of Triple-Track and Comb-Pattern Leakage Current Measurements, *Polymeric Materials for Electronics Packaging and Interconnection*, J.H. Lupinski and R.S. Moore, Eds., pp. 249-267 (American Chemical Society, Washington, D.C., 1989).
4. Anderson, J.E., Dielectric Constant Effects on Water Dissociation and Electrical Conductivity in Water-p-Dioxane Solutions, *J. Phys. Chem.*, 95, 7062-7064 (1991).

Table I

EXPERIMENTAL SOLVENT CONDUCTIVITY [Λ_{liq}], SOLVENT SORPTION [W]
AND BULK CONDUCTIVITY [Λ_{blk}] OF SOLVENT-EQUILIBRATED
POLYSILOXANE FILMS

Solvent	Λ_{liq} [mho/cm]	W [wt. fraction]	Λ_{blk} [mho/cm]
None (dry)	-----	-----	2×10^{-16}
Water	$1.5 \pm 1 \times 10^{-6}$	0.0015 ± 0.0005	2×10^{-16}
Methanol	$2 \pm 1 \times 10^{-6}$	0.02 ± 0.002	6×10^{-13}
Ethanol	$4 \pm 1 \times 10^{-7}$	0.04 ± 0.01	3×10^{-11}
Isopropanol	$6 \pm 4 \times 10^{-8}$	0.22 ± 0.01	5×10^{-10}

Table II

SURFACE AND INTERPHASE CONDUCTIVITIES OF COMB TEST PATTERNS;
CALCULATED INTERPHASE CONDUCTIVITIES (22°C). VALUES IN Mho.

Solvent	Bare Comb	Encapsulated	Calculated
None (dry)	$(6 \pm 1 \times 10^{-14})^{**}$	$(3 \pm 2 \times 10^{-14})^{**}$	1.4×10^{-15}
Water	$4 \pm 1 \times 10^{-9}$	$6 \pm 1 \times 10^{-12}$	1.4×10^{-15}
Methanol	$5 \pm 4 \times 10^{-8}$	$7 \pm 5 \times 10^{-12}$	4.1×10^{-12}
Ethanol	$2 \pm 1 \times 10^{-9}$	$6 \pm 2 \times 10^{-8}$	2.0×10^{-10}
Isopropanol	$2 \pm 1 \times 10^{-8}$	$2 \pm 1 \times 10^{-9}$	3.5×10^{-9}

** Experimental values, given for completeness, that lie below the 5×10^{-14} mho resolution limit of our instrumentation.

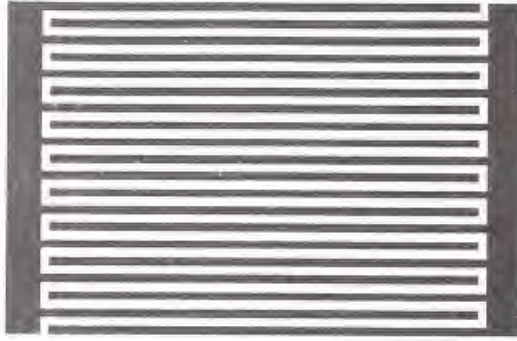


Fig. 1 Schematic representation of comb specimen.

Fig 2a. Schematic representation of bulk conductivity measurement.

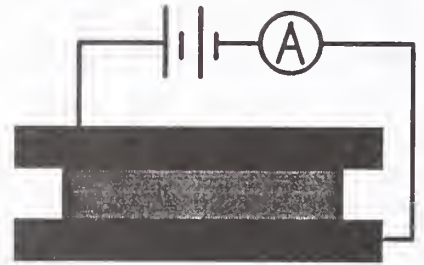


Fig. 2b. Schematic representation of surface conductivity measurement.

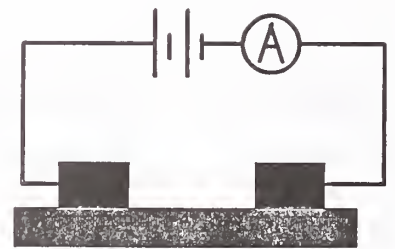
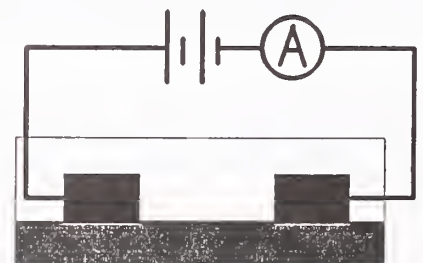


Fig. 2c. Schematic representation of interphase conductivity measurement.



CORROSION OF CHIP RESISTORS WITHIN A HYBRID INDUCED BY TANTALUM CHIP CAPACITOR OUTGASSING PRODUCTS

by

Joe Abbott, Thomas J. Green, and Kerry Huntington
Martin Marietta
Denver, CO

ABSTRACT

Hybrids fabricated by Martin Marietta failed burn-in testing due to open nichrome resistors. Although eighteen types of nichrome resistors were present within each hybrid package, corrosion always occurred on one resistor type at one circuit location.

Testing demonstrated the following:

1. Manufacturer A's tantalum chip capacitors must be present within the hybrid package for corrosion to occur.

2. Corrosion is minimal or nonexistent on resistors protected with a polyimide coating.

3. Corrosion is minimal or nonexistent on resistors to which power is not applied.

4. The corrosion rate and pattern is dependent on the resistor orientation within the circuit.

5. The corrosion rate can be decreased by using an increased preseal-bake temperature during hybrid fabrication.

6. The corrosion rate can be decreased by using a better preseal-bake vacuum during hybrid fabrication.

HISTORY

Two of three Heater Controller Hybrids (HCH) failed burn-in testing. Each HCH contains two identical circuits (see Figure 1). On each unit, one of these two circuits failed.

These were the first three hybrids of this type built by the Martin Marietta microelectronics facility. However, this hybrid type had been successfully built by an independent laboratory for some time with piece parts supplied by Martin. Piece parts supplied to the independent lab were from the same lots as were used in

the Martin build.

Prior to the hybrid failures, a liftoff problem had been observed on soft-body tantalum chip capacitors fabricated by Manufacturer A (capacitor debond during centrifuge testing). Analysis had shown these capacitors outgass fluorine when heated, and that fluorine was present throughout the inside of packages which contained them. Six of these capacitors were present within each Heater Controller Hybrid.

FAILURE ANALYSIS

Troubleshooting isolated both hybrid failures to a resistor in the R15 circuit position being used as a pullup. This resistor is a 13.9k ohm $\pm 0.1\%$ nichrome resistor with no protective coating. Visually both failed resistors exhibited evidence of corrosion, and electrically both measured open. In addition to the two failed resistors, evidence of corrosion could be seen on both R15 resistors in the redundant circuit positions. No anomalies were observed on any other resistors in the failed units, or on any resistors in the unit which passed the testing.

Two corrosion patterns were present on the four R15 resistors from the two failed units.

Corrosion Pattern A can be seen in Figures 2, 3, and 4. Corrosion is concentrated near the laser trim area of the resistor tophat bar. This pattern was present on both failed resistors and one of the redundant circuit resistors.

The Type B Corrosion Pattern is shown in Figure 5. Corrosion is concentrated at the shorting bar trim away from the tophat bar. This pattern was present on one redundant circuit resistor. Besides being the only R15 resistor of the four which exhibited this corrosion pattern, this was the only one which did not exhibit a resistance increase.

SEM inspection of resistor corrosion areas showed nichrome was present in these areas, but differed structurally from nichrome in areas away from the corrosion. Figure 6 shows a SEM backscatter electron image of the corrosion area of the first failed resistor. Figure 7 shows a combination secondary electron/backscatter electron image of the same area. Comparison of the two photos shows that nichrome in the corrosion areas of Figure 6 exhibits charging in Figure 7. This confirms these areas are nonconductive, and are responsible for the resistance increase.

EXAMINATION OF UNITS FABRICATED BY THE INDEPENDENT LAB

Although no resistor corrosion failures had been observed on HCH units fabricated by the independent lab, two of these units which had passed burn-in testing without incident were opened and examined. One of the four R15 resistors showed visual evidence of corrosion. Electrical testing confirmed a resistance increase (14.23k ohm, S/B 13.90k ohm $\pm 0.1\%$). This indicated that the same corrosion mechanism was present on these units, although the rate was apparently not high enough to result in failure.

EXAMINATION OF STOCK PARTS

No anomalies were observed in the course of examination of a sample of resistor dice from the lot used to supply R15 parts.

OVERSTRESS SIMULATION TESTING

Overstress simulation testing was performed on two stock resistors. Figure 8 shows a stock resistor opened by ESD overstress (2 kV Human Body Model). Figure 9 shows a stock resistor opened by DC electrical overstress (100 V DC stress applied for approximately ten seconds before the resistor opened). The appearance of both these failures differs substantially from the production failures.

BURN-IN TESTING

Two sets of burn-in tests were performed to understand the corrosion problem.

a. Initial Burn-In Test - A group of four hybrids containing eight resistors each were fabricated for burn-in testing. Results of the test are shown in Table 1. The burn-in test included the following details:

1. Two of the units were fabricated with Manufacturer A's capacitors and two without in order to determine if the presence of the capacitor was necessary for resistor corrosion (see Table 1 - No Cap and W/Cap).

2. R15 resistors of the type which failed were included both with and without a polyimide coating in order to determine if the coating inhibited corrosion (in Table 1 "R15 Poly" and R19 resistors have a polyimide coating, all other resistors in Tables 1 and 2 have no coating).

3. R15 resistors were included which were oriented each way with respect to the power supply in order to determine if the corrosion pattern and/or rate was dependent on this parameter. (The only difference between resistors with Type A and Type B Corrosion Patterns was orientation within the circuit. As shown in Figure 10, resistors in the "A" Orientation exhibited Type A Corrosion Patterns, while the single resistor in a "B" Orientation exhibited a Type B Corrosion Pattern. The "R15 OrB" resistors of Table 1 were positioned in a B Orientation, all other R15 resistors in Tables 1 and 2 were positioned in an A Orientation.)

4. Resistors were included in which the nichrome had been trimmed by Martin personnel in the shorting bar trim area to determine if the presence of the electric field was responsible for corrosion always concentrating here (Figure 11 documents the cut, resistors identified as "R15 Cut" in Table 1 had this modification).

5. Four other nichrome resistor types from the Heater Controller Hybrid were included to determine if corrosion was limited to the R15 resistor type and layout (Table 1 - R5, R14, R18, R19).

The sample parts were manufactured per the standard Martin process. The parts were then leak tested, subjected to a 24-hr/150°C bake, and ten temperature cycles (-55°C to 125°C) prior to the burn-in. A temperature of 110°C, and voltage of 10 V across each resistor, was used for the burn-in test.

As can be seen in Table 1, no resistor degradation occurred in packages which did not contain capacitors, or on resistors with a polyimide coating.

Large resistance degradation was observed on R15 resistors without the polyimide coating which were in an "A" orientation. Large resistor degradation was also observed on resistors which had been trimmed to minimize the magnitude of the electric field at the shorting bar trim area.

The correlation between corrosion pattern and resistor orientation within the circuit was confirmed. Resistors positioned in an A orientation exhibited large resistance shifts, and a Type A Corrosion Pattern (see Figure 12). Resistors positioned in a B orientation exhibited minimal resistance shift, and a Type B Corrosion Pattern (see Figure 13).

It is noted from Table 1 that power was removed from two resistors twenty-four hours into the burn-in after moderate resistance increases. No further degradation occurred on the resistors in the course of the burn-in,

indicating power application across the resistor is necessary for a high corrosion rate.

It is also noted that of the four resistors in hybrid 4I which were of a type different than R15, three exhibited some resistance increase (R5, R14, R18). R19, the only resistor which did not increase in resistance, was also the only one with a polyimide coating. However, visual examination of R18 found the actual cause of the open was electrical overstress (possibly ESD damage during testing), and resistance increases in R5 and R14 were small. These results are inconclusive.

b. Second Burn-In Test - A second burn-in test was performed on fifteen hybrids containing ten resistors each (eight R15 types, one R14 type, and one R18 type). The primary purpose of this testing was to determine why corrosion rates on hybrids fabricated by the Independent Lab were lower than those fabricated by Martin, despite use of the same piece parts.

Table 2 summarizes results of the testing (Initial Burn-In results are included in the table). The burn-in test included the following details:

1. Some parts were subjected to processing which simulated normal Martin HCH fabrication procedures up to the preseal vacuum bake, and others to processing that simulated the Independent Lab's procedures up to the preseal vacuum bake.
2. Parts were subjected to a variety of Preseal Vacuum Bake conditions (Martin used a 130°C/16-hr preseal bake with house vacuum, the Independent Lab used a 150°C/24-hr bake with nitrogen purge followed by a 150°C/1-hour bake with a vacuum of less than 1 Torr).
3. Some parts were fabricated with Manufacturer A's capacitors, and others with Manufacturer B's capacitors of the same type. The initial burn-in testing had shown corrosion did not occur without capacitors. This test would show if corrosion occurred with capacitors of the same type from another manufacturer.

After sealing the parts were leak tested, subjected to a 24-hr/150°C bake, and ten temperature cycles (-55°C to 125°C) prior to the burn-in. A voltage of 10 V was placed across each resistor for the test. Burn-in temperatures of both 85°C and 110°C were used.

As seen in Table 2, only four of the nineteen units showed any evidence of resistor degradation in the course of all burn-in testing. These were the four parts which: a) contained Manufacturer A soft-body capacitors, and b) were fabricated using Martin preseal vacuum bake conditions

(130°C, house vacuum, 16 hours).

Table 2 data indicates resistor degradation can be minimized by increasing the temperature of the preseal vacuum bake, or by using a better vacuum during the bake. This apparently decreases the corrosion rate by more thoroughly removing outgassing products generated by Manufacturer A's capacitors during the preseal vacuum bake. These two preseal vacuum bake parameters appear to be the primary cause of the variation in corrosion rates between Martin-fabricated and Independent-Lab-fabricated hybrids.

Table 2 also shows that Manufacturer A's capacitors must be present for corrosion to proceed at a high rate. Resistors in hybrids containing Manufacturer B capacitors of the same type showed negligible resistance change as a result of the burn-in.

No change in resistance was observed on any of the R14 or R18 resistors in this second test. If corrosion does occur on other resistor types, it is at a slower rate.

EDX/AUGER/RGA ANALYSIS

EDX spectra performed at resistor corrosion sites showed no anomalies.

Auger spectra and mapping consistently showed the presence of fluorine throughout the inside of units which contained Manufacturer A's capacitors. The fluorine appeared to be present in even higher concentrations at R15 corrosion sites. This was the only anomaly observed in extensive Auger analysis of production units and burn-in test samples.

RGA analysis on a sample of devices from the burn-in test showed differences between units which did and did not contain Manufacturer A's capacitors. Table 3 shows this data.

It can be seen from Table 3 that all six devices passed the Mil-Std-883 Method 1018 requirement for internal water vapor content (5000 ppm max).

It is also noted that in the two packages where corrosion occurred there is a significantly higher carbon dioxide level and correspondingly lower oxygen level. This may suggest a reaction is taking place in which oxygen is being consumed and carbon dioxide generated.

All six units passed hermeticity testing. This style package is prone to the "one way leak" phenomenon, which

may account for the presence of some He in the packages^{1,2}.

CONCLUSIONS

Manufacturer A's capacitors outgass material which initiates corrosion.

The corrosion rate is dependent on preseal vacuum bake conditions.

The corrosion rate is dependent on resistor orientation in the circuit.

The corrosion rate is minimal or nonexistent on resistors to which power is not applied.

The corrosion rate is minimal or nonexistent on resistors with a polyimide coating.

CORRECTIVE ACTION

Only resistor chips with a polyimide coating are now used in the R15 circuit position. Martin hybrid-fabrication parameters used in the preseal bake have been changed to 18-hr/150°C at 10 mTorr vacuum, with a dry-nitrogen backfill three times during the bake. Use of soft-body tantalum capacitors fabricated by Manufacturer A has been discontinued.

ACKNOWLEDGEMENTS

Bob Anselmi, Larry Bell, Cathy Flowers, Karen Miles, Harry Schumacher, Steve Smith, and Dave Wilson were all involved in useful technical discussions related to this analysis.

REFERENCES

1. "One Way Leakers", D.D. Dylis and G.H. Ebel, 1990 IES Symposium.
2. "How to Test for One Way Leakers", C. Epstein, Hybrid Circuit Technology, March, 1988.

Hybrid	Resistor	R (kohm, initial)	Resistance Change During Bake (ohms)							R (kohm, final)
			24 hrs	44 hrs	66 hrs	136 hrs	178 hrs	228 hrs	318hrs	
	R15	13.90	0	0	0	0	0	0	0	13.90
	R15	13.91	0	0	0	0	0	0	0	13.91
	R15 OrB	13.90	0	0	0	0	0	0	0	13.90
#1I	R15 OrB	13.90	0	0	0	0	0	0	0	13.90
NO CAP	R15 Cut	13.90	0	0	0	0	0	0	0	13.90
	R15 Cut	13.91	0	0	0	0	0	0	0	13.91
	R15 Poly	13.90	0	0	0	0	0	0	0	13.90
	R15 Poly	13.90	0	0	0	0	0	0	0	13.90
	R15	13.90	0	0	0	0	0	0	0	13.90
	R15	13.91	0	0	0	0	0	0	0	13.91
	R15 Poly	13.90	0	0	0	0	0	0	0	13.90
#2I	R15 Poly	13.91	0	0	0	0	0	0	0	13.91
NO CAP	R5	0.02603	OPEN+	OPEN+	OPEN+	OPEN+	OPEN+	OPEN+	OPEN+	OPEN+
	R14	3.501	0	0	0	0	0	0	0	3.501
	R18	99.70	0	0	0	0	0	0	0	99.70
	R19	398	0	0	0	0	0	0	0	398
	R15	13.91	870	870*	870*	870*	870*	870*	880*	14.78
	R15	13.90	2670	OPEN	OPEN*	OPEN*	OPEN*	OPEN*	OPEN*	OPEN (Fig. 12)
	R15 OrB	13.90	10	10	10	20	20	20	20	13.92
#3I	R15 OrB	13.91	0	0	0	0	0	0	0	13.91 (Fig. 13)
W/CAP	R15 Cut	13.91	380	380*	370*	380*	380*	380*	380*	14.29
	R15 Cut	13.89	OPEN	OPEN	OPEN	OPEN	OPEN	OPEN	OPEN	OPEN
	R15 Poly	13.91	0	0	0	0	0	0	0	13.91
	R15 Poly	13.90	0	0	0	0	0	0	0	13.90
	R15	13.90	80	130	130	410	810	1040	1630	15.53
	R15	13.91	40	60	60	130	190	260	430	14.33
	R15 Poly	13.90	0	0	0	0	0	0	0	13.90
#4I	R15 Poly	13.90	0	0	0	0	0	0	0	13.90
W/CAP	R5	0.02602	0.00001	0.00001	0.00002	0.00009	0.00025	0.00017	0.00021	0.02623
	R14	3.501	70	70	70	70	70	70	70	3.571
	R18	99.77	21670	12170	12270	13020	OPEN+	OPEN+	OPEN+	OPEN+
	R19	398	0	0	0	0	0	0	0	398

* = power not applied during bake

+ = open due to electrical overstress

TABLE 1. A Summary of Initial Burn-in Test Results.

Four hybrids were in this group of test parts. The two identified as "No Cap" indicates no capacitors were present in the package. The two identified as "W/cap" indicates six Manufacturer A soft-body capacitors were present in the package.

Eight resistors were present in each package. Resistors identified as "R15", "R15OrB", "R15Poly", and "R15Cut" are 13.9k ohm nichrome resistors of the type which failed. "R15OrB" indicates a "B" Orientation of the resistor (see Figure 10). "R15Poly" indicates the resistor has a polyimide coating. "R15Cut" indicates a cut has been made to the resistor to minimize the electric field strength in the shorting bar trim area (see Figure 11). R5, R14, R18 and R19 indicate resistors of the same types as were in these positions in the Heater Controller Hybrid.

HYBRID	PROCESS	PRESEAL VACUUM BAKE	CAPACITORS	BURN-IN TEMP	CORROSION
1I	Martin	130°C/House/16Hr	None	110°C	No
2I	Martin	130°C/House/16Hr	None	110°C	No
3I	Martin	130°C/House/16Hr	Manufacturer A	110°C	Yes
4I	Martin	130°C/House/16Hr	Manufacturer A	110°C	Yes
1	Independent Lab	150°C/<1Torr/1Hr	Manufacturer A	110°C	No
2	Independent Lab	150°C/<1Torr/1Hr	Manufacturer A	110°C	No
3	Martin	130°C/<1Torr/16Hr	Manufacturer A	110°C	No
4	Martin	150°C/<1Torr/16Hr	Manufacturer A	110°C	No
5	Martin	130°C/House/16Hr	Manufacturer A	110°C	Yes
6	Martin	150°C/House/16Hr	Manufacturer A	110°C	No
7	Independent Lab	150°C/<1Torr/1Hr	Manufacturer A	85°C	No
8	Independent Lab	150°C/<1Torr/1Hr	Manufacturer A	85°C	No
9	Independent Lab	150°C/<1Torr/1Hr	Manufacturer A	110°C	No
10	Independent Lab	150°C/<1Torr/1Hr	Manufacturer A	110°C	No
11	Independent Lab	150°C/<1Torr/1Hr	Manufacturer A	110°C	No
12	Independent Lab	150°C/<1Torr/1Hr	Manufacturer A	85°C	No
13	Martin	130°C/House/16Hr	Manufacturer B	110°C	No
14	Martin	130°C/House/16Hr	Manufacturer B	110°C	No
5*	Martin	130°C/House/16Hr	Manufacturer A	110°C	Yes

TABLE 2. A Summary of Burn-in Test Results

This table summarizes all the burn-in testing performed for this report. Hybrids 1I through 4I are from the Initial Burn-in Test, Hybrids 1 through 14 are from the Second Burn-in Test. The device identified as 5 failed hermeticity testing. A new sample was fabricated, and this test was repeated (hybrid 5*). In the Process column, "MARTIN" indicates samples were subjected to pre-vacuum-bake processing which simulated Martin HCH fabrication procedures. "INDEPENDENT LAB" indicates pre-vacuum-bake processing which simulated those of the Independent Lab. The "Preseal Vacuum Bake" column identifies conditions of the preseal vacuum bake. "House" refers to the house vacuum, which is around 460 Torr. For corrosion to occur, Manufacturer A's capacitors must be present, and a low temperature or poor vacuum used during the preseal bake (in this table, corrosion is defined as a 0.1% resistance increase on at least one resistor in the unit).

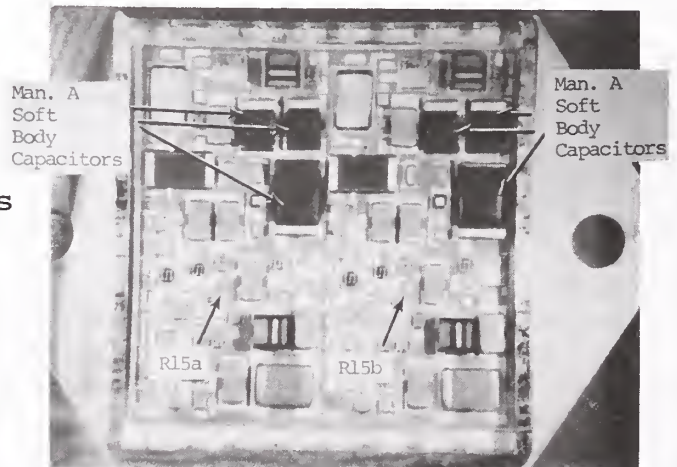
MEASUREMENT	UNITS	SAMPLE					
		1I	2I	3I	4I	9	10
Pressure	torr	13+	13+	13+	13+	13+	13+
Nitrogen	%	89.8	86.8	90.2	94.5	92.9	92.8
Oxygen	%	5.09	6.67	ND	ND	1.14	1.84
Argon	ppm	3643	4096	4250	1109	1879	2648
Carbon Dioxide	%	0.41	0.41	6.36	4.00	1.40	2.36
Moisture	ppm	4484	4221	3790	1528	4313	3690
Hydrogen	ppm	6662	5429	2651	5693	2131	1990
Helium	%	ND	1.74	1.91	0.20	3.02	1.90
Fluorocarbons	ppm	ND	<100	ND	ND	6707	2706
Ammonia	%	3.04	2.90	0.09	0.14	ND	ND
Isopropyl Alcohol	ppm	1450	1140	529	662	ND	ND
Hydrocarbons	ppm	154	123	1170	1044	ND	ND
Methanol	ppm	ND	ND	1962	1231	ND	ND

ND = NOT DETECTED
 SAMPLES PREBAKED @ 100C FOR 24 HOURS

TABLE 3. A Summary of RGA Test Results.

RGA test results on samples from the Table 1 and 2 burn-in testing. Samples 3I and 4I contained Manufacturer A's capacitors and exhibited extensive resistor corrosion. Samples 1I and 2I did not have capacitors, and exhibited no resistor corrosion. Samples 9 and 10 contained Manufacturer A's capacitors but were processed using the Independent Lab's fabrication parameters, which generally produced moderate corrosion.

FIGURE 1.
 Optical photograph showing a Heater Controller Hybrid. Locations of the R15 resistors are shown, as well as the six soft-body Manufacturer A chip capacitors believed to be the source of the corrosion product.
 1x Magnification



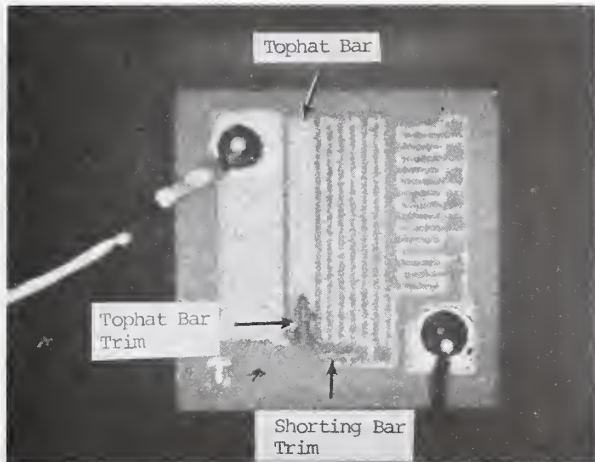


FIGURE 2.
Low-magnification optical
photograph of the failed R15b
resistor from the first
production unit. (Type A
Corrosion Pattern)
70x Magnification



FIGURE 3.
High-magnification optical
photograph of the failed R15b
resistor from the first
production unit. (Type A
Corrosion Pattern)
370x Magnification



FIGURE 4.
High-magnification optical
photograph of the failed R15a
resistor from the second
production unit. (Type A
Corrosion Pattern)
370x Magnification



FIGURE 5.
High-magnification optical
photograph of the R15b
resistor from the second
production unit. This
resistor did not fail, but
shows evidence of corrosion
(arrows). (Type B Corrosion
Pattern)
500x Magnification



FIGURE 6.
Low-magnification SEM
backscatter image of the
Figure 3 resistor.
670x Magnification

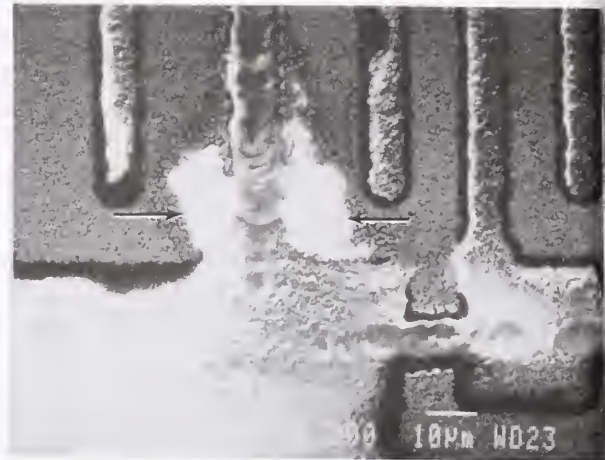


FIGURE 7.
Combination
backscatter/secondary electron
image of the Figure 3
resistor. Nonconductive areas
of the resistor exhibit
charging (arrows). Comparison
to Figure 6 shows these
nonconductive areas correlate
well with the NiCr structural
anomalies.
670x Magnification

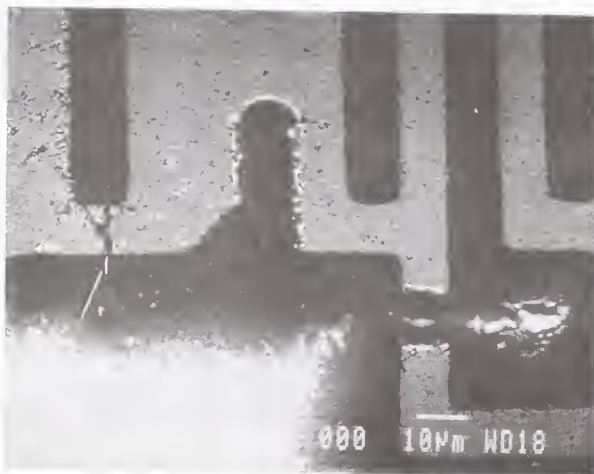


FIGURE 8.
SEM backscatter electron image
of a resistor overstressed
with a 2 kV HBM ESD pulse.
670x Magnification

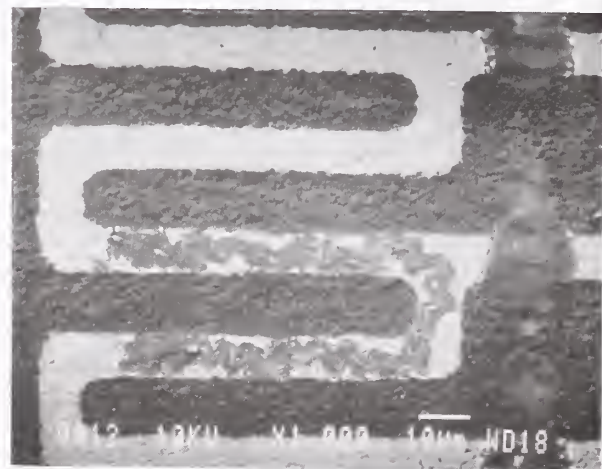


FIGURE 9.
SEM backscatter electron image
of a resistor electrically
overstressed with 100 V DC.
670x Magnification

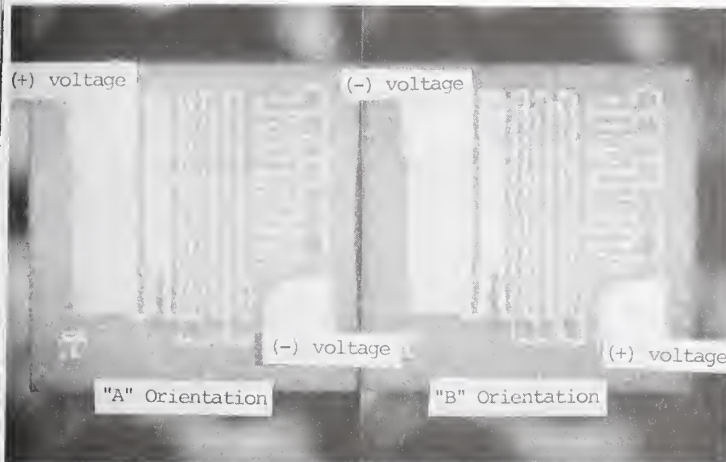


FIGURE 10.
The corrosion rate and pattern depend on resistor orientation within the circuit. Resistors positioned in an "A" Orientation corroded at a high rate in a Type A Pattern. Resistors positioned in a "B" Orientation corroded at a low rate in a Type B Pattern.
70x Magnification



FIGURE 11.
This resistor type has a large electric field across the shunting bar trim. Corrosion always concentrated on one side of the shunting bar or the other, depending on resistor orientation within the circuit. Resistors designated as "R15 Cut" in Table 1 were trimmed as shown to eliminate the field. (This was not found to affect corrosion rate or location, however.)
190x Magnification



FIGURE 12.
Optical photograph of an R15 resistor from the Initial Burn-in Test. This device was positioned in an "A" Orientation, and exhibits a Type A Corrosion Pattern (similar to Figures 3 and 4).
370x Magnification



FIGURE 13.
Optical photograph of one of the R150rB resistors from the Initial Burn-in Test. This device was positioned in a "B" Orientation, and exhibits a Type B Corrosion Pattern (similar to Figure 5).
370x Magnification

MOISTURE EFFECT AND MEASUREMENT ON SEMICONDUCTOR GAS PROCESS

by

Anthony F. Amato, Yadan W. Chen, and Edward T. Flaherty
Matheson Gas Products, Inc.
East Rutherford, NJ

ABSTRACT

This paper discusses the many problems moisture contributes to the semiconductor process. The main problem results from moisture's ability to form hydrogen bonds. The combination of moisture and oxygen is very reactive with most semiconductor gases. Determination of moisture in semiconductor process gases using different technologies is well known. Most methods presented are not absolute and require standardization. Stability of moisture standards at low concentrations in high pressure cylinders were studied. Factors which affect cylinder stability, such as cylinder material, temperature and pressure, are examined. This paper emphasizes the importance of calibrating moisture analyzers to ensure accurate and consistent analysis. Determination of moisture in hydrogen chloride and hydrogen bromide by the condensation method, and chlorine by FTIR are also discussed.

INTRODUCTION

Gaseous impurities, such as moisture and oxygen in semiconductor process gas systems, can increase defect densities in device films, generating particles and corrosion by-products {1}. Therefore, measurement and removal of these contaminants are important to both the electronic gas supplier and the electronic gas user.

Water is sometimes referred to as the "universal solvent" because of its unique chemical and physical properties. These properties present problems to the semiconductor industry because they have ability to hydrogen bond and hydrolyze many semiconductor gases. The atmosphere, for instance, has an average 50 percent relative humidity which can be introduced into cylinders or bulk gas delivery systems at many points during assembly or maintenance. This moisture will be adsorbed onto walls of containers and form hydrogen bonds to the active sites on surfaces. It differs from other environmental contaminants, such as CO, CO₂, O₂ and N₂, which can be introduced into the system with moisture, but can be removed by simple purging or vacuum. Moisture, once absorbed, can be removed only by the addition of energy (heat) and vacuum {2}.

CORROSION

Most of the process gases used in the semiconductor industry are very reactive, and a majority of them are very corrosive. Moisture in these

gases react to form by-products which can be in gaseous, solid or liquid form. These unwanted by-products can clog and contaminate semiconductor piping systems. Process gases that experience complete reaction with water and oxygen are listed in table #1. They hydrolyze rapidly to form the corresponding hydrogen halide and metal oxides. These hydrogen halides then corrode all wetted surfaces (valves, regulators, tubing) of the system. Metal oxides that are insoluble in gas and liquid phases result in particulates. These particulates coat the wall of the system, and, when exposed to moisture, act as a catalyst to further perpetuate the reactions. Further complications are found when oxygen is present with moisture.

MOISTURE MEASUREMENT OF SEMICONDUCTOR GASES

No one technique or method is universal for the detection of moisture; therefore, we must apply several analytical methods depending on the nature of the component. The following are the analysis methods and techniques presently being used: mass spectrometry, infrared spectrometry, condensation, piezoelectric, electrolytic, dielectric and gravimetric. Mass spectrometry can be used to identify the presence of moisture and hydrolysis species, which will help explain contamination mechanisms and confirm the results from other methods. Infrared spectrometry is very useful in understanding moisture analyses in chlorine. Trace moisture in corrosive gases, such as hydrogen chloride and hydrogen bromide, can be measured using a condensation technique {3}. Most techniques mentioned above are not absolute. It is necessary to standardize or calibrate the specific instruments using moisture standards when quantitating moisture in sample gas. The dew point determination is considered as an absolute method with free gases, but a condensation point versus moisture concentration calibration curve has to be determined empirically for corrosive gases.

MOISTURE STANDARDS IN HIGH PRESSURE CYLINDERS

Stability Study

A moisture calibration standard is necessary in assuring the proper operation of moisture analyzers. There are many methods of generating known amounts of moisture in the gas phase; such as: combustion of hydrogen and oxygen, catalytic conversion of hydrocarbons, diffusion or permeation of water vapor through a membrane, dilution of water vapor in high pressure cylinders with dry gas, etc. Preparation of moisture standards in high pressure cylinders would appear to be a convenient and simple method for use as long as the gas mixtures are both accurate and stable.

It is known that preparation of moisture standards in high pressure cylinders is a difficult task due to absorption on, or reaction with, cylinder walls {4}. It can be affected by many factors, such as cylinder material, pressure, temperature and moisture concentrations, etc.

To examine these factors, several moisture standards were prepared in high pressure aluminum and carbon steel cylinders at low concentration levels, nitrogen balance. Each cylinder was analyzed over a period of six weeks as cylinder pressure decreased. The moisture analyzer used was a piezoelectric moisture analyzer. Evaluation of these cylinders was carried out under various pressure and temperature conditions. One aluminum cylinder was tested until it was emptied. The results are illustrated in figure #1.

As can be seen from figure #1, the moisture concentration in the aluminum cylinder is very stable from full cylinder pressure to 50 psig. It fluctuated in a range of <1 parts per million in a six week period to within ± 2 percent.

Figure #1 also indicates the moisture in a carbon steel cylinder is much less stable and varies within 6 ppm in 1700 to 600 psig range. This indicates that moisture has more interaction with carbon steel walls than with that of aluminum.

Figure #1 illustrates that when a cylinder becomes empty the moisture concentration increases rapidly and significantly {5}. It is suspected that the increase of moisture is due to de-absorption of moisture.

Temperature effect was also examined with the two cylinders, aluminum and carbon steel. Cylinder temperatures can easily change during transportation or storage. It has been commonly considered that moisture concentration would decrease as the cylinder temperature decreases. When these cylinders are cooled to low temperatures and then allowed to warm, the moisture content re-equilibrates to its initial value after a period of 300 to 400 minutes; as illustrated in figure #2. It also appears that aluminum cylinders re-equilibrate themselves faster than carbon steel cylinders.

Similarly, the moisture content increases as cylinder temperature rises to 40°C {4} (Figure #3). Ambient temperature control is essential to ensure the stability of moisture cylinders, exclusive of other factors such as the detector type, sampling system, etc.

The research has led to the following conclusion: moisture standards at a level of 20 ppm can be very stable (within ± 2 percent range) for a period of time if the following conditions are met: (a) the use of treated aluminum cylinders; (b) the use of cylinder pressure no lower than 100 psig; (c) cylinders kept in a temperature controlled environment to ensure stable moisture content. If it has been exposed to the extreme temperatures and the value has shifted, the cylinder is able to rebound to its normal value when the conditions are restored.

To study long term stability and instrument comparison, fifteen moisture standards in aluminum cylinders were prepared. These aluminum cylinders were filled simultaneously from one batch of mixture gas. If the cylinders were treated and filled uniformly the result would be a homogeneous mix upon analysis. Each cylinder was analyzed by a piezoelectric moisture analyzer three or four times in a 16 day period. The results in table #2 show that the precision of analysis appears to be within the experimental error of ± 2 percent, and the batch average value is within ± 6.4 percent.

Eleven of these cylinders were labeled and sent to other laboratories for analysis using methods available to that location. Instructions on how to maintain cylinders in a temperature controlled environment for accurate results were emphasized. Results were collected and compared with the initial values. It was hoped that a uniformly prepared set of moisture standards would ensure lab to lab consistency.

In comparing their results with the cylinder initial moisture values, there was clearly a serious problem with the moisture detection instruments.

There were four major types of moisture analyzers tested in this program; results from each type are listed in table #3. Presently, the piezoelectric and P_2O_5 electrolytic type are recognized as leading moisture analyzers by the semiconductor industry {6}. Each type of analyzer seems to agree with itself, but not with any other type. The following experiments were designed to resolve the disagreement between these two types of moisture analyzers.

INSTRUMENT COMPARISON

As can be seen from table #3, the piezoelectric instrument versus P_2O_5 electrolytic yield different results.

To further confirm the disagreement, simultaneous comparison was made by using a permeation system to calibrate two instruments in 2 to 15 ppm region, see figure #4 for system setup. Both instruments generated lower values than calculated from the permeation device at higher concentrations. In figure #5, the two instruments agree at approximately 5 ppm. Above 5 ppm, the P_2O_5 cell results in a higher response than the piezoelectric. Below 5 ppm, the piezoelectric gives slightly higher value than the P_2O_5 cell.

It appears that the factory settings of both instruments result in a different value of moisture than that calculated from permeation devices. Additionally, the response is dependent on the moisture concentration. Multipoint calibration appears to be necessary.

CALIBRATION

Given the differences noted above with different types of instruments, it was interesting to compare units of the same type. The P_2O_5 and piezoelectric units were chosen. Table #4 illustrates the results of comparing two piezoelectric units with a series of moisture standards at concentrations of 2, 4, and 15 ppm. Clearly, before recalibration, significant differences existed in the units when analyzing high concentrations of moisture. Recalibration at the factory improved the consistency between the two units.

With the P_2O_5 unit, the manufacturer indicated that it was an absolute reading instrument and no calibration was necessary. In either case, we created the calibration curve using permeation tubes and did notice a difference in initial response versus the theoretically calculated

moisture from permeation tubes. Table #5 shows the response of calibrated and uncalibrated P_2O_5 units along with the two previously recalibrated piezoelectric units. We have finally achieved some degree of consistency among these moisture units.

It should be realized that improper calibration might be a major source of error and inconsistency in moisture analyzing units. Some manufacturers perform calibration at the factory and generate calibration curve for users, other manufacturers call their instruments absolute and claim no calibration is necessary. Both situations could misguide users because the instrument may lose calibration over a period of time - recalibration is necessary. Additionally, direct methods need to be verified due to the imperfect efficiency and deterioration of detective cells. It is our belief that calibration and recalibration of both analyzers was the only way to resolve the problem and obtain consistency. One can argue about the accuracy of a permeation device, or any moisture generator currently available. Certainly, the integrity of the calibration system and the procedure used for the standardization is of importance, but, ultimately the hierarchy of the standard used for this recalibration is of prime importance.

MEASUREMENT OF MOISTURE IN CORROSIVE GASES

Expanding moisture analysis techniques to the more reactive gases, such as hydrogen chloride, hydrogen bromide and chlorine, further complicates the situation due to the reactivity of these gases. In the few examples that we will present, you will see that the techniques used for the measurement of moisture in the corrosive gases were not absolute methods, and required calibration with known absolute standards.

HYDROGEN CHLORIDE AND HYDROGEN BROMIDE

The determination of trace amount of water in hydrogen chloride had been of considerable interest to manufactures of semiconductor materials. One of the current industry methods for analyzing moisture in HCl gas is to measure a condensation point when using the chilled mirror technique {3}. Hydrogen chloride and moisture readily form a hydrogen bond when contacted. We suspect that in utilizing this condensation technique we are measuring the condensation of hydrates of hydrogen chloride.

Figure #6 illustrates a calibration curve for condensation point versus moisture concentration for air, hydrogen chloride and hydrogen bromide. Table #6 gives the equation to calculate moisture content in hydrogen chloride and hydrogen bromide, which has been determined empirically using a calibration procedure. This technique has been verified, although it does have some limitations. First, it is not an on line analysis and requires some time to actually carry out the determination. The current detection limit, 1 ppm, appears to be the limit. The technique is not an absolute technique. Additionally, all condensation point determinations are subject to operator errors and can be disrupted by the collection of foreign matter on chilled mirror surfaces giving false readings.

CHLORINE

Moisture has been alleged to be an impurity in chlorine by semiconductor manufactures. A study was undertaken to determine the identification and concentration of moisture in chlorine by FTIR.

This FTIR system used is a Nicolet 520, Fourier transform infrared spectrometer, equipped with a liquid nitrogen cooled HgCdTe (MCT) detector with a Wilks 20m long path cell with a resolution of 2 cm⁻¹. The sample manifold is made of 316 stainless steel and all connections are VCR with diaphragm valves - refer to figure #7. All experimental conditions are kept identical including the use of helium for background spectra and the pressure sampling for samples, as well as standards.

The chlorine molecule is, for the most part, transparent to the FTIR because of its diatomic structure, and only reveals the fingerprints of its impurities {7}, see figure #8. The impurity bands identified are as follows:

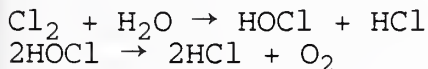
HCl	3100-2700 cm ⁻¹
CO ₂	2400-2250 cm ⁻¹
CO	2230-2050 cm ⁻¹
COCl ₂	900-800 cm ⁻¹
H ₂ O	4000-3400 cm ⁻¹
	2000-1300 cm ⁻¹
HOCl	1245; 967 cm ⁻¹

An experiment was devised to observe chlorine with the addition of moisture. A 50/50 mixture of chlorine and a 12 ppm moisture standard was introduced into the gas cell. The moisture bands were observed initially, then they disappeared over a short period of time. The data show that hydrogen chloride is formed with time. This was repeated several times with the same results, see figure #9.

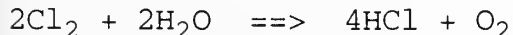
In aqueous systems, the reaction of moisture and chlorine sets up the following equilibrium:



Our data bring us to the conclusion that the reaction in the gas phase is not equilibrium controlled. We postulate that hypochlorous acid may be formed quickly and instantly decomposes to hydrogen chloride and oxygen.



We were not able to observe any HOCl bands in the frequency ranges of 1245 cm⁻¹ and 967 cm⁻¹; supporting the instability of HOCl. The overall reaction of moisture in chlorine appears to go to completion in the presence of excess chlorine, according to the stoichiometry.



Oxygen cannot be measured using FTIR because it, too, is a diatomic molecule lacking oscillating dipoles, and is infrared inactive.

It is proposed to monitor HCl and oxygen as an indicator of moisture contamination in chlorine. Measurement of oxygen in chlorine can be examined by gas chromatography. If the ratio of nitrogen to oxygen exceeds the normal 4:1 ratio due to atmospheric contamination, it is logical to assume it is from the presence of moisture.

CONCLUSIONS

First, the significant impact of moisture on bulk gas systems and specialty gases used in the semiconductor industry has been discussed. Complicated reactions of specialty gases with moisture and oxygen are summarized. Determination of moisture in corrosive gases can be achieved using various technologies. Most methods employed are not absolute but require calibration using reliable moisture standards.

Second, the use of moisture standards in high pressure cylinders can be found to be easy as well as convenient in verifying instrument performance. This stability study indicates that preparation of moisture mixtures in aluminum cylinders can provide a stable moisture source.

Third, a comparative study of various moisture analyzers, using a series of uniformly correlated moisture standards in cylinders and permeation devices was carried out, particularly between piezoelectric and electrolytic moisture analyzers. It is realized that the improper calibration of the instruments is the major source of error and inconsistency. Through calibration and recalibration of both analyzers we were able to resolve the problem and reach an agreement at various concentration levels.

Lastly, determination of moisture in hydrogen chloride, hydrogen bromide and chlorine is discussed. Trace moisture in hydrogen chloride and hydrogen bromide can be measured using the condensation method. The condensation temperature versus moisture concentration calibration curves determined empirically for HCl and HBr are provided. FTIR has been very useful in understanding moisture analyses in chlorine. In gas phase, chlorine reacts with moisture to form hydrogen chloride and hypochlorous acid which instantly decomposes to hydrogen chloride and oxygen. Therefore, no moisture exists in chlorine gas.

It is important to realize that sufficient and frequent instrument calibration using a reliable moisture source is necessary to promise accurate measurement. The advantage and limitation of each instrument must also be fully understood. Ideally, moisture standards must be verified by methods traceable to NIST.

Since there is no moisture standards available, a method that is traceable to NIST must be used. "Traceable" leads to many interpretations.

REFERENCES

1. E. Flaherty, A. Amato, L. Johns, Solid State Technology, January, 1992.
2. E. Flaherty, et al, Solid State Technology, July, 1987.
3. E. Flaherty, et al, Analytical Chemistry, vol.58, p.1903 (1986).
4. S. G. Wechter; F. Kramer, Jr., the 21st National Symposium of the Analysis Instrument Division, Instrument Society of America at King of Prussia, Pa., on May 8, 1975.
5. C. B. Blakemore; P. L. Collier, "Monitoring Moisture to Boost Semiconductor Yields", DuPont Company, Wilmington, Delaware.
6. J. J. McAndrew; D. Boucheron; Solid State Technology, p.55, February, 1992.
7. H. A. Szymanski, "IR Theory And Practice of Infrared Spectroscopy", Plenum Press, New York, 1966.

Acknowledgments

The authors would like to express their thanks to Ann Marie Brzychcy, Jack Simmermon, Doug Peterson, Edward Pavina and Thomas Beck for their invaluable discussion and technical assistance.

Table #1 - Specialty Gas Reactions with Oxygen & Moisture

HYDRIDES

<u>Gas</u>	Reactions with	
	<u>H₂O</u>	<u>O₂</u>
AsH ₃	-	Slow Oxidation As ₂ O ₃
PH ₃	-	Reacts to P ₂ O ₅
NH ₃	NH ₄ OH	-
B ₂ H ₆	H ₃ BO ₃	B ₂ O ₃ , H ₂ O

SILICON SOURCES

<u>Gas</u>	Reactions with	
	<u>H₂O</u>	<u>O₂</u>
SiH ₄	-	SiO ₂ , H ₂ , H ₂ O
SiH ₂ Cl ₂	SiH _x Cl _y OSiH _x Cl _y HCl	SiO ₂ , H ₂ , H ₂ O SiH _x Cl _y OSiH _x Cl _y
SiHCl ₃	"	"
SiCl ₄	"	"
Si ₂ H ₆	-	SiO ₂ , H ₂ O SiH ₃ OSiH ₃
SiF ₄	HF, SiF ₃ OSiF ₃	-

ACID GASES

Reactions With

<u>Gas</u>	<u>H₂O</u>	<u>O₂</u>
HCl	Hydrates	-
HBr	Hydrates	-
BCl ₃	HCl, H ₃ BO ₃	-
BF ₃	BF ₃ -H ₂ O, HF, BF ₂ OH	-
Cl ₂	HCl, O ₂	-

TABLE #3

COMPARISON OF MOISTURE ANALYZERS

SAMPLE LABELED	ANALYSIS (ppm)			
	PIEZO ELECTRIC	P2O5 ELECTROLYTIC	Al2O3 DIELECTRIC	DEW POINTER
14.2	13.2 ± 2.3			
14.1		18.8 ± 1.7		
14.4			11.4 ± 3.8	
14.3				6.7 ± 5.9
# of Analyzer	5	6	3	3

TABLE # 4

ANALYSIS OF MOISTURE CYLINDERS BY PIEZO TYPE ANALYZERS
BEFORE & AFTER RE-CALIBRATION

Analysis (ppm)

CYLINDER #	A1		A2	
	Before	After	Before	After
1	15.6	22.15	18.2	22.64
2	1.87	1.97	1.71	2.14
3	-	3.99	-	4.24

"-": NOT ANALYZED

TABLE # 5

COMPARISON OF PIEZO & P2O5 ELECTROLYTIC TYPE ANALYZERS

CYL.#	Analysis (ppm)				
	B1 Before Cal.	B1 After Cal.	A1 After Cal.	A2 After Cal.	A TYPE AVG
1	18.37	22.08	21.48	23.50	22.49
2	16.77	20.34	20.59	21.45	21.02
3	16.09	19.53	19.92	20.94	20.43
4	14.20	17.08	17.87	18.68	18.28
5	3.62	4.10	3.97	4.04	4.01
6	1.97	2.08	1.91	2.29	2.10

A : PIEZO ELECTRIC TYPE ANALYZER

B : P2O5 ELECTROLYTIC TYPE ANALYZER

Table #6 Equation of HCl and HBr - dewpoint vs. ppm water

$$y = A * \exp (b * x)$$

y: water ppm by volume

x: dew/frost point (°C)

Gas	Factor A	Factor b	Coefficient r
---	-----	-----	-----
HCl	830	0.14	0.953
HBr	51.7	0.15	0.989

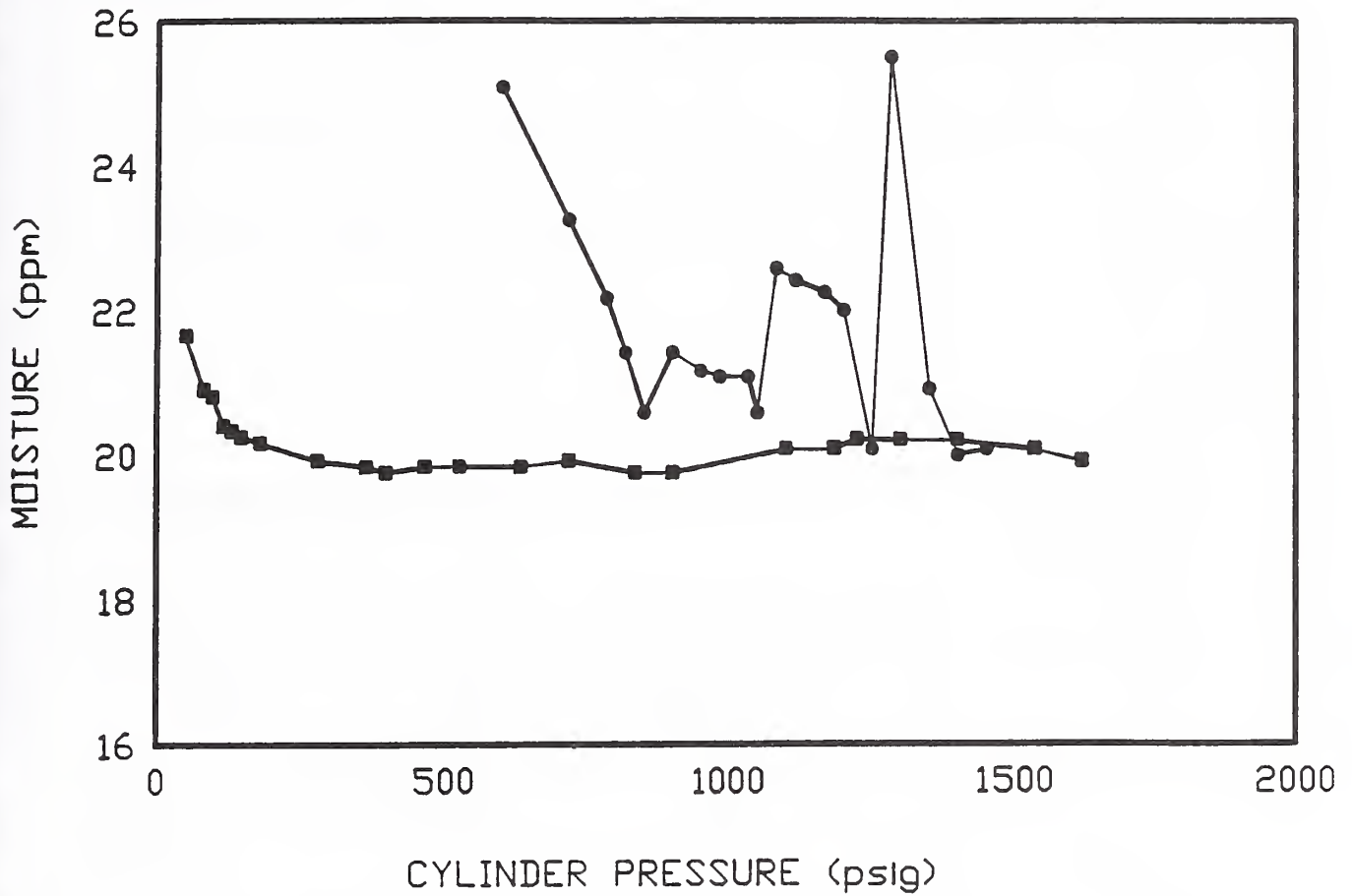
Flow requirement: 1 slpm

Detection Limit: 1 ppm

FIGURE 1

MOISTURE IN CYLINDER VS PRESSURE

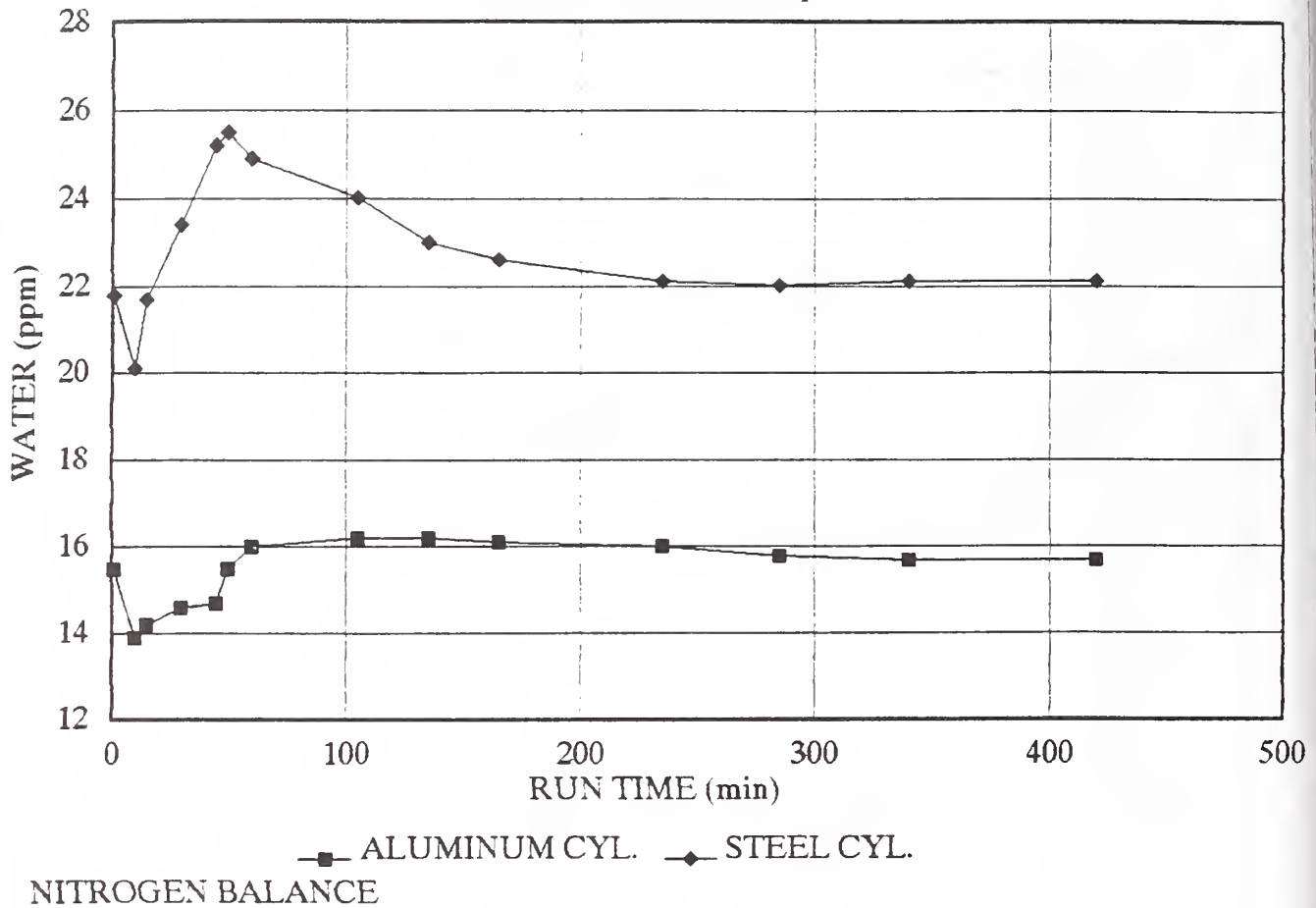
NITROGEN BALANCE



ALUMINUM = ■

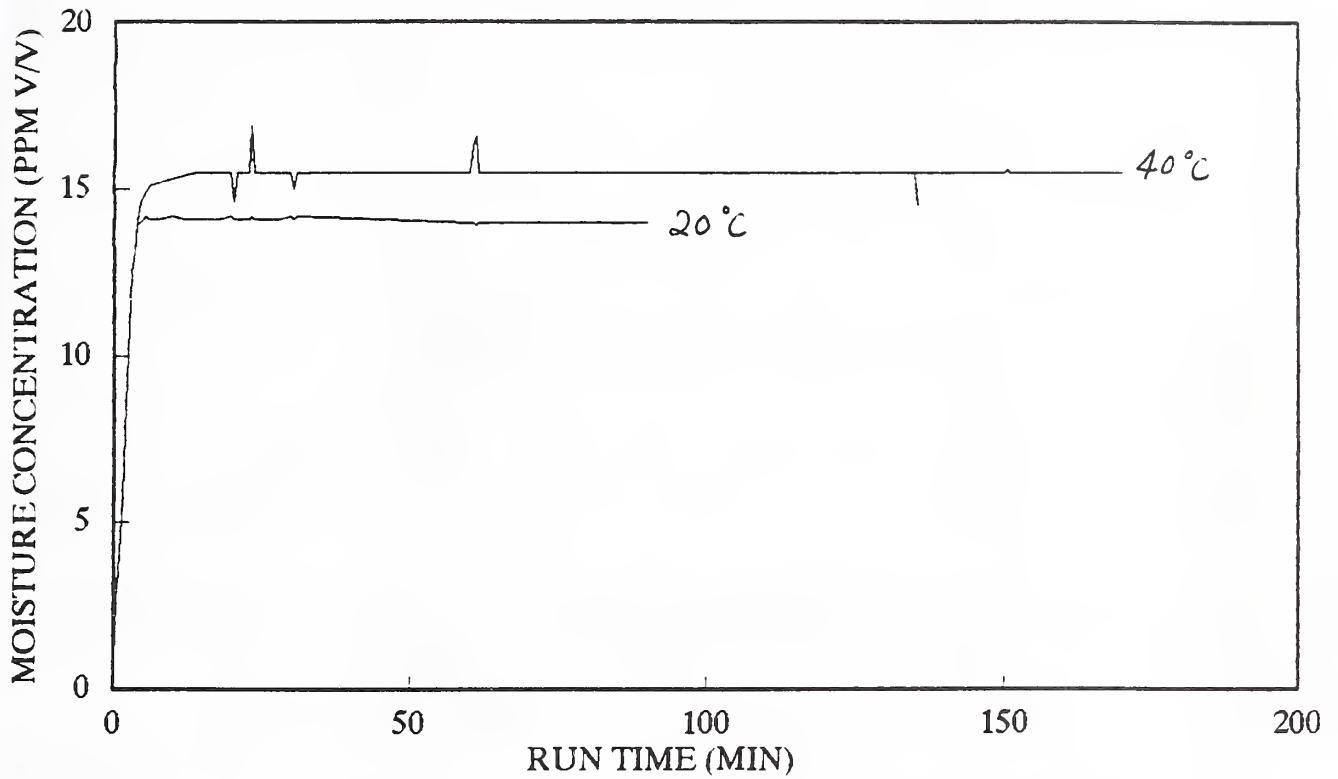
STEEL = ●

FIGURE #2 RE-EQUILIBRATION OF MOISTURE STANDARDS
from 0°C to Room Temperature



THE FIRST POINT MEASURED AT ROOM TEMPERATURE

FIGURE #3 EFFECT OF HIGH TEMPERATURE
ON MOISTURE RESULTS



— CYL. HEATED TO 40 °C

— CYL. @ ROOM TEMP 20 °C

CYL. # SX-20948 (14.1 ppm)

Nov. 1991

FIGURE 4

CALIBRATION SYSTEM

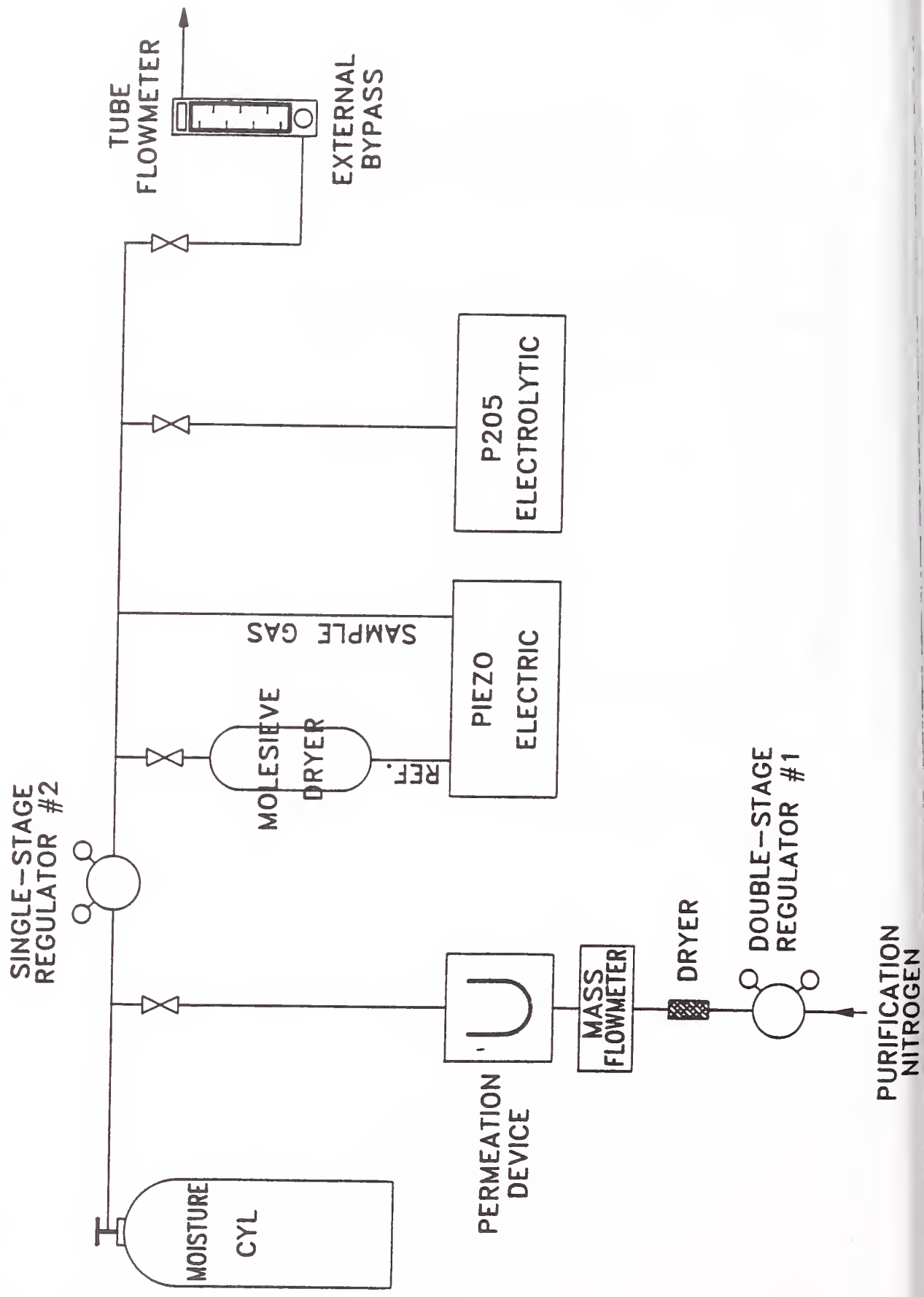
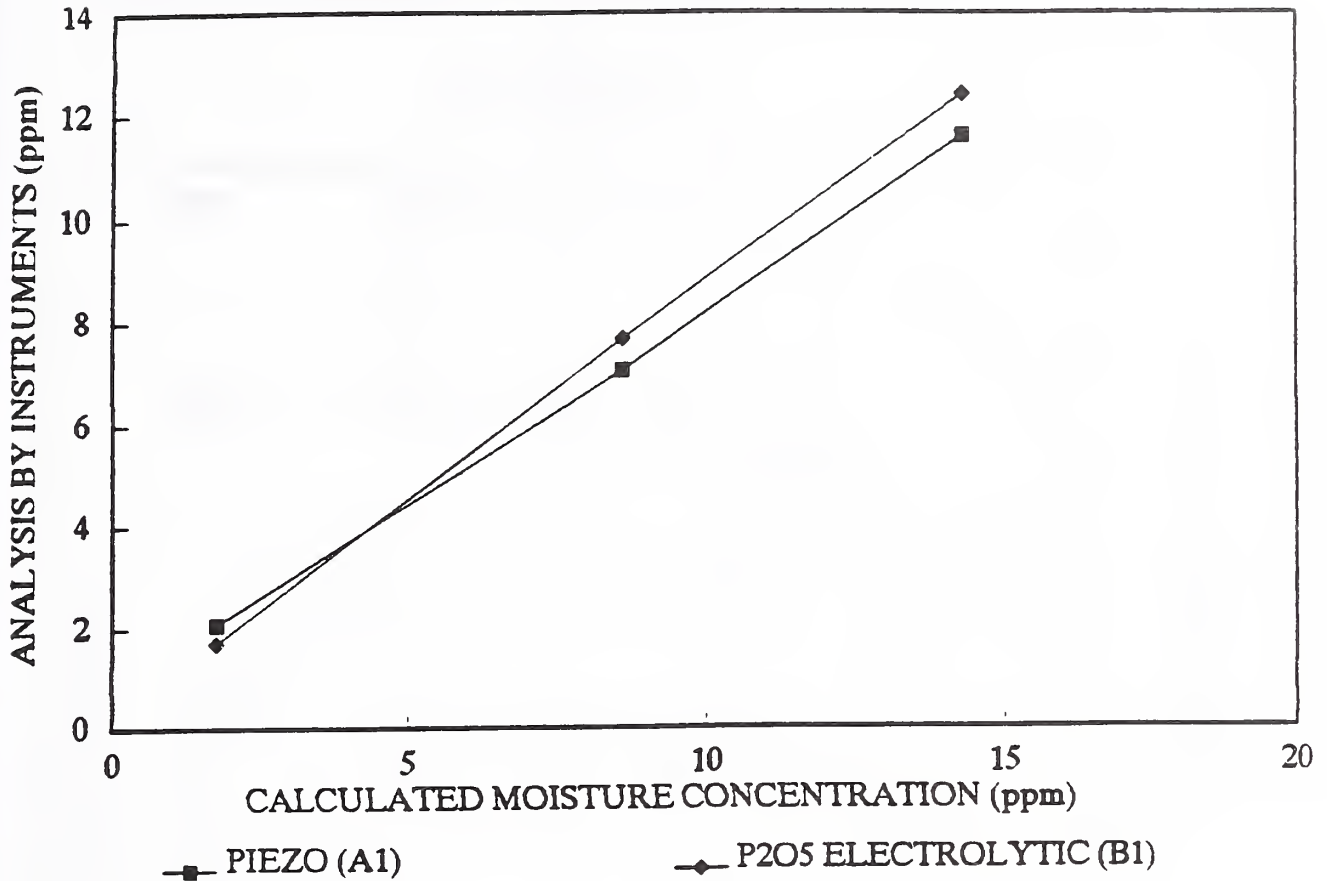


FIGURE 5 COMPARISON OF PIEZO & P2O5 ELECTROLYTIC ANALYZERS USING A PERMEATION METHOD



DEC. 1991

FIGURE #6 MOISTURE vs. CONDENSATION POINTS

CALIBRATION

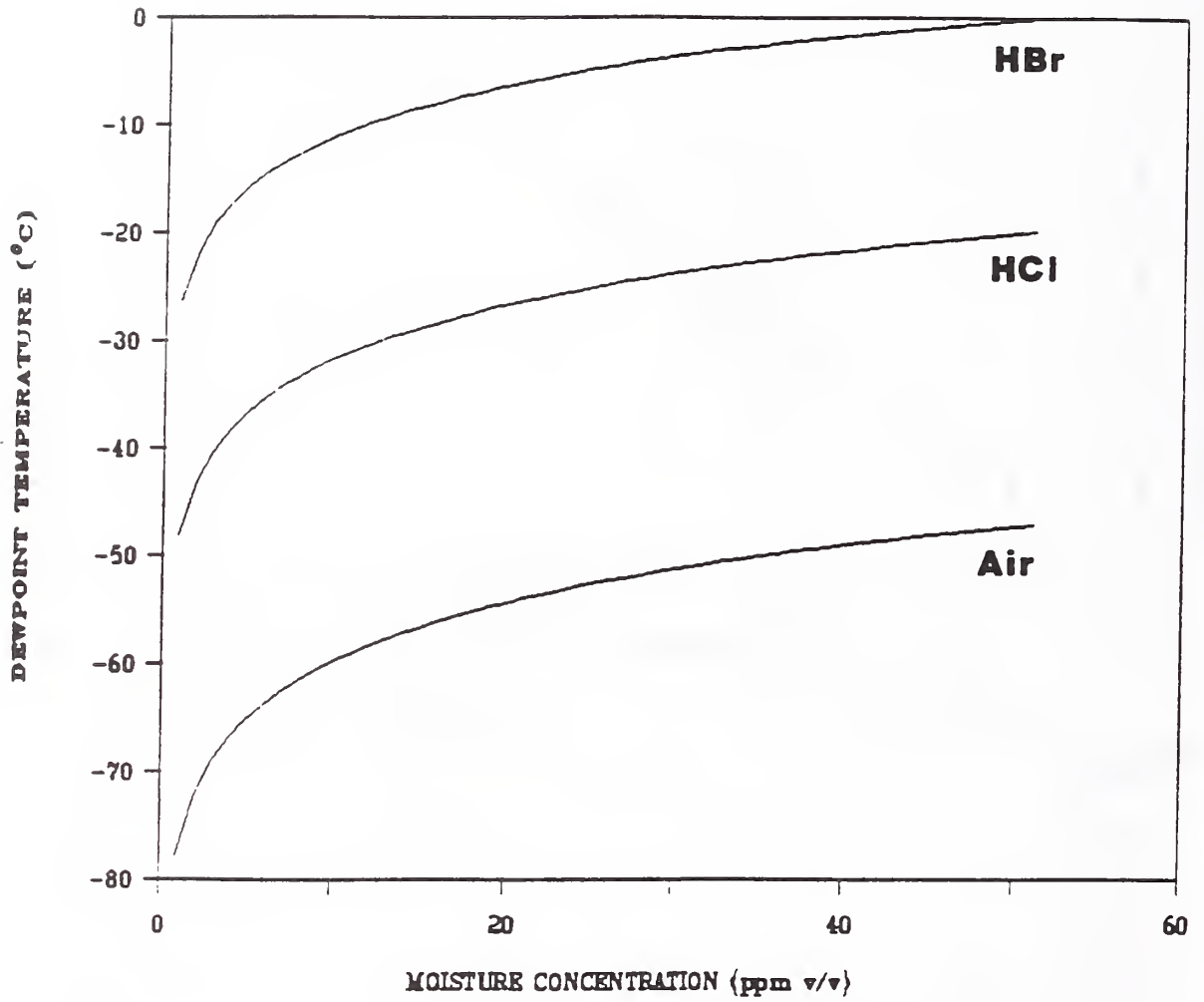


FIGURE 7 F.T.I.R. FILLING APPARATUS

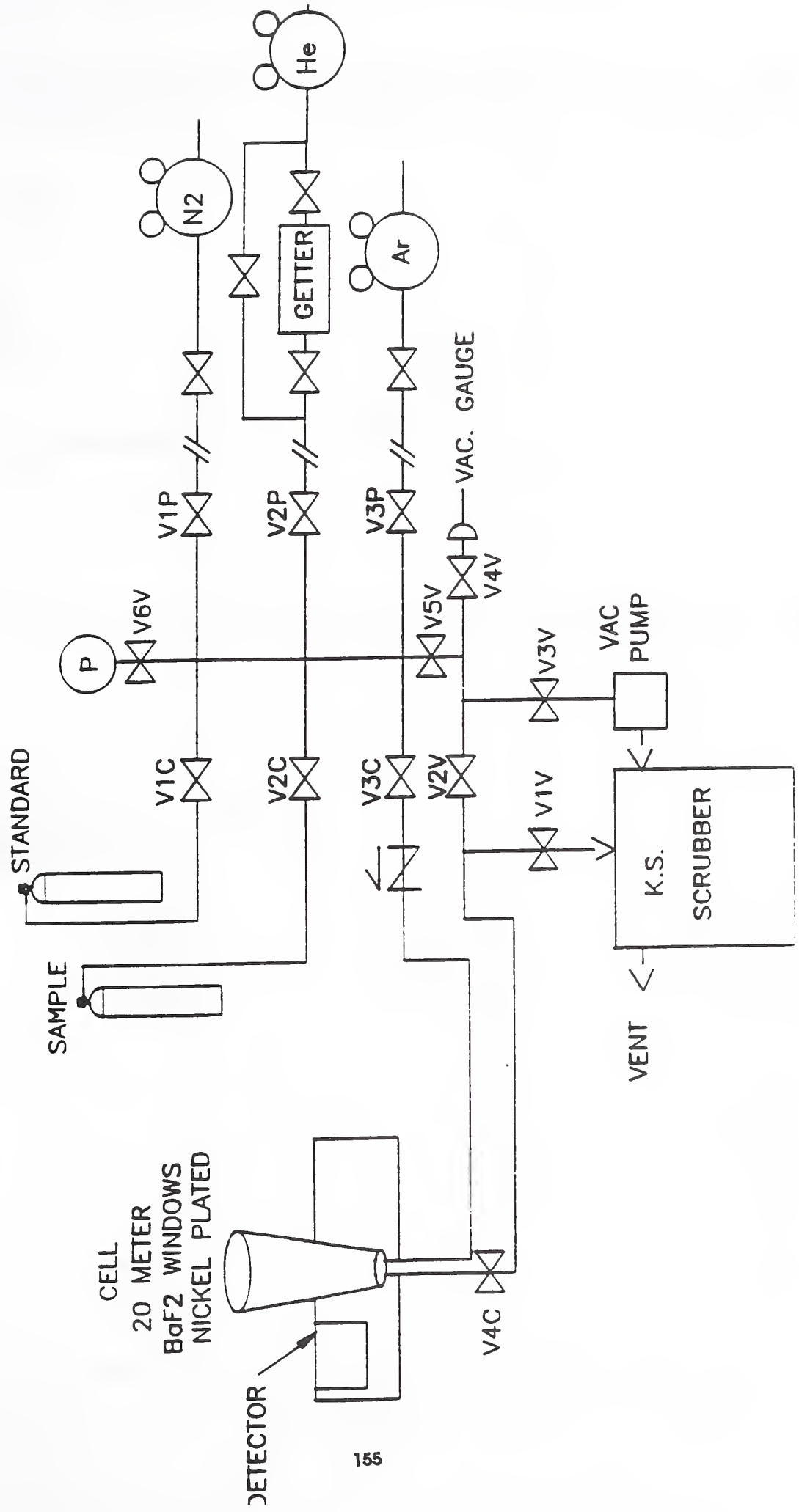


FIGURE 8

SPECTRA
 Cl_2

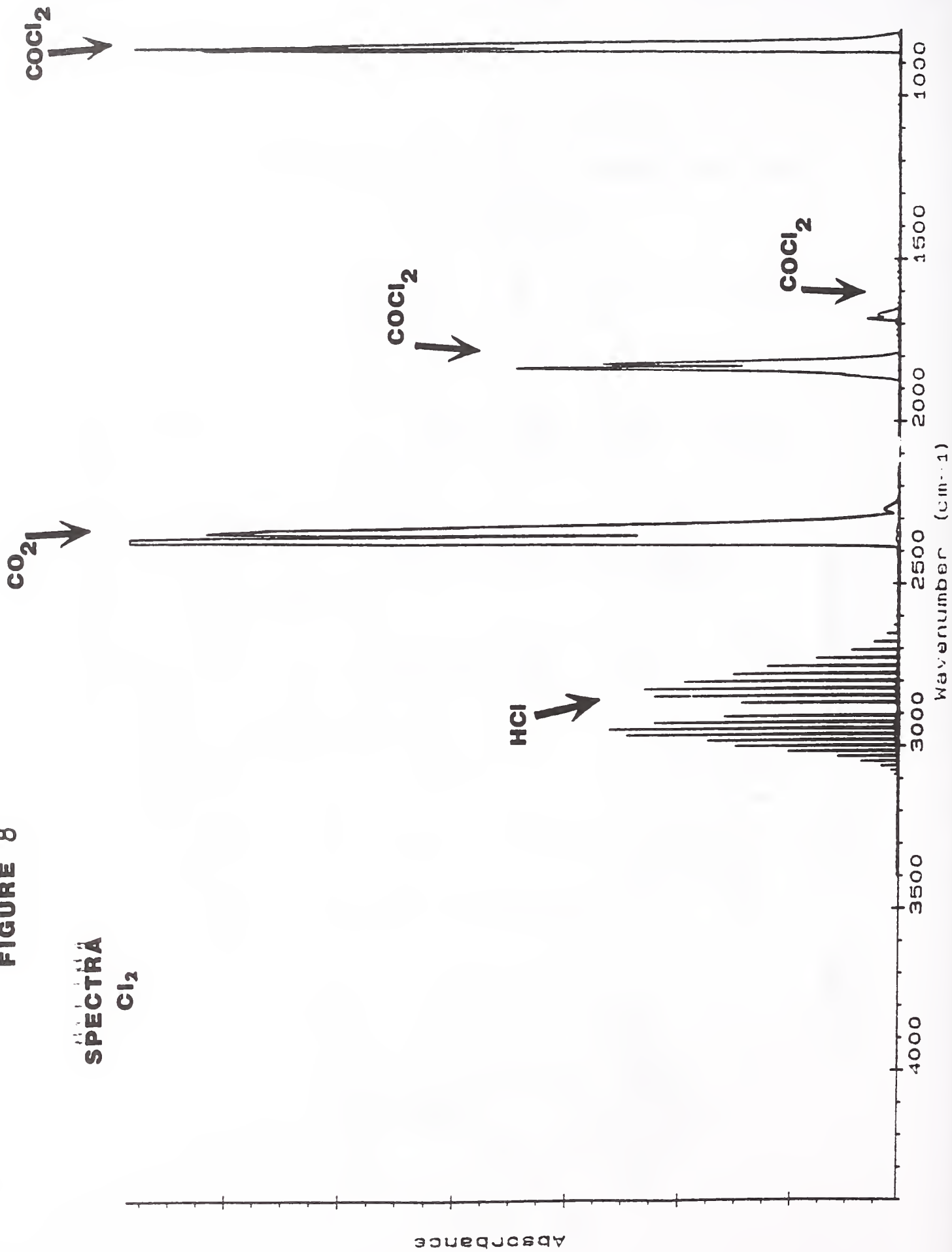
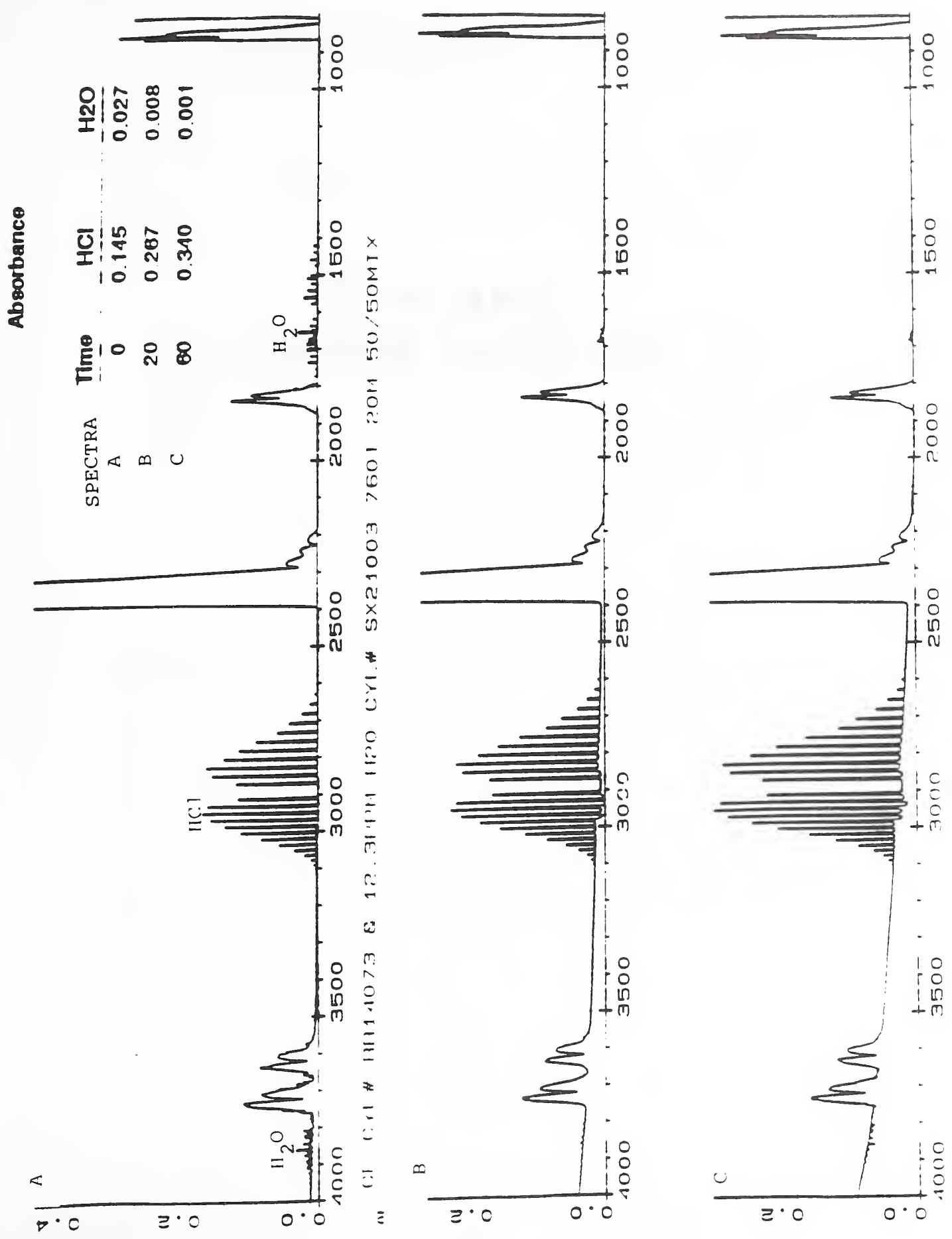


FIGURE 9



CELL # 1111-1073 & 12.34PH IPO CYL.# SX21003 7601 20M 50/50MTX

Session III

Moisture Effects

MILITARY SPECIFICATIONS AND LABORATORY SUITABILITY FOR MIL-STD-883 METHOD 1018

by

Alan R. Clark
Defense Electronics Supply Center
Dayton, OH

Abstract: A presentation of the general requirements for military laboratory suitability to MIL-STD-883 Method 1018, MIL-M-38510, MIL-H-38534, and MIL-I-38535. A listing of currently suitable laboratories to Method 1018 along with those seeking future suitability and the volume capabilities that they are approved for. The points of contact at D.E.S.C for the various military specifications listed above.

Key Terms: MIL-M-38510, MIL-H-38534, MIL-I-38535,
MIL-STD-883, Laboratory Suitability

1. INTRODUCTION

There are three major military specifications (MIL-M-38510, MIL-H-38534, MIL-I-38535), and one military standard (MIL-STD-883) that reference the Internal Water Vapor Content in microcircuits where laboratory suitability is required. Although each of the specifications is different in its approach to qualification and reliability, there are some similar requirements that they all share. These similarities and differences will be discussed further. The original specification was MIL-M-38510, that covered monolithic microcircuits, with MIL-H-38534, and MIL-I-38535 following to cover hybrid and some more complex devices. All of these specifications contain requirements for all qualification and quality conformance inspection testing to be done at facilities with government Laboratory Suitability. MIL-STD-883 method 1018 falls under these suitability requirements.

2. REQUIREMENTS

MIL-M-38510

Qualification Requirements: Section 4.4.2.4 "Groups C and D tests shall be as specified in method 5005 of MIL-STD 883."

METHOD 5005- Table IV. Subgroup 6- MIL-STD-883 method 1018
-5000 ppm maximum water @100°C
-Sample 3(0) or 5(1)

Quality Conformance Requirements: Section 4.5.5 "Group D inspection (package related tests) shall be in accordance with test method 5005 of MIL-STD-883 ..."

MIL-H-38534

Incoming Inspection for Adhesives: Section 4.3.8 "The polymeric adhesives used in hybrid microcircuit applications shall be subjected to and pass the evaluation procedures detailed in MIL-STD-883, Method 5011."

METHOD 5011- Section 3.8.7.1 "The packages shall be subjected to ambient gas analysis in accordance with MIL-STD-883 method 1018 procedure 1."

Qualification Requirements: Section 4.6.5.8 Internal water vapor
-Sample 3(0) or 5(1)
-5000 ppm @100°C
-if failure, test another sample, same size

Quality Conformance Requirements: Section 4.7.3.3 Group C Table XIc
-method 1018 @100°C
-Sample 3(0) or 5(1)

MIL-I-38535

Qualification Requirements: Section 3.5.2.2 Qualification test plan "All demonstration vehicles must be screened to requirements of 4.3 and tested in accordance with tables III, IV, V, VI..."

Table VI Group D -subgroup 6-method 1018
-5000 ppm @100°C
-Sample 3(0) or 5(1)

Technology Conformance Requirements: Section 4.4.2.4 "Group D inspection shall include package related tests which are performed periodically". Same as table VI Group D above.

3. PROCEDURE

There is a standard procedure for obtaining Laboratory Suitability for testing military microcircuits. It is used for all types of test methods included in MIL-STD-883. Test method 1018 has a few additional steps to standard procedure which are included below.

DESC PROCEDURE FOR COMMERCIAL LABORATORY SUITABILITY:

1. Manufacturer requests, to DESC, the use of the laboratory facilities and the applicable test methods.
2. The request is forwarded to Rome Labs to receive a correlation test packet with samples to test.
3. When samples are tested they are to be returned to Rome Labs with the applicable data.
4. Laboratory then submits to DESC procedures and forms which include the DESC forms 2, 36, 695. These forms are suitability request, test equipment list, and system calibration procedures.
5. DESC then audits the facility for the requested methods.
6. Written notification of suitability issued.
7. Laboratory performs requested testing and records on DESC form 36F or equivalent.
8. Laboratory submits annual summary report of testing on military parts to DESC.
9. Laboratory is reaudited, typically every two years to maintain Laboratory Suitability.

POINTS OF CONTACT

MIL-M-38510/MIL-I-38535

ALAN CLARK: DESC-EQM

(513) 296-6270

MIL-H-38534

RICK BARKER: DESC-EQC

(513) 296-8714

4. STATUS OF COMMERCIAL LABORATORIES SUITABLE
FOR INTERNAL WATER VAPOR

COMMERCIAL LABORATORIES HAVING DESC SUITABILITY

- | | |
|--|--|
| 1) AT&T
Bell Laboratories
555 Union Blvd.
Allentown, PA 18103
0.01 - 20.0 ccm | 4) Northrop Corporation
P.O. Box 5032
Hawthorne, CA 90251-5032
0.1 - 4.0 ccm |
| 2) Atlantic Analytical Lab
P.O. Box 220, Bldg. 4
Salem Industrial Park
Whitehouse N.J. 08888
0.01 - 20.0 ccm | 5) Oneida Research Services, Inc.
One Halsey Road
Whitesboro, NY 13492
0.01 - 20.0 ccm |
| 3) BNR Europe Limited
London Road
Harlow, Essex 17 9NA
United Kingdom
0.01 - 10.0 ccm | 6) Pernicka Corporation London
112 Racquette Drive
Fort Collins, CO 80524
0.01 - 20.0 ccm |

COMMERCIAL LABORATORIES AWAITING DESC SUITABILITY

- | | |
|--|---|
| 1) DESC-QTF
1507 Wilmington Pike
Dayton, OH 45444-5630 | 2) Seal Laboratories
250 North Nash Street
El Segundo, CA 90245 |
|--|---|

**HERMETICITY SPECIFICATIONS AND THEIR EFFECTS
ON METHOD 1018**

by

A. Dermarderosian, Sr.
Raytheon Company
Sudbury, MA

OUTLINE

- PURPOSE
- REVIEW OF METHOD 1014 HERMETICITY LIMITS
 - FIXED METHOD HELIUM LEAK TESTS
 - FLEXIBLE METHOD HELIUM LEAK TESTS
 - FIXED METHOD OF RADIOISOTOPE LEAK TESTS
- MOISTURE INGRESS RATES IN PACKAGES
- CONCLUSIONS
- SUMMARY OF ROME LAB/RAYTHEON CONTRACT WITH RECOMMENDED 1014 CHANGES.

PURPOSE

TO CRITIQUE THE HERMETICITY REQUIREMENTS OF THE PRESENT MILITARY STANDARD (MIL-STD-883D, METHOD 1014.9) AS IT MAY AFFECT THE RESULTS OF THE MAXIMUM INTERNAL MOISTURE REQUIREMENTS OF METHOD 1018 RGA TESTS.

MOISTURE PENETRATION TIMES

VOLUME CC	METHOD 1014.9	MAX. ALLOWABLE LEAK RATE (L) ATM CC / SEC ; AIR	TIME TO REACH 5000PPM AVG. AMB. =10,000PPM (7.6 TORR)
<0.05 R1=5E-8cc/sec	FIXED He (0.049 CC) (0.01 CC)	1E-7 cc/sec	HOWL & MANN 74 HRS
		4.5E-8 cc/sec	EXPERIMENTAL 336 HRS
≥0.05-<0.5 R1=5E-8cc/sec	FIXED He (0.49 CC) (0.05CC)	2.2E-7 cc/sec	338 HRS
		7E-8 cc/sec	108 HRS
≥0.5-<1.0 R1=1E-7cc/sec	FIXED He (0.9 CC) (0.5 CC)	5.4E-7 cc/sec	253 HRS
		4E-7 cc/sec	190 HRS
≥1.0-<10.0 R1=5E-8cc/sec	FIXED He (9.9 CC) (1.0 CC)	1.2E-6 cc/sec	1251 HRS
		3.6E-7 cc/sec	421 HRS
≥10.0-<20.0 R1=5E-8cc/sec	FIXED He (19.9 CC) (10.0 CC)	1.1E-6 cc/sec	2743 HRS
		8E-7 cc/sec	1895 HRS
			EXPERIMENTAL 336 HRS 110 HRS
			2554 HRS 411 HRS
			2715 HRS 1509 HRS
			19000 HRS 3840 HRS
			46,400 HRS 24,690 HRS

MOISTURE PENETRATION TIMES

VOLUME CC	METHOD	MAX. ALLOWABLE LEAK RATE (L) ATM CC / SEC ; AIR	TIME TO REACH 5000PPM AVG. AMB. =10,000PPM (7.6 TORR)
≤0.01	1014.9 FLEXIBLE He (0.01 CC) (0.005CC)	5E-08	HOWL & MANN 30 HRS 15 HRS EXPERIMENTAL 96 HRS 48 HRS
>0.01-≤0.4	FLEXIBLE He (0.4 CC) (0.015 CC)	1E-07	606 HRS 23 HRS
>0.4 - ≤20.0	FLEXIBLE He (19.9CC) (0.41CC)	1E-06	3017 HRS 62 HRS 49,128 HRS 1012 HRS

MOISTURE PENETRATION TIMES

VOLUME CC	METHOD 1014.9	MAX. ALLOWABLE LEAK RATE (L) ATM CC / SEC ; AIR	TIME TO REACH 5000PPM AVG. AMB. =10,000PPM (7.6 TORR)
<0.01	RADIOISOTOPE (0.009 CC) (0.005CC)	1.7E-08	HOWL & MANN 80 HRS 45 HRS EXPERIMENTAL 149 HRS 82 HRS
≥0.01-≤0.4	RADIOISOTOPE (0.39 CC) (0.01 CC)	8.5E-08	696 HRS 18 HRS 2942 HRS 175 HRS
>0.4	RADIOISOTOPE (19.9CC) (0.41CC)	8.5E-07	3549 HRS 73 HRS 52,100 HRS 1017 HRS

CONCLUSIONS

- PRESENT TEST PROCEDURES A1, A2 AND B HAVE INCONSISTENT AIR LEAK RATE REQUIREMENTS
 - A FACTOR OF TEN (10) FOR SAME VOLUME (< 0.05 CC)
 - A FACTOR OF TEN (10) FOR NEARLY THE SAME VOLUME (~ 0.4 CC)
- ALTHOUGH DEVICES CAN PASS THE REQUIREMENTS OF THESE PROCEDURES, ENOUGH MOISTURE CAN PENETRATE LEAKERS BELOW THESE LIMITS WHICH CAN RESULT IN FAILURE TO PASS THE LIMITS OF METHOD 1018.

CONCLUSIONS (CONT'D)

- THESE INCONSISTENCIES AND INADEQUACIES HAVE BEEN AT THE ROOT OF MANY PROBLEMS BETWEEN SUPPLIERS AND CUSTOMERS
 - THE INCONSISTENCIES BETWEEN FINE LEAK TEST PROCEDURES CAN RESULT IN A LEGAL STANDOFF.
 - THE INADEQUACIES OF THE LIMITS USED IN THE FINE LEAK TEST PROCEDURES CAN RESULT IN COSTLY PRODUCTION SHUTDOWNS.

- BOTH THE LEAK TEST PROCEDURES AND LIMITS MUST BE CHANGED IN ORDER TO REDUCE THE COST IMPACT NOTED ABOVE.

SUMMARY OF ROME LAB/RAYTHEON STUDY FOR METHOD 1014

- ELIMINATE FIXED HELIUM PROCEDURE
 - COMPROMISE/INCONSISTENT
- ADD BACKFILL TRACER GAS PROCEDURE
 - ALLOWS TIGHTER LIMITS ON LARGER VOLUME PARTS
- USE MOLECULAR FLOW EQUATION FOR RADIOISOTOPE TEST
 - CORRELATION BETWEEN HELIUM AND RADIOISOTOPE
- ALLOW HIGH TEMPERATURE BAKE AFTER BOMB
 - ALLOWS FOR MULTIPLE TESTING AND INCREASED SIGNAL TO NOISE RATIO.
- MAXIMUM ALLOWABLE LEAK RATE FOR ALL VOLUMES LOWERED TO 1×10^{-8} ATM CC/SEC; AIR

HERMETIC PACKAGE MOISTURE CONTROL AT HARRIS SEMICONDUCTOR

by

Robert K. Lowry
Harris Semiconductor
Melbourne, FL

Abstract: This paper summarizes operational and technical experiences gained from ten years of running an in-house internal water vapor (IWV) measurement service. A facility geared for large sample volumes can provide IWV measurements to its in-house customers at lower cost and with faster cycle time than commercial laboratories. This enables assurance of low moisture in hermetic products using statistical process control based on statistically significant sample sizes. True process control of IWV, and rapid attack on control problems when they do occur, is difficult to achieve when relying on contract laboratories.

INTRODUCTION

Controlling moisture in hermetic packages has been a priority for Harris Semiconductor since metallization corrosion was first known as a device failure mechanism. Concern for moisture control was driven beginning in the 1970's by the use of thin nichrome film less than a few hundred angstroms thick in microcircuits fuse or resistor structures [1].

Thin nichrome is especially prone to corrosion. Water is always the necessary (though not always sufficient) condition for corrosion to occur. Under the right conditions, corrosion can occur even when only a few monolayers of chemisorbed water have access to device structures made of nichrome [2]. This fact, combined with the broader concerns for preventing corrosion of aluminum interconnect metal and package metallization [3-7], compelled the development and maintenance of a robust moisture control plan.

INTERNAL WATER VAPOR (IWV) ANALYSIS OPERATIONS

At Harris Semiconductor the Analytical Services Laboratory provides Residual Gas Analysis (RGA) measurements of hermetic package internal water vapor content. The laboratory has operated mass spectrometers for this purpose since 1981. Defense Electronic Supply Center (DESC) suitability for MIL-STD Test Method 1018 [8] IWV testing was attained in 1983. Since that time, 96 percent of

all package analysis needs have been fulfilled by in-house measurement. In some years, no samples were submitted to outside laboratories.

Package Styles Analyzed

The mix of IC packages received at the in-house facility consists of Cerdip (glass seal), braze (metal lid), and weld-seal (metal cans). Sealing ambients are dry natural air or synthetic air, forming gas or high-purity nitrogen, and high-purity nitrogen, respectively. Eutectic die attachment accounts for about 75 percent of the samples. The remainder contain organic die attach materials requiring a pre-analysis bake. Virtually all package styles have an internal cavity volume <0.2 cc.

Character of the Sample Population

Figure 1 shows that the types of samples analyzed by the in-house facility are almost evenly divided among three main categories:

1. Shipment Lot Qualifications (35 percent)-- Includes samples submitted by outgoing quality functions for IWV testing required by customer specification. As supplier/customer relations evolve to be more trust-oriented, customers will be more willing to accept product from statistically-controlled sealing processes (the next category), and the volume of samples in this category will shrink.

2. Manufacturing Process Control (32 percent)-- Samples in this category are taken at specified intervals from each hermetic sealing operation (furnace, welder, etc.). They are analyzed usually within 24 hours (often on the same day) and the results plotted on control charts. Charts govern all sealing processes. As long as IWV content remains in control for a given sealing operation the process keeps running. All sealed product from any such process is deemed to be in control with respect to IWV content. Out-of-control action plans govern events if a moisture reading violates control limits. These plans generally involve sampling product sealed before and after the out-of-control reading to time-bracket statistically significant moisture events. At the same time, process flows and equipment status are reviewed for assignable causes.

3. Engineering Sustaining (30 percent)-- Includes samples submitted by assembly engineering during process improvement work. Many of these parts are from statistically designed experiments being run as part of continuous improvement studies.

4. Other (3 percent)-- Includes field returns and special studies like the very long term hermeticity study described later in this paper.

Ten Years of In-House Analysis Operations

Figure 2 shows the annual volume of IWV measurements at commercial laboratories and at the in-house facility since 1976. Some characteristics of the analysis operations are as follows:

1. Pre-1982-- Before start-up of the in-house facility, 100-300 packages per year were analyzed at commercial laboratories. Package moisture control was surmised from this small sample volume.
2. 1982-1985-- DESC suitability for in-house IWV measurement was achieved in 1983. A steady rise in sample volume to 3000 packages per year occurred. The volume of samples sent to commercial laboratories was steady or slightly higher than in prior years. This was due to check sampling as internal customers built confidence in data from the in-house facility.
3. 1986-1988-- Sample volume in-house stayed level while sample volume sent to commercial laboratories dropped to zero. The flat in-house volume reflects the one-shift operating capacity of the RGA equipment. The decline in samples sent outside reflects full confidence of internal customers in the internal facility.
4. 1988-1991-- Sample volume in-house soared, to a high of 8322 packages in 1991. In 1988 General Electric Solid State was merged into Harris Semiconductor. The merger quadrupled the number of hermetic assembly sites requiring moisture monitoring, from two to eight. Accordingly, a second shift was added to the RGA facility. This more than doubled the analysis capacity to accommodate the volume of hermetic product being sealed by the "new" company. During this period the number of samples sent to commercial laboratories remained nil except during 1990, when some were analyzed externally to help resolve measurement anomalies described later in this paper.
5. 1992-- Sample volume dropped by 33 percent, reflecting the consolidation of hermetic assembly sites from eight to three. Second-shift machine operation was also eliminated. The machine operated at a one-shift sample capacity greater than that prior to 1988, due to improvements in operations and scheduling.

Analysis Logistics

The in-house facility allots blocks of time to the various sample categories. Samples arrive on planned schedules, permitting rapid cycle times. Eighty percent of all units are tested the same day as received. More than 90 percent are tested within 24 hours. This enables real-time information for statistical process control and lot clearance. Astute use of air express shipment services enables IWV data to be returned to overseas locations by fax

generally within 6 working days.

Benefits of the In-House Facility

Results from ten years of in-house RGA operations have been gratifying. In particular:

1. Process control is established and maintained.
2. Only compliant product is shipped to customers.
3. Measurement cycle time is fast.
4. Per sample cost is low.
5. A significant technical resource is immediately available to production and engineering.
6. A worrisome reliability problem of the 70's is relegated to a matter of process control.

Economy of scale in a dedicated facility enables low analysis cost. In 1991 the cost was \$8.77 per package sample. With the intensity of surveillance and the statistical control of sealing processes enabled by in-house RGA testing, not one field failure due to sealed-in moisture has been known to occur during the entire ten-year period.

CHALLENGES, DISCOVERIES, AND ENLIGHTENMENTS

The task of measuring water vapor, the most non-ideal of all gases, is challenging and even surprising on occasion. Some items of particular interest encountered by the in-house facility are described here.

The Bicycle Seat Phenomenon

With the business merger referred to earlier, the mix of part types arriving at the IWV facility changed suddenly and dramatically. One significant change was much larger numbers of packages containing organic die attach material. Such parts require a pre-analysis bake at $100 \pm 5^{\circ}\text{C}$ for 12-24 hours. To accommodate the greatly increased number of units requiring this bake, thrifty, resourceful personnel replaced the small air oven being used with a surplus infrared (IR) oven from equipment storage, at remarkably low cost (zero!).

However, when pre-analysis baking in this oven commenced, an increase in the IWV content of organic die-attach units occurred. Some parts even failed the 5000 parts per million by volume (ppmv) moisture limit, delaying some product shipments. The product had never previously failed for IWV content.

Table 1 summarizes IWV data and the associated hydrocarbon content for a common group of organic die attached product baked in various ways. It is clear that IR baking elevated both IWV and hydrocarbon content. Though the IR bake oven's calibrated thermometer indicated baking temperature of exactly 100°C, a Cr-Al thermocouple placed on the floor of the oven indicated the temperature there to be 151°C. IR baking actually produced an "out-of-spec" condition which artificially raised sample temperatures. Organic die attach materials were heated to well above 100°C, outgassing quantities of moisture that would not outgas at 100°C. The elevated level of hydrocarbon offgas products in the IR baked packages confirms this observation.

The RGA facility dubbed this incident the bicycle seat phenomenon. When a bicycle with a black seat is parked outdoors in the sun for any length of time, the seat gets quite hot, even on a cool day. On a cloudy day or indoors, the temperature of the seat does not rise above that of its surroundings. The dark seat absorbs radiant energy from the sun, elevating its temperature well above that of its surroundings. The same thing happens to units baked under IR energy. Dark-colored ceramic and thermally conductive metal surfaces absorb radiant IR energy, elevating the effective temperature of the sample above the 100°C required for pre-analysis baking.

Replacing the IR oven with a standard convection oven resolved the pre-analysis bake moisture problem.

The Low-Z Gas Problem

More than 5% hydrogen and helium in packages has been observed to affect IWV values.

1. One assembly site produced braze sealed metal lid packages in a forming gas environment. Normally the level of hydrogen in the forming gas was about 5%, and this product easily passed IWV tests. However, a series of product began arriving which failed IWV tests, delaying product shipments. The wet product had unusually high levels of hydrogen, in the 20-30% range. In an urgent effort to find acceptable product, the assembly site contracted for IWV tests from commercial laboratories, with mixed results. Some units passed, others continued to fail. It was soon noticed that results were laboratory-specific, as shown in Table 2.

A common group of units was sub-divided and measured at Harris and at three commercial laboratories. Results from Commercial Lab A were about the same as those from the in-house Harris facility. However, when measured at Commercial Labs B and C, the product met specification, Despite this disagreement on IWV content, all four laboratories agreed that the parts contained hydrogen above 20%. When similar parts containing lower levels of hydrogen (about 5%)

were tested, they not only passed the moisture requirement at all four laboratories, all measurement sites were in general agreement that moisture was below 1500 ppmv.

Elevated hydrogen levels clearly interfered with measurements at Harris and at Commercial Lab A. The interference unnecessarily delayed product shipment. However, the ultimate conclusion was that all product actually contained acceptable levels of moisture.

This problem was resolved by controlling forming gas composition for sealing to keep hydrogen $\leq 5\%$, since at this level there is no measurement interference. This was the best solution, since there was no practical reason for higher levels of hydrogen in the sealed product. If there were practical reasons for hydrogen to exceed 5%, the mass spectrometer would have to be calibrated in humidified forming gas mixtures with hydrogen levels comparable to the cavity ambient, in place of pure nitrogen normally used for calibration.

2. The same anomaly has been observed with packages containing $> 5\%$ helium. Helium added to the sealing ambient, and thereby incorporated in the package cavity, can be useful for hermeticity testing. But helium is not commonly used in package sealing. As for hydrogen, it is necessary to use humidified helium mixtures requiring extra calibration time and effort, when helium is known to be an interferent.

Very Long Term Hermeticity

Long term hermetic package integrity has always been somewhat uncertain. Time constants for moisture ingress show that a 0.01 cc semiconductor package, meeting a maximum air leak rate of $1E-7$ atm cc/sec air would attain 500 ppmv moisture in its cavity in 2.3 days and 5000 ppmv moisture in its cavity in 32 days.[2]

The in-house facility cooperated in a hermeticity study initiated by the Reliability Analysis Center. Dozens of still-functional IC's, with date codes from 1974-1986, were collected during aircraft avionics system upgrades and returned for IWV analysis as part of the Microcircuit Field Failure Return Program. [9]

Standard leak test results on the units prior to the RGA work are shown in Table 3. Forty-eight of 72 parts failed fine leak test.

Results of RGA analysis on the entire group of 72 units are summarized in Table 4. Of the full group of units, 43 contained undetectable moisture < 100 ppmv, 23 contained detectable moisture < 5000 ppmv, and 6 contained moisture > 5000 ppmv. Of the 48 fine leak failures, 21 contained undetectable moisture < 100 ppmv, 22 contained detectable moisture < 5000 ppmv, and 5 contained moisture < 5000 ppmv.

From an evaluation of cavity ambient gases other than water vapor (carbon dioxide, nitrogen, argon), only one unit (a fine leak failure) actually had air ambient composition.

These results indicate that the fine leak failures did not really leak. Parts remained hermetic, at least from the standpoint of water vapor ingress, for as long as 18 years.

Process Control

Statistical approaches enabled by real-time measurements at the in-house facility are powerful means of controlling processes to avoid line shutdowns, shipment delinquencies, and quality uncertainty.

Figure 3 shows a 20-month portion of an actual process control chart for a dual in-line package sealing furnace. The center line for the process (\bar{x}) is 716 ppmv, and the 3σ upper control limit is 3580 ppmv. The process operated in control until September 1992, when several out-of-control and two out-of-specification readings occurred. Searches for assignable causes began immediately. Package assembly process and equipment variables as well as piece part performance were examined in statistically designed experiments. No equipment or process variables gave statistically significant results.

However, a study of the piece parts revealed that a change in raw materials was the assignable cause for the increased moisture. Lids and bases from a second supplier began to enter the process during 1992. Table 5 summarizes IWV results measured on Supplier A and Supplier B piece parts. The "null hypothesis" that IWV in materials from Suppliers A and B is the same can be rejected with 95% confidence. The conclusion from the controlled experiments is that the assignable cause for the rise in IWV was the entry of piece parts from Supplier A into assembly production.

"Check It At Another Lab!"

It is only natural for Engineering or Quality functions to split lots and send them to a second RGA facility to "double-check results".

Everyone's first reaction to the out-of-control readings in Figure 3 was to question the operation of the mass spectrometer, and, of course, to request check analyses. However, statistical data on mass spectrometer variability control was reviewed. Chronological plots of IWV data in other part types from different assembly sites, analyzed at the same time as the out-of-control parts and showing no IWV increases, were also reviewed. These data quickly established that the mass spectrometer was operating reliably and that the out-of-control points in the control chart were

statistically significant indications of a loss of process control. This enabled quick-start of an organized search for assignable cause, using the same mass spectrometer that produced data for the control charts. This averted the time, expense, and inevitable confusion of engaging a second machine to work on the problem.

In our experience, the likelihood of check analysis requests follows a rigid, one-sided step function. That is, the probability is very high that a check analysis will be requested if one or more parts in a group reads >5000 ppmv (or more generally, 1 ppmv over any SPC control limit or specification limit). The high probability holds even if one part reads 5001 ppmv and all others read 5000 ppmv. The probability of a check analysis request is zero when all parts in a group measure <5000 ppmv. Zero probability holds even if every part in the group reads exactly 5000 ppmv.

CONCLUSION

This paper has summarized operational and technical experiences from ten years of running an in-house IWV facility. A facility geared for large sample volumes provides IWV services to in-house customers at lower cost and with faster cycle time than commercial laboratories. This assures low moisture in hermetic products using statistical process control based on significant sample sizes. True process control of IWV, and rapid attack on control problems when they do occur, is difficult to achieve when relying on contract laboratories.

ACKNOWLEDGMENTS

The following people are gratefully acknowledged for their work, which has contributed much to the success of the in-house RGA facility and which made this paper possible.

Dr. Jack Linn...for sustaining and advancing the technical capability of the in-house RGA facility.

Josh Daar.....for analyzing package after package after package.

Dave Decrosta...for teaming his assembly engineering expertise with the RGA facility for (1) knowledgeable engineering of low-moisture sealing technologies, and (2) resolving out of control moisture events like that in Figure 3.

REFERENCES

1. Paulson, W., 11th Annual Proceedings, International Reliability Physics Symposium, April, 1973.
2. DerMarderosian, A., Proceedings RADC/NBS International Workshop, Moisture Measurement and Control for Microelectronics (IV), November, 1986.
3. Kolesar, S., 12th Annual Proceedings, International Reliability Physics Symposium, April, 1974.
4. Harman, G., "Wire Bonding in Microelectronics", monograph, International Society for Hybrid Microelectronics, 1989.
5. Lowry, R.K., Van Leeuwen, C.J., Kennimer, B.L., and Miller, L.A., 16th Annual Proceedings, International Reliability Physics Symposium, April, 1978.
6. Uhlig, H.H., Corrosion and Corrosion Control, John Wiley & Sons, 1971.
7. Shumka, A., and Piety, R., 13th Annual Proceedings, International Reliability Physics Symposium, April 1975.
8. MIL-STD 883D, Test Method 1018.2.
9. Dylis, D.D., Proceedings of the 18th Annual International Symposium for Testing and Failure Analysis, October, 1992.

TABLE 1

I WV RESULTS AFTER CONVECTION OVEN AND INFRARED
OVEN PRE-ANALYSIS BAKES

	NO BAKE	CONVECTION OVEN BAKE	INFRARED OVEN BAKE
Effective Bake Temp	25°C	100°C	151°C
Average Moisture Content, ppmv	650	550	2240
Average Hydrocarbon Content, ppmv	855	710	2750

TABLE 2

MOISTURE CONTENTS OF HIGH-HYDROGEN UNITS MEASURED AT FOUR DIFFERENT LABORATORIES

	HARRIS	LAB A	LAB B	LAB C
Average Moisture Content, ppmv	11200	13650	1510	610
Average Hydrogen Content, %	30.0	29.0	20.6	31.0

TABLE 3

LEAK TEST RESULTS, LONG TERM HERMETICITY STUDY

Pass both fine and gross leak test..	24
Fail gross leak test.....	4
Fail fine leak test.....	48

TABLE 4

MOISTURE LEVELS, LONG TERM HERMETICITY STUDY

	All 72 Units	48 Fine Leak Failures
<100 ppmv.....	43	21
Between 100 and 5000 ppmv....	23	22
>5000 ppmv.....	6	5

TABLE 5

MOISTURE LEVELS INHERENT IN MATERIALS FROM TWO DIFFERENT PIECE PART SUPPLIERS

Supplier	Bases, sealed base-to-base		Lids, sealed lid-to-lid	
	A	B	A	B
Moisture, ppmv	1581	676	1796	647
Std deviation, ppmv	1484	459	1476	445
p statistic	0.0108		0.0010	

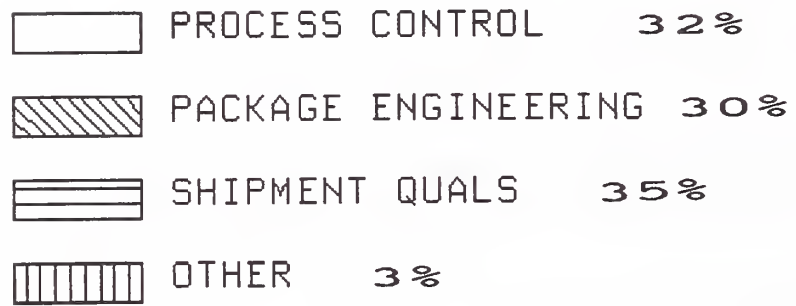
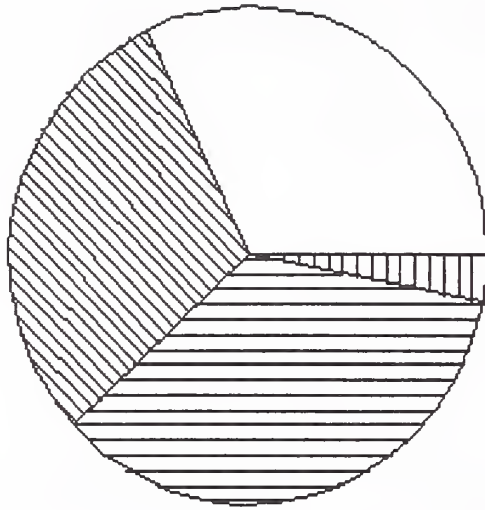


Figure 1. Character of the sample population at in-house IWV facility.

MASS SPEC ANALYSIS

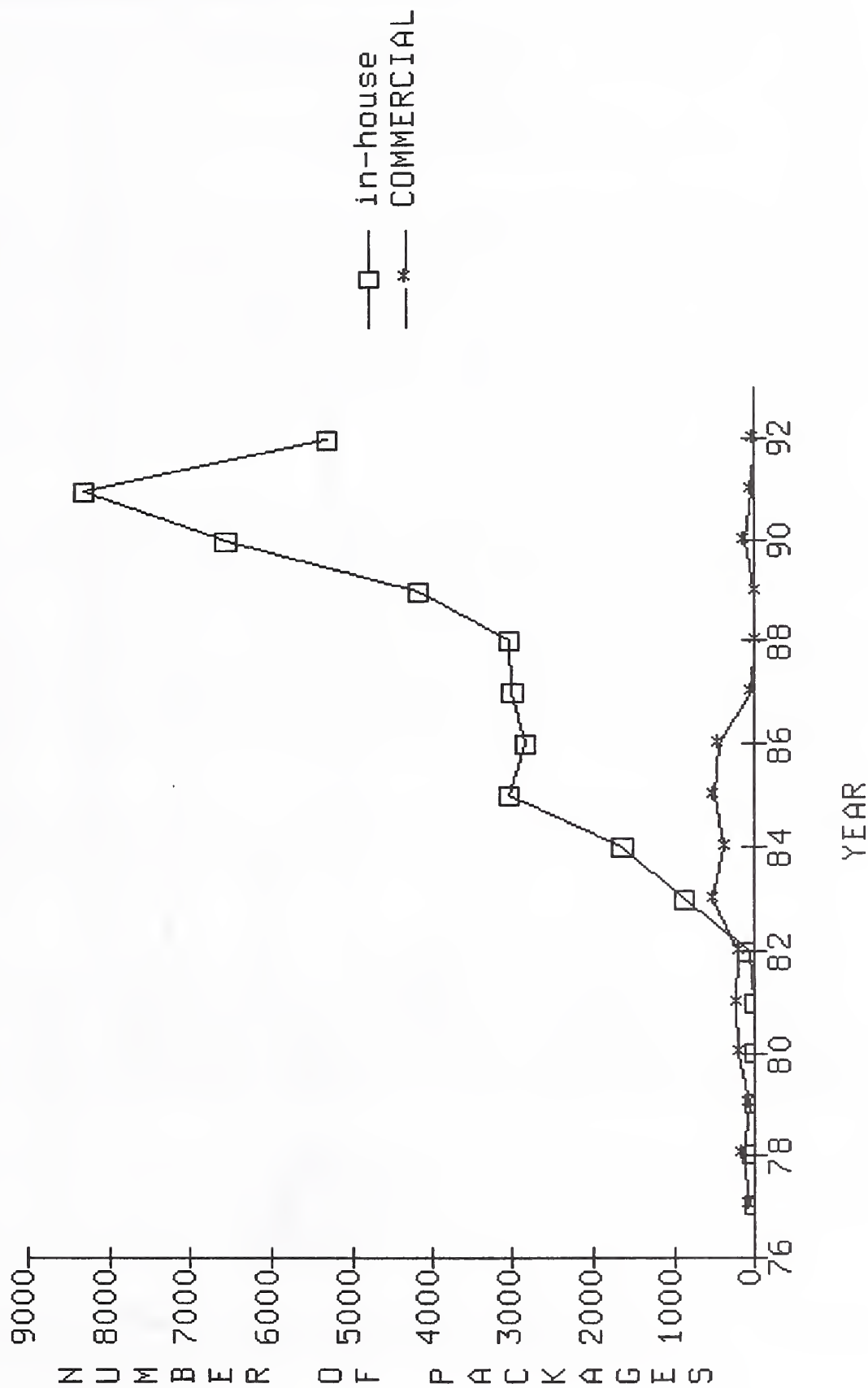


Figure 2. Annual volumes of IWV samples run at in-house and commercial service laboratories.

FURNACE F3 MOISTURE

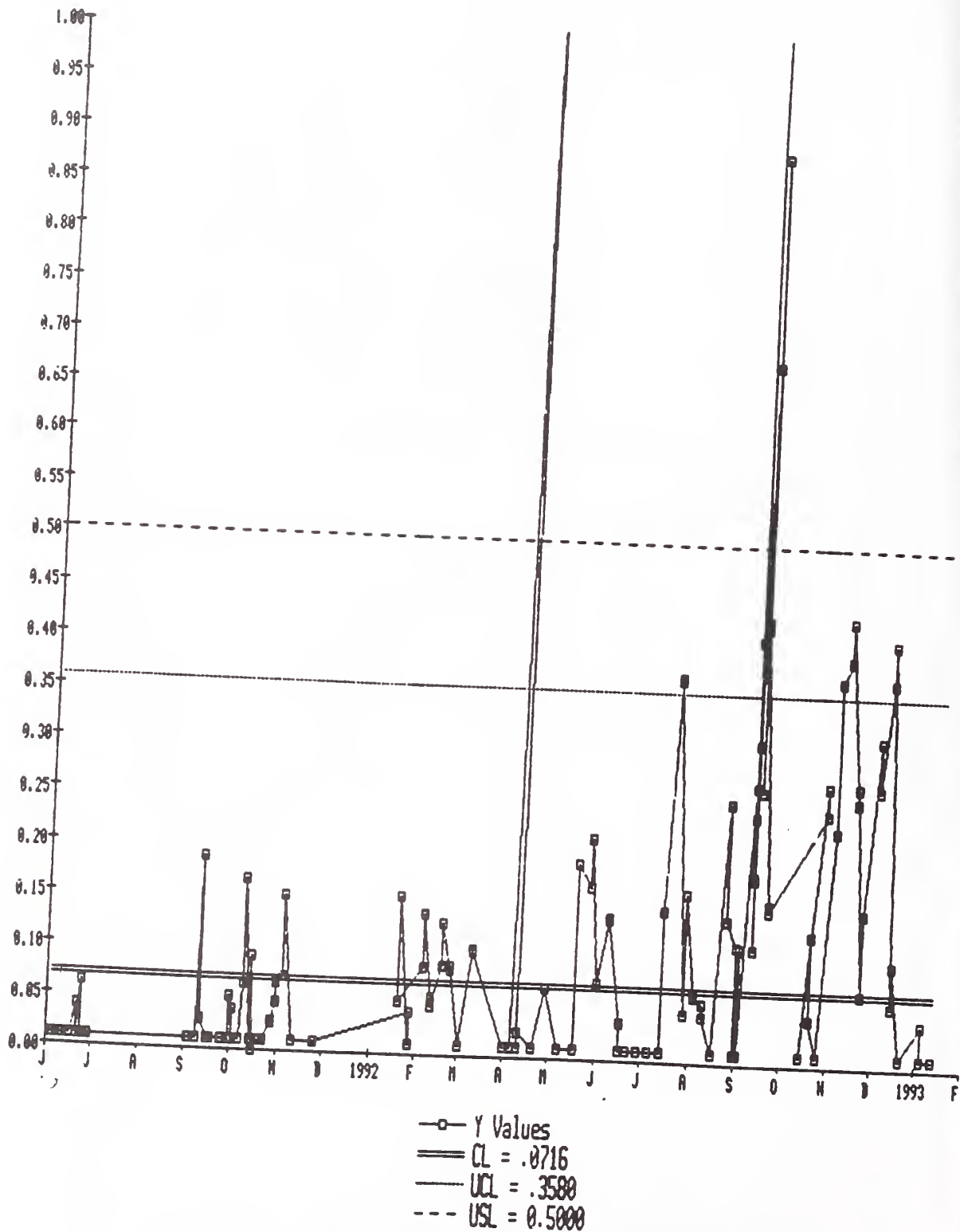


Figure 3. Sealing furnace process control chart.

IMPROVING DEVICE RELIABILITY THROUGH RESIDUAL GAS ANALYSIS (RGA)

Arun Kumar, Ph.D. and James O. McClain, Jr.
SEAL Laboratories
250 North Nash Street
El Segundo, California 90245

Abstract: Residual Gas Analysis provides excellent information about the gaseous atmosphere within the cavity of sealed packages. Although the water vapor content is of greatest importance, the presence of other gases and their amounts provide additional information regarding the chemical reactions that have occurred within the package, subsequent to sealing. The reliability of devices is therefore directly dependent on the package atmosphere for time dependent degradation mechanisms like corrosion, electromigration, ionic migration causing surface electrical leakage, etc.. The RGA data thus are not only useful for quality control but also extremely valuable for failure analysis.

During RGA testing, moisture, nitrogen, oxygen, argon, carbon dioxide, hydrogen, helium, fluorocarbons, methane and ammonia are normally reported. However, a review of the complete spectrum from 1 to 100 atomic mass units (AMU) reveals if any "other" gases are present in the package. Once the gases present in the as-sealed packages are analyzed, baseline data are created. Exposure of the package to temperature will continue to show a change in gas composition until the chemical reaction occurring within the package, if any, is completed. This data can then assist in determining the appropriate baking procedures (temperature and time) required for a given device prior to lidding. In most cases, vacuum assisted or dry nitrogen baking of the devices prior to lidding at maximum permissible temperature shortens the time required for baking.

The significance of each gas, constituting the internal atmosphere of the package, is described. The usefulness of RGA data in failure analysis and its implementation in quality control to improve the device reliability is also presented with a few examples.

INTRODUCTION

At present, residual gas analysis (RGA) per MIL-STD-883D, Method 1018.2 requires the cavity type electronic devices to contain less than 5000 ppmv moisture, with no other requirement for other gases. During RGA, however, all the gases present in the package are analyzed. Whether the package passes or fails the MIL-STD moisture requirements, the internal gas composition can be carefully analyzed to determine (a) the major composition of the sealing gas, and (b) the post-seal chemical reactions or outgassing that have occurred within the package. Of course, if the internal gas composition is similar to ambient air (78% nitrogen, 20.95% oxygen, 9340 ppm argon, 0.8-1.5% moisture, 330 ppm carbon dioxide and 5-6 ppm helium), the package has lost its hermeticity and another package should be analyzed.

All the RGA data analyzed in this paper are obtained using a Millipore/Extrel RGA system. Other conclusions are drawn from data published in the literature.

INTERNAL ATMOSPHERE AFTER LID/COVER SEAL

The RGA data obtained immediately after the lid/cover sealing operation provides the composition of the sealed gas. If the composition is not as intended, either an air leak has occurred in the sealing chamber or the sealing gas composition is questionable. Even though MIL-STD-883 requirements for moisture content is 5000 ppmv maximum, the moisture content after sealing should be as low as possible since further reactions within the cavity over time and upon temperature exposure will generally increase the moisture content. The device package and the cover should be pre-seal baked, preferably in vacuum or in dry nitrogen, to remove the maximum amount of absorbed and adsorbed moisture, other organic contaminants and outgassed products from organics (e.g., epoxies, if used).

INTERNAL ATMOSPHERE AFTER ENVIRONMENTAL TESTING AND AGING

After the sealed packages have been subjected to the reliability tests, e.g., thermal cycling, thermal shock, burn-in, bias bake, etc., the changes in the internal gas composition from the post-seal condition indicate the chemical reactions that have occurred within the package. Most of these changes, individually or combined, should be examined carefully to assess the long term reliability of the device. If the chemical reaction is still occurring within the package cavity, further RGA testing after additional temperature exposures is recommended. After the internal chemical reaction has been brought to full completion, examination of the internal atmosphere can conclusively determine the long term reliability of the package.

A brief review of the RGA data interpretation was recently presented by Shuman [1]. The significance of each gas component analyzed in the package cavity is presented as follows:

(i) Nitrogen: Nitrogen is used as the main sealing gas in most of the electronic devices. Air has 78% nitrogen by volume, and this amount of nitrogen along with 21% oxygen indicates that the package has an air leak. Nitrogen does not form within the package cavity by any known common chemical reaction or breakdown.

(ii) Oxygen: In general, the devices should not contain any oxygen. Its presence indicates a poor sealing atmosphere or that the package is a slow leaker. The presence of 21% oxygen along with 78% nitrogen shows an air leak. Normally higher moisture levels are found concurrent with higher oxygen levels. If any oxidation reaction has occurred within the package since cover seal, the oxygen is generally used up. Oxygen is a highly reactive gas and can cause failures due to oxidation.

(iii) Argon: Should not be present unless (a) used as a sealing gas mixture, or (b) hermeticity of the package has been compromised. Ambient air has 9340 ppmv argon and the ratio of oxygen to argon is approximately 20:1, therefore, this ratio is used to see if the package is a slow leaker.

(iv) Carbon Dioxide: Generally should be less than 100 ppmv, however, for leakers it could be up to 400 ppmv. Carbon dioxide is generally produced within the package by the aerobic reaction of epoxies, which consume oxygen and produce carbon dioxide, moisture, and hydrocarbons.

Excessive temperature exposure of the devices (thermal cycling, repeated burn-in, etc.) cause breakdown of organic materials within the devices and produce carbon dioxide, generally accompanied with moisture generation. Hydrocarbons present in the package may also oxidize to form carbon dioxide upon heating.

(v) Moisture: The moisture level could be higher due to the following reasons:

- (a) Moist sealing atmosphere due to the presence of moisture in the sealing gas or a leak in the sealing chamber.
- (b) Package and/or cover had absorbed/adsorbed moisture before sealing due to inadequate pre-seal baking procedures.
- (c) Package is a leaker.
- (d) Organic or other materials present in the package are outgassing and producing moisture.

Corrosion of metallized integrated circuits, aluminum bond wires and end terminations of other components due to moisture has been studied in great detail. Such corrosion is further catalyzed by the presence of halides (chlorides and fluorides). An excellent review of aluminum bond pad and interconnect segment corrosion has been presented by Lowry [2].

Electromigration by solder and flux residues, and with silver filled conductive epoxy, also occurs in the presence of moisture (electrolyte). Advances in hermetic packaging and moisture control through RGA has reduced the possibility of corrosion and electromigration failures and has improved device reliability.

(vi) Hydrogen: Some metallic packages and lids, e.g., Kovar, have been known to outgas hydrogen. Packages with nickel or nickel/gold plating reduce the outgassing to almost 10% of that of bare Kovar. Brazed ringframes of hybrid packages also absorb hydrogen if brazing is performed in a hydrogen (reducing) atmosphere. The presence of hydrogen increases the possibility of high moisture formation within the package. The amount of hydrogen in leakers is generally in the 100 ppmv range.

Packages with silicon die(s) and a gold eutectic die attach material produce hydrogen by the following reaction at the expense of moisture [3]:



This process appears to be a good method to reduce the internal moisture content.

(vii) Helium: Helium mixed with nitrogen is sometimes used as a sealing gas. If not, its presence indicates a leaker if fine leak testing was performed using helium. Background helium in ambient air is in the 5-6 ppmv range.

(viii) **Fluorocarbons:** Since fluorocarbons are used in gross leak testing, their presence indicates a leaker. Generally, there is no other source for fluorocarbons in the package.

(ix) **Methane:** Methane is generally analyzed as an indication for hydrocarbons present in the package. Less than 100 ppmv methane could be present due to a variety of organic contaminants present within the package. Generally, the epoxies used in the packages produce a large amount of methane during curing and breakdown, both by anaerobic and aerobic reactions.

(x) **Ammonia:** Ammonia is produced by anaerobic thermal decomposition of amine containing epoxies used as die attach materials. Large amounts of ammonia indicate that the pre-seal bake temperature and/or time should be increased. A vacuum assisted bake is preferred to remove the maximum amount of outgassed products from the epoxy die attach. Higher ammonia is generally associated with higher amounts of moisture, carbon dioxide, hydrogen and methane (hydrocarbons).

USE OF RGA DATA IN IMPROVING DEVICE RELIABILITY

EXAMPLE 1. Effect of Increasing Vacuum Bake Time on Moisture Content of Hybrids:

Large hybrids containing several dies attached with a non-amine epoxy in a Kovar package with nickel underplating and gold plating, with solder cover seal had shown high moisture, carbon dioxide and hydrocarbon contents, after being sealed in a dry nitrogen atmosphere after 8 hours of baking at temperature. Increasing the baking time to 24 and 72 hours revealed a cleaner internal atmosphere and a lower moisture content; Table I.

EXAMPLE 2. Effect of Increasing Baking Time, Temperature and Vacuum on Moisture Content of Hybrids:

Hybrids containing two dies attached with a non-amine epoxy in a Kovar package with nickel underplating and gold plating, with solder cover seal had shown very high moisture, carbon dioxide, hydrogen and hydrocarbon contents, after being sealed in a dry 80% nitrogen- 20% helium atmosphere. Table II shows the changes in RGA data after (a) increasing the baking temperature, (b) adjusting the gas composition and increasing the baking time, and (c) vacuum baking in addition to improvements in (b). The moisture content and other outgassed species were lowered to reasonable limits by the changes in the pre-seal bake procedures.

EXAMPLE 3. Outgassing of Epoxy From the Coil of Relays:

Large relays with tin plated steel cans had shown high moisture content due to outgassing of epoxy from a coil and an aerobic reaction consuming the intended small amount of oxygen in nitrogen. After tests were run with an empty can, with a Kapton insulator, with a coil, and after prebaking the coil individually and then sealing in the relay can, the complete chemical reaction sequence could be determined; Table III. After prebaking the coil at the highest possible temperature, the epoxy still reacted with some oxygen, however, left some oxygen in the relay for the beneficial "lubrication" so that the contacts do not stick during long term operation of the relay.

EXAMPLE 4. Electrical Leakage Through Ionic Conduction in the Presence of Moisture:

A hybrid with 36-pin metal DIP revealed electrical leakage failure at low temperatures that disappeared at elevated temperatures. The hybrid failed fine leak test and the RGA data were as follows:

Nitrogen 67.2%, oxygen 20.3%, argon 8065 ppm, carbon dioxide 1775 ppm, moisture 5.9%, helium 5.4%, ammonia 699 ppm.

The RGA data indicate a very high moisture content inside the package due to the outgassing of the epoxy die attach as well as an air leak. The high helium content was introduced during the fine leak testing of the hybrid.

After delidding, Secondary Ion Mass Spectrometry (SIMS) of the leaky die surface revealed high amounts of sodium, potassium, calcium and chloride ions. In the presence of moisture, these ions form an electrical leakage path, showing the observed failure mode.

Table I. Effect of Increasing Vacuum Bake Time on Moisture Content in Hybrids

Sealing Gas: Dry Nitrogen

Die Attach: Non-amine epoxy

Package & Cover: Ni/Au Plated, Kovar, Solder Seal

SAMPLE NO.	1		2		3	
	(8 hr. Bake)		(24 hr. Bake)		(72 hr. Bake)	
NITROGEN, %	99.0		99.2		99.5	
OXYGEN, ppm	97		70		30	
ARGON, ppm	185		155		15	
CO ₂ , ppm	3701		973		683	
MOISTURE, ppm	4760		3901		2212	
HYDROGEN, ppm	255		180		102	
HELIUM, ppm	33		20		13	
CH ₄ , ppm	1631		870		83	

Table II. Effect of Increasing Baking Time, Temperature and Vacuum on Moisture Content in Hybrids

Sealing Gas: 80% Nitrogen + 20% Helium
 Die Attach: Non-amine epoxy
 Package & Cover: Ni/Au Plated, Kovar, Solder Seal

SAMPLE NO.	1	2	3	4	5	6	7	8
NITROGEN, %	81.1	81.3	83.2	82.5	75.6	78.7	78.3	78.5
OXYGEN, ppm	87	72	129	136	3146	3918	--	--
ARGON, ppm	40	37	114	--	73	104	80	61
CO ₂ , ppm	6620	5439	1897	1731	1191	326	2029	1129
MOISTURE	1.9 %	1.6 %	7402ppm	6154ppm	4167ppm	2841ppm	3611ppm	2023ppm
HYDROGEN, ppm	1774	1606	2862	2591	466	490	166	165
HELIUM %	15.7	16.0	15.3	16.3	22.6	19.3	20.9	20.9
CH ₄ , ppm	868	783	113	110	37	32	64	21

↑ Baking Temp. ↑ Adjusted Gas Composition + Baking Time → Vacuum Baked

Table III. Outgassing of Epoxy from the Coil of a Relay

SAMPLE NO.	1		2		3		4	
	NITROGEN, %	95.8		95.9		99.2		97.1
OXYGEN, %	4.1		4.0		ND		2.1	
ARGON, ppm	ND		ND		ND		ND	
CO ₂ , ppm	ND		ND		5586		2293	
MOISTURE, ppm	479		510		2307		2418	
HYDROGEN, ppm	ND		ND		ND		ND	
HELIUM, ppm	ND		ND		ND		ND	
FLUOROCARBONS, ppm	ND		ND		ND		ND	
CH ₄ , ppm	10		10		47		27	
NH ₃ , ppm	ND		ND		ND		ND	

Sample Description:

- 1 - Empty Can, Tin Plated Steel
- 2 - Kapton Insulator
- 3 - Coil Containing Epoxy; Aerobic reaction consumed O₂ and produced CO₂ and moisture
- 4 - Relay with Prebaked Coil

REFERENCES

1. Shuman, D.T., *Residual Gas Analysis at O.R.S. and Interpretation of RGA Data*, (Abstracts of Microcircuit Atmosphere Workshop, ISHM, Santa Barbara, California, July 28-30, 1992).
2. Lowry, R.K., *Microcircuit Corrosion and Moisture Control*, pp. 63-69, (Microcontamination May 1985).
3. White, M.L., Striny, K.M., and Sammons, R.E., *Attaining Low Moisture Levels in Hermetic Packages*, pp. 253-259, (Proceedings of IRPS, IEEE, 1982).

MOISTURE LEVEL FLUCTUATIONS WITHIN HERMETICALLY SEALED MICROELECTRONIC DEVICES

Larry Henke, Steve VanDerlick, Mark Alderton
Cardiac Pacemakers, Inc.
4100 Hamline Avenue North
St. Paul, MN 55112

Abstract: Experimental studies show the variation of internal vapor phase moisture concentrations within sealed microelectronic devices. Metal shells containing significant quantities of polymeric materials and circuitry were tested. A molecular sieve reduced 40 cm³ of free internal volume from 24000 ppmv moisture to less than 1 ppmv. Temperature changes from -20°C to 60°C produced fluctuations of as much as 40000 ppmv moisture in non-desiccated devices. Polymeric materials were identified as a source of the moisture fluctuations and it was observed that the rate of adsorption and desorption was relatively equivalent. Moisture concentrations measured by mass spectrometer averaged 5 to 6 times greater than those measured by aluminum oxide sensor chips at the same temperature.

INTRODUCTION

Pulse generator devices for treating electrical heart abnormalities contain an assortment of construction materials known for adsorbing and desorbing moisture. Several types of polymers and epoxies are used, the total volume of which approaches that of the free internal volume of the device.

The vapor phase moisture concentration inside simulated pulse generator devices was studied from -20°C to 60°C, the maximum environmental temperature range allowed for the product. To obtain this data, it was necessary to use an in-situ moisture sensor which could capture moisture levels as a function of temperature and time. Panametrics MM-HT aluminum oxide sensor chips were used for this purpose, with data recorded by the Panametrics 770MM moisture meter.

The experiments focused on: 1) changes in device moisture levels through short term and long term durations at temperatures typical in production process steps, 2) the effect of a desiccant on those moisture levels, and 3) how mass spectrometer measurements (residual gas analysis, or RGA) compare with those of the aluminum oxide sensors at 37°C.

MOISTURE LEVEL VARIATIONS WITH AND WITHOUT DESICCANT

Test Device Construction

Two groups of four test devices each, were fabricated using identical methods and components. Each test device consisted of a metal shell that contained typical microelectronic components with a larger quantity of polymeric components. The internal volume measurements are given in table 1.

Each device in the first group contained 0.5 grams of molecular sieve desiccant in a pouch. (Davison Chemical, Type 4A formed molecular sieve.) The devices of the second group did not contain any molecular sieve. Both groups contained one Panametrics MM-HT aluminum oxide moisture sensing chip mounted in an open ceramic 16 pin lead-less chip carrier. Small gage Teflon coated wires joined the chip carrier to electrical feedthroughs that terminated outside of the metal shell. After all fabrication steps were performed, each moisture sensor's response was measured with the Model 770MM instrument to verify electrical continuity and stability through the feedthroughs.

The completed metal shells were joined to a cover followed by a seam weld. No vacuum bake was performed on the devices. Through a small port the internal atmosphere was purged and replaced with dry nitrogen, followed by a closure weld of the port. The welded devices were fine leak tested and verified to meet $< 1.0 \times 10^{-8}$ cc He/sec.

Testing

Both groups of test devices were exposed to temperature fluctuations typical for electronic assembly manufacturing. At the completion of each temperature cycle all test devices were allowed to return to room temperature prior to the next temperature exposure, except during the transition from -20° to 55°C (process steps 8 and 9) where the temperature transition was immediate. The process temperatures used and their exposure times are given in table 2.

Measurements of each moisture sensing chip were taken at various times during the temperature cycles. During long cycle durations where the internal temperatures of the devices were stable, measurements were as far as 24 hours apart. However, during the ramp up or ramp down portion of each cycle measurements were taken at least every hour. The recorded values from each of the test devices in each group were averaged together. At the completion of all process cycles, moisture sensing chips inside the test devices were calibrated by Panametrics. The resultant calibration curve was used to convert the moisture measurements to parts per million by volume (ppmv). The results are shown in figure 1.

Results

As the temperature of the device increased, moisture was driven from the internal components from both the desiccated and non-desiccated devices. As shown by figure 1, during the 45

minutes that both groups were exposed to the first 50°C process oven the moisture level in the non-desiccated devices increased from 17000 to 40000 ppmv . However, the moisture level in the desiccated devices only increased from 7800 to 15000 ppmv. The difference in moisture between the desiccated and non-desiccated devices shows that this type of molecular sieve was adsorbing moisture very quickly, while the internal components were going through a water desorbing phase.

Figure 1 also shows a steady drop in the moisture levels in the non-desiccated devices after the internal temperature inside the device had stabilized. The 672 hour exposure of these units to a 37°C stabilizing chamber resulted in a 10000 ppmv drop in moisture. This phenomenon is also displayed during the 25°C phase between the 37°C stabilize oven and the 37°C process oven. This trend suggests that internal components in the non-desiccated devices go through a partial re-adsorption phase.

Both groups of devices started out at roughly 25000 ppmv after weld and leak test. The majority of the moisture in the desiccated devices was adsorbed early in the testing. Figure 1 shows that within the first 50 hours after sealing, the moisture level in these devices had dropped to below 500 ppmv at room temperature. Later, even with increased temperature exposures of 60°C, the moisture level increased from < 1 ppmv to only 480 ppmv. By comparison, the non-desiccated device moisture levels remained above 7500 ppmv throughout the test and reached 31000 ppmv at 60°C. For all increased temperature excursions some moisture would be released into the vapor phase and then quickly re-adsorb when the temperature was decreased.

It should be noted that the water vapor concentration values cited thus far are minimum moisture levels. The sensor chips are known to lose sensitivity at temperatures higher than 25°C due to decreased surface adsorption [1]. This results in measured values being lower than actual at those temperatures. The values so far mentioned are based on 22°C calibration curve readings. No correction factor was identified for the levels of moisture in this experiment. However, below 40 ppmv the temperature effect is very small.

MOISTURE LEVEL VARIATION AS A FUNCTION OF TEMPERATURE

Procedure

Seven electronic devices were built with Panametrics moisture sensing chips (MM-HT) installed in them to record moisture values with changing temperatures. The free internal volumes ranged from 2.0 to 3.0 cm³. Again the devices contained typical microelectronic components and a significant volume of polymeric materials. Each device, with its sensor chip, was vacuum baked at 50°C for a minimum of twelve hours. Following the vacuum bake cycle, the devices were hermetically sealed in an inert gas environment and to verify hermeticity, each device was subjected to a helium leak test. The devices were heated from 0°C to 60°C in 10 degree increments, and held for 30 minutes at each temperature before taking a measurement. The experiment was repeated from 60°C to 0°C in like manner. The temperature cycling was

performed twice on each device to verify results. After temperature cycling was complete, moisture in each device was measured by RGA so that a correlation between the two methods of moisture analysis might be derived. Midway through the temperature cycling phase, one of the sensor chips failed and the data from that device could not be used.

Results

Chip sensor moisture measurements were recorded in ppmv on each device. These values were then temperature corrected by estimating correction factors from sensor calibration data at different temperatures supplied by Panametrics. Figure 2 illustrates the devices' change in moisture with respect to increasing and decreasing temperature, the decreasing temperature curve being slightly above the increasing temperature curve. Readings from devices with identical makeup and free internal volumes were averaged together for ease of analysis. The figure shows that increasing and decreasing moisture levels follow essentially the same path with little hysteresis, inferring that the moisture is re adsorbed by the internal components at the same rate as it is desorbed.

To verify that the plastics were a source of moisture, a follow on experiment was done. This experiment compared empty devices to devices which contained only 0.45 grams of polypropylene and a free internal volume of approximately 7 cm³. Again each device was hermetically sealed by a seam weld in an inert gas environment and contained a Panametrics sensor chip. Table 3 describes the test conditions and sample size. The temperature ramping experiments previously described were repeated for these devices.

Figures 3 and 4 show the data for the vacuum baked and non-vacuum baked devices. Both figures show a larger increase in moisture at elevated temperatures when the polymer is present than when it is absent. This observation supports the idea that the polymeric materials do desorb and re adsorb moisture with change in temperature. They are a large contributor to the moisture increases seen at elevated temperatures in these experiments.

COMPARISON OF RGA AND MOISTURE SENSOR DATA

Moisture levels inside the devices from the above mentioned experiment were measured by RGA to compare the results of the two techniques. Since vapor phase moisture levels change with temperature, a temperature common to both methods was chosen, which in this case was 37°C. This yielded some enigmatic results which are presented in figures 5 and 6.

Although the RGA data was in most cases higher than the sensor chip value at the same temperature, a direct correlation between the two measurement methods was not established. RGA values averaged 5 to 6 times higher than corresponding chip sensor values for devices with electronic and polymeric components, with individual values ranging from 3 to 19 times higher. For the empty devices with and without polypropylene, the difference between RGA and sensing

chip diminished. In some cases the sensing chip indicated a higher moisture level than the RGA measurement.

CONCLUSIONS

Molecular sieve is effective in reducing relatively high moisture levels to less than 1 ppmv inside sealed devices containing a large amount of moisture adsorbing materials. This is true even when no vacuum bake is performed on the components.

While total moisture remains constant inside a hermetically sealed device, the vapor phase concentration changes considerably as temperature changes, at least when large quantities of polymeric materials are present. Internal components, and specifically polymers, desorb water vapor rapidly when the device temperature increases. The process is reversible and the moisture re absorbs just as rapidly.

Moisture measurements by mass spectrometer and aluminum oxide sensor chips are not equal for this type of device, even when taken at the same temperature. The difference is related to the presence of moisture adsorbing materials inside the device, but the variability of the data sample is inconclusive at this point.

ACKNOWLEDGMENTS

We wish to thank Victor Fong and Panametrics, Inc. for performing the calibration curves and supplying the temperature correction data. We also wish to thank Al Edgar for his critical review of this manuscript.

REFERENCES

- [1] Kovac, M. G., Performance Characteristics of Al_2O_3 Moisture Sensor Inside Sealed Hybrid Packages, *ISHM Proceedings*, October 1977, pp. 249-252.

Table 1. Internal Volume - Desiccated and Non-Desiccated Devices

DESCRIPTION	VOLUME (CM ³)
Internal Components	73
Free Internal Volume	40
Total	113

Table 2. Process Temperatures - Desiccated and Non-Desiccated Devices

Process #	Process Description	Temp (°C)	Exposure Time (hrs)
1	Gross Leak Test	120	0.008
2	Process Oven	50	0.75
3	Process Oven	50	2
4	Stabilize Chamber	37	672
5	Process Oven	37	2
6	Process Oven	55	8
4	Process Oven	60	48
8	Environmental Chamber	-20	3
9	Environmental Chamber	55	3

Table 3: Testing Matrix - 0°C to 60°C Temperature Variation Test

Test Condition	Sample Quantity	
	With Polypropylene	Without Polypropylene
Vacuum bake	2	3
No vacuum bake	2	3

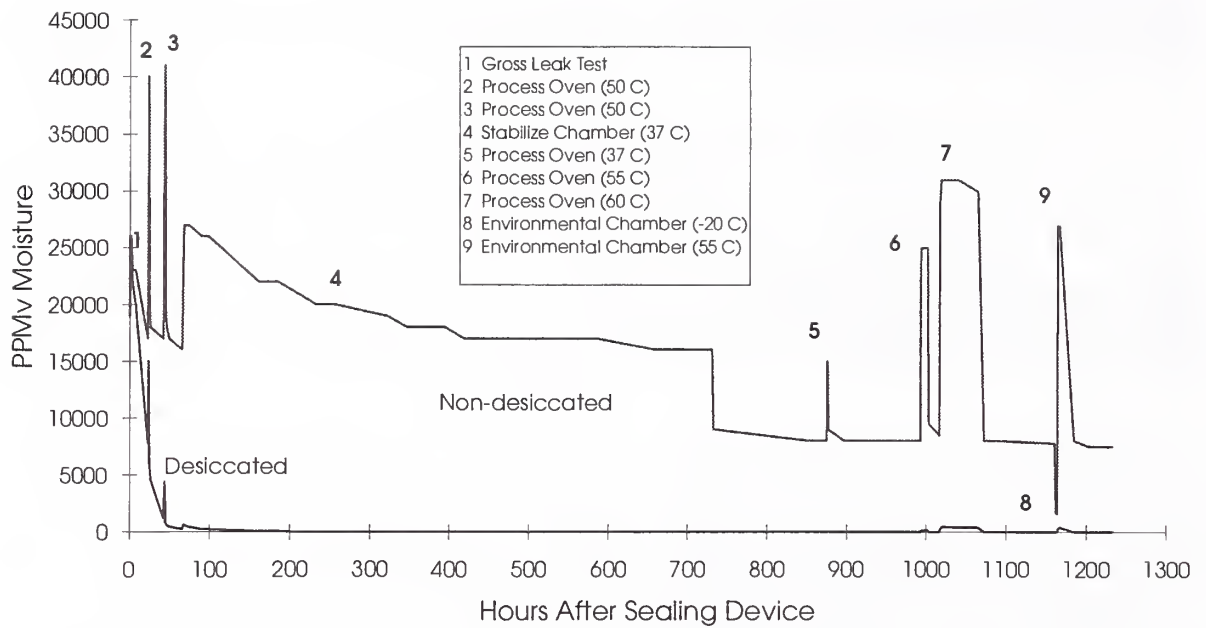


Figure 1: Device moisture levels through typical process temperatures. Free internal volume is 40 cm³. Measurements are not temperature corrected and are therefore represent minimum values.

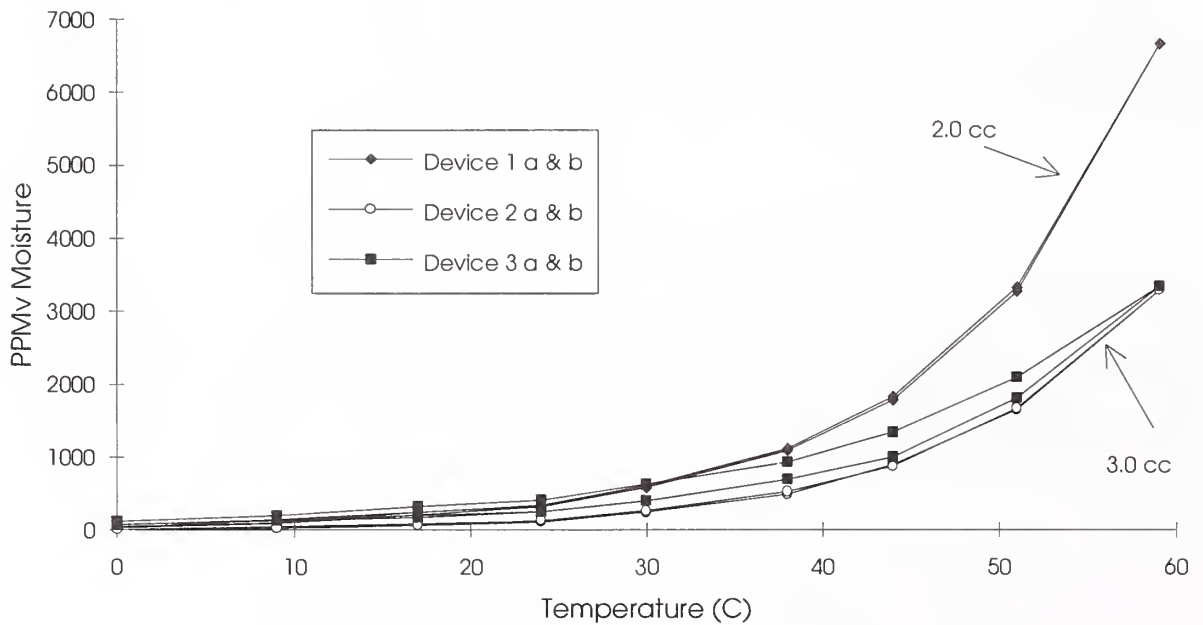


Figure 2: Device moisture as a function of increasing and decreasing temperature. Free internal volume is 2.0 to 3.0 cm³.

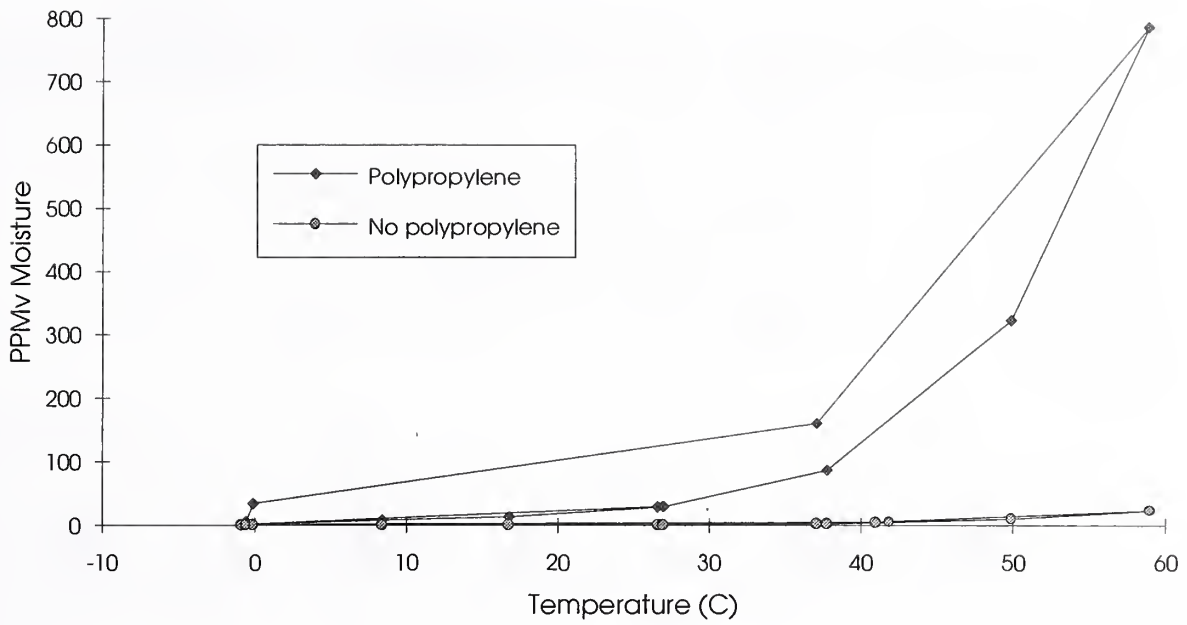


Figure 3: Vacuum baked device moisture as a function of increasing and decreasing temperature. Free internal volume is approximately 7 cm³. Lines are an average of 2 to 3 samples.

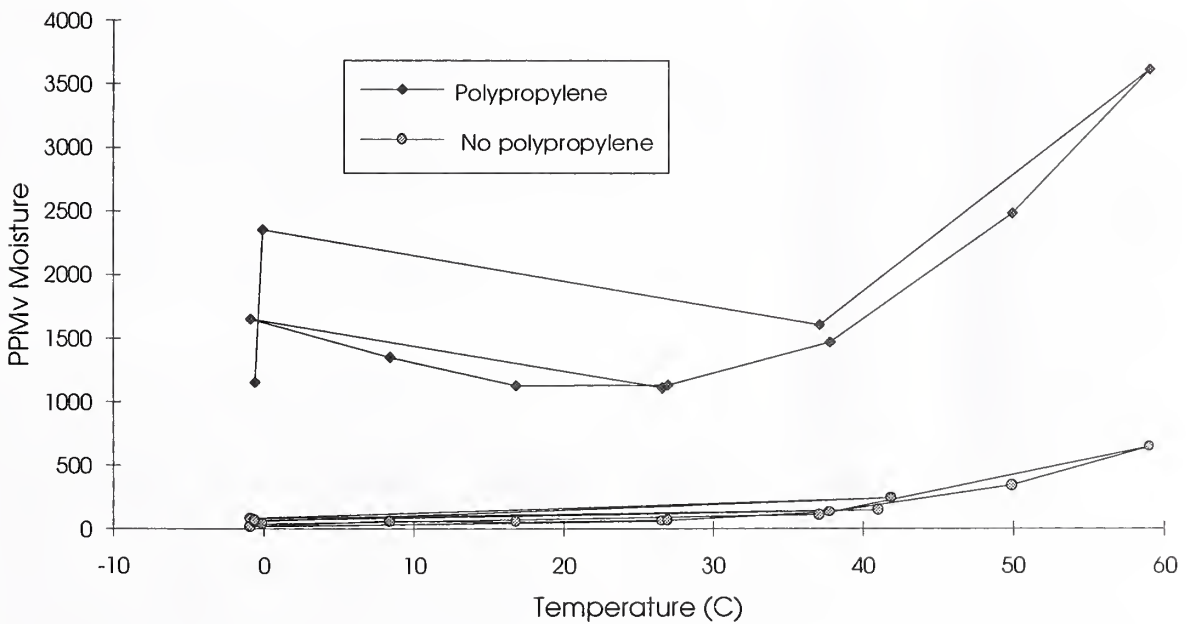


Figure 4: Non-vacuum baked device moisture as a function of increasing and decreasing temperature. Free internal volume is approximately 7 cm³. Lines are an average of 2 to 3 samples.

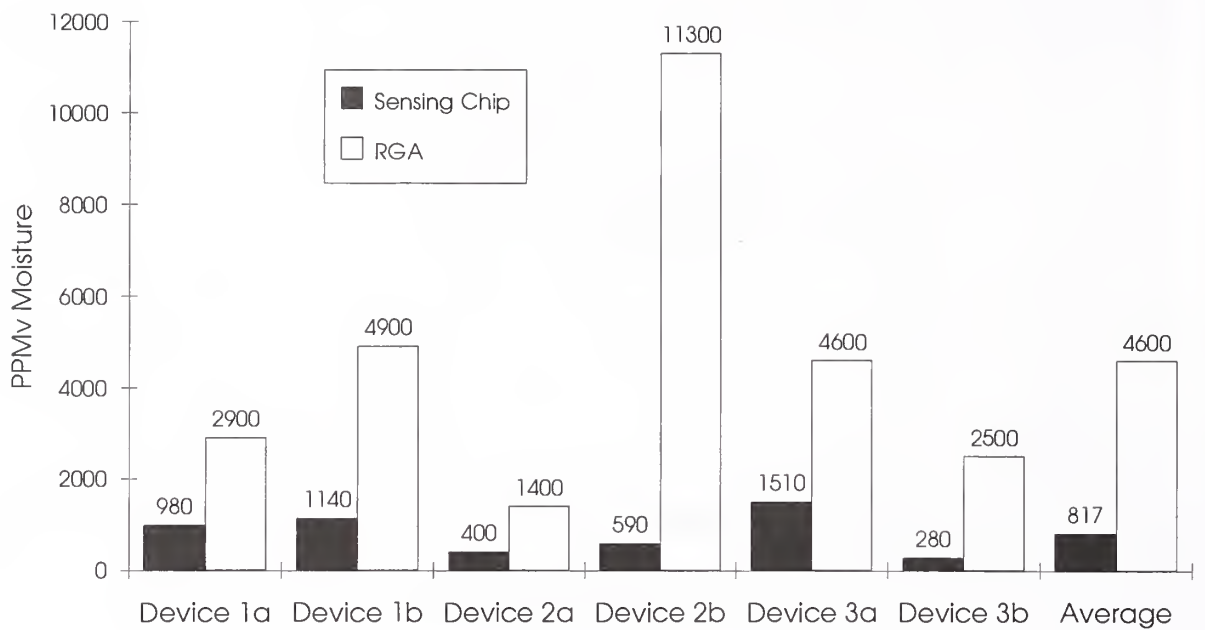


Figure 5: Comparison of moisture measurement readings by two techniques at 37°C. Free internal volume is 2.0 to 3.0 cm³. Samples contain electronic components, polymers and other materials.

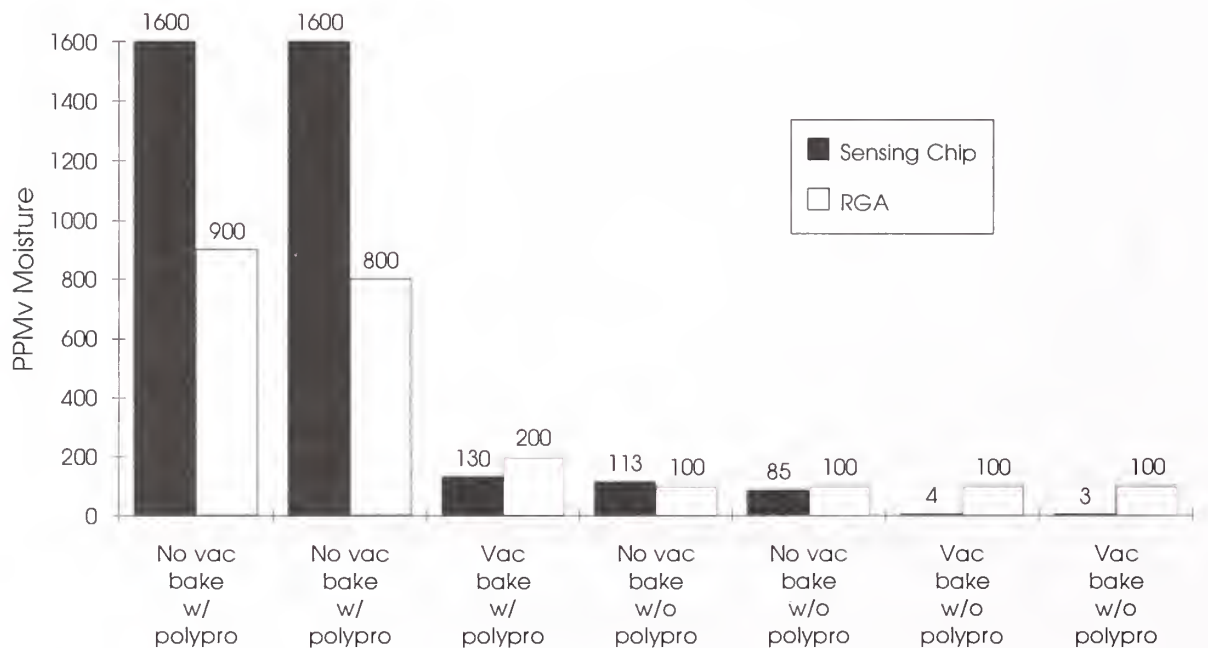


Figure 6: Comparison of moisture measurement readings by two techniques at 37°C. Sample volume is approximately 7 cm³. Samples contain only sensor chip and a polypropylene liner or the sensor chip alone.

High Reliability Sealed Chip Technology, What's Needed For Determining Corrosion Protection

**David O. Ross & James F. Reilly
Rome Laboratory/ ERDR
525 Brooks Road
Griffiss RFB, NY 13441-4505**

Abstract

The utilization of Sealed Chip Technologies for high reliability applications has been delayed for several years, in part, due to the lack of effective measures for determining the level of corrosion/contamination protection provided by the technology and the process related variability of that protection. While sealed chip technologies must provide both mechanical and corrosion protection to all the ICs in a device, determining the level of mechanical protection provided is currently much easier than determining the level of corrosion/contamination protection provided. This paper will discuss the needs of the high reliability industry in terms of finding effective measures for determining corrosion/contamination protection.

Introduction

A Sealed Chip Technology (SCT) is a packaging technology which relies on a barrier layer or an interface layer to provide the level of corrosion and contamination protection needed for the application. SCTs fall into the following broad categories: organic [silicone gels], ceramic [silicon carbide (SiC) and silicon nitride (SiN)], and metal film on dielectric. To some extent, the epoxy encapsulant used for plastic encapsulated devices (PEDs) is also included.

Use of SCTs for high reliability applications has been delayed for several years due to the lack of effective measures for determining the level of protection provided by the specific technology and the process related variability of that protection. While SCTs must provide both mechanical and corrosion protection to the ICs in a device, determining the level of mechanical protection provided is currently much easier than determining the level of corrosion or contamination protection provided by that technology. Many existing (traditional) test methods are still adequate and appropriate for determining mechanical protection.

The crux of this determination problem is that with SCTs, a thin barrier or interface layer is providing the necessary protection, rather than the traditional, dry, hermetically sealed volume. This hermetic volume is relatively easily tested for its essential parameters (quality of seal and dryness of atmosphere). The protection determination problem can be subdivided by identifying appropriate product evaluation methods in three basic areas: analysis techniques for understanding the protective layer, effective SCT qualification test methods, and process control test methods that correlate with qualified product. These three product evaluation areas need not be exclusive; a basic test method may be usable in all three areas.

The need for these three groups comes from a basic requirement of Statistical Process Control (SPC), that one must understand the essential parameters of product quality in order to produce a quality product. In order to have an accurate assessment of product quality, one must have analysis techniques for developing an understanding of how that critical layer works. Appropriate qualification test methods, based on the knowledge of how the protective layer works, are needed to demonstrate whether the necessary protection is being provided. The environmental conditions applied during evaluation should be chosen to accelerate the probable weaknesses of the SCT. The process control test results should be acquired on the qualification test samples in order to determine their correlation with the qualification test results. In production, that SCT can then be demonstrated as being applied at least as well as it was during the qualification testing. While it is true that one could use extensive, long term destructive testing methods to qualify the SCT, using the same approach for production process control may be expensive and inefficient.

The previous discussion points to a need to develop test methods which can rapidly, and non-destructively, probe the critical SCT layer for its integrity and composition on the process line. In order to successfully probe the critical layer, one must understand how that layer works, which may require the development of a variety of test methods. Additionally, one must know how the critical layer responds to the non-destructive probe, both when the layer passes the qualification tests, and when the layer does not pass those tests. Rome Laboratory and other organizations are working to develop the product evaluation techniques needed.

Qualification vs. Process Control Testing

Traditionally, the military system has relied on "qualification" tests to ensure that it was buying a quality product. While qualification tests usually provide a high level of confidence in the product, in many cases there are less expensive techniques which could be used to achieve a similar level of confidence. The most basic of these techniques is the use of SPC to ensure that an established process consistently produces a high quality product. For example, if an excess of flame retardant causes high failure rates of PEDs under HAST (Highly Accelerated Stress Test) conditions, monitor infrared spectra of the epoxy molding compound prior to encapsulation, instead of using the lengthy, destructive HAST test on the finished parts. Another potential SPC technique is the use of optical scatter techniques to monitor contamination levels and die conditions on a production line. The earlier in the process flow these monitoring techniques are used, the lower the cost for high confidence in the product. This will also increase the potential for significant quality improvements to occur.

The main cost impact experienced in this area occurs when fabricators use qualification tests as process control techniques. Traditionally, qualification type tests were required as acceptance tests on hermetic product. Using lot acceptance tests provides a high confidence level, however, that confidence comes at a high cost and often significantly increases the fabricators level of in-process-product. On the other hand, using appropriate process control techniques should still provide the high confidence levels while delivering a lower cost product. The fabricators usage of a Qualified Manufacturing Line (QML) approach would allow the use of process control techniques to replace their current qualification/acceptance tests. The crux of the current problem is that standard qualification tests and process control techniques are needed and not available for emerging SCTs.

Potential qualification tests include: thermal shock, HAST at 130°C, 85% RH and forward biased, HAST as above with contamination and/or a corrosive environment, moisture induced stress sensitivity, a standardized moisture test chip, vacuum enhanced dye penetrant, scanning acoustic microscopy, and sequential tests involving any combination of the above.

Potential process control tests include: dye penetrant, scanning acoustic microscopy, chronoamperometry, electroimpedance

spectroscopy, differential absorption laser spectroscopy (DIAL), FTIR, optical scatter, and a standardized moisture test chip.

Weaknesses of Current Testing Methodologies

The current industry standard test methods typically are based on test methods produced by standards writing organizations (Rome Laboratory (MIL-STD-883), IPC (Institute For Interconnecting & Packaging Electronic Circuits), JEDEC (Joint Electron Device Engineering Council), Electronic Industries Association (EIA), ASTM (The American Society for Testing and Materials), etc.). Test methods for traditional hermetic products are well established, but available standard, test methods for plastic encapsulated devices (PEDs), and SCTs do not address the full range of potential failure mechanisms. Some manufacturers are attempting to develop and use their own test methods, however, this approach is inefficient for the manufacturer, due to the duplication of effort, and inefficient for the customer, due to the inability to directly compare data from different test methods.

Test Method Development

The development of standardized test methodologies should occur in a disciplined manner, such that reusability is maximized. Ideally, the same property or characteristic would be measured in each product evaluation technique, and across SCTs. The test method should identify whether the test method is intended as an analysis technique, a qualification test, a process control test, or for multiple applications. Further, the test method should define the types of defects or failure mechanisms it has been developed to identify [coating quality (composition, coverage, durability, contamination), mechanical flaws (interface delamination, cracks), permeability (bulk transport, transport mechanisms and blockage thereof), corrosion (lead frame, die interconnect, pad), etc.]. Potential acceleration conditions, recommended pass/fail criteria, and advantages and disadvantages of use, should be included in the test method application notes.

Intrinsic Vs. Extrinsic Contamination

Many current "qualification" tests only evaluate the intrinsic (as shipped condition) contamination of the devices under test, and do not stress the SCT protective capabilities against extrinsic (external environmental) contamination. Extrinsic contamination will exploit any intrinsic weaknesses in either the SCT or its process defects. A significant example of a test method which only evaluates intrinsic contamination are the current HAST methods, which are carried out

under conditions of extreme cleanliness in order to achieve reproducibility. It has been shown that the varying levels of cleanliness of the devices under test has a significant impact on the variability of test results. However, this level of cleanliness is unrealistic since the real world is not very clean. Tests with deliberately contaminated parts show significantly shorter lives with many SCTs.

Current Approaches

Some of the existing efforts to develop and standardize test methods for SCTs follow:

Rome Laboratory Data Exchange With The French MOD

The French DOD has extensive data on lab testing of commercial plastic parts (130°C/85% Relative Humidity HAST). Based on this data, they are currently testing field military radios built with plastic parts and collecting the field reliability data. The results from this experiment will allow accurate correlation to be drawn between lab test data and actual field reliability. The data will provide a basis to define potential MIL-STD- 883 Test Methods and update MIL-HDBK-217 in a realistic manner.

DLA (Defense Logistics Agency) Plastic Packaging Program

The purpose of the DLA Plastic Packaging Program (contract number DLA900-92-C-1647) is to develop test methods, procedures, qualification levels, and specifications which allow for the low risk procurement and use of reliable plastic packaged devices. The prime contractor is National Semiconductor, with several subcontractors: Dow Corning, Honeywell, Sandia National Laboratory, and Rohm & Haas (Plaskon). Dow Corning is refining the process for depositing their SiC coating. Honeywell is gathering field data concerning PED reliability. Sandia is improving their moisture test chip, and Plaskon is supplying their high purity molding compounds. This program has the active participation of, and is provided technical support by, the Air Force, Navy, Army, and DESC. The program is a 3 year, \$2.7M effort, due for completion in September 1995. The first drafts of specifications, test methods, and procedures are due in September, 1993.

JEDEC 26A

The proposed revision to JEDEC Standard 26A "General Specification For Plastic Encapsulated Microcircuits For Use In Rugged Applications" is designed to provide uniform requirements for PEDs in systems used in environments requiring reliable performance. The standard is a

tremendous improvement over the current problem of no uniform standards and it is being used as a starting point by Rome Laboratory. However, data is needed to substantiate the qualification and process monitoring test levels, and the tests and test levels are not necessarily appropriate for SCTs and the use of PEDs in harsh, life critical applications.

RwoH

RwoH (Reliability without Hermeticity) is a pair of Mantech contracts intended to develop SCTs for use in military and high reliability environments. One contractor (National Semiconductor) used a reasonably successful ceramic approach, while the other contractor, MCC is using a more risky, organic approach. The efforts of both contractors have led to many of the insights presented herein (any errors are not theirs).

MIL-STD-883 Updates

MIL-STD-883 is currently a set of test methods which was designed for traditional hermetic military packaging technologies. However, many of the test methodologies which are appropriate for the emerging SCTs do not exist in MIL-STD-883. Several efforts are being made to modernize MIL-STD-883 by utilizing the pertinent results of other efforts, such as the DLA plastic packaging availability effort, and the JEDEC 26A committee. The French MOD has developed test methods of their own, which may be translated and adapted for inclusion in MIL-STD-883. Finally, organizations such as the IPC and ASTM have developed, or are in the process of developing, numerous test methods for emerging technologies. Rome Laboratory plans to leverage off of this work by referencing as many of these test methods as possible.

Conclusions

The use of SCT for high reliability applications has been delayed in part due to the lack of effective measures for determining the level of corrosion protection provided. The crux of the determination problem is that with SCT, a thin barrier or interface layer is providing the necessary protection. Current test methodologies are often inappropriate, or only suited as qualification tests. The protection determination problem is divided into three basic areas: understanding of the protective layer, qualification tests, and process control tests. Innovation and standardization is needed in all three areas.

The development of standardized test methodologies should occur in a disciplined manner, such that reusability is maximized. This should be carried out within the auspices of existing standardization organizations. DOD work related to this area include the Rome Laboratory Data Exchange with the French DOD, the DLA Plastic Packaging Availability Program, and the MIL-STD-883 updates.

LONG TERM PACKAGE INTEGRITY IN A MILITARY ENVIRONMENT

D. David Dylis and George H. Ebel
IIT Research Institute
201 Mill Street
Rome, NY 13440

ABSTRACT

Recently there have been several papers presented on the detailed results of failure analyzed parts collected during the performance of the Field Failure Return Program (FFRP). The substantial payback for these efforts has been well documented (see references). There are also global issues that could have even larger returns on the investment. One of these is a study of long-term package integrity of microelectronics in a military environment.

One of the major long-term failure mechanisms that exists in microelectronics are moisture-induced problems such as corrosion, electro-chemical metal migration and electrical parameter shifts. Moisture can occur in a package by a lack of hermeticity, by outgassing of materials inside of the package or by poor processing controls during the manufacture of the device. The FFRP is gathering RGA (Residual Gas Analysis) data as part of a long-term package hermeticity study. This study should also yield valuable information on the outgassing of materials inside of a hermetically sealed-package.

Specific items that will be reported on in this paper are:

- (1) Differences in long-term outgassing of metal and ceramic packages
- (2) RGA data on polymer sealed hybrid microcircuits that have functioned properly for over 23 years on an airborne inertial navigation system
- (3) A comparison of two leak rate detection methods (Bergquist and standard helium bomb) for parts that functioned satisfactorily for over ten years in a military environment

ACKNOWLEDGMENT

Support for initial FFRP efforts was provided by the United States Air Force, Rome Laboratory, Griffiss AFB, New York. Support for initial DoD FFRP efforts has been provided by the U.S. Air Force under Contract F30602-91-C-0002.

KEYWORDS

Bergquist Method
FFRP
Field Failure Return Program
Hybrid

Integrated Circuit
Leak Testing
Reliability
Residual Gas Analysis

INTRODUCTION

As part of the FFRP (Field Failure Return Program), a study of long-term package integrity was initiated. Parts that have operated successfully in a military environment for 8 to 25 years have been collected and analyzed to determine package integrity and its effect on long-term reliability. To date the investigation has had a three pronged approach. The first approach was to look at metal and ceramic packaged microelectronics. By using Residual Gas Analysis (RGA) data, package types using the two materials were analyzed to see if there were any peculiarities after extended use in a military operation. The second effort was to investigate the performance and failure mechanisms relating to three types of polymer sealed hybrid microcircuits that had been operative in a fighter aircraft environment for over 23 years. The last effort was to compare the standard helium leak rate test to the newer Bergquist method.

METAL AND CERAMIC PACKAGE STUDY

Since Residual Gas Analysis (RGA) in Method 1018 of MIL-STD-883 has been imposed, there have been many discussions and publications on it's results and the effectiveness of seal testing. Recently, papers have been published that indicate that microelectronic packages will, within a year or two, leak to the point where they would be in equilibrium with the associated ambient. In most cases that would mean filled with moist air. While there is still work to be done on package integrity, the amount of data collected by the FFRP to date would refute these paper studies. Table 1 shows the results of an RGA run on two one-inch square flat packs after eight years of service from an avionic Inertial Navigation Unit. These parts were manufactured in 1981 and removed from service in 1989. Sample 1 was sealed during the 18th week and Sample 2 was sealed during the 43rd week of 1981. Each hybrid was both dry and free of both Argon and Oxygen. RGA data was not available on "as made" parts from the supplier during the 1981 time interval. However, these parts were obviously hermetic during the eight years of field environment.

Table 2 shows data from a similar study on a hybrid microcircuit in a 40 pin platform package. In this case, the "as-made" RGA data was available and is

represented by samples A and B. Sample C was removed from an avionic Missile Remote Interface Unit that had been exposed to 8 years of field environment (date coded October 1980). Sample D is a seven-year-old part that was used for Quality Conformance Inspection (QCI) testing and stored since 1982. Again, this data shows that parts approaching ten years of field usage can maintain their hermetic integrity.

From the data presented in Tables 1 and 2, it can be seen that the major difference in ambient content as measured by the RGA between "as made" parts and long term usage is the higher hydrogen content. The hydrogen appears to increase by an order of magnitude after 8 to 10 years of storage. It has been documented that both the base metal and plating can contribute to hydrogen outgassing after package seal. The fact that the hydrogen level is high supports the fact that these packages were truly hermetic.

During a recent visit to an Air Force Depot, seven UVPROMs removed from a fighter aircraft were obtained. The parts were not causing a known problem and no circumstances pertaining to their removal was available. These devices were entered into the FFRP as part of the long-term RGA/hermeticity study. The seven samples were assembled in the 1979 through 1984 time frame and RGA was performed to characterize what happens to the moisture content of the hermetic cavity after six to eleven years in actual military usage. As shown in Table 3, all devices had moisture levels of less than 1000 parts per million by volume (ppmv). This is well below the military specification limits of 5000 ppmv and indicates that the parts sealed in dry air have maintained their hermeticity very well. The device manufacturer reported to us that when the parts were made, the typical moisture levels were running in the 2000 to 4000 ppm range. This would suggest that the package materials are acting as a moisture getter and it further suggests that ceramic parts should have lower moisture content with time. A second study is underway using about 100 CERDIPs (Ceramic Dual-In-Line Packages) made from 1974 to 1986. Before the RGA testing is done on these parts, leak rates will be measured in an attempt to correlate package hermeticity with internal water vapor.

The only anomalies in the RGA data is in the CO₂ and Oxygen categories. Those parts having higher CO₂ levels have corresponding lower Oxygen levels which suggests that some chemical reaction is taking place that is using Oxygen and generating CO₂. In any event, this mechanism does not appear to be a reliability problem.

In the last example of long-term hermeticity, five 2N598 transistors manufactured in 1964 were acquired from Howard Dicken of D-M Data, Incorporated. These parts which had been in storage in their original packing were checked for hermeticity and passed both fine and gross leak tests. The actual fine leak rate for all parts was measured as better than 1×10^{-9} cc/sec air. Table 4 summarizes the RGA results for these parts. They were sealed in dry air and apparently have not changed significantly in the 26 years since they were made.

Although the data accumulated thus far in the RGA data bank is small, it covers many of the commonly used packages. It shows that it is possible to use many packages that have long term integrity but we also know that not all packages have long-term hermeticity. As the program expands, the magnitude of the problem will become more apparent. One advantage of this study is that it will include electrically good parts as well as failed parts. Parts that have high internal moisture contents as well as those that have low moisture contents will be examined so that the physics of making good hermetic packages can be determined.

RGA DATA ON POLYMER SEALED HYBRID MICROCIRCUITS

Recently, several hybrids that had just been removed from a fighter aircraft Inertial Navigation Unit were obtained. These hybrids had date codes in the late sixties and early seventies. The lids of these 5/8" square hybrids were attached using a polymer seal. These devices had operated for 23 to 25 years in an unprotected fighter aircraft environment and even after their removal, many of the hybrids were still functioning properly. The hybrids are mounted in stacks of three so even if only one fails, all three hybrids are scrapped. Because of diagnostic procedures, in many cases, two and sometimes even three stacks of the hybrids are removed before the problem is corrected. Fifteen of these hybrids (five of each type) were selected for analysis having date codes ranging between the 50th week of 1967 to the 7th week of 1970.

Two samples were selected for RGA and Table 5 lists the internal gases found in their package cavities. The results were about what was expected - very moist air. The 20% moisture content, which is an order of magnitude above the dew point at room temperature, was higher than we expected.

The 15 hybrids were delidded and visually inspected from 7x to 200x and no signs of any corrosion or other moisture related problems were detected. Of the three failures found, two were attributed to electrical overstress that opened 1 mil gold substrate to package leads on the output and ground connections. No damage was done to any semiconductor devices which indicates that a transient pulse in excess of 100 microseconds is at fault. The third failure was a loose substrate caused by insufficient heat to melt the substrate attach eutectic preform.

Table 6 provides the composite parts and part hours for components contained in the 15 hybrids. For failure rate calculation, one can assume that the high moisture levels found in the hybrids (above a monolayer at room temperature) were present six months after seal date. The data is listed by element type including wirebonds and by passivation/glassivation of semiconductor devices and nichrome resistors.

The lack of any moisture related corrosion or metal migration is believed to be due to the cleanliness of the hybrid internal cavity and all included materials. The functional performance of the hybrids required plus and minus 15 volts, so there was plenty of voltage for gold migration. Also, over two thirds of the LM709 operational amplifiers were unglassivated. In the late 1960s and early 1970s, the LM709 was considered one of the most sensitive ICs for moisture/contamination testing. If there is voltage, moisture and halogens and/or sodium present, the literature is full of results showing catastrophic failures. Since we know voltage and moisture were present, we can only conclude that the hybrids were clean and no halogens or sodium was present. These particular hybrids did receive an extensive cleaning operation, including a Cobehn spray, just prior to sealing.

To confirm that the surfaces inside of the hybrids were clean, two polymer sealed hybrids received extensive evaluation using both Auger and ESCA. Each hybrid was carefully opened just prior to the surface analysis in order to assure that no contaminants were added to the hybrids. No halogens, sodium, potassium or other detrimental elements were detected. Figure 1 shows an ESCA plot of one of the hybrids in the vicinity of a ceramic chip capacitor. During the 23 plus years that these hybrids have been in the field, extensive moisture (200,000 ppmv) has penetrated the polymer seals but apparently no detrimental material has done so. It is thought that although moisture diffuses through the polymer, contaminants are filtered out and only pure water enters the hybrid cavity.

This study shows the extreme importance of a good cleaning process, especially as the pressure to use more non-hermetic parts is increasing. To be reliable, parts must not only have clean well-controlled processes during manufacturing, but also have a design to filter out contaminants during the life cycle of the part.

STANDARD HELIUM LEAK TEST CORRELATION WITH THE BERGQUIST METHOD

The first attempt to correlate the standard helium leak test with the Bergquist method using 15 ceramic dip packages that had been in the field for 10 years resulted in limited success. The problem arose because all 15 parts were virtual leakers and only the background helium was being detected. Nevertheless, even in this limited test, there were some interesting pieces of information uncovered. Table 7 summarizes the results of the testing. All 15 parts were tested using the Bergquist method with bomb pressures of 30 psig and a bomb time of 40 minutes. This was compared to the standard helium leak test using a bomb time of 40 hours and a bomb pressure of 75 psig. The Bergquist results always were lower than the standard helium. The ratios of the leak rates of the two methods ranged from 1.7 to 20 with an average of 5.7. Six of the parts were retested using the Bergquist method with bomb times of 140 minutes at a bomb pressure of 45 psig. In this case, there was good correlation with leak rate ratios ranging from .9 to 2.6 with an average of 1.6. This indicates that for good correlation, the Bergquist method should use bomb pressures of 45 psig or greater and bomb times over 2 hours.

SUMMARY

Although there is still more data being collected, a large number of hermetic parts (over 100) randomly selected from the FFRP have shown that after about 10 years in avionics applications, most parts still retain their hermeticity. There have been no leakers detected in these parts. Most of these parts are ceramic dual in line packages. About 20 percent of the RGA data has been collected from metal package tests. The data shows that ceramic parts become drier with time. Metal packaged components contain the same moisture levels but can have a significant increase in hydrogen level with time. Metal flat packs and platform packages exhibited this phenomena while the TO5 metal cans did not.

Cleanliness is an important factor in preventing moisture related problems. Even though parts in the field for 23+ years had about 200,000 ppmv of moisture, they functioned properly and showed no signs of corrosion or metal migration.

REFERENCES

1. Capt. T.J. Green, "A Summary of RADC's Microelectronic Field Failure Collection & Analysis Program", ASM International Conference, October 1987.
2. Capt. T.J. Green, "Getting the Facts from the Field... Real World Failure Data Collection and Analysis", Government Microcircuit Applications Conference (GOMAC), November 1987, pp. 105-108.
3. Capt. T.J. Green, "A Review of IC Fabrication, Design, and Assembly Defects Manifested as Field Failures in Air Force Avionics Equipment", International Reliability Physics Symposium (IRPS), April, 1988, pp. 226-229.
4. Capt. T.J. Green and William K. Denson, "A Review of EOS/ESD Field Failures in Military Equipment", Electrical Overstress/Electrical Static Discharge Symposium (EOS/ESD), September, 1988, pp. 7-14
5. D. David Dylis and George H. Ebel, "The DoD Microcircuit Field Failure Return Program", Institute of Environmental Sciences (IES), April, 1990
6. John P. Farrell and George H. Ebel, "New Approaches to Microcircuit Quality and Reliability", National Aerospace & Electronics Conference (NAECON), May, 1990.
7. D. David Dylis and George H. Ebel, "Field Failure Return Program, The Missing Link", Institute of Environmental Sciences (IES), November, 1990, pp. 1-12.

8. Lt. Col. R.W. Stegmaier, "RADC Field Failure Return Program (FFRP), An Overview", Government Microcircuit Applications Conference (GOMAC), November, 1990, pp. 589-592.
9. D. David Dylis, "A Review of the Field Failure Return Program", GOMAC, November, 1990, pp. 593-595.
10. George H. Ebel, "Long Term Failure Mechanisms of Microcircuits", GOMAC, November 1990, pp. 597-600.
11. James J. Dobson and Edgar A. Doyle, "RADC FFRP, Its Impact on System Operational Readiness and Reliability", GOMAC, November, 1990, pp. 601-604.
12. George H. Ebel, "Practical Statistical Process Control Tools for Predictive Technology", Predictive Technology Symposium, November, 1991.
13. D.D. Dylis, "Selected Case Histories from the DoD Field Failure Return Program", International Society of Testing and Failure Analysis (ISTFA), October, 1992, pp. 67-72.
14. D.D. Dylis, "Organization and Operation of the DoD Field Failure Return Program", Government Microcircuit Applications Conference (GOMAC), November, 1992

TABLES

TABLE 1: GAS ANALYSIS RESULTS ON 1" x 1" FLAT PACK HYBRIDS

Serial Number	% (V/V)	
	1	2
Hydrogen	0.615	0.341
Helium	ND	ND
Methane	ND	ND
Water Vapor	0.046	ND
Nitrogen	99.325	99.648
Oxygen	ND	ND
Argon	ND	ND
Carbon Dioxide	0.014	0.010
Pump Oil	ND	ND
Freon	ND	ND

ND = not detected

Note: 1% (v/v) = 10,000 ppmv; 0.1% (v/v) = 1,000 ppmv

TABLE 2: GAS ANALYSIS RESULTS ON 40 PIN PLATFORM PACKAGE HYBRIDS

A - As made part early 1983

B - As made part early 1983

C - Part removed from a fighter aircraft after eight years of service

D - Quality conformance inspection part stored seven years

Serial Number	% (V/V)			
	A	B	C	D
Hydrogen	.024	.021	.192	.251
Helium	ND	ND	ND	ND
Methane	.006	.007	.030	.029
Water Vapor	.465	.472	.418	.489
Nitrogen	99.216	99.189	99.208	99.036
Oxygen	ND	ND	.004	.004
Argon	.030	.030	.011	.043
Carbon Dioxide	.242	.258	.134	.144
Pump Oil	.002	.004	.002	.003
Freon	ND	ND	ND	.001

ND = not detected

Note: 1% (v/v) = 10,000 ppmv; 0.1% (v/v) = 1,000 ppmv

TABLE 3: GAS ANALYSIS RESULTS ON UV PROM CERDIPs

A - Made in late 1979
 B - Made in early 1984
 C,D,E,F,G - Made in mid 1981

Serial Number	% (V/V)						
	A	B	C	D	E	F	G
Hydrogen	ND	ND	ND	ND	ND	ND	ND
Helium	ND	ND	ND	ND	ND	ND	ND
Methane	ND	ND	ND	ND	ND	ND	ND
Water Vapor	.042	.050	.035	.046	.090	.043	.047
Nitrogen	83.1	81.2	79.8	80.1	80.0	80.4	80.8
Oxygen	3.86	17.2	15.3	16.5	17.5	15.7	12.4
Argon	.862	.847	.873	.871	.859	.804	.857
Carbon Dioxide	12.2	.69	3.96	2.49	1.58	3.03	5.90
Pump Oil	ND	ND	ND	ND	ND	ND	ND
Freon	ND	ND	ND	ND	ND	ND	ND

ND = not detected

Note: 1% (v/v) = 10,000 ppmv; 0.1% (v/v) = 1,000 ppmv

TABLE 4: GAS ANALYSIS RESULTS ON THREE LEAD TO-TYPE METAL CAN TRANSISTORS

Serial Number	% (V/V)				
	1	2	3	4	5
Hydrogen	.017	.017	.014	.025	.021
Helium	ND	ND	ND	ND	ND
Methane	ND	ND	ND	ND	ND
Water Vapor	.384	.396	.326	.387	.383
Nitrogen	78.038	77.600	77.435	78.084	78.945
Oxygen	20.553	20.996	21.243	20.501	19.633
Argon	.948	.939	.932	.936	.949
Carbon Dioxide	.060	.052	.050	.066	.070
Pump Oil	ND	ND	ND	ND	ND
Freon	ND	ND	ND	ND	ND

ND = not detected

Note: 1% (v/v) = 10,000 ppmv; 0.1% (v/v) = 1,000 ppmv

TABLE 5: GAS ANALYSIS RESULTS ON POLYMER SEALED HYBRIDS

Sample ID		70E918	70F401
Pressure	torr	3.72	4.30
Nitrogen	%	65.5	69.7
Oxygen	%	11.8	8.52
Argon	ppm	7642	8149
CO ₂	%	0.67	1.29
Moisture	%	21.2	19.6
Hydrogen	ppm	245	275
Helium	ppm	ND	ND
Fluoro-carbons	ppm	ND	ND
ISP Alcoh	ppm	405	

ND = not detected

Note: 1% (v/v) = 10,000 ppmv; 0.1% (v/v) = 1,000 ppmv

TABLE 6: IN-SERVICE HOUR SUMMARY OF HYBRID ELEMENTS IN 15 POLYMER SEALED HYBRIDS

In-service hour summary of hybrid elements in 15 polymer sealed hybrid successfully working in a military fighter aircraft (uncontrolled environment) for 23 to 25 years in ~200,000 ppm H₂O.

IC's - LM709	operational amplifiers	4,011,840	hrs total
		2,832,480	hrs unglassivated
		1,179,360	hrs glassivated
Transistors	2N930 -	8,127,168	hrs unglassivated
	2N1893 -	4,060,224	hrs unglassivated
	2N2905 -	4,060,224	hrs unglassivated
	2N2946 -	4,066,944	hrs total
		412,272	hrs glassivated
		3,647,952	hrs unglassivated
	Total transistors	20,321,280	hrs
		412,272	hrs glassivated
		19,909,008	hrs unglassivated
Diodes	1N914 -	2,030,112	hrs unglassivated
MOS Capacitors -		10,108,896	hrs
Ceramic Capacitors -		12,139,008	hrs
Resistors	Nichrome Passivated Chip	7,592,256	hrs
	Tantalum Nitride Passivated Chip	15,528,912	hrs
	Thick Film Substrate	15,974,616	hrs
Wirebonds	Au/Au Wedge	224,710,416	hrs
	Au/Au Ball	80,179,344	hrs
	Au/Al Ball	144,531,072	hrs

TABLE 7: COMPARISON OF INDICATED LEAK RATES USING STANDARD HELIUM AND BERGQUIST METHODS

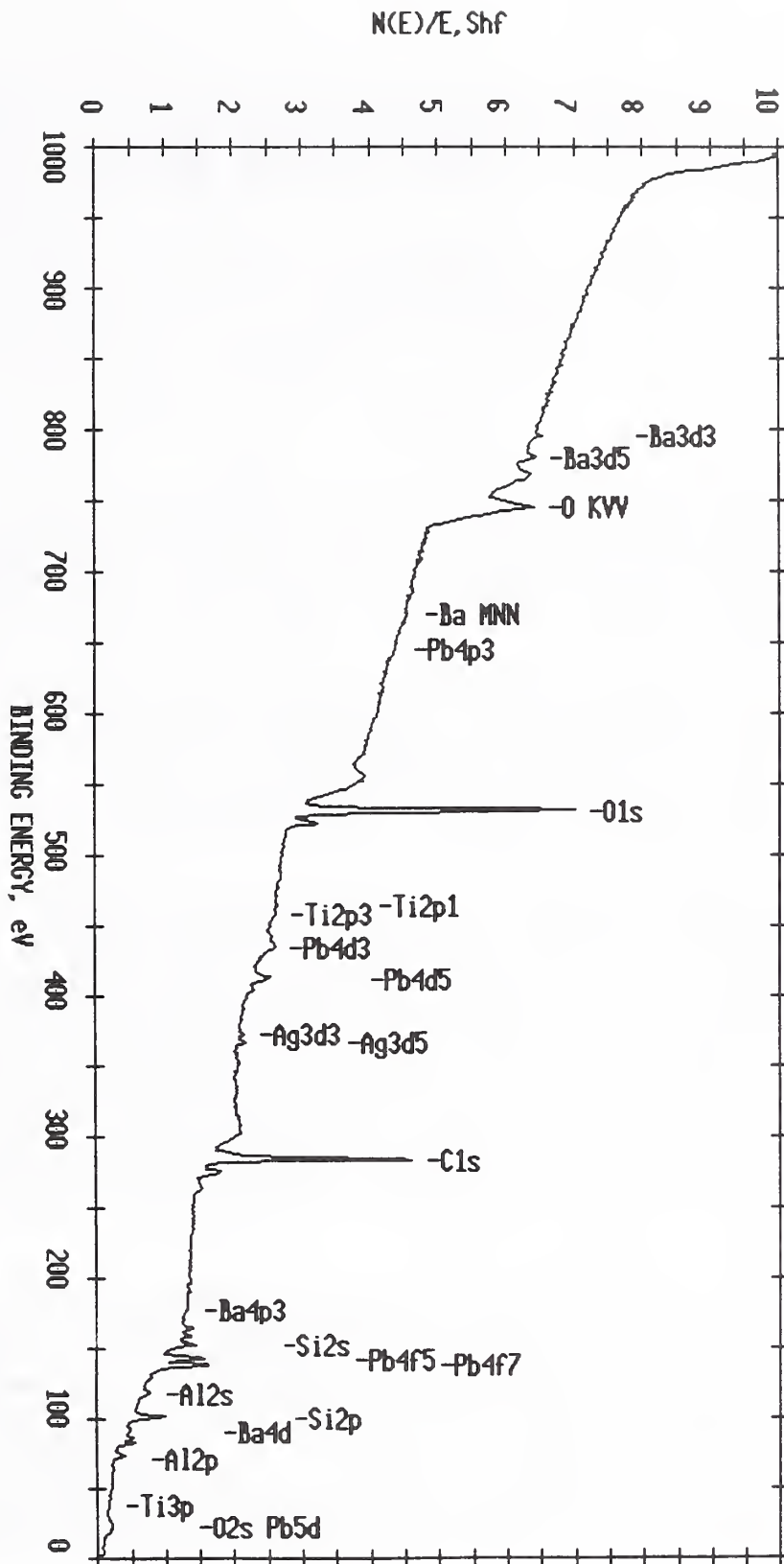
Serial #	Bergquist Bomb Pressure PSIG	Bergquist Bomb Time	Dwell Time	Indicated Bergquist He Leak Rate	Indicated Standard He Leak Rate*	Ratio of Standard Leak Rate/Bergquist Leak Rate
109	30	40 min	2 min	4E ⁻⁷	too far out of range	
109	30	40 min	85 min	2E ⁻⁹	1E ⁻⁸	5.0
110	30	40 min	54 min	7E ⁻⁹	2E ⁻⁸	2.9
111	30	40 min	50 min	1E ⁻⁸	9E ⁻⁸	9.0
112	30	40 min	58 min	8E ⁻⁹	2E ⁻⁸	2.5
113	30	40 min	17 min	6E ⁻⁸	1E ⁻⁷	1.7
114	30	40 min	25 min	1E ⁻⁸	2E ⁻⁷	20.0
115	30	40 min	44 min	3E ⁻⁹	3E ⁻⁸	10.0
116	30	40 min	30 min	8E ⁻⁹	4E ⁻⁸	5.0
117	30	40 min	35 min	9E ⁻⁹	4E ⁻⁸	4.4
118	30	40 min	39 min	2E ⁻⁸	6E ⁻⁸	3.0
119	30	40 min	76 min	6E ⁻⁹	4E ⁻⁸	6.7
120	30	40 min	68 min	4E ⁻⁹	1E ⁻⁸	2.5
121	30	40 min	72 min	5E ⁻⁹	2E ⁻⁸	4.0
122	30	40 min	80 min	1E ⁻⁹	6E ⁻⁹	6.0
123	30	40 min	63 min	6E ⁻⁹	2E ⁻⁸	3.3
109	45	2 hr 20 min	10 min	1E ⁻⁷	9E ⁻⁸	.9
109	45	2 hr 20 min	50 min	9E ⁻⁹	2E ⁻⁸	2.2
110	45	2 hr 20 min	17 min	4E ⁻⁸	6E ⁻⁸	1.5
114	45	2 hr 20 min	22 min	9E ⁻⁸	2E ⁻⁷	2.2
117	45	2 hr 20 min	45 min	2E ⁻⁸	3E ⁻⁸	1.5
121	45	2 hr 20 min	33 min	3E ⁻⁸	5E ⁻⁸	1.7
122	45	2 hr 20 min	40 min	8E ⁻⁹	1E ⁻⁸	1.2

Note: Average Ratio of Standard Leak Rate/Bergquist Leak Rate

For 30 PSIG = 5.7

For 45 PSIG = 1.6

*Bomb Time 40 Hours
Bomb Pressure 75 PSIG



ESCA SURVEY 4/1/93 ANGLE= 75 deg ACO TIME=47.71 min
 FILE: singer2 amp module
 SCALE FACTOR= 7.857 K C/S, OFFSET= 1.034 K C/S PASS ENERGY= 89.450 eV Mg 200 M

FIGURE 1: ESCA PLOT OF SURFACE CONTAMINATION ON A POLYMER SEALED HYBRID

ALTERNATE PACKAGING SCHEME TO
GUARANTEE LOW INTERNAL MOISTURE CONTENT

James C. Lau/Doug B. Nord
TRW
One Space Park
Redondo Beach, CA 90278

SUMMARY

An Alternate packaging scheme that can guarantee low moisture levels inside electronic packages is described in this paper. The overall electronic system cost should be less than "presently designed" systems. System reliability should be greatly improved.

Packages initially sealed in low moisture "protective" condition may be unable to maintain the protective environment for the designed mission lifetime. The MIL-STD-883 method 1014 leak testing specification (and equipment sensitivity) limits causes the "guaranteed" low internal moisture (less than 5000 ppm) storage time to range from several days to several months.

The alternate packaging scheme is able to maintain a package internal condition similar to the typical initial sealing condition. The existing initial protective environment is achieved by sealing packages in a dry sealing station that is maintained by a constant flow of dry gas. In this alternate packaging scheme, the drying tubes supply the dry gas to each package interior. Each removable small ultrahigh vacuum drying tube adds less than 0.04 cubic inches and 0.03 ounces to the system. Packages connected by these drying tubes can maintain the assured protective environment for the required life of the systems. The removable connections used crushed metal gaskets to achieve "ultra high vacuum" level seals.

Dry gas going into and out of each of the packages in the system during storage and operation can be obtained through various means. Dry nitrogen bottle, "air conditioning" (compression and cooling to condense and remove moisture), use of desiccant, and venting in space (vacuum in space is dry) are examples of dry gas generating schemes. Patent applications for options of this scheme are in progress. There is no need to develop new technology before implementation of this alternate scheme. The increased demand for the components provided in this scheme should reduce the unit cost.

Packages regarded as hermetic in the present system can minimize the overall dry gas flow (supply) requirement. Packages that failed the existing hermeticity standard may be made usable in this scheme if increased dry gas is supplied to the "defective" components to accommodate the increased drying demand. It would not be convenient to increase the dry gas flow rate in this scheme to maintain adequate internal moisture level for systems with large leak rates. (greater than 1 atm-cc/sec air). Several "special arrangements" to accommodate specific operational conditions are also discussed. The tubing connection as system overhead for this alternate scheme should be more than justified by the increase in reliability and reduction in overall system cost.

The advancement of multichip modules for both digital and microwave systems should reduce the number of hermetic packages for each functional unit and make this approach more attractive.

INTRODUCTION

High reliability electronic circuits are enclosed in "hermetic packages" so that failure (due to water vapor) is less likely in the protective environment. Proof of hermetic protection must be furnished by sample testing. Specification details related to part testing (theory for test, equipment accuracy and sensitivity) and storage condition cause the actual application of this approach to be a complicated issue. For example, this is the fifth workshop organized by National Institute of Standards and Technology (NIST)/Rome Laboratory to discuss the problem. There are many more "other discussions" sponsored by other organizations.

The "traditional approach" which is discussed extensively in previous workshops or other meetings is to rely on a hermetic package seal to maintain the "sealed in" protective environment. Numerous discussions related to the finite detectable leak sizes and the corresponding guaranteed time with protective (low moisture) environment were made. The conclusion is definitely that for packages initially with "sealed in" dry environment, the finite detectable leak rate makes "guaranteed" internal protective environment beyond corresponding storage/ operation time in potentially harmful condition impossible [1-4].

The applicable specification requirements have been changed several times in the last ten years (some merely to correct typographical errors). The current Mil-Std-883D method 1014.9 requirement and one previous requirement are illustrated in figure 1. The "irregular" shape curve for the fixed method is an obvious symptom that the rejection thresholds are not clearly connected to the basic laws of nature (and are arbitrary).

The RGA test for parts stored in potentially harmful environment demonstrated that many parts stored/operated beyond the "corresponding" time period do maintain the protective environment. There is the statistical basis to project probable internal low moisture level for sealed packages, but the actual condition for each package cannot be known "non-destructively."

The proposed approach of actively maintain internal moisture level can guarantee the protective environment indefinitely, or as long as effort to operate and monitor the system is made. The concept is similar to the typical approach used for keeping the "sealing" environment dry (using sufficient dry gas flow). The effort needed to implement this approach is more than compensated by eliminating other efforts (helium bomb and RGA). The enhanced reliability and the ability to accommodate parts that fail to meet the existing specification requirement should also reduce overall system cost.

This approach has not been implemented in any actual system, so successful records have not been established. The details (and experience) associated with actual application is also nonexistent now. Feasibility demonstrations at levels adequate to establish customer confidence can be set up with adequate support. A "technology program" to demonstrate feasibility is desirable. The details (cost and schedule) of the demonstration program will depend on "customer" perception of hermeticity requirements and associated necessary test data. It is possible to argue that there is no need for the demonstration program because the fundamentals are so well established. The details for use in a project may be defined at the time of a funded design phase like any design effort.

"Protective" coating is also being investigated as another RWOH (reliability without Hermeticity) approach. Experiences did not demonstrate that protective coatings consistently improve reliability in "moisture" environment. The reason may be coating materials could act as an "electrolyte" to sustain moisture related chemical reaction and prevent the formation of "natural oxide passivation." Evidence that one type of coating can protect all possible surfaces is difficult (impossible) to obtain with limited funding. New technology research and development is necessary for the coating approach. The subject drying tube approach does not rely on unknown new material technology.

Sealed containers (presumed to be maintained dry) such as those used for the "Patriot" (and Tomahawk) missiles used in "Desert Storm" is another protection method. Operational constraints limit the use of the sealed containers.

Basic Description of the Proposal

Dry gas supplied to the interior of electronic packages during storage (and long duration operation) can guarantee dry internal moisture level for systems without large (to be defined later) leak rate requirements.

All packages that require the guaranteed low internal moisture level have two small removable ultrahigh vacuum connections. The removable connections used crushed metal gaskets made of soft metal such as OFHC copper, aluminum, silver, or gold between harder material such as steel. One of the connections is for dry gas in-flow and the other is for gas out-flow. All packages are connected in networks of parallel or series tubings (or combinations of both). The addition of these features will obviously increase package size and weight. The penalty can be minimized with lower package count. Integrating more functions into each package as a basic design approach (such as IMA and MCM) which has been known to reduce overall system size and weight is compatible with this approach. A patent pending design for making the small "ultrahigh vacuum" connectors using 6-32 screw thread should minimize the weight and size penalty [5]. This small tube should be able to maintain greater than 0.1 atm cc/sec gas flow with low pressure (several psi). A typical package is illustrated in figure 2. Patent application for the small connector (at the size of a 6-32 machine screw as an example) design is underway. Dry gas supply line partition similar to the electrical function modular partition is preferred.

Valves connected to the overall system dry gas inlet and outlet are probably desirable for most applications. Protection during transportation or between connections to different dry gas supply sources can be made with the valves closed.

A small system with total package internal volume of less than 100 cc may be made with less than 25 hermetic packages. All the packages may be connected with the tubings in series. The 0.1 atm cc/sec gas flow rate can "replenish" package internal gaseous content in less than 20 minutes. For system to be stored (or used) in "saturated" atmospheric moisture condition (35,000 ppm moisture) the dry gas can make sure that the internal moisture level is 5,000 ppm even if there are leaks up to 0.01 atm cc/sec. Figure 3 is a representative scheme.

Parallel dry gas supply lines may be necessary for larger systems or system with known "non-hermetic" package. The routing of the dry gas lines may be modified to provide higher dry gas flow through leaky packages. The required seal conditions for packages in a system can be optimized for maximum reliability at minimum system cost. Figure 4 is an example. Figure 4 arrangement strongly suggests that stacked slices of multichip modules (or IMA, without the conventional printed circuit boards) may be the preferred overall packaging approach. For the power divide and switch unit example, each "slice" is one hermetic package of approximately 5" x 2.5" x 0.4".

Stainless steel (or another material with similar strength) used to construct the dry gas delivery system is among the strongest materials used for electronic packaging. This system would not cause structural weakness. The requirements for electrical power and signal connections are more likely to be the structural weak links.

The cut off frequency for the 0.015 inch diameter tubing as circular waveguide is in more than 400 GHz (in the dominant TE₁₁ mode). Lower frequency signals cannot be propagated and higher frequency signals are attenuated.

ADVANTAGE IN COMPONENT/SYSTEM RELIABILITY

Reliability for present component/systems built to existing specification requirements is debatable. For packages with 0.43 cc internal volume, the requirement according to Mil-Std-883 method 1014 is $L < E-6$ atm cc/sec air. For storage in ambient environment with 15,000 ppm moisture level, (50 % RH at 23 C) the guaranteed "dry interior" storage time is only 6 days. Larger (4.3 and 43 cc internal volume) packages would have longer (60°C and 600 days) guaranteed "dry storage" times. The period is too short for most applications.

There are situations where leak test clearly indicated that the package seal is not meeting the specification requirement, but there is no replacement (or other alternative) available. Severe program delay or taking risk (with customer waiver) may be the only options available under existing approach. Neither option is desirable. The effort to justify the "risk" option may be costly. If drying tubes are used, a package with less than E-4 atm cc/sec air leak would not become a reliability problem, and the dilemma can be avoided. The justification for using packages with leaks greater than the existing "hermeticity" limit (but no more than E-4 atm cc/sec air) can be achieved "automatically" with the adoption of the drying tube. "Standardized" tube re-routing procedure and analysis to justify the decision may be set up.

Failure to meet the requirement of Mil-Std-883 method 1018 (RGA) may be caused by outgassing of sealed in materials. There are also reports that hydrogen outgassing from metals may react with oxides to form moisture. GaAs device performance degradation in the presence of hydrogen has been reported [6]. The drying tube would be able to carry away the undesirable gaseous contents and eliminate these potential problems. This is a most significant "purge" benefit from the subject approach to monitoring dry hermetic sealing.

Packages with no or small leaks minimize the required dry gas flow rate. The typical Mil-Std-883 method 1014 requirement for packages with internal volume of more than 0.4 cc is $L < 1 \text{ E-6 atm cc/sec}$. Large system with up to 1,000 packages all meeting this requirement can be maintained dry indefinitely using only one drying tube connected serially through all packages. This is the assurance level the existing system cannot deliver.

Small presumed hermetic packages stored inside packages maintained dry using this approach would be under "double protection." If the small, presumed hermetic package is actually damaged, enclosed in a package with the drying tube would slowly improve the "protective environment."

Evidence that the requirements are satisfied during manufacturing and operation (for the complete system) will be monitored and provided continuously.

RADC which is responsible for Mil-Std-883 is hereby requested to clarify if constant monitoring of the system internal atmosphere with adequate sensors and obtaining no indication of more than 5,000 ppm moisture is sufficient evidence for meeting the method 1018 RGA requirement.

Procedure 3 (paragraphs 2.3 and 3.3) in Mil-Std-883D method 1018 is the following: 2.3 Procedure 3.3 (procedure 3 measures the water vapor content of the device atmosphere by measuring the response of a calibrated moisture sensor or an IC chip which is sealed within the device housing, with its electrical terminals available at the package exterior) The apparatus for procedure 3 shall consist of one of the following:

- a. A moisture sensor element and readout instrument that is capable of detecting a water-vapor content of 300 ± 50 ppm while sensor is mounted inside a sealed device.
- b. Metallization runs on the device being tested (isolated by back-biased diodes which, when connected as part of a bridge network) can detect 2,000 ppmv within the cavity. The device shall be cooled below dew point and then heated to room temperature as one complete test cycle.

NOTE: Suitable types of sensors may include (among others) parallel or interdigitate metal stripes on an oxidized silicon chip, and porous anodized-aluminum structures with gold surface electrodes.

Surface conductivity sensors may not be used in metal packages without external package wall insulation. When used, the sensor shall be the coolest surface in the cavity. It should be noted that some surface conductivity sensors require a higher ionic content than available in ultraclean CERDIP packages. In any case, correlation with mass spectrometer Procedure 1 shall be established by clearly showing that the sensor reading can determine whether the cavity atmosphere is more or less than the specified moisture limit at 100°C.

3.3 Procedure 3. The moisture sensor shall be calibrated in an atmosphere of known water-vapor content, such as that established by a saturated solution of an appropriate salt or dilution flow stream. It shall be demonstrated that the sensor calibration can be verified after package seal or that post seal calibration of the sensor by lid removal is an acceptable procedure.

The moisture sensor shall be sealed in the device package or, when specified, in a dummy package of the same type. This sealing shall be done under the same process, with the same die-attach materials and in the same facilities during the same time period as the device population being tested.

The water-vapor content measurement shall be made, at 100°C or below, by measuring the moisture sensor response. Correlation with procedure 1 shall be accomplished before suitability of the sensor for procedure 3 granted. It shall be shown the package ambient and sensor surface are free from any contaminating materials such as organic solvents which might result in a lower than usual moisture reading.

3.3.1 Failure criteria. A specimen with a water-vapor content greater than the specified maximum value shall constitute a failure.

The paragraphs in the method 1018 specification is included in this discussion to emphasize the difficulty in the present procedure 3. The complete system can be regarded as one package (and demonstrated to be "leak tight"). This makes meeting procedure 3 requirements using drying tubes simple. One sensor for a complete system is sufficient evidence that the method 1018 RGA requirement has been satisfied. Multiple sensors in large systems is recommended. Additionally, instead of calibration against the procedure 1 sensors, the primary standard used at NIST for water-vapor sensing that is far more accurate, may be included in this test circuit.

ADVANTAGES DURING MANUFACTURING/SYSTEM INTEGRATION

Detection sensitivity for sealed package helium leak testing is worse than the "open face" test. The helium bomb is typically able to "fill" the interior of the sealed package with less than 10 percent helium (normal bomb time for package leak at the acceptance threshold). The detected helium flow is proportional to the helium partial pressure inside the package. For sealed package leak test, the internal helium pressure is usually much less than atmosphere pressure and the resultant sensitivity is proportionally lower. The "bomb" cycle also causes schedule delay. Removable drying tube allows for helium leak test immediately after seal (or even during seal) at full atmospheric (or higher) helium pressure differential.

The "convenient" 16 hour, 15 psi overnight helium bomb used by many manufacturers for leak testing packages with 20 cc internal volume (or larger) would result in the rejection criteria of $4E-8$ atm cc/sec helium (or lower) flow rate. This low helium flow level may be confused with "adsorbed" surface helium inside the test chamber. For the case of packages with 100 cc (or larger) internal volume, the rejection criteria are less than $8 E-9$ atm cc/sec and are more difficult to distinguish from the "detector background." Packages made with helium absorbing materials such as fused quartz (silica) or epoxy on the surface would release helium in the test chamber. Increase bomb/dwell time can help resolve the confusion but the cost would be higher. "Open face" type procedure can be used for system (component) with the drying tube so differential of one atmospheric pressure (or more if desired) can be applied immediately without the "bomb" time.

RGA test for destructive samples is needed for packages made to meet existing specifications before delivery. Systems with drying tubes do not need RGA samples. The internal moisture level can be continuously monitored by inserting moisture monitors (permanently or temporarily during processing) in the system. RGA, if performed is trivial because the result would be the drying gas composition (and the removed outgassing products).

In case of damage to any package seal before delivery, the monitoring system can assist detection of the occurrence. "System" leak test can be conducted with connecting the dry gas lines to leak testing equipment and place the (complete) system inside helium chamber. Nondestructive procedures to identify the leak location can be established with selected connections re-arrangement. Replacement of the damaged unit or re-routing of the dry gas supply can restore the assured environmental condition.

Extensive visual inspection is now required so cracked but leak tight glass feedthroughs can meet the "visual criteria" as a protection against possible future degradation. With the drying tube making "true hermeticity" information readily available, the inspection for potential future "seal damage" may be eliminated. The visual inspection can be simplified.

In the case the tubing connection interferes with the manufacturing process (such as soldering to mother board) the removable tube may be removed and replaced with "plug" seals with the same type metal gasket. The unit would then be just like other hermetic packages with adequate seal. If the desire to conduct sealed package leak testing is strong enough, sealed package leak testing according to the existing specification can be performed.

ADVANTAGES IN COST AND SCHEDULE

For systems or components already in production, accommodating this approach by redesign and retooling would add cost. The long term savings may be achieved when the volume is sufficiently large. New designs are the effective vehicles to demonstrate overall cost reductions.

The reduced/eliminated "waiting" (bomb) time for leak testing (and seal rework) speeds up the manufacturing process. The elimination of RGA test reduces the time and cost for "quality assurance" (no need for destructive RGA samples). More effective methods to prevent "failures" reduce repair and rework.

Many aerospace electronic manufacturers have the experience of forming "tiger teams" to deal with the consequence of RGA/seal failure. Debates related to accuracy of RGA testing have been a cost increase factor. Suggestions to abolish the present method 1018 procedure 1 RGA test have been made [7].

A PDSU (power divide and switch unit) design started in 1992 is used as an example to estimate the manufacturing cost saving. The "old" and "new" designs are compared.

a. "Old" Design

This is a 12 x 12 PDSU for frequency up to 4.5 GHz. There are more than 500 hermetic packages in 16 slices. 3 set of leak tests (fine and gross) are normally necessary for each hermetic package. They are:

1. leak test immediately after seal (advisory, may omit gross)
2. final leak test before leaving hybrid production area
3. after lead forming in higher level integration

There is no requirement for leak test after the installation into higher level assembly. Leak test is practically impossible after this point.

At least 3000 leak tests are necessary. Actual time consumed in leak test alone is more than 3000 hours.

The cost estimate for this 144 cross points PDSU is more than one million dollars per unit. The space and weight requirements are 11" x 7" x 8" and 15 pounds.

b. "New" Design

The new design is a 16 x 16 switch for frequency up to 10 GHz using 16 slices as 16 hermetic packages. The space and weight requirements are 7.5" x 6.7" x 5.3" and 12 pounds. The cost estimate is less than 800,000 dollars and is less than half the cost of the previous old design at the "per cross point" basis. This design is compatible with the drying tube approach with the need for only 16 sets (32 total) of removable tube connections. The space for the required coaxial cables is not included in the volume estimate. The drying tubes could occupy the space around the coaxial cables and should not add to the space requirement. The weight increase is less than one tenth of a pound.

The wait for leak test and possible rework immediately after seal is eliminated as integral leak test become part of the sealing process. There is no more need for gross leak tests. The other leak tests can be performed without the pressurization cycle (replaced by the effort of connecting the tubes to leak detector).

The drying tubes (or the integrated hermetic package) obviously make internal hermetic packages unnecessary. This is an important reason for the reduction in volume and weight, as well as cost for package installation.

Validity of the cost estimates is to be determined. The unit using the "new" design has not yet been made. There are many "old" designs in existence and conversion to the "new" design approach should reduce size and weight by a similar factor. The schedule and cost impact of losing the more expansive highly integrated module is a higher risk. The drying tube can reduce/eliminate the risk.

OPTIMIZATION FOR SELECTED APPLICATIONS

A. Spacecraft Electronic

The low pressure (less than E-5 torr) in space guarantees low moisture level (and the corresponding low dew point of lower than -100 degrees Celsius). Meeting the RGA requirement is assured if the packages are vented. The drying tubes connected to valves obviously can be vented (slowly) and achieve the low moisture condition. For high voltage circuits, the ultimate pressure is so low that avoidance of arc discharge is guaranteed. In the case "inert gas atmosphere" is needed, the connected interior can make system monitoring and inert gas replenishment management more effective.

B. Stationary Installations

Stationary installation such as ground systems, storage areas, offices, and homes can be arranged such that dry gas supply is part of the basic utility. Dry nitrogen lines are already in place for most manufacturing and test areas. Dedicated dry gas supply system with flow rate of more than ten (atmospheric) liters per minute is readily available. The dry gas supply installation should occupy approximately 1 cubic foot of space. Air conditioning unit with moderate compressor pressure and/or "cold" temperature would be able to remove most moisture content (to less than 500 "ppm" moisture level). Desiccant that can be regenerated may also be used. The installation should have the electric (or other) power to operate the dry gas source.

C. Large Platform and Missile

The dry gas source is similar to the stationary installation except the platform should include the electric (or other) power source. Each missile or other electronic system launched from the platform should be equipped with (at least) two valves. Dry gas flow through all packages (where needed) is maintained as long as connection to the platform is maintained. Shortly before the launch (or separation from the platform), the valves in the missile are closed. The resultant seal is expected to be adequate for maintaining the internal environment throughout the short flight time. Otherwise, the dry gas supply described in the "portable units" section, dry gas storage tank, or vent to space (if the flight path is through space) can be used.

D. Portable Units

A dual compressor/desiccant container dry gas supply unit design with the ability to regenerate the desiccant is described in another invention disclosure [8]. The volume for this dry gas supply may be less than 0.5 cubic inch. This design is scalable to larger sizes. In situations such as using battery power where system operation power diverted to the dry gas supply is not desirable, the valves may be closed and the system operates as a normally sealed package. At places where external electrical power is available, the power battery can be recharged, the desiccant may be regenerated and the dry gas flow may be turned on.

These benefits are realized by paying the price of added tubings and gas connectors. Millimeter/microwave circuits where additional electrical connections (feedthroughs) means additional noise and insertion loss have been moving in the direction of integrated assembly (IMA). Direct chip mounting and multichip modules (MCM) also make digital circuit directed the way of larger packages. These developments are compatible with this approach of assuring adequate package internal atmosphere control.

When the use of this approach is more common, the "standardized components and practices" can reduce the unit cost. Soon, a complete drying tube arrangement for small systems may be available for about 1000 dollars. For large systems with more than 100 packages, the added cost for each package may be less than 100 dollars. There is industrial or commercial application potential. Further price reduction at high volume (more than one thousand units) scale economics production by factors of ten is possible.

References

1. "Permissible Leak Rates and Moisture Ingress" Aaron DerMarderosian (Raytheon Company) in RADC/NBS International Workshop Moisture Measurement and Control for Microelectronics (IV) November 1986
2. "Test Methods and Their Limitations" R.P. Merrett (British Telecom Research Laboratories)
3. "1984 International Reliability Symposium Hermeticity Tutorial" Stanley Ruthberg (National Bureau of Standards)
4. "Calculations for Leak Rates of Hermetic Packages" J. Gordon Davy. IEEE Transactions on Parts, Hybrids, and Packaging, Vol. PHP-11, No. 3 September 1975
5. "Small, Removable Ultrahigh Vacuum Tubing" TRW invention disclosure dockett number 13-0139.
6. "Hydrogen Effects on Reliability of GaAs MMIC's" William O. Camp, Jr., Randall Lasater, Vincent Genova, Robert Hume IBM Systems Integration Division Owego NY 13827
7. "A Critical Evaluation of RGA Testing" R. F. S. David, A. Andrew Shores, and M. Friedlander. IEEE Transactions on Components, Hybrids, and Manufacturing Technology. Vol. 12 No. 4 December 1989
8. "Scalable Dry Gas Supply for ROWH" TRW invention disclosure dockett number 13-0152.

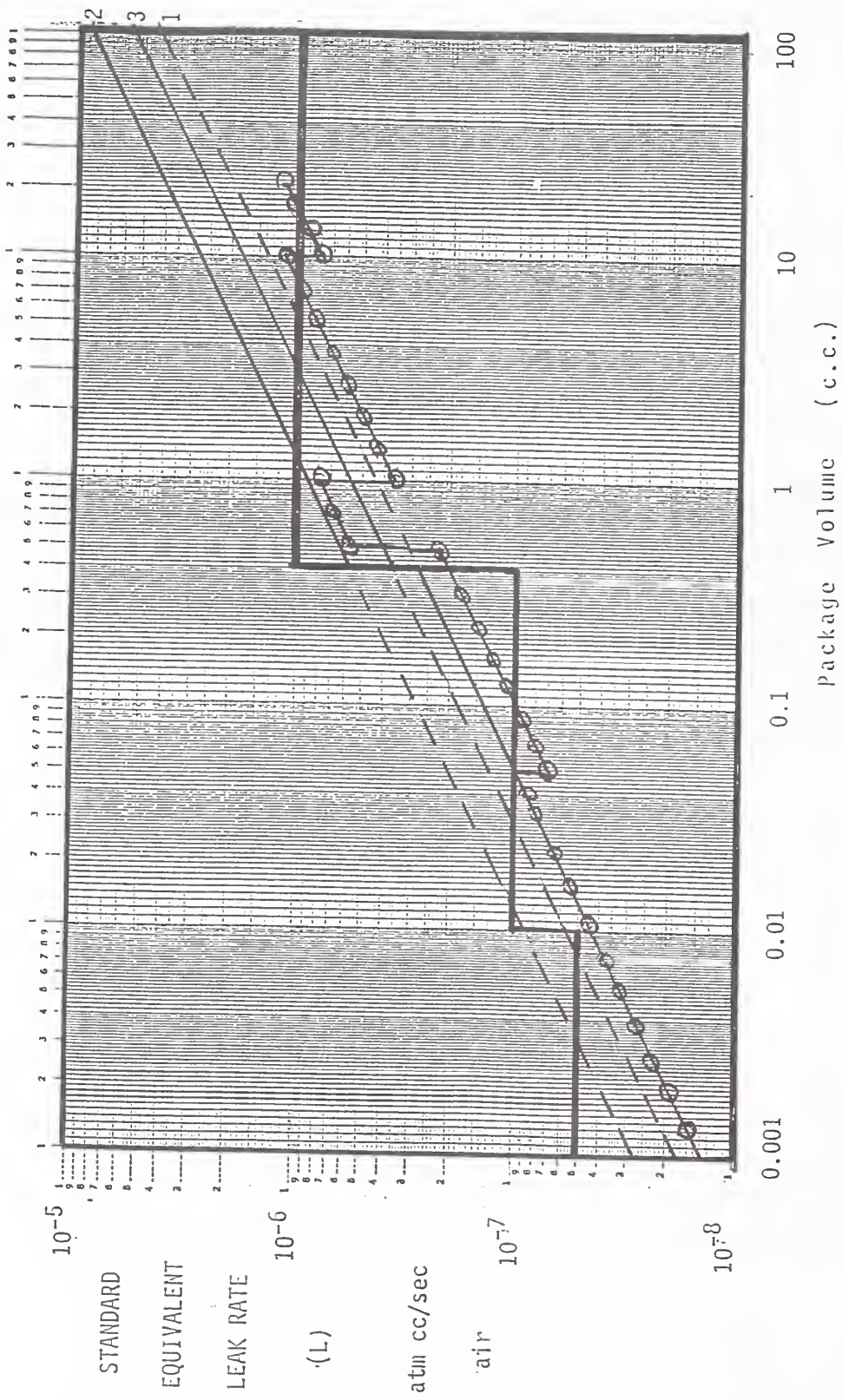


Figure 1. MIL-STD-883 Hermeticity Requirement

- Dark Solid Line - Flexible Method
- Light Solid Line - Fixed Method, Notice 4
- Circled Line - Fixed Method, Notice 5
- Dashed Line - Extrapolated Requirements

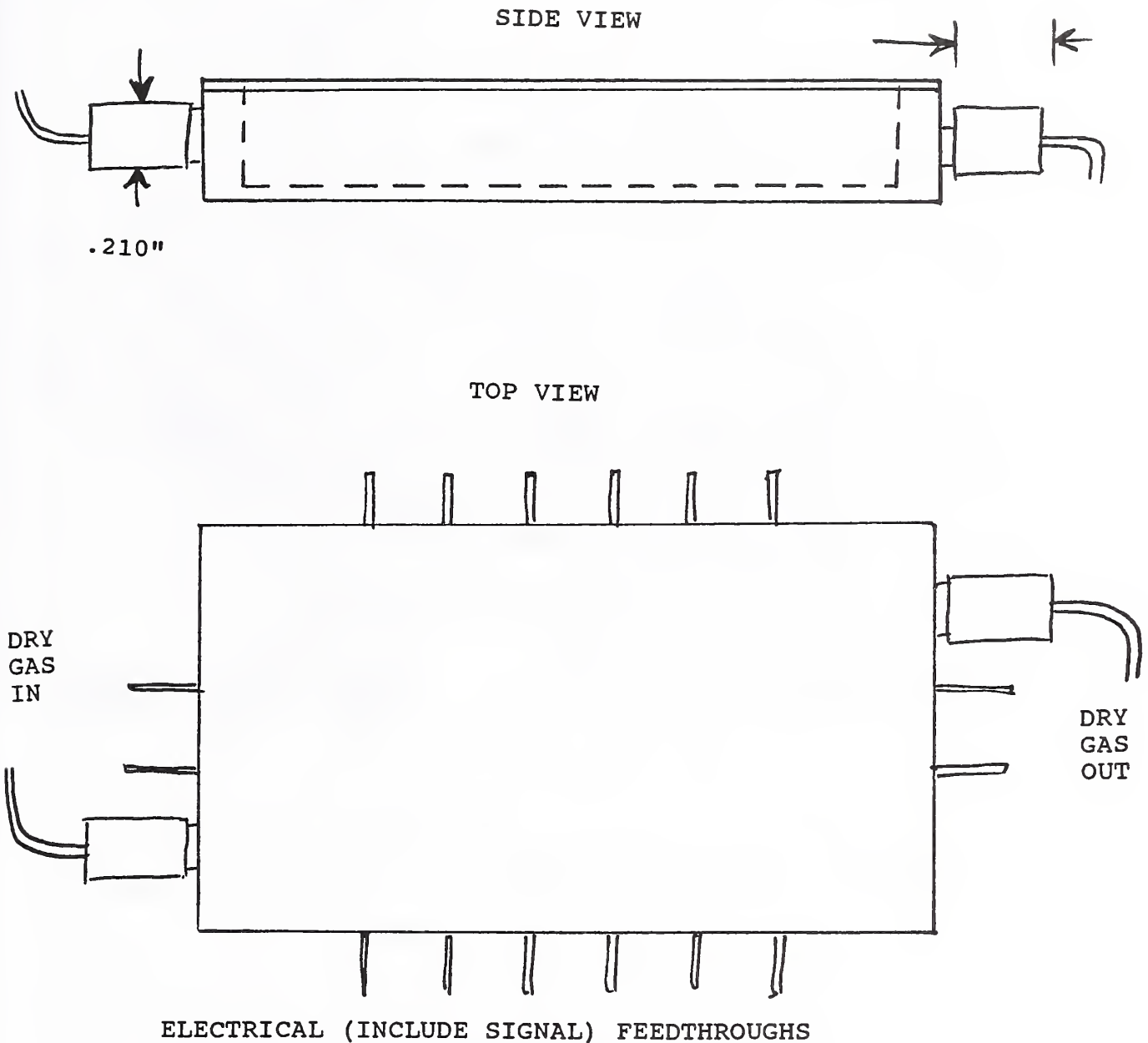
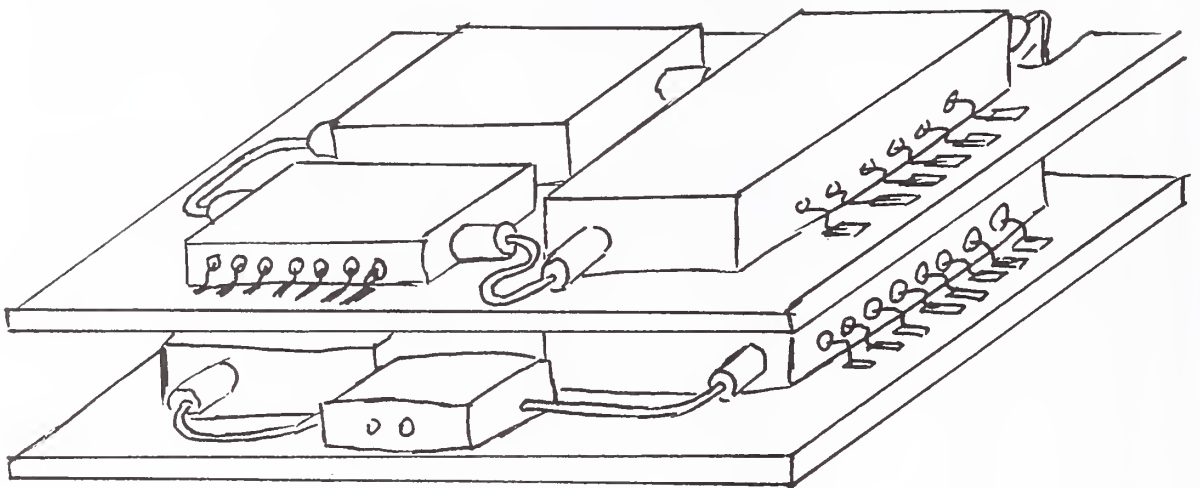


Figure 2. Dry Gas Tubes For A Typical Package

(Internal Volume \approx 10cc)

8 \times Actual Size

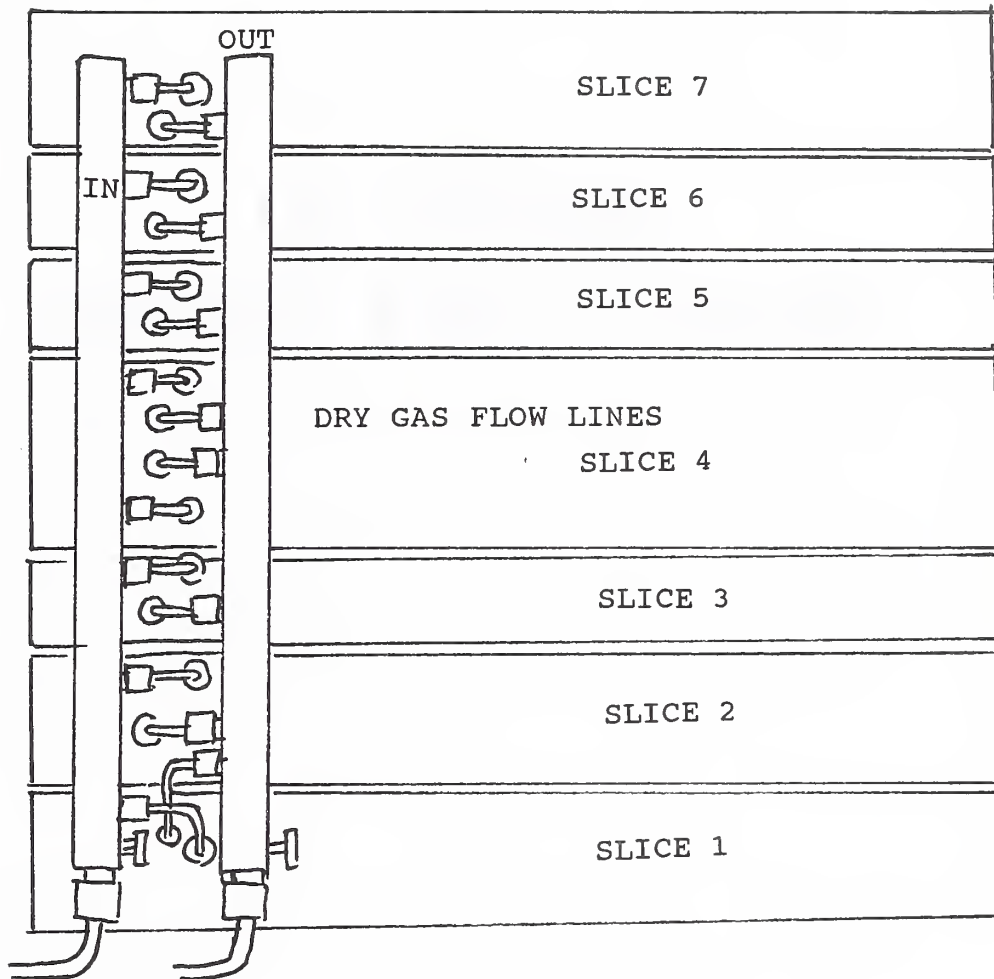
DRY GAS CONNECTORS AND TUBES



CONNECTIONS TO DRY GO SUPPLY
(VALVE ASSEMBLY)

MOTHER BOARD OTHER
HIGHER LEVEL ASSEMBLY

Figure 3. Small System With All Drying Tubes In Series
(Near Actual Size)



CONNECTORS (LARGE SIZE)

Figure 4. Larger System With Parallel Drying Tubes
 Each Slice Is Connected With At Least A Pair Of Tubes

Session IV

Moisture and Organic

DECREASING MOISTURE CONTENT OF EPOXY AFTER HIGH TEMPERATURE STRESS, BY ALTERING PRE-SEAL BAKE TIMES.

Bill Vigrass, Jack Linn and Jim Walling
Harris Semiconductor
MS 59/065
PO Box 883
Melbourne, Fl. 32935

ABSTRACT: A correlation has been determined between die attach cure processes, pre-seal bake processes and sealed package moisture content after high temperature stress. While pre-seal bake times may be reduced to 4 hours and residual gas analysis, RGA, through mass spectroscopy shows a dry package after assembly, << 0.5 percent of moisture, results after a high temperature bake can be markedly different. A part with a 4 hour pre-seal bake will show up to 3.0 percent of moisture content after 24 hours at 175°C, after a 48 hour pre-seal bake it will only show 0.2 percent moisture. With the decomposition of the epoxy other gases are produced besides water such as methane, carbon dioxide, and hydrocarbons any and all of which can cause corrosion or create charged particles in the package, changing device performance characteristics.

KEYWORDS: Packaging; Reliability; Die Attach; Design

1. INTRODUCTION

With the increasing power dissipation and stress sensitivity of semiconductor mixed signal devices, a low cure temperature, low die stress die attach with a high decomposition temperature is necessary for hermetic packaging. Currently, new parts are producing upwards of 2 Watts which in a hermetic package can translate to a 60 to 70 degree Celsius internal junction temperature rise above the package temperature. Combined with small packages and constrained placement on PC boards with little heat extraction, a chip could easily see 150°C at the silicon junctions in a 70°C ambient. Any moisture in a package could cause a failure by introducing charged particles at a surface junction, gate oxide area, or corrosion on a metal interconnect line.

At Harris a cross functional team from Process Reliability, Packaging and Analytical Services has recently been working to reduce the moisture content and improve the reliability of a high power dissipation, stress sensitive and assembly temperature restrictive hermetic packaged devices which uses an epoxy as its die attach medium. Work was specifically aimed at a new package, product, process development effort. The epoxy die attach studied meets the requirements of having a low cure temperature, ~200°C and produces low die stress while having a sufficiently high stud pull values.

The purpose of this work was to establish the reliability implications of the out gassing of moisture from the epoxy under expected operating conditions and to investigate ways to reduce it. Of particular interest was the cure cycle and the pre-seal bake time and temperature.

2. PROCEDURE

Work includes RGAs before and after storage bakes at different temperatures, with different pre-seal bake times, thermal gas analysis (TGA) weight loss for a simulated cure and pre-seal bake cycle, and die stud pulls to determine the strength of the epoxy before and after stress. All package testing was done with the same die size, 0.200 X 0.280 mils, in the same 40 pin dip package type. TGAs were performed on epoxy from the same batch as was used during the packaging experiments.

The first design of experiments, DOX, was a three way split in stress temperatures, 125°C, 150°C, 175°C using cure cycle A, which is a three step cure with a final cure temperature of 200°C. The results show that at sustained temperatures above 125°C a significant amount of outgassing can occur, graph 1. At low temperature, 125°C, there is an initial outgassing of moisture but it quickly saturates and does not seem to increase over time indicating a very stable package environment. At higher temperatures, 150°C and 175°C there seems to be a fairly constant increase in moisture over time that continues to increase even after 1600 hours. It is reasonable to assume that the outgassing will saturate before the epoxy completely breaks down since the stress temperature is lower than the cure or pre-seal bake temperature. Methane, carbon dioxide, CO₂ and hydrocarbons, HC_x were measured along with H₂O and the changes over time are listed in table 1. For low temperature stress, 125°C, methane, CO₂ and HC_x are stable after an initial increase mimicing what was seen for moisture while for higher stresses, 150°C and 175°C all gasses continue to increase with time. The rise in organics and moisture indicates a decomposition of the epoxy.

In conjunction with the first DOX a high temperature operating lifetest, HTOL, was conducted on the same product @ 100°C. The product dissipates approximately 2 Watts leading to an internal temperature of 160°C and the results for moisture outgassing are shown in graph 2. The results correlate well to what was expected if the data from DOX 1 was extrapolated to 160°C. Even with the high moisture content after HTOL stressing for 3000 hours no parts failed due to device shift that could be attributed to moisture. Visual inspection also showed no corrosion of the metal at the bondpads or internal to the circuitry.

DOX two was a three way split in pre-seal bake time of 4, 24, and 48 hours. It was started to answer some of the questions raised by DOX 1, about the complete curing of the epoxy in the pre-seal bake oven and to find out if there is a saturation point for the epoxy when stressed at 150°C. The initial RGA showed no difference in moisture, methane, CO₂ or HC_x for virgin units out of packaging assembly. The units were then stressed at 150°C or 175°C. The results in table 2 shows significant outgassing of moisture for short pre-seal bake times, 4 hours, after stress at 175°C or 150°C. A long pre-seal bake time, 48 hours, significantly reduces moisture content after the part has been stressed but the epoxy still continues to outgas H₂O, methane, CO₂ and HC_x. The results from DOX 2 confirm the findings of DOX 1, the epoxy is breaking down at a stress temperature of 175°C, and while longer pre-bake times help in reducing moisture content, it does not cure the problem.

At 150°C the results are not so clear. The moisture, methane, CO₂ and HC_x content peaks at 1500 hours and then decreases at 2000 hours. The ceramic package, lead frame, the die and/or even the epoxy may be absorbing some of the moisture and the other gases leading to the decrease in out-

gassing. The data is inconclusive but a peak in moisture seems to occur after 1500 hours of high temperature stress. ¹

The epoxy while degrading and outgassing at 150°C and 175°C, still has significant bonding strength since no apparent degradation was found in stud pull testing even after 2000 hours of stress and a pre-seal bake time of 48 hours, table 3.

A TGA was also performed to simulate the outgassing of cure cycle A and the pre-seal bake, graph 3. The problems with the epoxy can clearly be seen here with outgassing continuing for the entire pre-seal bake time and not stabilizing even after 48 hours confirming results seen with RGAs in DOX 2.

A second cure cycle, cycle B, was tried with a four hour vacuum pre-seal bake that showed a significant increase in outgassing during the cure cycle but a decrease in the pre-seal bake. The TGA is shown in graph 4 of the outgassing during a simulated pre-seal bake. Stressing it at 150°C the moisture outgassing is comparable to the 48 hour pre-seal bake of DOX 2 at 150°C, graph 5. Increased amounts of CO₂ and hydrocarbons are visible probably due to the reduction of oxygen in the cavity package itself due to the vacuum pre-seal bake, table 4, although the packages are backfilled with nitrogen during seal.

3. CONCLUSIONS

The outgassing process is very temperature dependant leading to a moisture saturation limit which for very high operating temperatures, 160°C and above, can have several percent water in a die cavity. At lower stress temperatures, 125°C, a low level of moisture saturation is quickly reached.

To reduce outgassing at higher temperatures, the cure cycle can be changed along with lengthening the pre-seal bake time or pre-seal method. A suitable cure and pre-seal bake combination could not be reached in this case unless, the ambient temperature of the package or the Θ_{ja} is lowered. A nitrogen pre-seal takes a longer time to ensure low moisture levels and leads to lower levels of CO₂ or HC_x than vacuum. A vacuum pre-seal method leads to lower moisture level than nitrogen but has increased levels of CO₂ and HC_x.

The effect of lengthening the pre-seal bake time in nitrogen has little effect on the die stud pull strength of the epoxy and does not increase the stress on the die significantly.

4. REFERENCES

1. J. H. Linn and J. Daar, RL/NIST Workshop on Moisture Measurement and Control for Microelectronics, 1993.

ACKNOWLEDGEMENTS

Special thanks to Josh Daar and Kris Hanley in Analytical Services for their time performing the RGA and TGA analysis

Table 1: DOX 1, Two Temperature Stress versus Time for Cure Cycle A.1

Time (hours)	Temp.	H ₂ O	Methane	CO ₂	HC _x
0 hrs	N/A	< 0.010	< 0.010	< 0.010	< 0.010
		< 0.010	< 0.010	0.012	< 0.010
		0.017	< 0.010	< 0.010	< 0.010
		0.021	< 0.010	< 0.010	< 0.010
		< 0.010	< 0.010	< 0.010	< 0.010
		< 0.010	< 0.010	< 0.010	< 0.010
192 hrs	125°C	0.020	< 0.010	< 0.010	< 0.010
		0.044	< 0.010	< 0.010	< 0.010
	150°C	0.045	< 0.010	0.028	< 0.010
		0.068	< 0.010	0.062	< 0.010
	175°C	0.820	0.079	0.849	0.298
		0.345	< 0.010	0.436	0.043
500 hrs	125°C	0.037	< 0.010	0.116	< 0.010
		0.036	< 0.010	0.075	< 0.010
	150°C	0.306	0.019	1.086	0.066
		0.237	< 0.010	0.252	0.034
	175°C	1.921	0.275	2.103	0.580
		1.070	0.115	0.768	0.406
1000 hrs	125°C	0.041	< 0.010	0.090	< 0.010
		0.033	< 0.010	0.045	< 0.010
	150°C	0.075	< 0.010	0.487	< 0.010
		0.243	< 0.010	1.037	0.070
	175°C	4.398	0.679	3.274	1.273
		1.553	0.246	1.074	0.323
1600 hrs	125°C	0.021	< 0.010	0.030	< 0.010
		0.038	< 0.010	0.026	< 0.010
	150°C	0.961	0.065	1.092	0.227
		0.543	0.052	0.804	0.162
	175°C	3.104	0.479	1.606	0.899
		2.672	0.508	2.129	0.791

1. Three step cure with final temperature at 200°C.

Table 2: DOX 2, Pre-Seal Bake Time vs. Stress Time at Two Temperatures.1

Stress Time	Stress Temp	Pre-Seal Bake Time	H ₂ O	Methane	CO ₂	HC _x
0	N/A	4 hrs	0.038 0.185	< 0.010 < 0.010	< 0.010 < 0.010	< 0.010 < 0.010
		16 hrs	0.703 < 0.010	< 0.010 < 0.010	< 0.010 < 0.010	< 0.010 < 0.010
		48 hrs	0.189 < 0.010	< 0.010 < 0.010	< 0.010 < 0.010	< 0.010 < 0.010
24 hrs	175°C	4 hrs	3.332	0.022	0.221	0.166
		16 hrs	0.726	< 0.010	0.710	0.026
		48 hrs	0.210	< 0.010	0.206	< 0.010
96 hrs	175°C	4 hrs	2.762	0.079	2.956	0.234
		16 hrs	1.161	0.040	0.535	0.200
		48 hrs	0.919	0.037	1.061	0.082
196 hrs	175°C	16 hrs	1.545 1.570	0.070 0.063	1.783 1.362	0.140 0.187
		48 hrs	0.449 1.560	< 0.010 0.054	1.034 1.588	0.050 0.124
832 hrs	150°C	16 hrs	4.612 1.179	0.086 0.042	0.865 0.699	0.255 0.164
		48 hrs	0.297 0.228	< 0.010 < 0.010	0.713 0.377	0.015 0.018
	175°C 2	16 hrs	3.342 6.411	0.576 0.707	4.791 2.983	0.980 1.190
		48 hrs	2.323 1.385	0.339 0.231	2.434 2.632	0.573 0.372
1500 hrs	150°C	16 hrs	1.135	0.061	1.651	0.199
		48 hrs	0.911	0.053	0.460	0.162
	175°C 2	48 hrs	3.099 4.019	0.978 0.714	5.771 2.297	1.542 1.146
2000 hrs	150°C	16 hrs	0.718 0.591	0.060 0.068	1.748 3.173	0.224 0.325
		48 hrs	0.422 0.095	0.019 < 0.010	1.035 0.875	0.074 0.021

1. Three step cure with final temperature at 200°C.
2. Elemental Oxygen starts appearing in RGA, possibly a secondary peak due to H₂O.

Table 3: Stud Pull Results from DOX 2.

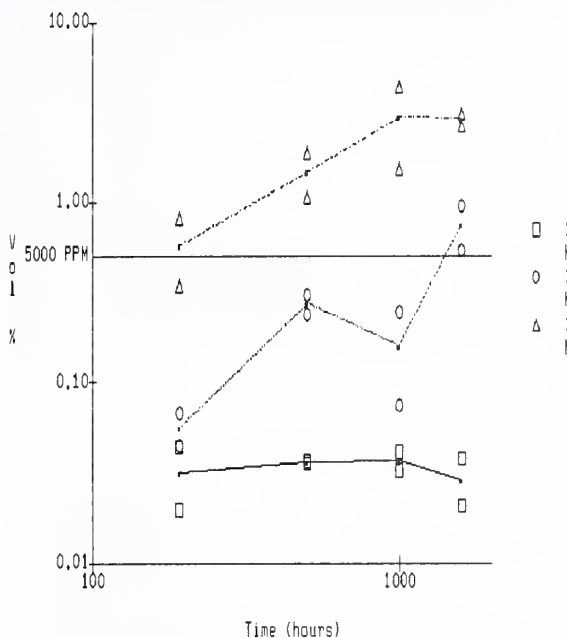
Time (hrs)	Temp.	Pre-Seal bake		
		4 hours	24 hours	48 hours
0 hrs	N/A	30.0	38.5	24.4
2000 hrs	150°C	48.2 38.0	45.5	40.7 22.7
	175°C	39.5		

Table 4: Cure Cycle B vs. Stress Time at 150°C.1

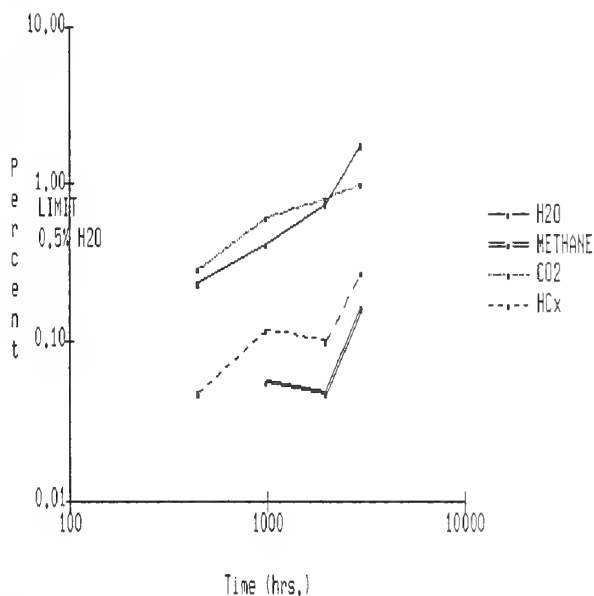
Time (hrs)	H ₂ O	Methane	CO ₂	HC _x
0 hrs	< 0.010	< 0.010	0.012	< 0.010
	0.025	< 0.010	0.014	< 0.010
280 hrs	0.361	0.071	0.312	0.354
	0.263	0.064	0.323	0.277
	0.262	0.056	0.271	0.212
500 hrs	1.298	0.090	0.558	0.472
	0.787	0.106	0.609	0.622
	0.356	0.051	0.949	0.222

1. Cured at 200°C.

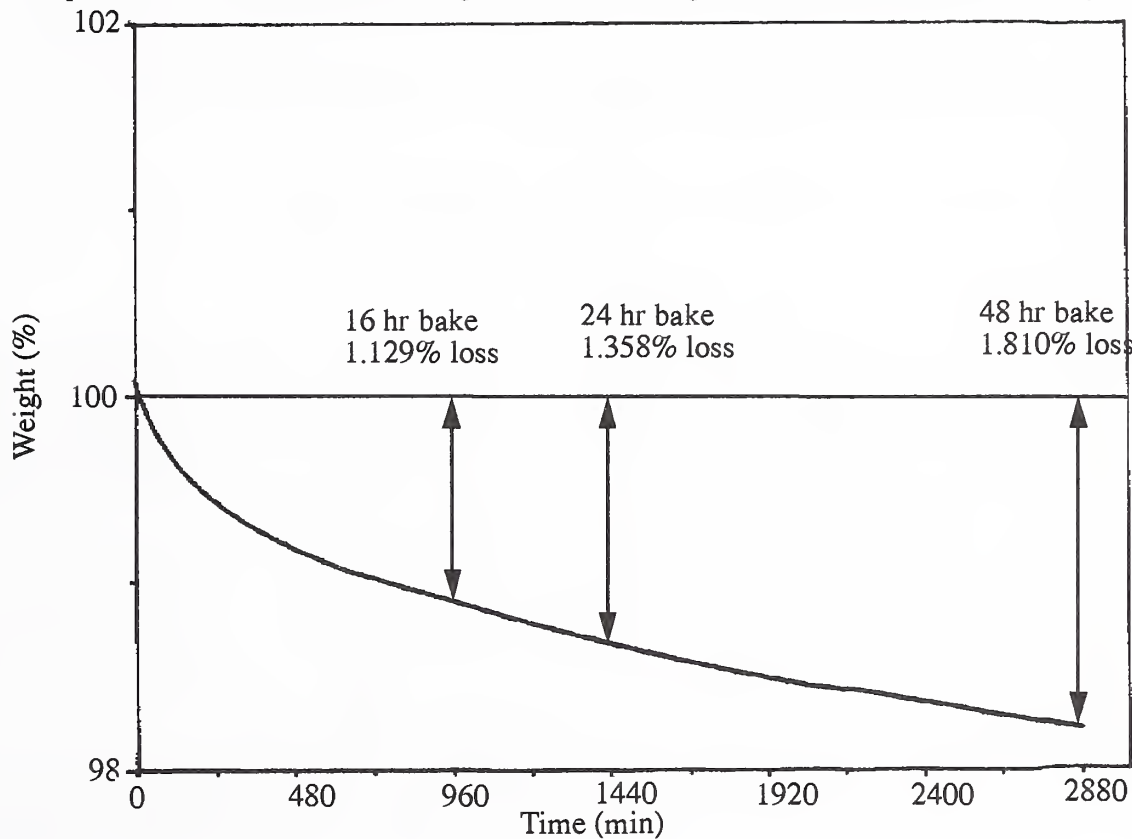
Graph 1: Moisture versus Time for Different Stress Temperatures with Cure Cycle A.



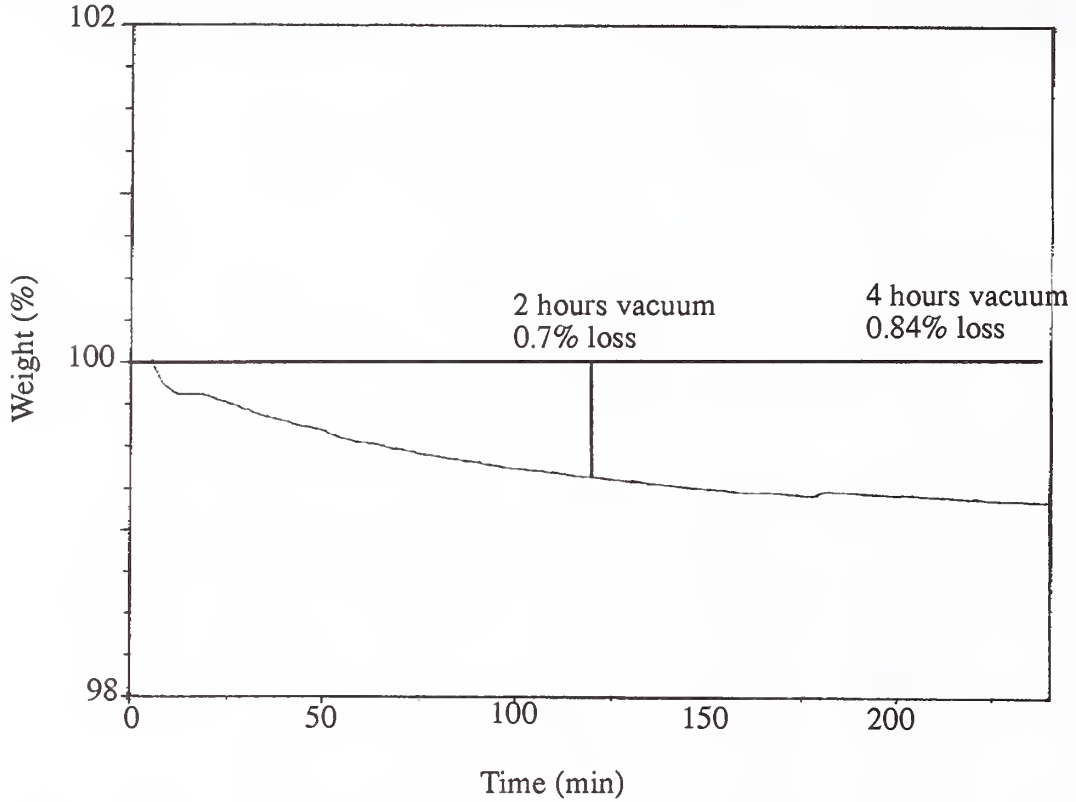
Graph 2: Moisture versus Time for HTOL Testing with Cure Cycle A.



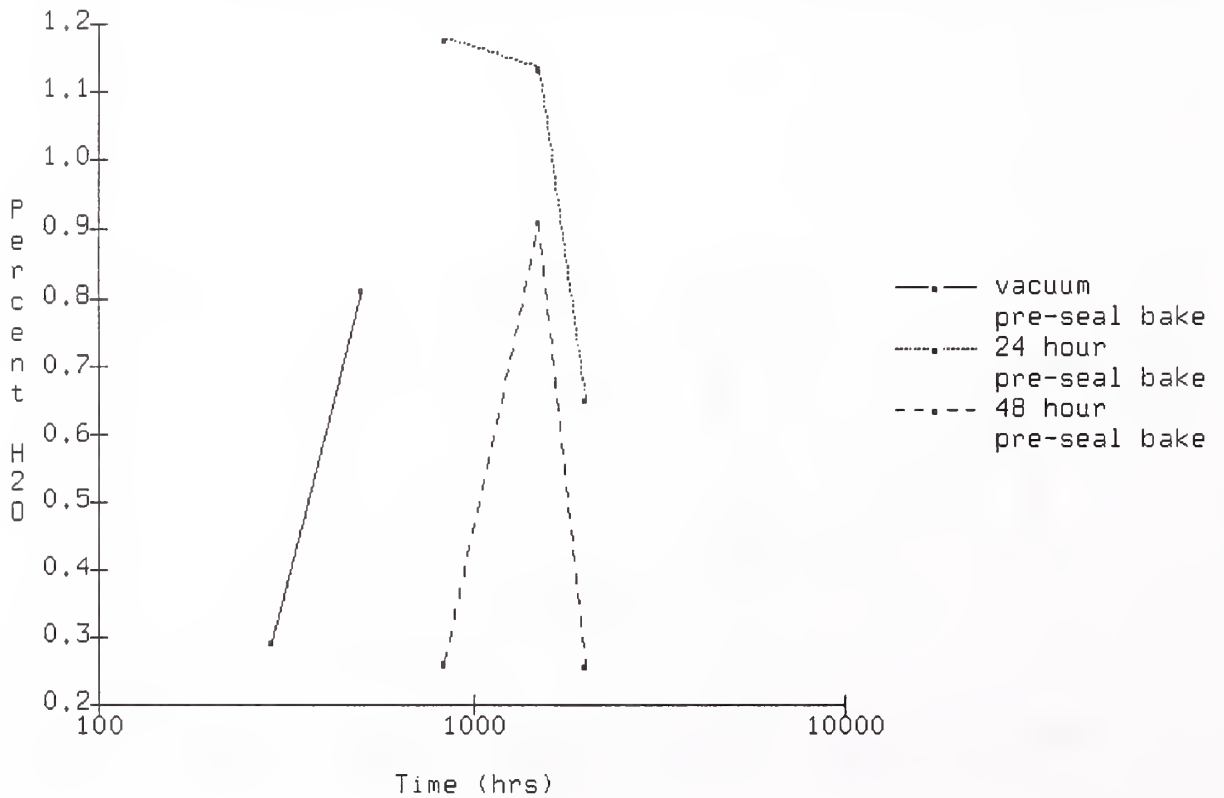
Graph 3: Time versus Percent Weight Loss for Nitrogen Pre-Seal Bake with Cure Cycle A.



Graph 4: Time versus Percent Weight Loss for Vacuum Pre-Seal Bake with Cure Cycle B.



Graph 5: Time versus Percent H₂O for Pre-Seal Bake Cycle.



EFFECTS OF PROCESS VARIABLES ON MOISTURE IN HERMETIC PACKAGES CONTAINING ORGANIC ADHESIVES

William H. Bardens
Beckman Industrial Corp.
An Affiliate of Emerson Electric Co.
4141 Palm Street
Fullerton, CA 92635

Terry E. Phillips and Richard C. Benson
Applied Physics Laboratory
The Johns Hopkins University
Johns Hopkins Road
Laurel, MD 20723

Abstract: The level of internal water vapor in a hermetic enclosure is the result of many variables. Two of the most important of these are the materials used internally in the construction of the device and the process steps utilized both, prior to, and following seal. The materials of greatest concern are organic adhesives, typically epoxy-based polymers, that are used for die and/or substrate attachment. The outgassing from these adhesives is dependent on the processing steps and can result in a surprisingly wide range of internal water vapor levels. This paper presents the results of experiments performed to investigate the effects of process variables on two commonly used substrate attach adhesives. These experiments involved mass spectrometric analysis of the internal atmosphere of hermetically-sealed packages that had been subjected to different preseal bakes and post-seal (burn-in) temperatures along with more detailed gas chromatographic/mass spectrometric analysis of the individual adhesives as a function of preseal bake and burn-in conditions. The results of these investigations led to the adoption of a particular system and process for use in manufacturing hybrids, which will also be discussed.

Key Words: Gas chromatography/mass spectrometry, hermetic packages, moisture, organic adhesives, outgassing, process variables.

1. INTRODUCTION

The investigation discussed in this paper was prompted by a failure to meet the 5000 ppmv maximum water vapor content specified in Mil-H-38534B during qualification testing of a newly designed hybrid microcircuit. It is generally accepted, and has been demonstrated by numerous researchers and by production experience over many years, that the water vapor level inside a sealed package is greatly affected by process variables prior to seal, the materials of construction inside the package, and the time and level of post-seal elevated temperature exposure (burn-in conditions). Previous articles have discussed, in general, the importance of adequate preseal bakeouts and the need to minimize the reabsorption/readsorption of water by the package and materials [1-6]. However, there have been few studies where the effect of preseal bakeout conditions on water content was investigated [7,8]. Indeed, one early study [9] found no correlation between water content and the presence of adhesives in the package nor between water content and preseal bakeout conditions, but rather the moisture level appeared to be more related to leak rates even though the packages had passed helium leak tests at the 10^{-7} cc-atm/sec level. Since even relatively small leak rates in packages can result in moisture levels that are comparable to (or even greater than) the water outgassed from organic materials, it is imperative that only residual gas analysis (RGA) data of adhesive outgassing in hermetic packages be used when investigating organic adhesives.

Experience has also shown that the organic adhesive used in the construction of hybrids is the primary contributor to water vapor under conditions where the sealing ambient contained low moisture and the package remained leak free. Previous work [8] by one of the authors had shown that for a given adhesive, water vapor levels will be decreased by longer preseal bakeout times and will be increased by post-seal elevated temperature exposure, with the increase being larger for higher temperatures and/or longer time periods. The latter observation was also reported by Ebel [3] and Ireland [10].

This previous work [8] resulted in the adoption of a different adhesive and preseal bake procedure at that time (1984). These materials and procedures have been utilized since the mid-1980s with generally effective results. There have, however, been periodic incidents of water vapor failure and, in investigating these, it became obvious that the adhesive and process in use resulted in a system which is subject to a very sharp increase in water vapor outgassing when the temperature is increased only marginally above 125°C. This increased outgassing of water vapor was not able to be reduced by modifications to the preseal process variables, at least within the range deemed acceptable for manufacturing.

After reviewing the history and taking into account the most recent failure on a major program, it was decided to pursue an investigation that would result in a system of materials and procedures that would significantly reduce water vapor levels and eliminate the periodic unanticipated failures.

2. EXPERIMENTAL METHOD

The goal of this work was to investigate a new material and preseal process which would result in lower water vapor content and which would reduce the temperature sensitivity of water outgassing in the 125°C range. Experience has shown that the adhesive used for substrate attachment, not the die mount adhesive, is the primary source of water vapor. This is certainly consistent with the fact that a typical hybrid contains from 5 to over 100 times as much substrate attach adhesive as die mount adhesive. The data obtained in this work provide comparative information on the water vapor levels resulting from the usage of two different substrate adhesive systems and variations in preseal bakeout procedures.

Materials

The organic adhesives used in these experiments were Ablefilm 555K and Ablefilm 5020K, which are epoxy preforms used for substrate attach. The package used was a Kovar plug-in style bathtub with a length and width of 1.765" x 1.245" (4.48 cm x 3.16 cm) with gold-plated leads on an electrolytic nickel-plated body. The lid was Kovar plated with electroless nickel and sized to fit the package. The lids were attached to the header by roller welding inside a glove box containing a dry nitrogen atmosphere with less than 20 ppm water vapor content. Except where noted, all packages had the lids attached prior to starting the preseal bake procedure by tack welding them in place with two small spot welds placed on opposite sides of the package. This positions the lid in place, but allows for atmosphere exchange through the unsealed areas of the lid-to-package interface. The internal volume of the sealed unit was approximately 4.1 cm³ without a substrate and approximately 3.4 cm³ with a substrate.

The adhesive substrate mounting preform had a length and width of 1.630" x 0.990" (4.14 cm x 2.51 cm) and had a volume of 0.132 cm³ for 5 mil (0.0127 cm) thick material and a volume of 0.158 cm³ for 6 mil (0.0152) thick material. In some experiments, the preform was not covered with a substrate, while in others, an alumina substrate was used in order to simulate the diffusion processes that occur in actual devices. The substrate, when used, was the same size as the preform and consisted of 25 mil thick 96% alumina.

Processing Conditions

The primary variables in the experiments are as follows:

1. A comparison of two materials: the currently used Ablefilm 555/555K and the proposed Ablefilm 5020K.
2. Post-seal high temperature storage at two temperatures, 125°C and 150°C, for varying times up to 1000 hours.
3. Preseal bakeout at 155°C with two different conditions of bakeout: 48 hours air prebake + 5 hours vacuum bake or 48 hours vacuum prebake + 5 hours vacuum bake.

This third variable needs some clarification as to the bake combination used. It is well-known and accepted that in order to obtain a dry package, some level of preseal baking is required. This bake could be performed entirely in the vacuum oven which is attached to, and opens directly into, the sealing chamber. However, the length of time required for adequate baking makes it impractical to utilize the attached vacuum oven for the total time period because of the severe limitation it places on production throughput. The bake cycle was, therefore, divided into two segments with the first portion being performed in an off-line oven. This bake is identified by the term "prebake" and this identifier will be used in the balance of this paper. Following prebake, the parts are transferred to the vacuum oven attached to the sealing chamber. Since the transfer between ovens results in exposure to room air, the transfer time is limited to a period of ten minutes maximum to minimize reabsorption of moisture by the adhesive materials. The two conditions which will be evaluated here are the use of either a forced air convection oven or a vacuum oven during prebake.

In order to make the results as meaningful as possible, conditions other than those previously discussed were kept as nearly identical as possible. There were some deviations from this due to the fact that the initial emphasis was to minimize the time required to recover from a qualification failure. Any deviation or additional variables from those discussed above will be noted as individual experiments are discussed. It should also be noted that regardless of whether it was prebake or final bake, a pressure of 10 mTorr or less was achieved at the end of the bake cycle for all vacuum bakes.

Residual Gas Analysis of Packages

The water vapor analyses on the sealed packages were all done by the same facility (Oneida Research Services, Inc.) utilizing the procedure specified in Mil-Std-883D, Test Method 1018.2 including pretest bake except where noted.

Gas Chromatography/Mass Spectrometry

In order to obtain more detailed outgassing information on the adhesives, volatile species were also measured with a modified gas chromatograph/mass spectrometer (GC/MS) which has been previously described in detail [11]. The sample configuration used in the GC/MS experiments was 9 each 0.3" x 0.5" (0.76 cm x 1.27 cm) Ablefilm 5020K preforms that were attached to electrolytic nickel-plated Kovar headers with the preform covered with an alumina substrate; no lids were used. Procedures were employed that were similar to those used for the hermetic packages. The adhesive samples were cured for 2 hours at 150°C in a chamber in ambient air. Following cure, samples were subjected to two different preseal bake conditions: 48 hours at 160°C in air plus 6 hours at 160°C in vacuum or 48 hours at 160°C in vacuum plus 6 hours at 160°C in vacuum. After the 48-hour portion of the bakeout (prebake) was completed, the samples were placed in the sample chamber attached to the GC/MS system while purging with helium; the chamber had been previously baked out in vacuum at 250°C. The 6-hour portion of the vacuum bakeout was conducted in this chamber.

The sample chamber and transfer lines were stainless steel with all seals made of metal except for the rotor seal in the gas sampling valve which was made of carbon-filled polytetrafluoroethylene. The chamber pressure was measured with a MKS Model 315BA capacitance manometer equipped with a 1330 Pa (10 Torr) head. The temperature of the sample chamber was regulated to $\pm 1^\circ\text{C}$ and the capacitance manometer, valves, and transfer lines were maintained at 150-170°C in order to minimize adsorption of chemical species on the internal metal surfaces of the apparatus.

The HP 5890A gas chromatograph was equipped with two capillary columns which are individually switched into the sampling stream. The first column, a HP-1, is a capillary column of cross-linked methyl silicone gum, 12 m long, 0.2 mm ID, and 0.33 μm film thickness. The second column, a Chrompack PoraPlot Q, is a capillary column lined with styrene-divinylbenzene porous copolymer, 10 m long, 0.32 mm ID, and 10 μm film thickness. It is the wide range of molecular weights, polarities, etc. of the volatile components outgassing from these samples that dictates the use of two distinctly different columns to provide the necessary chromatographic separation. The Chrompack column was typically used to provide separation of the lower molecular weight compounds, in particular water. Because of the emphasis on water in this work, analyses using the Chrompack column were given priority in cases where the outgassing pressure in the chamber was rather low and there was sufficient gas for only one run. Higher weight compounds were separated by the HP-1 column. Helium (99.9995% purity) was used as the carrier gas. The GC column was connected to a HP 5970B quadrupole mass spectrometer using a capillary direct interface. Electron impact ionization was used with an electron energy of 70 eV.

The results obtained from the GC/MS measurement are reported as total ions (generated and measured by the MS) per unit time as a function of the column elution time, and are presented as a total ion chromatogram (TIC). Each data point on this TIC represents the total number of ions contained in the mass spectrum taken at the indicated time. By examining the mass spectrum of the peaks in the TIC, the identity of the corresponding molecular species can usually be determined. Furthermore, the total number of ions in each peak is proportional to the number of molecular species eluting from the column, which is related to the original concentration in the sample cell. The response of the GC/MS system to water was determined by introducing known water vapor pressures into the sample chamber, followed by transfer to the GC and detection by the MS. This was done for a range of water concentrations.

An alternative water calibration method is also being pursued which utilizes the evolution of a known quantity of water from a hydrated salt. The requirements for such a material are: it is non-hygroscopic, it is thermally stable below 60°C, it exhibits a reproducible water loss via heating, and that this water loss occurs in the temperature range 60 to 160°C. The primary advantage of this method is that the desired water vapor concentration in the sample chamber is achieved on the basis of first-principal measurement of the hydrated salt mass. Furthermore, no vapor phase transport to the sample chamber occurs. Rather, the water vapor is generated *in situ* in the chamber in a manner similar to the outgassing from the adhesive samples. Since no liquid water is produced, there should be no vapor phase transport of ions from the salt as is occasionally observed from saturated salt solutions. We have investigated several hydrated salts using thermogravimetric analysis (TGA), and have determined that $\text{CaSO}_4 \cdot 2\text{H}_2\text{O}$ seems to meet all of our requirements. Low levels of water vapor would require extremely low masses of hydrated salt, which could be difficult to handle. However, this small quantity can be easily achieved by diluting $\text{CaSO}_4 \cdot 2\text{H}_2\text{O}$ in a non-hydrated salt such as KBr. Mixtures have been prepared and the TGA results are reproducible. The TGA measurements show that the water begins to evolve at ~100°C and is essentially complete by 150°C. Follow-on experiments will be conducted in the GC/MS system.

3. RESULTS AND DISCUSSION

Experiments Using Hermetic Packages

The first experiment, as outlined in Table 1, was intended as an initial look at the effect on water vapor resulting from usage of the new adhesive (Ablefilm 5020K) to determine if this alternative was viable. Substrates were mounted in all samples (except Group 5) by the adhesive listed. One group (#2) had lids, which had previously been vacuum baked, placed on the package in the glove box after preseal bake was completed instead of the standard procedure of tack welding the lid in place prior to starting the preseal bake. A second group (#3) had a moisture getter (Staydry 1000 manufactured by Staystik, Inc.) applied to the inside surface of the lid prior to lid attachment. A third group (#5) consisted of empty package controls to help determine if all other portions of the process were in control. All

Table 1 Effect of Adhesive Type and Process Variables on Water Vapor Levels

Test Group	Adhesive Preform Material	Preform Thickness	Other Variables	Water Vapor Level (ppmv)
1	Ablefilm 555K	5 Mil		4039
				4191
2	Ablefilm 555K	5 Mil	Lids Placed on Headers <u>After</u> Preseal Bake	4223
				4290
3	Ablefilm 555K	5 Mil	Moisture Getter Used	4315
				4356
4	Ablefilm 5020K	6 Mil		4491
				4496
5	None	—	Empty Package Controls	4732
				4289
6	None	—	Empty Package Controls	4298
				4427
7	None	—	Empty Package Controls	4429
				4581
8	None	—	Empty Package Controls	4636
				<100
9	None	—	Empty Package Controls	<100
				340
10	Ablefilm 5020K	6 Mil		2625
				2836
11	None	—	Empty Package Controls	2936
				3119
12	None	—	Empty Package Controls	589
				779

samples in this experiment were subjected to a prebake seal procedure consisting of 48-hour air prebake + 5 hours vacuum bake at 155°C. After seal was completed, all samples were subjected to the screening steps of leak test, stabilization bake, temperature cycling, and burn-in required by Mil-H-38534B with burn-in being simulated by temperature storage at 125°C for 168 hours. At the completion of these screening steps, the samples were subjected to water vapor testing.

The second experiment consisted of samples built without a substrate - the adhesive preform was simply cured in place on the base of the package. This allowed an evaluation of the outgassing of water vapor without having to be concerned with the effect, if any, of the rate of diffusion of water vapor to the edge of the preform where it could be released to the package atmosphere. Also evaluated at this time was the effect on both adhesive systems of performing the prebake in air or vacuum. These samples were sent to the testing facility after seal without exposure to any additional screening steps except leak test. The testing facility then baked the samples under the conditions specified in Tables 2 and 3 and performed water vapor analysis immediately after removal from the bake oven.

The third experiment, as outlined in Table 4, was performed primarily to provide confirmation of the results of previous experiments as concerns the Ablefilm 5020K material. The samples were built the same as before, but six months later using a newer and different manufacturing lot of adhesive. These samples were sent to the testing facility after seal without exposure to any additional screening steps except leak test. The testing facility then baked the samples under the conditions specified in Table 4 and performed water vapor analysis immediately after removal from the bake oven.

RGA Results from Package Experiments

Table 1 shows the results of the first experiment in terms of the water vapor levels achieved. Several observations may be made concerning this data. The first of these is that the control samples exhibited very low water vapor levels, indicating that the levels obtained in the other sample groups were truly related to the material contained within the package enclosure and not related to some external factor such as bakeout oven temperature control or high levels of water vapor in the seal chamber. The second observation is that the usage of the moisture getter results in remarkably low levels of water vapor. Although the use of this material is not currently acceptable for all applications, the possibility of introducing its usage should definitely be explored. The third observation is that, with the process parameters used, there is no difference in water vapor levels whether or not the lids are positioned on the package during preseal bakeout; this is consistent with prior tests and production experience. The fourth observation is that the water vapor levels in the packages containing Ablefilm 5020K are significantly lower than those in the packages containing Ablefilm 555K. The improvement resulting from the usage of Ablefilm 5020K is probably even better than that shown here when the different thicknesses of the two materials are considered. The amount of water vapor outgassed from a material is certainly related to the volume of material present. Although the water vapor level inside the package may not be directly proportional to the volume of the adhesive, there is no doubt that had the thickness of the Ablefilm 5020K been 5 mils thick instead of 6 mils, the water vapor levels would have been even lower.

Tables 2 and 3 show the results of the second experiment in terms of water vapor levels achieved for Ablefilm 555K and Ablefilm 5020K, respectively. Run 1 was data collected on samples which had received a 48-hour air prebake, and Run 2 was data collect on samples which had received a 48-hour vacuum prebake. For the samples with Ablefilm 555K, there is a Run 1A and 1B because on Run 1A,

Table 2 Water Vapor Using Uncovered Adhesive (No Substrate).
Ablefilm 555K, 5 Mil Thick.

Preseal Bake Conditions	Run 1A	Run 1B	Run 2
	48-Hr. <u>Air</u> Prebake + 5-Hr. Vacuum Bake 155°C	48-Hr. <u>Air</u> Prebake + 5-Hr. Vacuum Bake 155°C	48-Hr. Vacuum Prebake + 5-Hr. Vacuum Bake 155°C
Post-Seal Bake Conditions	Water Vapor, ppmv	Water Vapor, ppmv	Water Vapor, ppmv
0 Hr. @ 125°C	<100 105	<100	—
40 Hr. @ 125°C	—	254 559	328
80 Hr. @ 125°C	3061 3275	864 972	—
183 Hr. @ 125°C	2124 3908	1304 1612	1534
383 Hr. @ 125°C	8266 8297	2618 2659	—
40 Hr. @ 150°C	—	4232 5013	7000
80 Hr. @ 150°C	18000 19600	8382 8920	—
183 Hr. @ 150°C	12600 15900	14000 14400	—
383 Hr. @ 150°C	33800 34300	27000 27900	—

the water vapor levels after 80 hours post-seal bake were higher than for 183 hours. It was felt that one of these two data points was anomalous. Therefore, a second set of samples was built using the same parameters as before and was submitted as Run 1B. This run had the more typical increase in water vapor level resulting from each added increment of time. Run 1B had generally lower values overall than did 1A, but illustrated the same trends. Run 2 for Ablefilm 555K contained fewer samples because it was only being used to confirm the results of considerable work done previously that had shown no difference between air prebake and vacuum prebake for Ablefilm 555K. The limited data contained in Run 2 is in agreement with this previous conclusion.

The most important observation to be made concerning the data in Tables 2 and 3 is the very significant decrease in water vapor levels for Ablefilm 5020K when a vacuum prebake is incorporated. For both 125°C and 150°C post-seal exposure, the reduction due to vacuum prebake compared to air prebake is on the order of 85%. No such reduction occurs with Ablefilm 555K. It is also interesting to note that for the time periods involved, Ablefilm 5020K with vacuum prebake appears to have none or a very small increase in water vapor due to increasing burn-in time.

Table 3 Water Vapor Using Uncovered Adhesive (No Substrate).
Ablefilm 5020K, 6 Mil Thick.

Post-Seal Bake Conditions	Preseal Bake Conditions	Run 1A	Run 1B*	Run 2
		48-Hr. <u>Air</u> Prebake + 5-Hr. <u>Vacuum</u> Bake 155°C	48-Hr. <u>Air</u> Prebake + 5-Hr. <u>Vacuum</u> Bake 155°C	48-Hr. <u>Vacuum</u> Prebake + 5-Hr. <u>Vacuum</u> Bake 155°C
		Water Vapor, ppmv	Water Vapor, ppmv	Water Vapor, ppmv
0 Hr. @ 125°C		<100 100	—	—
40 Hr. @ 125°C		—	—	186 389
80 Hr. @ 125°C		2863 2863	—	425 674
183 Hr. @ 125°C		2998 3120	—	548 556
363 Hr. @ 125°C		6165 7324	—	300 357
40 Hr. @ 150°C		—	—	—
80 Hr. @ 150°C		15400 15700	—	1334 1597
183 Hr. @ 150°C		12500 14300	—	2143 2730
383 Hr. @ 150°C		30100 30600	—	1470 2260

*There was no need to conduct Run 1B; the column is included to enable clear comparison with Table 2.

Table 4 shows the results of the third experiment in terms of the water vapor and carbon dioxide levels achieved. Several observations may be made concerning this data. The first and most important of these is that the reduction in water vapor levels obtained when vacuum prebake is used, as was seen in the previous experiment, was observed in this experiment also. This reduction occurs for samples subjected to both 125°C and 150°C post-seal temperature exposure, but is particularly dramatic at 125°C. The second observation is that it made little or no difference whether a substrate was attached on top of the preform or if the surface of the adhesive preform was exposed to the package atmosphere. This would indicate that for the time and temperature involved in this particular preseal bakeout, diffusion of the water vapor to the edge of the substrate plays no part in the eventual water vapor levels. The third observation comes from the evaluation of the carbon dioxide levels in these same packages. The bottom half of Table 4 lists the values of carbon dioxide in the same order as given for water vapor in the top portion of the table. It is obvious from this data that carbon dioxide levels have the same dependency on vacuum vs air prebake that water vapor level does. Although the carbon dioxide level is not subject to any specification limit, and thus not of interest in terms of attempting to control it, it may be of some value when attempting to determine the mechanism involved in the vacuum vs air prebake differences.

Table 4 Effects of Variations in Preseal Conditioning and Post-Seal Temperature Storage on Water Vapor Levels. Ablefilm 5020K Adhesive, 5 Mil Thick.

Pre-Seal Conditioning \ Post Seal Exposure	Water Vapor, ppmv		
	168 Hours at 125°C (Burn-In Simulation)	1000 Hours at 125°C	1000 Hours at 150°C
Empty Package 48-Hr. <u>Vacuum</u> Prebake + 5-Hr. Vacuum Bake at 155°C	447	620	—
Adhesive with No Substrate 48-Hr. <u>Vacuum</u> Prebake + 5-Hr. Vacuum Bake at 155°C	—	1035 1611	7600 11500
Adhesive With Substrate Attached 48-Hr. <u>Vacuum</u> Prebake + 5-Hr. Vacuum Bake at 155°C	175 257 902	712 932 —	10200 12100
Adhesive With Substrate Attached 48-Hr. <u>Air</u> Prebake + 5-Hr. Vacuum Bake at 155°C	916 1295 3578	5873 7178 7864	24100 28800
Carbon Dioxide (CO₂), ppmv			
Adhesive With No Substrate 48-Hr. <u>Vacuum</u> Prebake + 5-Hr. Vacuum Bake at 155°C	—	5607 6149	14900 16500
Adhesive With Substrate Attached 48-Hr. <u>Vacuum</u> Prebake + 5-Hr. Vacuum Bake at 155°C	1547 1579 3299	4891 5300	16300 15500
Adhesive With Substrate Attached 48-Hr. <u>Air</u> Prebake + 5 Hr. Vacuum Bake at 155°C	5508 4914 5253	19000 17700 22100	58800 51900

In addition to the water vapor results shown in Tables 1-5 and the carbon dioxide results shown in Table 4, the mass spectrometer gives information on other components of the gas contained within the sample. When looking at the detailed residual gas analysis reports of the packages, the following was noted:

1. There were a small number of leak-test escapes as identified by helium and/or fluorocarbon content. The data from these were considered invalid and were not included in these results.
2. No major differences or trends in the gas composition were obvious except for water vapor and carbon dioxide already discussed.
3. There was no hydrogen in any of the empty packages nor in the packages containing only the substrate attach adhesive. The only packages containing hydrogen were those that were complete operating hybrids, and these contained hydrogen up to 8000 ppmv.
4. Samples containing Ablefilm 555K had no ammonia detected regardless of the test conditions.
5. Samples containing Ablefilm 5020K had no ammonia detected as long as the post-seal temperature exposure was limited to 125°C. Samples stored at 150°C began to show ammonia after 40 hours, with the maximum value obtained being 3167 ppmv after 1000 hours.
6. Low levels of methyl alcohol were reported in a few of the packages, but there was no correlation with processing conditions nor with any other species.

Table 5 represents the practical application of the results obtained from the experiments. The top portion of this table shows the data from the qualification units which failed and prompted this investigation. The first four data points are from the units submitted as required by Mil-H-38534B. The bottom portion shows the data from the second qualification after units were rebuilt using the material (Ablefilm 5020K) and revised process identified as acceptable by the experiments. As is obvious, these units passed the water vapor requirement and would have done so even at the end of a 1000-hour operating life.

Table 5 Water Vapor Levels in Mil-H-38534 Hybrids.
Data are From Qualification Units.

Material	Pre-Bake Atmosphere	Post Seal Exposure Time at 125°C			
		Burn-In 168 Hours	Operating Life 1000 Hours	Water Vapor ppmv	
555K	Air	Yes	—	5498	
			—	5945	
			—	6052	
			—	6065	
		—	Yes	—	7157
				—	8200
				—	8800
				—	10300
				—	10400
				—	12500
5020K	Vacuum	Yes	—	586	
			—	670	
			—	879	
		—	Yes	—	544
				—	608
—	—	797			

GC/MS Analysis of Adhesive Outgassing

GC/MS measurements of the outgassing from Ablefilm 555K were conducted prior to the hermetic package experiments on Ablefilm 5020K. Since the Ablefilm 555K package studies did not exhibit any post-seal outgassing dependence on the prebake conditions, the primary motivation of the GC/MS investigation was to determine the source of water production and whether backside substrate metallization (silver/palladium) had any effect on the water vapor level. The latter investigation was motivated by our work that showed that the presence of silver flake in some conductive die attach adhesives can lead to enhanced outgassing [11-14]. However, the experiments on Ablefilm 555K did not reveal any effect on the outgassing due to the silver/palladium metallization. After these measurements were completed, the RGA results were obtained for the hermetic package experiments and indicated the strong dependence on the preseal bake conditions for Ablefilm 5020K; the GC/MS studies were then focused on this issue.

Although the hermetic package results above, using samples prepared on a hybrid manufacturing line, indicate that the differences observed in water vapor levels for the air and vacuum preseal bakeouts of Ablefilm 5020K were due to adhesive properties, it was thought useful to verify this using controlled experiments in a laboratory environment. Because of the high sensitivity of the GC/MS technique, it was expected that changes in the composition of the outgassed species could be correlated with the preseal bakeout conditions. If this were indeed the case, then information would be obtained regarding the chemical reactions involved that result in water production.

As discussed earlier, the adhesive samples were placed in the GC/MS sample chamber following cure and the 48-hour preseal bake (either air or vacuum). They were then subjected to a 6-hour vacuum bake and the sample chamber sealed under vacuum to allow the outgassing products to collect in the sample chamber at 125°C, with the chamber pressure monitored as a function of time. The outgassing products were analyzed with the GC/MS at the following approximate times: 40, 90, 136, and 185 hours. The entire contents of the sample chamber was transferred to the GC/MS at the end of each time interval, the chamber resealed, and the outgassing collected for the next time interval. Thus, the GC/MS data is for the entire time interval; e.g., 0-40 hours, 40-90 hours, etc.

Shown in Figure 1 are the total ion chromatograms using the Chrompack column obtained for the 40-90 hour time interval of the simulated burn-in at 125°C for Ablefilm 5020K that had been subjected to either an air prebake (Figure 1a) or a vacuum prebake (Figure 1b). The outgassing species detected were (listed in order of increasing retention time): carbon dioxide, propene, methyl chloride, water, dimethyl ether, butene, methyl alcohol, propanal, acetone, methyl acetate, and tetrahydrofuran. (The benzene is from a system impurity.) An important observation in the GC/MS experiments is that ammonia was never detected during outgassing from Ablefilm 5020K at 125°C. This substantiates the RGA results from the hermetic packages where ammonia was detected only in samples that had been subjected to extended heating at 150°C.

Note the lower water concentration in the sample subjected to the vacuum preseal bakeout. This was the case for all of the measurements obtained during the simulated burn-in period. This is evident in Figure 2 where the cumulative amounts of the three dominant outgassing species (carbon dioxide, methyl alcohol, and water) are shown as a function of burn-in time, where the results have been normalized with respect to the mass of adhesive used in each experiment. The water level in the sample subjected to the air prebake was approximately twice that of the sample that was prebaked in vacuum. This is the same trend as observed in the hermetic package experiments, but the magnitude of the effect is much lower. The corresponding results for carbon dioxide and methyl alcohol exhibit a 25-30% increase for the sample that was prebaked in air. Again, this trend for carbon dioxide was observed in the hermetic package experiments, but the effect is lower in the GC/MS studies. Methyl alcohol was not consistently observed in the hermetic package experiments, yet is always a strong peak in the GC/MS data which indicates the high sensitivity of the GC/MS measurement.

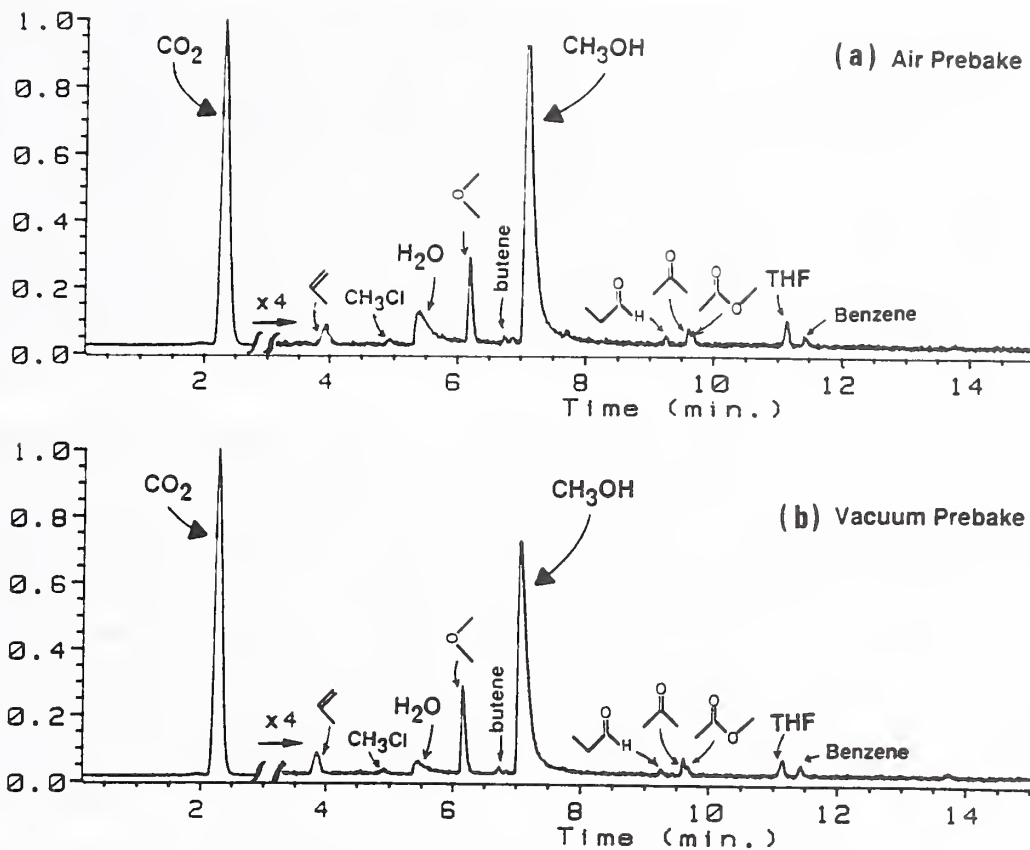


Figure 1 Total ion chromatograms obtained using the Chrompack column for Ablefilm 5020K outgassing during the 40-to-90 hour period of simulated burn-in at 125°C. Note that each chromatogram is plotted with the carbon dioxide peak intensity set at full scale. Adhesive subjected to (a) 48-hr. prebake in air at 160°C + 6-hr. vacuum bake at 160°C and (b) 48-hr. prebake in vacuum at 160°C + 6-hr. vacuum bake at 160°C.

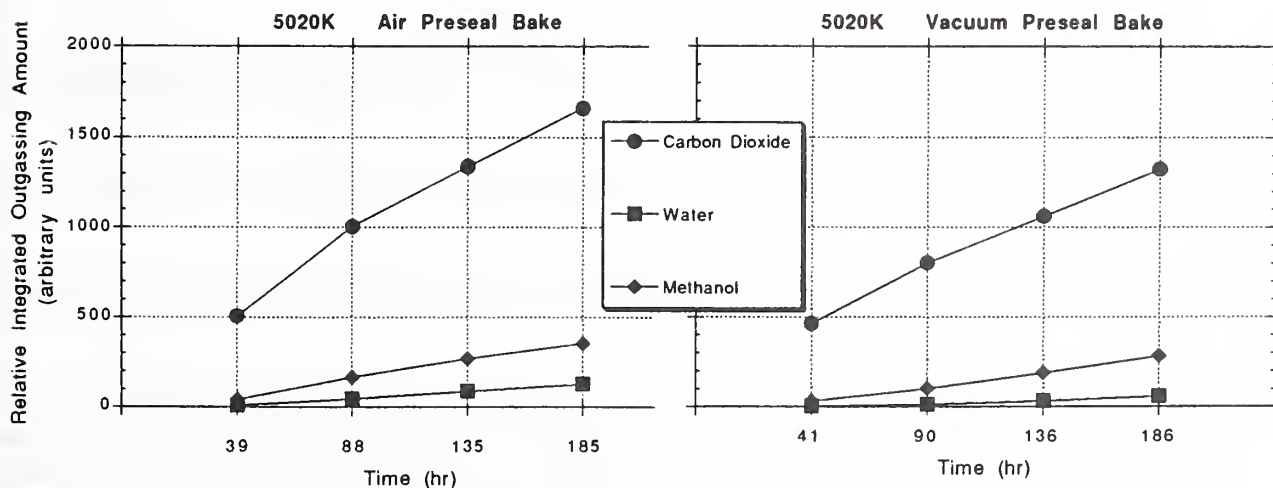


Figure 2 Cumulative outgassing amounts for carbon dioxide, water, and methyl alcohol as function of simulated burn-in time at 125°C for Ablefilm 5020K subjected to air or vacuum prebake.

This high sensitivity enables the detection of several organic species (see Figure 1) which potentially can provide information on chemical reactions that may occur in the adhesive; e.g., if the adhesive undergoes thermal degradation during burn-in. Our previous work has indicated that thermal degradation of the polymer system can occur at 125°C [11-14]. At the present time, we do not know which outgassing species from Ablefilm 5020K (Figure 1) may be additives, impurities, or degradation products. Comparing the GC/MS results for the minor outgassing constituents of the air and vacuum prebaked samples unfortunately did not reveal any significant differences in chemical composition nor concentration. Furthermore, the small sample size in some cases precluded the use of the HP-1 GC column which is used to separate and detect higher molecular weight organic species. Thus, we were not always able to analyze the gas using both the Chrompack column and the HP-1 column. Future experiments will utilize a larger mass of adhesive in order to increase the detection sensitivity for the minor outgassing species.

The total pressure rise in the sample chamber (volume = 20 cm³) over the 186-hour burn-in period at 125°C was 0.46 Torr for air prebaked Ablefilm 5020K and 0.25 Torr for the vacuum prebaked samples; these values have been corrected for the adhesive sample mass. In terms of total outgassing per unit adhesive mass, the values were 2.3 Torr/g and 1.25 Torr/g for the air and vacuum prebake, respectively. The chamber pressure continued to increase throughout the 186-hour burn-in period, which is in agreement with the behavior of the dominant species shown in Figure 2. However, this is not in agreement with the results of the hermetic package experiments, where it was observed that the air prebaked samples continued to outgas water and carbon dioxide, but the vacuum prebaked samples exhibited little or no increase in water and carbon dioxide outgassing as a function of burn-in time at 125°C. The GC/MS adhesive samples outgassed into an evacuated chamber while the adhesive in the hermetic packages outgassed into an enclosure that was approximately one atm of nitrogen. It is not known at this time what the effect, if any, of an atm of inert gas is on the adhesive outgassing rate.

Future experiments will address this issue by conducting the process with, and without, one atm of inert gas present in the chamber. Furthermore, additional GC/MS experiments will be conducted on Ablefilm 5020K using larger quantities of adhesive in each experiment in order to increase the sensitivity for the detection of minor species. In this manner, we may be able to detect any difference in the chemical composition or the concentration of outgassed species depending on whether an air or vacuum prebake is used. We propose that oxygen present during the air prebake may participate in chemical reactions that affect the water level outgassing. Therefore, experiments will be conducted using prebakes where the oxygen partial pressure is greater than 20% to determine if the water vapor level is correlated with the oxygen concentration during prebake.

4. CONCLUSIONS

The results of the hermetic package experiments and the GC/MS measurements are in agreement with respect to the overall trends that were observed. Based on the above discussion of these results, the following conclusions can be reached:

1. Given equivalent conditions of processing and temperature exposure, Ablefilm 5020K will result in a lower water vapor level than will Ablefilm 555K.
2. Performing the off-line prebake portion of the preseal bakeout process in vacuum instead of air will result in a significantly lower water vapor level when Ablefilm 5020K is used, but has essentially no effect on Ablefilm 555K.
3. The hermetic package experiments indicate that the all-vacuum preseal bakeout for a total of 53 hours (48 hr. + 5 hr.) appears to have essentially stopped water vapor evolution from Ablefilm 5020K at a post-seal temperature of 125°C--at least up to 1000 hours of exposure. The GC/MS measurements indicated a lower outgassing rate for the vacuum prebaked Ablefilm 5020K, but both the air and vacuum prebaked samples continued to evolve water over the 186-hour period that was studied.

ACKNOWLEDGEMENT

This work was partially supported by the Department of the Navy.

REFERENCES

1. Thomas, R. W., Moisture, Myths, and Microcircuits, *IEEE Trans. Parts, Hybrids, Packaging*, PHP-12, 167 (1976).
2. Messenger, C. G., Improved Reliability Through Dry and Hermetic Microcircuit Packaging, *Proc. 27th Elec. Components Conf.*, 1977, p. 172.
3. Traeger, R. K., Organics Used in Microelectronics: A Review of Outgassing Materials and Effects, *Proc. 27th Elec. Components Conf.*, 1977, p. 408.
4. Vasofsky, R. W., Czanderna, A. W., and Czanderna, K. K., Mass Changes of Adhesives During Curing, Exposure to Water Vapor, Evacuation, and Outgassing, Part I: Ablefilms 529, 535, and 550, *IEEE Trans. Comp., Hybrids, Manuf. Technol.*, CHMT-1, 405 (1978).
5. Ebel, G. H., Application of 1018.2 to Hybrid and VLSI Devices, *Proc. 21st Int. Reliability Phys. Symp.*, 1983, p. 274.
6. Schuessler, P., Adhesive Die Attach Materials: Their Pros and Cons, *Int. J. Hybrid Microelec.*, 6, 342 (1983).
7. Koudounaris, A. and Wargo, E. E., Detection and Control of Moisture in Space Hybrids, *Int. J. Hybrid Microelec.*, 4, 148 (1981).
8. Bardens, W. H., Mass Spectrometric Evaluation of Epoxy Adhesive Systems, *Proc. RADC/NBS Workshop, Moisture Measurement and Control for Semiconductor Devices (III)*, NBSIR 84-2852, 1984, p. 271.
9. David, R. F. S., Effects of Leak Rate and Package Volume on Hybrid Internal Atmosphere, *Int. J. Hybrid Microelec.*, 6, 433 (1983).
10. Ireland, J. E., A Performance Evaluation of a High Density, Hermetic Assembly using Epoxy Die Attachment, *Int. J. Hybrid Microelec.*, 6, 352 (1983).
11. Phillips, T. E., deHaas, N., Goodwin, P. G., Benson, R. C., and Bonneau, M., Studies of a Model Five-Component Epoxy Adhesive, *Proc. 5th SAMPE Electronics Conf.*, 1991, p. 52.
12. Benson, R. C., Phillips, T. E., and deHaas, N., Volatile Species from Conductive Die Attach Adhesives, *IEEE Trans. Comp. Hybrids Manuf. Technol.*, 12, 571 (1989).
13. Benson, R. C., Phillips, T. E., deHaas, N., and Bonneau, M., Investigations of a Model Die Attach Adhesive, *Proc. 4th SAMPE Electronics Conf.*, 1990, p. 267.
14. Phillips, T. E., deHaas, N., Goodwin, P. G., and Benson, R. C., Silver-Induced Volatile Species Generation from Conductive Die Attach Adhesives, *Proc. 42nd Elec. Components and Technol. Conf.*, 1992, p. 225; and in *IEEE Trans. Comp. Hybrids, Manuf. Technol.*, 15, 956 (1992).

LOW MOISTURE POLYMER DIE ATTACH ADHESIVE FOR SOLDER SEAL PACKAGES

My N. Nguyen
Johnson Matthey Electronics,
10080 Willow Creek Rd.
San Diego, CA 92131

ABSTRACT

Low internal cavity moisture (less than 5000ppm) is one of the key requirements for hermetic packages to prevent the possibility of moisture-induced corrosion failures of the chip. Conventional inorganic adhesives like silver-glass and Au-Si preform/ribbon are commonly used in die-attachment in solder seal hermetic packages. However, these two die-attach technologies have major process limitations during assembly.

Silver-glass requires excessive controls in bondline thickness, temperature profiles and dry air-flow during firing to ensure consistent adhesion and low internal cavity moisture. In addition, silver-glass process is die-size dependent and for large die the firing process can be up to several hours long. Both silver-glass and Au-Si eutectic require high temperature processing, typically above 340°C, which are detrimental to today's sub-micron geometry devices. Die backside conditions can impact adhesion or voids formation with either Au-Si eutectic or silver-glass paste. Low internal cavity moisture is not only achieved by ensuring dry atmosphere in the firing furnace but also by selection and preconditioning of package materials [1].

In this paper, we discuss the processing requirements and performance of a novel thermoset polymer die-attach paste developed for ease of manufacturing. Although it is organic in nature, the paste has moisture reduction properties and thus open up manufacturers to a wide range of metal lids and ceramic packages. Careful control of furnace or oven atmospheres is no longer critical to achieve low internal cavity moisture.

The advantages of this material are highlighted in comparison to conventional epoxies, polyimides, Au-Si preforms and silver-glass pastes. The paste can be cured in less than 60 seconds at 200°C and applicable to a wide range of die sizes. Reliability tests such as temperature cycling, and high temperature storage have shown that the high adhesion does not degrade and low moisture is still maintained after 1000 cycles or 1000 hours at 150°C.

I. Introduction

Advances made in the semiconductor wafer fabrication have resulted in large chip with high I/O and sub-micron geometry. At the same time, semiconductor assembly houses are focussed on improving

productivity and reducing cycle time. These have placed stringent demands on packaging materials for improved performance, robustness and faster processing.

Die-attach adhesive is important to the reliability performance of solder seal packages. Their key requirements are :-

1. Low internal cavity moisture and particle count.
2. Fast cure capability.
3. High and consistent adhesive strength.
4. Low temperature processing.
5. High temperature stability, above 360°C.
6. High speed dispensing capability.
7. No void, hence solventless paste.
8. Very low ionic contaminants.
9. No bondline control.

The conventional Au-eutectic die bonding is not suitable for big die without suffering from high yield losses due to chips and cracks cause by manual handling at die bonding step. Furthermore, the thermal mismatch for such large devices between the package, preform and die would generate high stress that could result in hair-line cracks and delaminations.

Silver-glass in comparison would not have a mismatch problem but the high temperature exposure in excess of 400°C would cause concern to the electrical performance of the device especially to the sub-micron geometry type and risk of nickel diffusion in the seal ring leading to hermeticity problems. The processing of silver-glass in such big die sizes would also require thick bondline which is difficult to achieve and control.

Conventional epoxy and polyimide systems offer efficient processing but are unable to give a "clean" cure resulting in high moisture level in the cavity of the package. This would fail military requirements of less than 5000ppm of moisture within the cavity. Besides, most epoxies are solvent based which tend to give bad voids after curing.

The new polymer die-attach paste, designated JM7000, addresses all the above requirements without any trade-offs. Its wide process window ensures maximum process flexibility. JM7000 lends itself to the current manufacturing process very well without requirement for further capital investment.

II. Material Characteristics

JM7000 is formulated based on a proprietary polymer and catalyst intersperse with Ag flake [2,3]. The paste is solventless but exhibits rheology similiar to an epoxy or polyimide.

A. Thermal Stability

The most significant performance enhancement of this material over conventional epoxies is its thermal stability. In Figure 1, thermal gravimetric analysis of the material shows no significant changes in weight during cure. The cured material is thermally stable until temperatures reach above 380°C at which point the onset of degradation occurs.

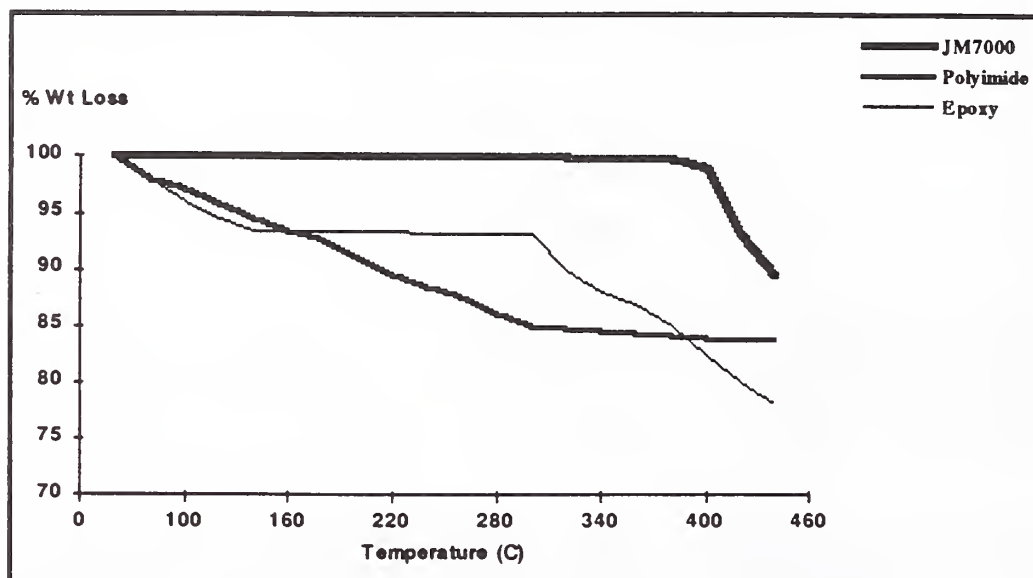


Fig 1. JM7000 Polymer Adhesive
Temperature Stability

The high thermal stability of JM7000 makes it an ideal candidate for application in solder seal packages where sealing temperatures are less than 360°C peak.

B. Cure Kinetics

Table 1 shows the cure kinetics of JM7000 at 200°C over various curing times. The degree of cure is calculated from the ratio of the residue heat of reaction to the total heat of reaction. These values are read off from the DSC (differential scanning calorimetry) traces of the material at different cure times.

<u>Times of 200 Deg C</u>	<u>DH of reaction</u>	<u>% Cure</u>
0 secs	-26.2	0
10 secs	-17.6	33
20 secs	-6.3	76
30 secs	-5.3	80
60 secs	-2.3	91
600 secs	-1.7	96

Table 1. Degree of cure

It is established that at least 90% conversion is required to achieved optimal adhesion properties [4]. In that light, it is noticed that JM7000 could generate adhesion as rapidly as within 60 secs at 200°C. The two important implications are :

- (i) The material can be processed in an inline mode if necessary and ;
- (ii) Be cured at a low temperature, thereby reducing possibility of nickel migration and electrical decadence of the circuitry.

C. Material Properties

The critical properties of this material are summarized in Table 2 in comparison to a conventional die-attach epoxy.

<u>Property</u>	<u>JM 7000</u>	<u>Epoxy</u>
Tg (°C)	240	130
Modulus (GPa)	10	12
Strain (%)	8.0	2.5
CTE (ppm)	36	40
TGA onset (°C)	380	306

Table 2. Material Properties

JM7000 has a higher Tg and onset of decomposition and much better thermal stability than epoxy based system. The high strain % at break also shows a high degree of flexibility in the material due to its unique structure of this proprietary system.

III. Processing Characteristics

A. Materials Preparation

This material like all other single component fast cure organic systems requires refrigeration at -40°C and has a shelf life of 6 months when stored at this temperature. Because the material is solventless, it will not separate out during operation and hence does not require jar rolling or stirring like in silver-glass. The material should be thawed before use and it could be done at room temperature in one hour or at elevated temperatures of 35°C for less than 20 minutes. No other material preparation is necessary prior to usage which makes this material very easy to implement on the production floor.

B. Dispensability

The other area of concern to manufacturers is the performance of the material during dispensing. Field trials have verified that the material dispenses as well as ordinary epoxy or polyimide. The material has been proven to work on high speed automated die bonders like Alphasem, Esec and

Shinkawa. In order to access the consistency of this material over the entire dispensing operation, a study was conducted using an Alphasem die bonder where the average dispensed weights for samples of JM7000 were taken at an hourly interval of up to 4 hours without machine adjustments. The results are shown in Figure 2 and indicate that there were no significant weight change during the trial period.

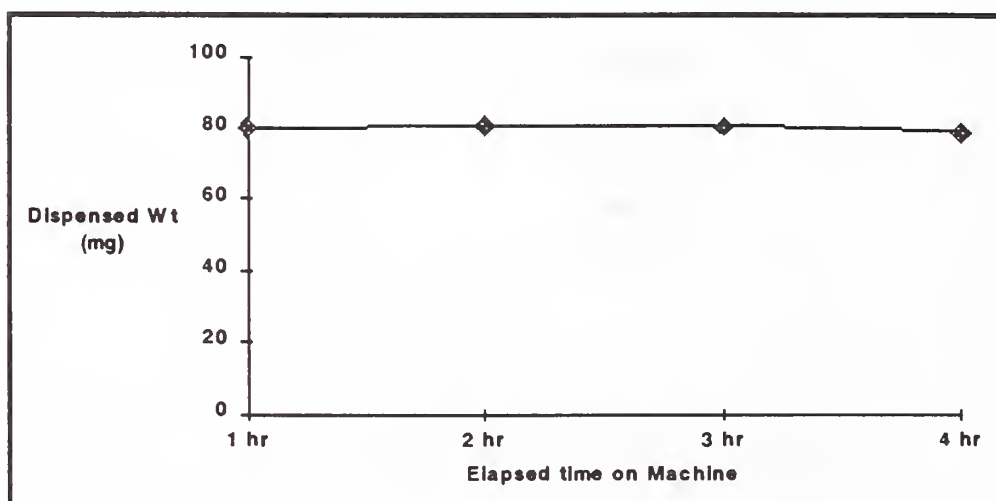


Fig 2. Dispensed Weight with time

This means that the material would dispense consistency for at least 4 hrs in running and on-going test shows that slight machine adjustment is necessary only by the end of an eight-hour period to maintain the same dispensed weight.

The pot life of this material would depend on its viscosity variations over time and this was verified by running a rheology check on the material at room temperature (25°C) using a Haake rotoviscometer. The increase in viscosity of the material is logged in as a function of time as in Figure 3. Based on this measurement, the rheology of the material will not increase significantly within the first 16 hours. This defines the pot life of JM7000.

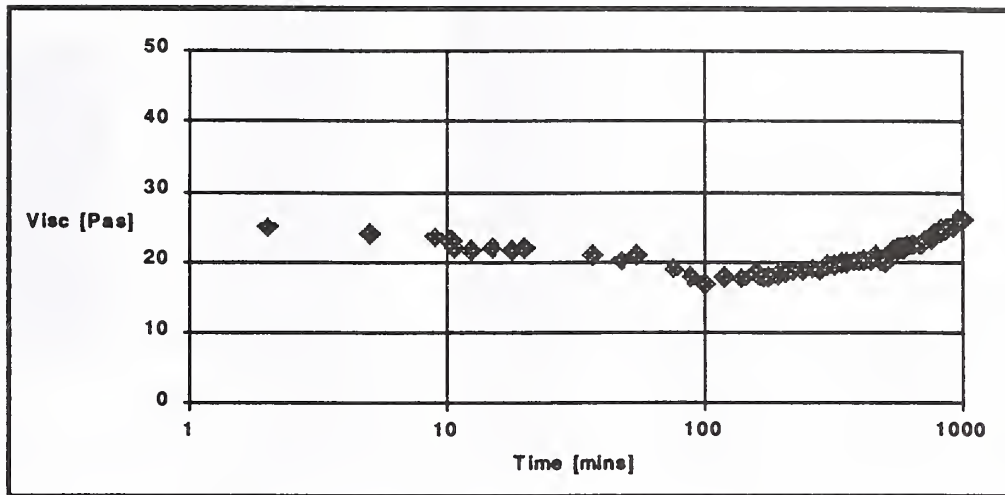


Fig 3. Viscosity Change with time

C. Curing Conditions

Because of the property of the catalyst in the material, the curing schedule could be accelerated at higher temperatures. A higher temperature could shorten the cure time to a minute or less, rendering the material snap curable. Table 3 shows the curing times at different temperatures.

<u>Cure Temp</u> (Deg C)	<u>Cure Temp</u> (secs)
150	240
160	120
180	60
200	40
250	20

Table 3. Curing Schedule

What is immediately apparent is that the material could be processed at a much lower temperature compared to silver-glass at a fraction of the processing time.

Curing could be effected by both oven and conventional furnaces and the adhesion strength of cured parts typically exceeds 1500psi. The bonding layer is void-free. The curing oven or furnace should be well circulated with air. Nitrogen or inert atmosphere is not required.

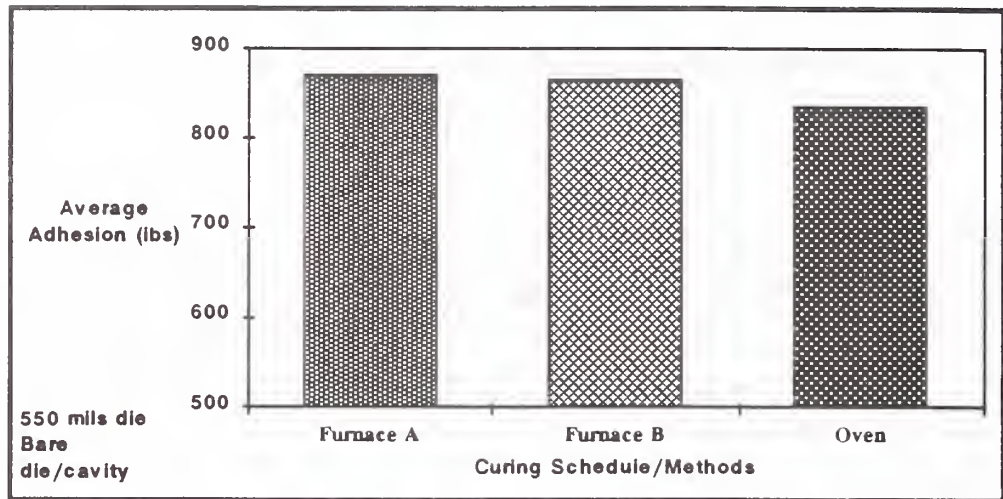


Fig 4. Adhesion with cure methods

Figure 4 illustrates the wide processing window achievable with this material. The chart contains adhesion results obtained with both furnace and oven curing. Results obtained under Furnace A and oven both had a 50-minute curing cycle whereas results under Furnace B were processed in a 10-minute curing profile. In all cases, the adhesion results obtained are similar. Voids under the die on all these 3 different splits were found to be less than 4% on the maximum.

The other desirable aspect of curing this material is that it is not dependent on die size. Figure 5 shows the relationship of adhesion to the die size. We observe that the adhesion strength does not vary with different die sizes.

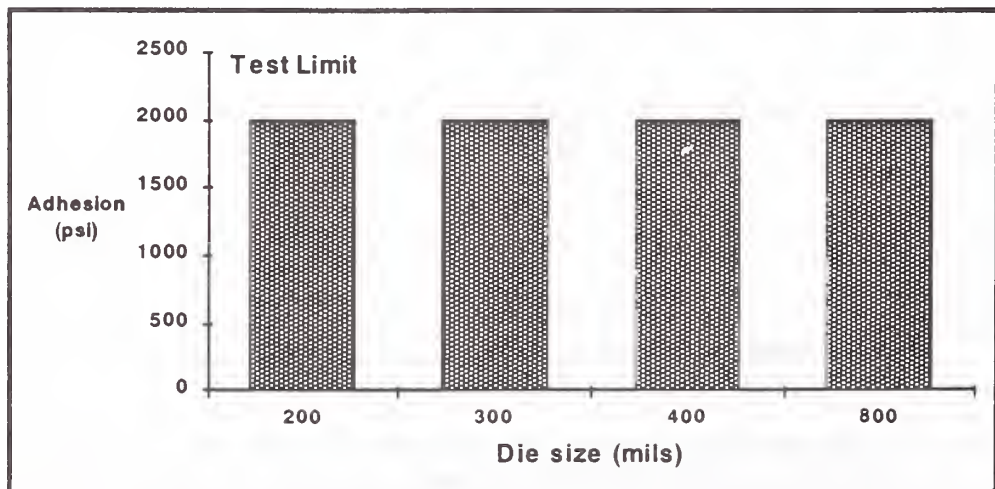


Fig 5. Die Size Robustness

In another separate study, we investigated if a variation in bondline would affect the adhesion of the JM7000. The results summarized on Figure 6 show that the material, unlike silver-glass, is independent of the bondline thickness.

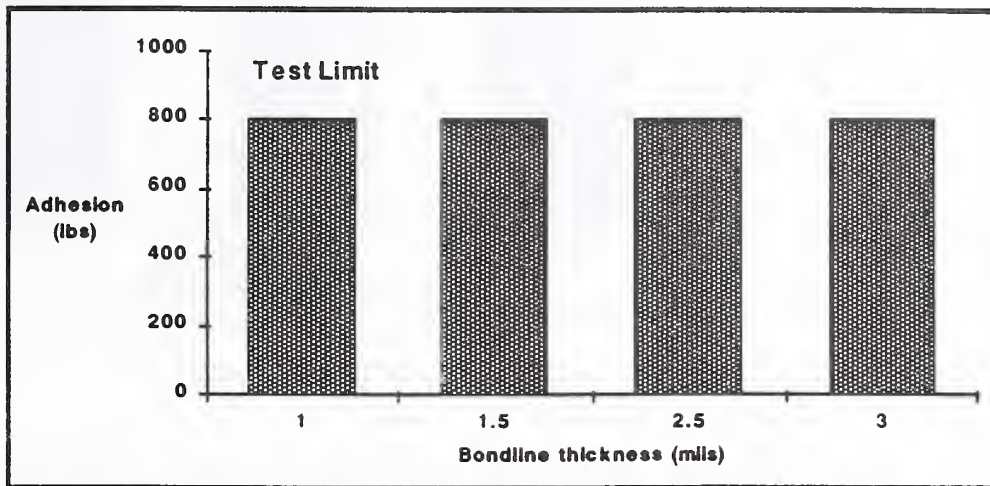


Fig 6. JM7000 Bondline Thickness

The adhesion strength is also found to be high regardless of die backside and cavity conditions from on-going studies [7].

This very wide processing window gives manufacturers the flexibility to go with either a furnace, oven or even an inline heater block cure while reducing the total processing time as well as the processing temperature. Particle count in cavity can be minimised if inline heater block curing method is used. High adhesion strength can be achieved for all configurations of die or package.

IV. Reliability

The reliability of JM7000 was investigated using 600 x 600 mils dice on ceramic PGA packages. These parts were cured in air atmosphere at 200°C for 10 minutes in an oven and subsequently sealed in nitrogen at 310°C for 5 minutes to simulate lid sealing process.

A. Adhesive Strength

The parts were subjected to a vertical pull test per Mil Std 883C, Method 2027 until delamination or when the maximum machine loading is attained.

Figure 7 summarizes the adhesion results up to 1000 cycles of thermal cycling between -65°C and 150°C.

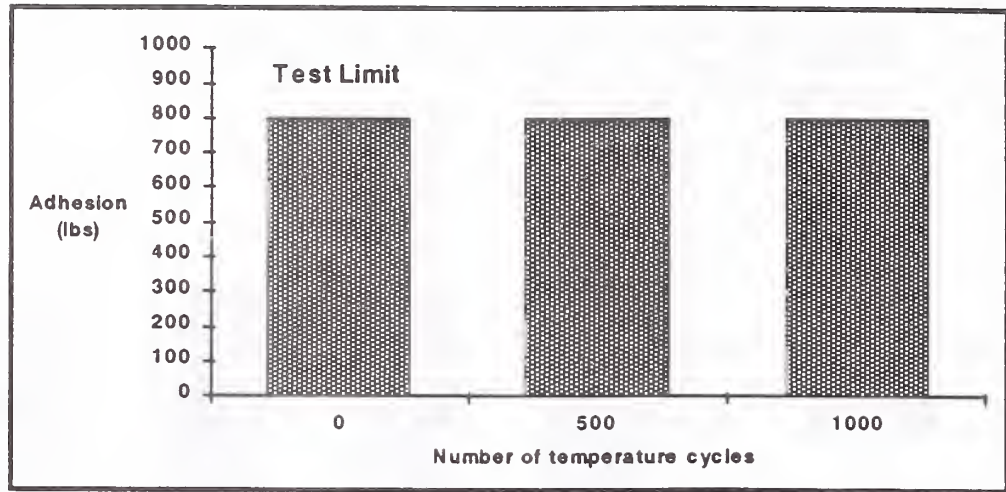


Fig 7. Adhesion at Temperature Cycling

The adhesive strength exceeded the maximum machine test limit. It was observed that after 1000 cycles of temperature cycling, the material did not degrade in adhesion performance.

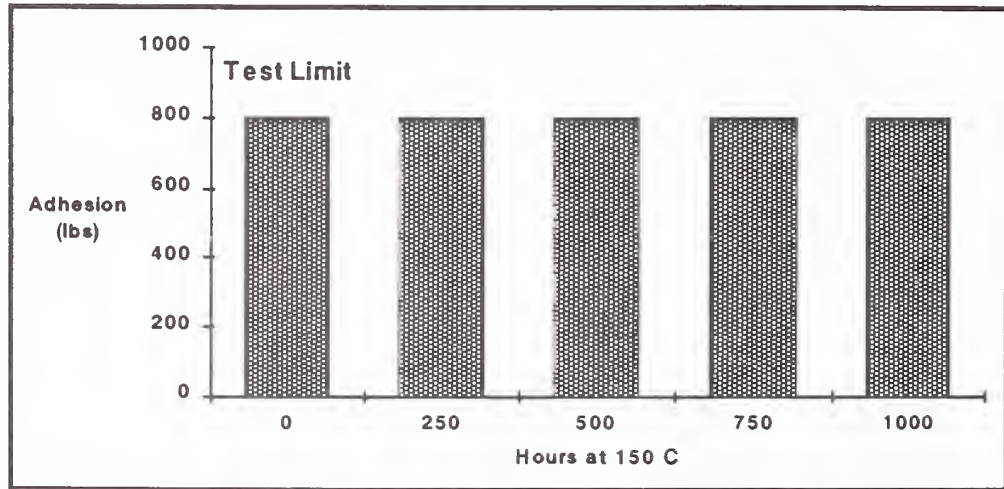


Fig 8. Adhesion at 150°C Aging

Similarly, results of 1000 hours storage at 150°C as shown in Figure 8 showed no deterioration in adhesive strength.

B. Residual Gas Analysis

JM7000 has a unique surface chemistry which breaks down the moisture in a hermetically sealed package at elevated temperature as in sealing process [2]. This reaction results in very low moisture within the sealed package in comparison to blank parts when processed under identical conditions

shown in Table 4. Typical empty solder seal packages have a moisture level of between 1000 to 5000 ppm after sealing [5].

<u>Elements</u>	<u>JM7000</u>	<u>Blank Parts</u>
Nitrogen (%)	95.2	99.6
Carbon Dioxide (%)	4.7	195ppm
Moisture (ppm)	< 100	1817
Hydro-carbon (ppm)	319	ND
Hydrogen (ppm)	700	1915

Table 4. RGA for Ceramic PGA package

We need to determine next if this reaction could be reversed during stress test. Figure 9 and 10 show the RGA of JM7000 over temperature cycling and 150°C and 225°C aging. Like adhesion results, the moisture level did not change after 1000 temperature cycles.

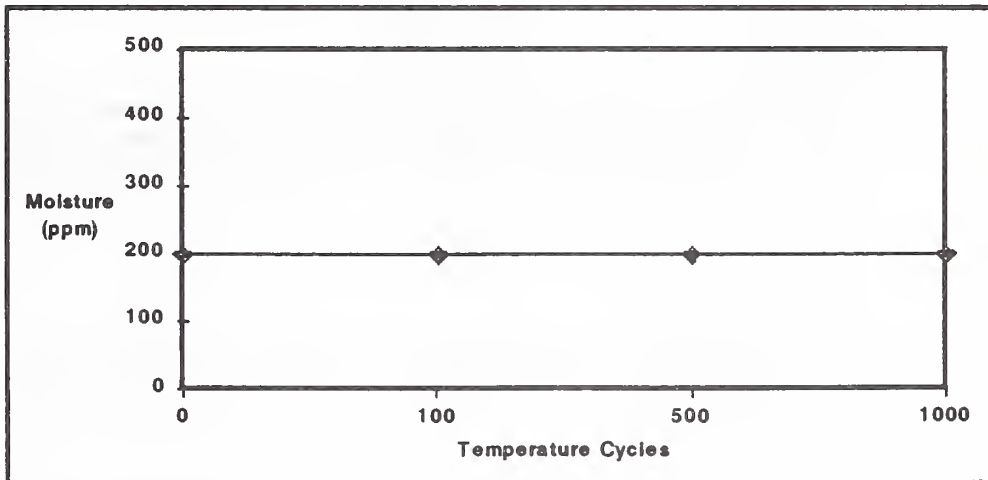


Fig 9. RGA at Temperature Cycling

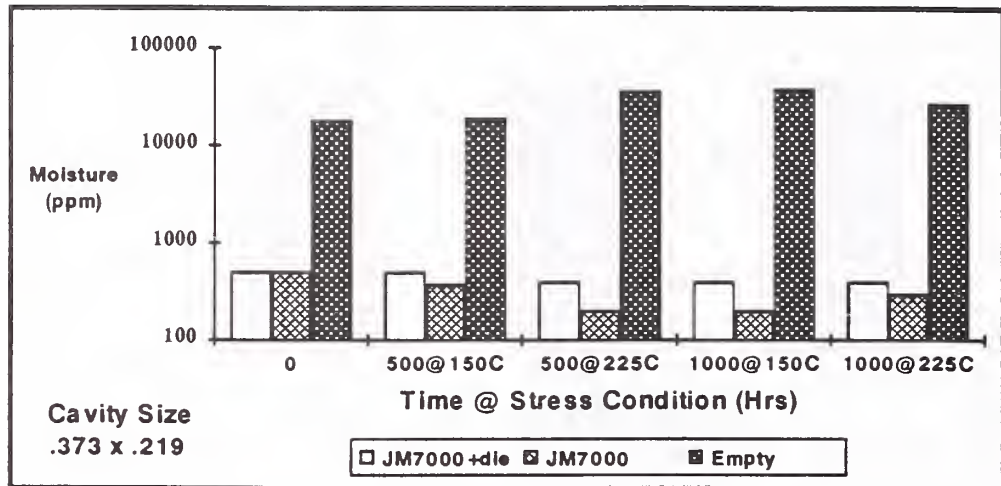


Fig 10. RGA after 150°C, 225°C Aging

The evaluation was extended to 150°C and 250°C aging tests. In this evaluation, packages with high moisture level were used. The moisture levels of packages with JM7000, with and without die, were significantly below those of empty packages. Storage at 150°C and 225°C showed no difference in moisture levels after 1000 hours. The results indicate that JM7000 is able to reduce moisture level in the cavity of the "wet" package to the level required by mil. specs.

C. Die Stress

The coefficient of thermal expansion mismatch between the die, die-attach media and substrate will result in the bending of the chip thereby affecting the surface curvature of the die. This could be correlated to the tensile stress experience by the die exerted by the die attach media and related by the equation below :

$$\text{Tensile Stress} = Et/2R$$

where

E = Young's modulus of Si (188GPa)

t = die thickness

R = radius of curvature

The minimum ultimate tensile strength for a 15 mil thick Si die is about 100 MPa [5]. The corresponding radius of curvature would need to be greater than 0.5 metres to avoid die fracture. This requires the radius of curvature of the attached die to be at least 1 metre to be considered low stress.

Measurement taken of the JM7000 material on a ceramic package for a 600 mils sq die was found to be 14 metres. The equivalent measurement on a silver-glass material gives a reading of 4 metres. This shows that both the material is able to impart a low stress level to the die and that JM7000 would induce equivalent or lower stress in comparison to silver-glass material.

D. Thermal Performance

The thermal performance of this material was investigated by attaching a thermal chip supplied by Delco Electronics to a large PGA package.

A comparison was made between JM7000 and silver-glass. The latter to serve as a control which historically has been used on ceramic packages with good thermal performance. The parameters that were of concern are the theta JA and theta JC. The former measures the thermal resistance from the junction of the test chip to the ambient and the latter the junction of the test chip to the case. Theta JC is the more meaningful assessment of the thermal effectiveness of the die attach material.

The theta JA and theta JC values were measured in accordance to thermal measurement methods in Mil Std 883C, Method 1012.2 using the OAI/SAGE 400 STAR Thermal Parametric Test System. Results are given in Figure 11.

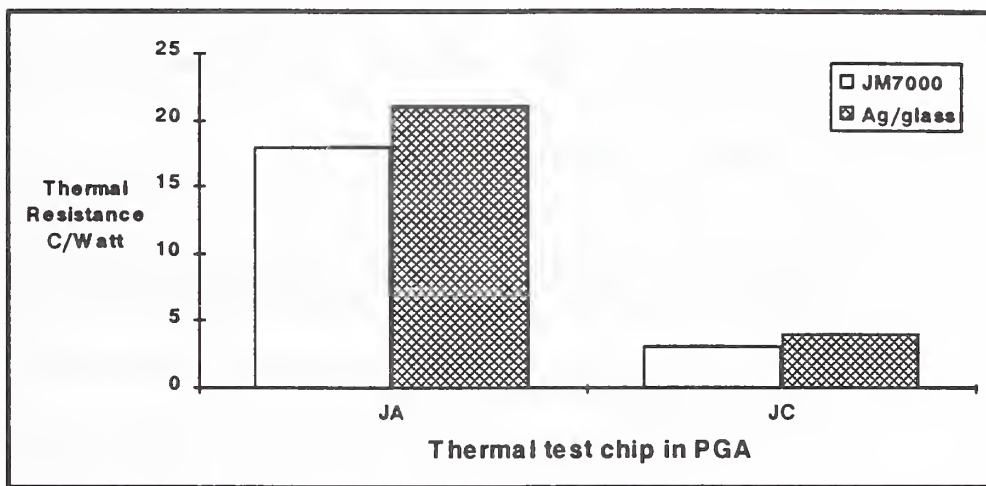


Fig 11. Thermal test - theta JA and theta JC

When compared with silver-glass, the thermal resistance of JM7000 as seen from above is not significantly different. This suggests that the thermal behaviour of JM7000 will be no different from currently accepted technology such as silver-glass.

V. Conclusion

JM7000 is a new polymer die-attach material that is designed to meet all military requirements for solder seal hermetic packages. The adhesion, residual gas analysis and the stress performance are found to be equivalent if not better than existing materials commonly used. The ease of processing this material makes it attractive for high speed assembly automation with existing assembly equipment. The desirable property of moisture reduction makes JM7000 a highly suitable material for advanced VLSI devices.

References

- [1] Tom Ramsey and Gail Heinen, "Controlling Moisture In Ceramic Packages", Semiconductor International, August 1988
- [2] M.N. Nguyen, US Patent pending
- [3] M.N. Nguyen, US Patent pending
- [4] Michael B. Grosse and My N. Nguyen, "Low Moisture Polymer Adhesive For Hermetic Packages", IEEE CHMT Processings, p. 239, 1992, San Diego, CA
- [5] M.L. White, K.M. Striny, R.E. Sammons, "Attaining Low Moisture Levels In Hermetic Packages", IEEE Proc. IRPS, p. 253, 1982
- [6] M.N. Nguyen, "Low Stress Silver-glass Die Attach Material", IEEE Trans on CHMT, Vol 3, p. 478, 1990
- [7] Sue Oliver, My Nguyen and Michael Grosse, "Silver/Ploymer Die Attach For Ceramic Package Assembly", IEPS Processings, 1992, Austin, Texas

INTERPRETATION OF RGA DATA
Including Recent Observations on the
Outgassing Characteristics of New Materials

Donald T. Shuman
Oneida Research Services, Inc.
One Halsey Road
Whitesboro, NY 13492

Abstract: Residual Gas Analysis of hermetic microelectronic devices has traditionally been treated solely as a means for measuring the device's internal moisture content. Too many times, the moisture reading is treated on a pass/fail basis using the Mil-Std criteria that all devices must contain less than 5000 parts per million (ppm) of moisture. In reality, the other gases routinely reported with the moisture contain a wealth of information that can be used to significantly improve product quality and reliability.

The intent of this paper will be to provide a cross-section of data examples that are representative of results obtained from various device technologies over the last 15 years at Oneida Research. Examples of both "good" and "bad" results for a variety of device/material combinations will be presented. Highlighted will be some observations regarding the outgassing characteristics of new die attach and overcoat materials that are now being evaluated in various segments of the electronics industry.

Typical problems that can be identified and eliminated using RGA are:

- o epoxy curing and bake-out (both under-curing and over-curing)
- o excessive thermal stresses (out-of-tolerance ovens, rework, etc.)
- o hermeticity failures (especially those that technically pass leak testing)
- o contamination problems (especially organic)
- o hydrogen outgassing (leading to moisture or hydride formation)
- o corrosion and dendritic growth sources (compounds other than moisture can promote these phenomena)
- o sealing environment problems (sealer leaks, poor helium circulation, etc.)
- o changes in vendor material formulations (adhesives, solvents, plating, etc.)

It is hoped that, by presenting this information, the RGA user will be better able to apply their gas analysis results to making process improvements that result in increased device reliability.

Key Words: Data interpretation; epoxy outgassing; hermeticity failures; hydrogen, Method 1018; moisture; Residual Gas Analysis.

1. INTRODUCTION

Residual Gas Analysis or Internal Water Vapor Analysis as outlined in Mil-Std-883, Method 1018, Procedure 1 has been used by the microelectronics industry as the prime method for measuring the moisture level inside of hermetic devices since the late 1970's. The advantage of Procedure 1 is that, as the Mass Spectrometric method, it also can quantify all of the other gases found in the device cavity.

However, as outlined in TM 1018, the test parameters revolve almost entirely around determining the moisture content of the package ambient. Failure criteria for moisture are found in Mil-Std-883, Methods 5005 and 5008. Other than an additional 1000 ppm limit for Oxygen found in MIL-S-19500, no limits or guidelines on any other gases exist. This has unfortunately caused many of the other substances routinely identified on an RGA report to be largely ignored. However, as will be shown, these substances often indicate the nature of high moisture as well as several other potential reliability risks.

The intent of this paper will be to summarize the historical observations made at Oneida Research over the past 15 years in order to provide a base of knowledge to the RGA end-user regarding the other gases found in devices. These observations have been made through direct experimentation, analysis of failed devices, and most importantly, through extensive personal contact with a significant number of device manufacturers. Several observations are made on some of the new and interesting materials currently being evaluated by various segments of the industry.

2. DISCUSSION

Sealing Gases

To begin, a review of what actually makes up typical sealing atmospheres is in order (table 1):

The most essential mixture to keep in mind is that of air (table 1a). As shown, air is a mixture of nitrogen, oxygen, argon, and carbon dioxide. Air also contains trace amounts of numerous other gases such as helium and neon. The moisture level in air will vary widely based on climatic conditions. Most Glass Frit seal devices are sealed in dry air. Devices sealed in other environments and that subsequently develop leaks will eventually contain air. A key factor to note is the ratio of oxygen to argon which is approximately 22 to 1 (20 to 1 is easier to remember and work with). This ratio will be useful in later discussions of leak phenomenon.

For most solder and welded seal devices the sealer atmosphere is dry nitrogen (table 1b). As shown, it is just that, dry nitrogen. The only common contaminant found is small (100 to 200 ppm) amounts of Argon, which is inert. Higher levels of argon accompanied by oxygen may indicate a leak somewhere in the gas handling system.

Many devices, especially hybrids, are sealed in an atmosphere containing helium as a tracer gas for enhanced leak test sensitivity. The most typical mixture is shown in table 1c, which is 90 percent nitrogen and 10 percent helium. Many other levels are often used, both intentionally and

otherwise. It has been found that, without adequate circulation, helium may tend to collect towards the top of the dry box. This results in lower than expected levels of helium being sealed into the devices. It is, of course, desirable to know the level of helium within a device as precisely as possible in order to more accurately calculate the leak rate of that device.

Glass Sealed Devices

Table 2 contains data typical of ceramic packages employing glass frit seal technology. Frit seals are usually reflowed in an air environment since the oxygen is needed in order to promote the oxide formation in the glass essential to a good seal. Glass sealed devices usually employ Eutectic gold/silicon die attach technology because of the high sealing temperatures (425 to 450°C) encountered.

The data in table 2a is representative of a glass sealed device with eutectic die attach. Note that the oxygen to argon ratio is slightly less than that typical of air due to the oxide formation described above and that the moisture level is very low. One interesting property of this technology is that cavity moisture levels tend to decrease with time. It is not unusual to find well handled glass sealed devices with less than 100 ppm of moisture after a year or so.

Of the problems that can be encountered with this technology, table 2b details the most common. This data indicates a device that has some sort of contamination in the cavity that is decomposing at the high sealing temperatures. The moisture exceeds 5000 ppm and is accompanied by an elevated level of carbon dioxide. Using the 20 to 1 oxygen/argon ratio, we can determine that the oxygen content has also decreased from normal levels.* In this case, it was determined that a new lot of piece parts had been received that were uncharacteristically "dirty". In particular, the lids had a hydrocarbon residue that was burning up during sealing, consuming oxygen and giving off carbon dioxide and moisture. The contaminant may have been from the manufacturing operation (i.e., a mold release agent) or from the packaging used in shipping (i.e., a residual plasticizer). The device manufacturer's usual cleaning process was insufficient to deal with this event.

It is important to note that all of the devices sealed using these lids failed. If the failure had been only one device out of many, the source of the failure would more likely have been at the assembly point. These more random failures are typically caused by some anomalous condition like a stray fiber or spittle contamination introduced during the assembly operation.

*Since argon is inert, it will not be involved in any reactions taking place within the package. As long as the reaction taking place involves the outgassing of other compounds, the level of argon reported will not change significantly and can thus be used to determine what the oxygen level "should" be. This fact is also useful when looking at leaks and their related problems later in this paper.

Table 3 contains data from glass seal devices that have a polyimide Alpha particle barrier applied to the die surface. Alpha particles have long been known to induce "soft" errors in devices and are more common in ceramic devices due to the higher number of radioactive decay events occurring in alumina. The polyimide layer has been found to significantly reduce the incidence of these errors.

The results shown in table 3a are typical of a device using this technology that has been properly processed. There are several interesting items in this data. The most pronounced effect is the severe amount of oxygen depletion occurring during sealing. This is to be expected whenever an organic material is exposed to such high temperatures in an oxidizing environment. The main gaseous byproduct appears to be carbon dioxide. Also given off is methane and, interestingly, hydrogen. Through extensive experimentation, several Integrated Circuit manufacturers have succeeded in getting acceptable moisture levels using this material.

Table 3b shows typical results obtained earlier in this experimentation. Most of the other gases are very similar in amount to a device exhibiting passing results. One significant factor influencing the moisture level is the ratio of the volume of the polyimide to the free volume of the package. As would be expected, the larger the cavity volume available per unit volume of polyimide, the lower the moisture level reported. Another interesting observation is that the initial reaction appears to be an oxidation of the polyimide and the outgassing of carbon dioxide and methane. Then, as the oxygen becomes depleted, a pyrolysis reaction takes over and hydrogen becomes the dominant outgassing product. As will be discussed later, hydrogen can be involved in a number of other reactions. Since many of the devices sealed in packages using glass seal technology are not usually exposed to hydrogen (as opposed to those in welded or solder sealed packages), the manufacturer should investigate whether the devices employing this technology might be susceptible to hydrogen induced anomalies.

One alternative when using polyimide that appears to be successful in keeping the moisture level fairly low is to custom blend the sealing atmosphere (table 4) rather than simply using compressed dry air (CDA). In this case, oxygen and argon are mixed with nitrogen at levels much lower than typical atmospheric concentrations. By keeping oxygen levels around 1 to 3 percent, a good glass seal can still be obtained but the oxidation reaction of the polyimide is severely curtailed. Interestingly, while some carbon dioxide and methane are still generated, hydrogen has not been observed. This implies that either the oxidation reaction may be a crucial precursor to the pyrolysis reaction or the lower level of hydrogen that may be being generated is more easily used up in some way.

Solder Sealed Devices

As mentioned above, devices that employ a solder to make the hermetic seal are typically sealed in dry nitrogen. RGA results of a solder sealed device using a nickel/gold plated Kovartm lid and eutectic die attach are listed in table 5. The atmosphere is predominantly nitrogen but usually with low levels of carbon dioxide and moisture. The carbon dioxide probably comes from trace organic residues found within the device such as organic brighteners used in the plating processes

on the lids. The moisture may also come from such a source or may come from entrapment sites within the device such as small scratches which can act as capillaries, filling with moisture before sealing, and then outgassing it during sealing or later post seal thermal stressing.

Also of note is the hydrogen, which is evolving from the lid. It has been shown that Kovartm and other ferrous alloys contain a great deal of hydrogen¹. Plating processes also generate significant amounts of hydrogen which can become entrapped within the plating layers. Any elevated temperature processing, from sealing to environmental screening, will cause this entrapped hydrogen to evolve out of the lid. As will be discussed later, hydrogen can be involved in forming moisture if the proper oxygen source is available.

Table 6 shows results from solder sealed devices that contain typical silver loaded lead borate glass die attach materials. This combination has become one of the most common in the industry. The results in table 6a are typical of devices that have been properly assembled and sealed. The only unusual gas associated with silver glass is the high amounts of carbon dioxide often reported, which appears to come from a dissociation of the silver carbonate in the glass².

The most common type of moisture failure associated with silver glass is illustrated in table 6b. As mentioned previously, significant amounts of hydrogen can evolve from the lids used on these packages. By its very nature, silver glasses of this type have large amounts of silver oxide, silver carbonate, and lead oxides. It has been shown² that these compounds are readily reduced by hydrogen, the byproducts being the base metal, moisture, and, in the case of silver carbonate, carbon dioxide. In the case shown here, hydrogen evolving from the lids has reduced these compounds at the fillet area of the die attach and produced unacceptably high moisture levels. The solution to this problem has been to introduce a preseal bakeout of the device in a forming gas (reducing) atmosphere immediately prior to sealing. While hydrogen will still evolve from the lids, this step limits the amount of oxides available for the hydrogen to react with and keeps moisture from forming.

A newer development in silver glass technology is the introduction of new "low temperature" lead vanadate glass systems. The low processing temperatures of these glasses (some below 300°C) is very attractive to manufacturers with large die size and small device geometries as the potential for thermally induced damage is minimized.

The results listed in table 7 are from devices employing this technology. Typically with these materials, as moisture levels increase, so do carbon dioxide levels (7a vs. 7b). This implies that the source of moisture is organic in nature, most likely the organic binders employed to give the glass proper dispensing properties during assembly. One significant processing difference between "high" and "low" temperature glasses is how these organic binders are removed during die attach. Traditional glasses employ a two step organic burn-off (OBO) and glass sinter profile. This allows the organic materials to be removed prior to reaching the glass transition temperature. The new lead vanadate materials employ a one step OBO/sinter profile which may be resulting in a higher level of residual organics being entrapped in the glass. This would then lead to the evolution of the thermal degradation by-products of the organics (chiefly carbon dioxide and moisture) into the device cavity with time. The solution is to carefully control the ramp rate of the temperature in order to achieve a more complete burn-off prior to the onset of glass sintering.

Another interesting new group of die attach materials currently under evaluation by several manufacturers are thermoplastics. These materials are very attractive in that they offer very low thermal stress, good bond strength, and very low moisture levels. Table 8 contains data typical of these materials. The most notable item is the extremely low moisture. It appears that, while moisture is generated during cure, the material itself reacts chemically with it and effectively acts as a getter, keeping the ambient dry. Very high levels of carbon dioxide are found in the cavity but is not in and of itself a problem. The other significant outgassing product is identified here simply as hydrocarbons. Current efforts to identify this compound(s) more thoroughly are underway, but they appear to be thermal degradation byproducts of the thermoplastic evolving during sealing.

Welded Seal Devices

Weld sealing is used on devices employing all metal package designs such as TO cans and hybrids. The sealing is performed in a dry box with a controlled atmosphere of nitrogen or combination of nitrogen and helium. Most TO packaged devices employ eutectic die attach technology and have internal atmospheres very similar to solder seal devices containing the same. Other TO's and most hybrids use epoxy die attach materials, which have their own particular processing problems.

For a number of years there were no formal guidelines in the industry as to what made up a proper epoxy. As long as such properties as bond strength, dispensibility, and thermal/electrical conductivity were acceptable, no other controls were deemed necessary. In the late 1980's it was found that several failure mechanisms could be traced to the epoxies used at the time and an effort was made to establish minimum guidelines for epoxy formulations. These guidelines were then implemented as Test Method 5011 in Mil-Std-883. Table 9 shows some of the differences between pre- and post-5011 epoxies from an RGA standpoint.

The most notable outgassing feature of some pre-5011 epoxies is ammonia (table 9a). These epoxies used a dicyandiamide curing agent which resulted in the formation of ammonia, which would then evolve out of the epoxy into the cavity of the device with later post-seal thermal screening. Ammonia has been shown to be corrosive to aluminum and it was postulated that the aluminum wires and metallization in the devices could be attacked. Unfortunately, this corrosion mechanism is difficult to prove since analysis of a corroded area would not reveal the presence of any ionic or corrosive agent as it would if something like chlorine were the culprit. However, device failures have been investigated where there did not appear to be any other assignable cause to a corrosion event.

With this in mind, post-5011 epoxies are designed as thermally curing systems that do not involve the amine curing agent. Typical RGA results for these adhesives are shown in table 9b. Notably, the ammonia is absent, but it has been replaced by the presence of some of the organic solvents used to maintain viscosity during dispensing (i.e., tetrahydrofuran). It was long thought that the commonly detected compounds MEK and methanol must also be processing solvents from the epoxy but recent investigations have found otherwise. Methyl ethyl ketone is apparently used as a viscosity modifier by the vendors of the silver flake used in conductive epoxies. Recent investigations³ have also shown that silver (a known catalyst) may be involved in a

number of reactions with the epoxy which result in the outgassing of such compounds as methanol.

Table 10 illustrates a recurring problem, that of an inadequate pre-seal bakeout. This is usually encountered when new equipment is brought on line or when new designs are introduced. It is also often the first indication of a malfunctioning bakeout oven (i.e., burnt-out elements). The pre-seal bakeout is, of course, intended to remove excess moisture and solvents from the device prior to lid seal. The key indicators, then, are high moisture accompanied by high residual solvents but with low levels of associated carbon dioxide. For most organic compounds and epoxies in particular, carbon dioxide is an excellent indicator of the amount of thermal stressing that has been applied. A low level of carbon dioxide associated with excess moisture indicates that additional baking is required in order to get acceptable moisture levels.

The opposite condition is shown in table 11. Excessive thermal stressing can be just as detrimental to internal water vapor levels as insufficient bakeouts can. The example in table 11a is the exact opposite of that shown in table 10. In this case, the pre-seal bakeout was too severe, as indicated by the complete absence of the typical solvent residues of a well handled device (table 9b) and the high level of carbon dioxide. The epoxy mass of the device has a certain total amount of thermal energy that it can withstand. This total is both temperature and time-at-temperature dependent. The total amount of thermal stressing that the device must withstand includes everything from curing to burn-in. As this total is exceeded, the epoxy begins to thermally degrade, albeit very subtly at first. The outgassed byproducts of this degradation are carbon dioxide and moisture. In this case, too much of the total was consumed during pre-seal baking, causing the necessary post-seal stressing to begin the degradation process.

Table 11b shows a similar overstress condition but one that has occurred after sealing. This condition actually contains the key features of the previous two examples: high residual solvents and high carbon dioxide. We can say that it was post-seal because the residual solvents would have been removed during pre-seal baking otherwise. This condition could indicate several problem areas such as an out of control burn-in oven, a malfunctioning power supply during biased burn-in, or even an oven with a poor or uneven thermal profile. Investigators have reported oven temperature variances as large as 70°C from top to bottom. RGA results will be greatly influenced by the particular position a device occupies in an oven such as this. In fact, this condition often accounts for erratic moisture readings encountered within a particular lot.

It should be noted here that such operations as element rework can have a dramatic impact on moisture readings for a particular device. The hot gas rework tools often used to remove bad elements from a substrate can generate very high local temperatures. The result is that the substrate attach adhesive under the element being reworked can be severely overstressed during this operation. The carbon dioxide and moisture generated by the overstress will then evolve out from under the substrate and into the package ambient. Depending on the size of the device and the severity of the overstress, this evolution may occur for a substantial period of time. Rework is also often the source of acetone reported during RGA. Many a bottle of nail polish remover has been found at rework stations.

Leak Phenomenon

One of the most serious problems facing the hybrid industry today is that of truly screening out leaking devices. Residual Gas Analysis results have long indicated that, while devices pass hermeticity testing, a significant number contain the high moisture, oxygen, argon, helium, and fluorocarbons that indicate the device is a leaker.

There are several factors that contribute to this apparent discrepancy. One is that the failing leak rate specified for devices in many programs is simply too lenient. Leak rate limits of 1×10^{-7} atm-cc/sec He and greater are not uncommon, yet devices close to these limits are actually true leakers. Passing such a limit does not mean a device is hermetic in any real sense, and this will be revealed during RGA. Another factor is the assumption that a device's leak rate remains constant under all conditions. Factors such as temperature and pressure have been found to alter a device's leak rate by several orders of magnitude. There is also a good deal of evidence that the leak test conditions in Method 1014 itself are not adequate when dealing with larger packages⁴.

The results summarized in table 12 are a good example of this problem:

The device shown in 12a passed hermeticity testing per Mil-Std-883, Method 1014 and yet is still obviously not hermetic. In this case, it appears that this is a pressure dependent leak. The presence of significant levels of helium and fluorocarbons with relatively low levels of moisture, oxygen, and argon indicates that this device is not leaking under all conditions. The physical effects of typical leak test bombing pressures on a package have been theorized to result in a temporary loss of hermeticity, most likely by disturbing the intergranular oxide boundary of the glass-to-metal seals.⁵ These stresses are the complete opposite of those put on the package during the detection portion of leak testing (i.e., vacuum or internal pressure induced by heat). This may make it easier for leak test materials to enter the package than for them to escape in a detectable quantity.

Table 12b shows results from a device with a leak that is more thermally dependent. This is evidenced by the presence of higher levels of oxygen and argon with no helium or fluorocarbons and very high levels of moisture. In this case, temperature cycle testing was found to be where the problem was most aggravated.

Most packages are built with "matched" glass seals, meaning that the package, glass insulator bead, and the lead all have matching temperature coefficients of expansion. At any given temperature, all parts of the package will, therefore, have expanded or contracted the same amount and package integrity should be maintained. However, because of their physical characteristics, each of these components will have a very different rate of change of expansion. The leads are a thin metal strip or wire with significant surface area, making them excellent radiators, while the glass bead is, by definition, a good insulator. The package body itself is likely somewhere in between, with significant surface area but also most of the thermal mass. This means that, when going from hot to cold for example, the lead will be contracting much faster than the insulator. In many cases this difference may be enough for hermeticity to be momentarily compromised, allowing moisture and other gases to move through the seal. This is where another aspect of temperature cycle testing contributes to the results of 12b; that is, that a significant amount of humidity is encountered in the cold side of most temp cycle chambers.

As the device is experiencing this momentary loss of hermeticity, it is also encountering a very moist environment. This would account for detected moisture levels often being much higher than the ambient humidity outside of the device can account for.

It follows that these problems are likely interrelated. A package seal that has been disrupted by thermal stresses will probably be more susceptible to pressure dependent phenomenon afterward. Table 12c contains data that is typical of this. Devices exhibiting results such as these have been traditionally called "One Way Leakers", wherein the thought was that moisture and other gases could leak into a device but not out. It would appear that this condition might more accurately be termed "Intermittent Leaker", since the leak actually only occurs during (or at least is greatly affected by) certain environmental conditions.

One often overlooked aspect of this problem is what these types of leaks might mean to a device later on. Most studies to date that have attempted to address the long term reliability of devices exhibiting this problem have been done by the device manufacturers. Devices suspected to have high moisture caused by this phenomenon have been subjected to severe life testing. The results of these experiments often lead researchers to believe that the devices will perform normally even though they contain elevated moisture levels. Overlooked is what affect later system level assembly operations are going to have. Such processes as Wave Soldering, Vapor Phase Reflow Soldering, and Vapor Degreasing all generate very similar temperature profiles to those shown to influence the "Intermittent Leak" phenomenon. The obvious difference here is the environment outside of the device, which now contains some very volatile and potentially corrosive compounds. RGA results obtained from field failed devices often look similar to those summarized in table 13. The presence of chlorinated solvents in the cavity is indicative of a leak that occurred during board level assembly. When mixed with moisture and exposed to temperature and, perhaps, electric current, it is possible for the chlorine (and other ionics such as fluorine) to dissociate from the solution and initiate corrosion reactions within the device.⁶ Limited data is available regarding what some of CFC replacements currently being implemented will do under similar conditions.

Another leak related phenomenon is illustrated in table 14. This device exhibits characteristic leak traits like the presence of helium and fluorocarbons as well as oxygen and argon. However, note that the oxygen to argon ratio is off significantly. This is indicative of an oxidation reaction taking place after the leak has allowed air to enter the device. This reaction is similar to that described previously in the section on Glass Sealed Devices. The oxygen is most likely participating in the thermal degradation of the epoxy during elevated temperature testing of the device. As before, the outgassing products are primarily carbon dioxide and water vapor. Thus, the leak not only allows moisture to enter the device, it also enhances the generation of more moisture by accelerating the thermal degradation of the adhesive.

The solution to the "Intermittent Leak" problem will likely involve a significant re-evaluation of the current design rules for glass-to-metal seal packages. Such parameters as Intergranular Oxide Thickness, Glass Bead Aspect Ratio, and Lead Pitch may need to be significantly rethought. Secondly, the inadequacies of Method 1014 need to be addressed. Extensive efforts to this end are currently underway in the industry.

Hydrogen Outgassing

A great deal of interest has been focussed on the role hydrogen plays in limiting long-term device reliability in recent years. Hydrogen, of course, has long been known to affect the formation of moisture within devices (see above section on solder seal devices containing silver glass). As devices have grown more complex, however, hydrogen has begun to be implicated in other types of failures, most notably in the formation of metal hydrides in Gallium Arsenide microwave devices.¹ Many of the metals being used in devices today (i.e.; titanium, platinum, palladium, etc.) are fairly reactive with hydrogen.

Table 15 shows the before and after affects of a hydrogen reduction reaction in a solder seal package. The results in 15a were typical of a particular device type. Occasional failures exhibited results similar to those in table 15b. It was found via Auger analysis that the failing devices had lids with a high level of nickel diffused to the surface of the gold plating. Nickel quickly forms a native oxide layer when exposed to air. After sealing, the evolved hydrogen reacted with the nickel oxide layer to form moisture. As can be seen, the elevated moisture levels were accompanied by a decrease in the average hydrogen level that was characteristic of this device type.

It should be emphasized that free oxygen is not necessary in order for hydrogen to form moisture. In fact, the reaction of free hydrogen and free oxygen usually requires significant activation energy. Many of the metal oxides routinely encountered in microelectronic devices, however, are much more likely to react with hydrogen. Oxides of silver, tin, lead, and nickel are very susceptible to this attack while oxides of aluminum and silicon are not. The Gibbs Free Energy calculations (a rough measure of the likelihood of a reaction proceeding) for many of these reactions is highly negative, indicating that these reactions are thermodynamically favored. It is highly probable that some of these reactions could occur at room temperature and very likely that they would occur at typical device operating and processing temperatures.

3. CONCLUSION

It has been shown that the amount of information contained in the typical RGA report far exceeds a simple measure of moisture content. While certainly not covering all possible problems that can be revealed by RGA, an attempt was made to cover the more common ones. By presenting the basics of interpreting this information, it is hoped that the RGA end-user will be able to better use the data to make the process improvements that lead to improved product reliability.

REFERENCES

1. Schuessler, P., and Feliciano-Welpe, D., *The Effects of Hydrogen on Device Reliability*, Hybrid Circuit Technology (January 1991).
2. Ramsey, Tom, and Heiner, Gail, Texas Instruments, *Controlling Moisture in Ceramic Packages*, Semiconductor International (August 1988).
3. Phillips, T.E., deHaas, N., Goodwin, P. G., and Benson, R.C., The John Hopkins University Applied Physics Laboratory, *Silver-Induced Volatile Species Generation from Conductive Die Attach Adhesives*, IEEE Proceedings, 1992.
4. Dermarderosian, Aaron, Raytheon, *Permissible Leak Rates and Moisture Ingress*, IRPS Hermeticity Tutorial, 1984.
5. Epstein, Dan, ILC Data Device Corporation, *How to Test for One Way Leakers*, Hybrid Circuit Technology (March 1988).
6. Dixon, Jeffrey B., Northrup, Mark R., and Rooney, Daniel T., Oneida Research Services, *Failure Analysis of a Hybrid Device Exhibiting Copper Dendrite Growth on Thick Film Resistors*, 41st Electronic Components & Technology Conference (1991).

Table I - Common Sealing Atmospheres

	a	b	c
Nitrogen	78.1%	99.9%	89.8%
Oxygen	20.9%	ND	ND
Argon	9320 ppm	125 ppm	130 ppm
Carbon Dioxide	310 ppm	<100 ppm	<100 ppm
Moisture	<100 ppm	<100 ppm	<100 ppm
Helium	ND	ND	10.1%
	Air	Dry Nitrogen	Dry Nitrogen/ Helium Mixture

Table II - Glass Sealed Device with Eutectic Attach

	a	b
Nitrogen	81.0%	78.8%
Oxygen	17.9%	15.6%
Argon	9221 ppm	1.03%
Carbon Dioxide	1053 ppm	3.67%
Moisture	541 ppm	8795 ppm
	"Good"	"Bad"

Table III - Glass Sealed Device with Eutectic Attach
and Polyimide Alpha Particle Barrier - Dry Air

	a	b
Nitrogen	86.1%	88.8%
Oxygen	5.09%	2.59%
Argon	9808 ppm	9950 ppm
Carbon Dioxide	5.49%	5.07%
Moisture	2207 ppm	5891 ppm
Hydrogen	1.29%	1.08%
Methane	8745 ppm	9089 ppm
	"Good"	"Bad"

Table IV - Glass Sealed Device with Eutectic Attach,
Polyimide Alpha Particle Barrier, and Custom Blended Air

Nitrogen	94.8%
Oxygen	1.55%
Argon	724 ppm
Carbon Dioxide	3.05%
Moisture	642 ppm
Methane	4458 ppm

Table V - Solder Sealed Device with Eutectic Attach

Nitrogen	99.4%
Carbon Dioxide	154 ppm
Moisture	473 ppm
Hydrogen	5845 ppm

Table VI - Solder Sealed Device with Silver Glass Attach

	a	b
Nitrogen	99.0%	99.8%
Carbon Dioxide	3420 ppm	3150 ppm
Moisture	439 ppm	6240 ppm
Hydrogen	5556 ppm	450 ppm
	"Good"	"Bad"

Table VII - Solder Sealed Device with "Low Temperature" Silver Glass Attach

	a	b
Nitrogen	99.2%	97.1%
Carbon Dioxide	4128 ppm	1.43%
Moisture	2877 ppm	1.26%
Hydrogen	1252 ppm	1985 ppm
	"Good"	"Bad"

Table VIII - Solder Sealed Device with Thermoplastic Attach

Nitrogen	89.6%
Carbon Dioxide	9.27%
Moisture	511 ppm
Hydrogen	4587 ppm
Hydrocarbons	5590 ppm

Table IX - Pre- Versus Post-5011 Epoxies

	a	b
Nitrogen	91.0%	85.1%
Carbon Dioxide	2091 ppm	5792 ppm
Moisture	1680 ppm	4720 ppm
Helium	8.34%	13.3%
Ammonia	3161 ppm	ND
MEK	ND	1446 ppm
Methanol	ND	1826 ppm
Tetrahydrofuran	ND	862 ppm

Table X - Epoxy - Poor Pre-Seal Bakeout

Nitrogen	95.3%
Carbon Dioxide	1220 ppm
Moisture	1.05%
Hydrogen	350 ppm
MEK	1.80%
Methanol	1.32%
Hydrocarbons	3250 ppm

Table XI - Thermally Overstressed Epoxies

	a	b
Nitrogen	95.6%	92.0%
Carbon Dioxide	2.35%	2.07%
Moisture	1.93%	1.89%
Hydrogen	1220 ppm	9780 ppm
MEK	ND	1.42%
Methanol	ND	1.20%
Hydrocarbons	ND	4725 ppm
	Pre-Seal	Post-Seal

Table XII - Intermittent Leak Phenomenon

	a	b	c
Nitrogen	96.1%	90.5%	87.7%
Oxygen	1225 ppm	6.07%	4.87%
Argon	274 ppm	2940 ppm	2415 ppm
Carbon Dioxide	1210 ppm	1575 ppm	2750 ppm
Moisture	3570 ppm	3.04%	2.72%
Hydrogen	897 ppm	425 ppm	890 ppm
Helium	2.44%	ND	3.07%
Fluorocarbons	7626 ppm	ND	1.02%
	Pressure Dependent	Temperature Dependent	Combined Effect

Table XIII - Intermittent Leak at System Level

Nitrogen	86.9%
Oxygen	6.85%
Argon	3220 ppm
Carbon Dioxide	8990 ppm
Moisture	1.20%
Hydrogen	1875 ppm
Helium	1.05%
Fluorocarbons	3540 ppm
Trichloroethane	6770 ppm
Isopropyl Alcohol	1.20%
Freon [®] TF	3525 ppm
Methylene Chloride	325 ppm

Table XIV - Leak with Oxygen Enhanced Thermal Degradation

Nitrogen	95.7%
Oxygen	1.2%
Argon	1550 ppm
Carbon Dioxide	1.02%
Moisture	8975 ppm
Hydrogen	273 ppm
Helium	8950 ppm
Fluorocarbons	1210 ppm

Table XV - Hydrogen Outgassing

	a	b
Nitrogen	98.0%	98.7%
Carbon Dioxide	915 ppm	890 ppm
Moisture	1220 ppm	8950 ppm
Hydrogen	1.15%	3025 ppm

WATER ADSORPTION AT A POLYIMIDE/SILICON WAFER INTERFACE

by

Wen-li Wu, William J. Orts, Charles J. Majkrzak
and Donald L. Hunston *

Polymers Division and Reactor Radiation Division
Institute of Materials Science and Engineering
National Institute of Standards and Technology
Gaithersburg, MD

Neutron reflectivity (NR) was applied to measure the concentration of water at the buried interfaces between an amorphous polyimide and silicon single crystal wafers. Excess water was discovered within 30 Å of the metal/polymer interface, where the water concentration reached 17% (by volume) for the samples without a coupling agent and 12% for the ones with coupling agent. Beyond the interface, the water concentration was measured at 2-3%, which is typical of bulk polyimide. The above results demonstrate conclusively the unique power of NR in determining water concentration near a buried interface, and provide the first quantitative evidence for a water concentration profile which peaks in the interface region.

* To whom correspondence should be addressed.

Introduction

Water is one of the most detrimental agents attacking adhesion joints, composites and multiple layer electronic modules, especially when high energy surfaces are involved¹. Metal surfaces in adhesion bonds, fiber glass surfaces in composites and silicon dioxide layers in electronic modules are common examples of pertinent high-energy surfaces. To alleviate moisture attack, polymers with low moisture absorption are often used in the above applications. Even with this precaution, coupling agents are added to help increase the resistance to environmental degradation, especially since it has been postulated that the water concentration near the interface can be significantly greater than in the bulk polymer matrix. This point has been inferred indirectly from experiments², although no method presently exists to quantify precisely the amount of water at or near the buried interface.

In this work we will demonstrate that neutron reflectivity (NR) can be used to quantify water trapped at polymer/solid interfaces. A polyimide (PI) film prepared by spin casting on a silicon single crystal was chosen for study. Polyimides have been used throughout the electronics and composite industries in a wide variety of applications. Their high melting point, good toughness, low dielectric constant and chemical inertness make them suitable for many high temperature composites, optoelectric fiber coatings, and multiple-layer electronic modules.

Typically, polyimides absorb a few percent moisture at room temperature. If an excess amount of water exists at the interfaces between PI and the components within an electronic or optoelectronic device, there can be damage to the underlying substrates or even total debonding at the interfaces.

NR has the capability to characterize water at buried interfaces due to its high spatial resolution, which is of the order of the neutron wavelength of 2.35 Å used in this work, and due to the penetration power of neutrons to a variety of single crystals. Silicon single crystal wafers with a diameter of 11 cm were used here. With an attenuation factor of less than 15% for a beam path of 11 cm, the wafer is essentially transparent to the neutron beam, which enables the study of the buried interfaces.

An important material constant which needs to be clarified for this discussion is the elastic cohesive scattering length per unit volume designated as Q_c^2 . This name derives from the fact that Q_c^2 is proportional to the second power of the critical angle defined in terms of the magnitude of the momentum transfer $Q_c = (4\pi/\lambda)\sin\Theta_c$. Total reflection of neutrons with wavelength λ will occur if the incident angle is less than Θ_c . It is noteworthy that in the above definition of Q_c or Θ_c , the interface between the material and vacuum is considered. Q_c^2 can be regarded as the height of the potential energy "barrier" for the surface. If the energy of the neutron beam transverse to the surface is less than Q_c^2 , total reflection occurs. More explicitly, $Q_c^2 = 16\pi Nb$ where N is the number density of

scattering nuclei and b is their average scattering length. Based on the composition of the PI used in this work and its bulk density of 1.37 g/cm^3 , Q_c^2 is calculated to be $1.57 \times 10^{-4} \text{ \AA}^{-2}$, while for the silicon wafer $Q_c^2 = 1.06 \times 10^{-4} \text{ \AA}^{-2}$. The high value of Q_c^2 for the PI sample results from the fact that it contains only a few hydrogen atoms. Since Q_c^2 for PI is higher than that of silicon, a critical angle for the PI/Si interface is readily seen in the NR results when the incident beam travels through the Si crystal to the interface. Deuterated water, D_2O , has a Q_c^2 of $3.21 \times 10^{-4} \text{ \AA}^{-2}$, which is much greater than that of Si and PI. Consequently, a minor amount of D_2O at the PI/Si interface changes the potential energy profile of the interface, hence the reflectivity results. This large difference in Q_c^2 between D_2O and the other constituents is responsible for the sensitivity of NR in detecting moisture at interfaces.

Experimental

Materials. A commercially available polyimide (Pyralin PI-2555*), made with an equal mole ratio of 4,4'-oxydianiline, m-phenylene diamine with 3,4'-benzophenone tetracarboxylic-anhydride was spin coated onto the (111) surface of silicon single crystal wafers. The coated film was baked at 135 C for 30

*Certain commercial materials and equipment are identified in this paper in order to specify adequately the experimental procedure. In no case does such identification imply recommendation or endorsement by the National Institute of Standards and Technology (NIST) nor does it imply necessarily the best available for the purpose.

minutes in air to remove the solvent and then cured at 350 C for 60 minutes in nitrogen. For one set of the samples, PI was coated directly onto the native oxide layer of the silicon wafer. For the other set, γ -aminopropyltrimethoxy silane was applied prior to the PI coating by spin coating (at 5000rpm) from a dilute solution of the silane coupling agent. These wafers were heated to 100°C for 10 minutes. For both cases, the thickness of the PI film was about 2 μ m.

Dry samples (i.e. the experimental controls) were prepared by leaving coated wafers under vacuum for at least one week. "Wet" samples were prepared similarly, followed by conditioning in a saturated D₂O atmosphere at 23 C for one week. During the NR measurements all samples were kept under their same respective conditioning humidities.

Reflectivity Measurements

All the NR measurements were conducted at the BT-7 reflectometer at the reactor of the National Institute of Standards and Technology. A graphite monochromator was used to select neutrons of wavelength $\lambda = 2.35\text{\AA}$ with width $\Delta\lambda/\lambda = 0.01$. Slit collimators reduced the incident beam divergence to ~ 0.016 . The detector acceptance angle was set at ~ 0.075 for the reflectivity measurements (the specular component) and ~ 0.012 for the transverse scan (the off-specular component). Most of the experimental data were derived from specular reflectivity data; thus, the intensity of the reflected signal was measured as a function of the angle of incidence, while the incident and

reflection angles were maintained as equal. To account for background corrections, the off-specular component collected when the detector was offset by $2\Theta = .05^\circ$ was subtracted from the data. In the off-specular experiment, the detector was held fixed at an angle of 0.4° with respect to the incident beam, while the sample was rocked from 0.1° to 0.3° .

Results and Discussion

The raw NR data of the wet/dry sample pair without coupling agent is given in Figure 1, with the low angle region highlighted in the inset. Reflected intensity is plotted as a function of the incident angle. Considering that the intensities (the ordinate) are presented in a log scale, the difference between the wet sample (solid circles) and the dry control (open circles) is about a factor of two. In addition, a minor increase in the critical angle of the wet sample is clearly visible in the inset. The raw intensities near zero angle exhibit a characteristic fall and rise, resulting respectively from acceptance into the detector of the main beam and the finite dimension of the sample. At extremely low incident angle, only a portion of the incident beam is intercepted by the sample and this portion increases with angle. A geometrical correction to account for sample size was made during the conversion of the raw intensity data into reflectivity profiles.

The converted reflectivity results were fitted using a matrix method algorithm^{3,4}. The reflectivity data for the dry

"control" sample (open squares) and the wet sample (open circles) are shown in Figure 2 along with their respective fit profiles (solid lines). During the least-squares fitting process only Q_c^2 for the silicon wafer was held fixed, whereas variable parameters included the asymptotic value of Q_c^2 for PI far from the interface, the Q_c^2 value and thickness of an intermediate layer which might be present, and the thickness of both transition zones, i.e. between PI and the intermediate layer, and between Si and the intermediate layer. The resulting potential energy profiles, expressed in Q_c^2 versus distance from the Si surface for both the dry (lower curve) and the wet (upper curve) samples are given in Figure 3. The origin on the distance axis was chosen arbitrarily and resulted in the PI/Si interface being located near 10\AA in Figure 3. The Q_c^2 to the left of 10\AA corresponds to the silicon wafer while the data to the right of this point describe the transition to bulk PI, which has a Q_c^2 of $1.5 \times 10^{-4}\text{\AA}^{-2}$. This transition occurs over a distance of 10\AA .

The transition distance seen here is far greater than that observed in previous experiments studying the interface between glassy polymethylmethacrylate and silicon wafer⁵. For this system the transition occurs within 5\AA of the interface, which is similar to that observed for silicon wafer/vacuum interfaces. The latter is attributed to interface roughness for the silicon wafer. Hence the extent of the transition region for the PI/Si interface is more than can be accounted for by the surface

roughness of the silicon wafer. The origin of this difference is not known, but the cross-linked nature of PI may play a role.

Figure 3 also shows the results for the wet sample. In addition to a conspicuous enhancement of Q_c^2 near the interface, the magnitude of Q_c^2 remote from the interface is also increased, presumably caused by absorption of D_2O throughout the entire thickness of the PI film. It is this increase in Q_c^2 remote from the interface which is responsible for the increase of the critical incident angle of the wet sample shown in Figures 1. In addition, Figure 3 shows a broad increase in Q_c^2 near the interface for the wet sample, which clearly suggests the existence of a high D_2O concentration near the interface. By assuming that any apparent changes in density (or in the potential energy profiles) are due to the addition of water to a polymer matrix with constant density, one can easily calculate the D_2O concentration profile. The assumption that the underlying polymer density remains constant, although a gross simplification, is analogous to what is commonly done in linear elasticity problems. In other words, no provision was allowed for the water to act as a plasticizer.

Based on the above assumption, the D_2O concentration profiles near the interface were readily calculated, and are shown in Figure 4 for samples without (open circles) and with (closed circles) silane coupling agent. For the sample with no coupling agent, a D_2O rich layer of $\sim 30\text{\AA}$ thickness exists near the interface in which the water content reaches 17% (by volume)

and then, further from the surface, falls back to 2.5% D₂O. The saturated bulk water content of this polymer at ambient temperature is about 3%. For spin-coated PI thin films, expansion is constrained laterally, so swelling is generally confined to the direction perpendicular to the interface. Hence it is not surprising that the measured water content is slightly below its bulk value.

The D₂O concentration profile for the sample set with aminosilane coupling agent, shown in Figure 4 (closed circles), was derived from the Q_c^2 curves shown in Figure 5. The density profile for the dry sample (lower curve in figure 5) merits some additional discussion. As noted above, the only parameter that was fixed during the data fitting process was the Q_c^2 for the silicon wafer. Clearly, the profile exhibits a ~20Å thick plateau which is absent in the corresponding sample without the coupling agent. Since the coupling agent is protonated, it has a low Q_c^2 value, and consequently, the results are consistent with the presence of a layer adjacent to the wafer which is rich in the coupling agent. Beyond the silane rich layer the potential reaches a value identical to that for PI in the dry sample without the coupling agent. The fully extended length of the silane molecule used is less than 10Å, hence the presence of a ~20Å silane rich layer strongly suggests that the silane molecules near the silicon wafer exist in a multiple layer form.

The potential energy profile of the wet sample is rather similar to that from the sample without silane; a broad maximum

occurs near the interface then tapers off to a value somewhat above that of the dry sample. The calculated D_2O profile derived from this sample pair is shown in Figure 4 (solid circles). Again, a thin water rich layer is present, reaching a maximum concentration of 12% compared with 17% for the sample without silane couplers. This result clearly demonstrates that the silane coupling agent used here does not completely expel all the water molecules from the PI/Si interfaces. The most noticeable difference in the D_2O concentration profiles occurs in the $\sim 10\text{\AA}$ region immediately next to the silicon wafer, where the presence of silane molecules lowers the water level by about 50%. Between 10\AA and 25\AA away from the silicon wafer, the silane effect is less pronounced but still reduces the water concentration significantly. Beyond that point, the silane has no effect. It is interesting to note that the asymptotic bulk water content values derived from these sample sets are virtually identical, as one would expect.

Although fitting the NR data to a potential energy profile is rather straightforward, it does not reach a unique solution. More than one possible Q_c^2 profile exists for any given NR data set. This uniqueness problem in deconvoluting the reflectivity results to structural information is common to all scattering related applications. The water concentration profiles reduced from the NR results, therefore, are not unique solutions. However, the potential energy profiles derived in this study have been kept in their simplest form, especially for the dry samples.

Profiles for the wet samples are created in the data fitting routine with the profile of the corresponding dry sample as the starting point. Therefore, although the water concentration profiles are not unique solutions to the NR data, they are believed to be very likely representations of the true picture.

A significant limitation of reflectivity experiments is that only structural information along the depth direction can be derived from specular data, since the momentum transfer vector stays perpendicular to the interface. It would be of added interest to acquire the average water concentration in directions parallel to the interface. This "in-plane" information is carried in the data from off-specular measurements, especially the transverse scan⁶. Extracting in-plane structural information from off-specular measurements is still in its infancy. Work in this area is actively being pursued, but the potential can be illustrated here with a few off-specular measurements and some qualitative interpretation of this data. The transverse scans from the wet/dry pair without silane, with the detector fixed at 0.4° , is given in Figure 6. The abscissa is the rocking angle; i.e. the angle between the incident beam and the interface. In general the widths of the specular peaks for both the dry (open circle) and the wet (solid circle) samples are the same within the instrument resolution. However, the off-specular intensity (tails of the peak) for the wet sample is noticeably higher than for the dry one. This implies that the in-plane distribution of the moisture (D_2O) is not uniform. Work is now in progress to

extract quantitative data from the transverse scans. For the pair with silane at the interface, the off-specular intensities of the dry sample are significantly greater than that shown in Figure 6, implying that the in-plane distribution of the silane is not uniform.

Conclusion:

A significant difference in the NR results was observed between the dry and the wet PI samples spin-coated on silicon single crystal wafers. Quantitative analysis of the NR data provides, for the first time, the evidence of a 30Å moisture layer at the interface. The maximum water content within this thin layer reaches 17% (by volume) for samples without any coupling agent, and 12% for samples with an aminosilane coupling agent at the interface.

References

- (1) Kinloch, A.J., "Adhesion & Adhesives Science & Technology," Chap. 8, Chapman & Hall, London, NY, (1987).
- (2) Nagarkar, P.V., Searson, P.C., Belluci, F., Allen, M.G., Latanision, R.M., Proceedings of the IEEE Conference on Components, Hybrids and Manufacturing Technology, Piscataway, N.J., IEEE, (1989), 160.
- (3) Dickman, R. and Hall, C. K., J. Chem. Phys. (1988) 89, 3168.
- (4) Lekner, J., "Theory of Reflection," Martinus Nijhoff Publishers, Dordrecht, (1987).
- (5) Wu, W., Majkrak, C.F., Satija, S.K., Ankner, J.F., Orts, W.J., Satkowski, M. and Smith, S.D., Polymer Communications, (1992) 33 (23), 5081.
- (6) Sinha, S.K., Sirota, E.B., Garoff, S., and Stanley, H.B., Phys. Rev. B (1988) 38, 2297.

Acknowledgement

The support of this work provided in part by an ONR grant N00014-92-F-0036 is gratefully acknowledged. The authors are also grateful to John C. Coburn and Michael T. Pottiger of E. I. duPont Company for preparing all the polyimide samples.

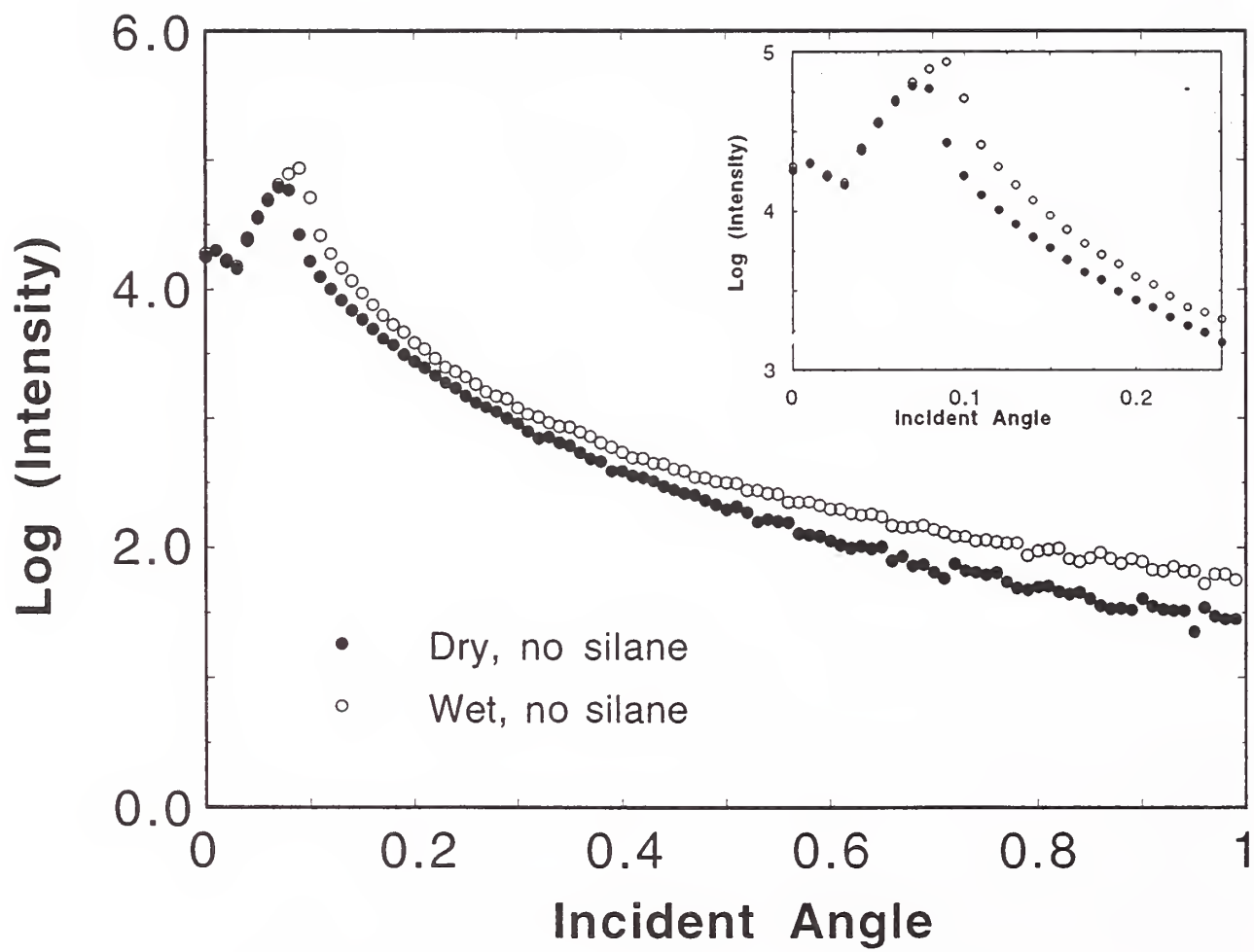
Captions

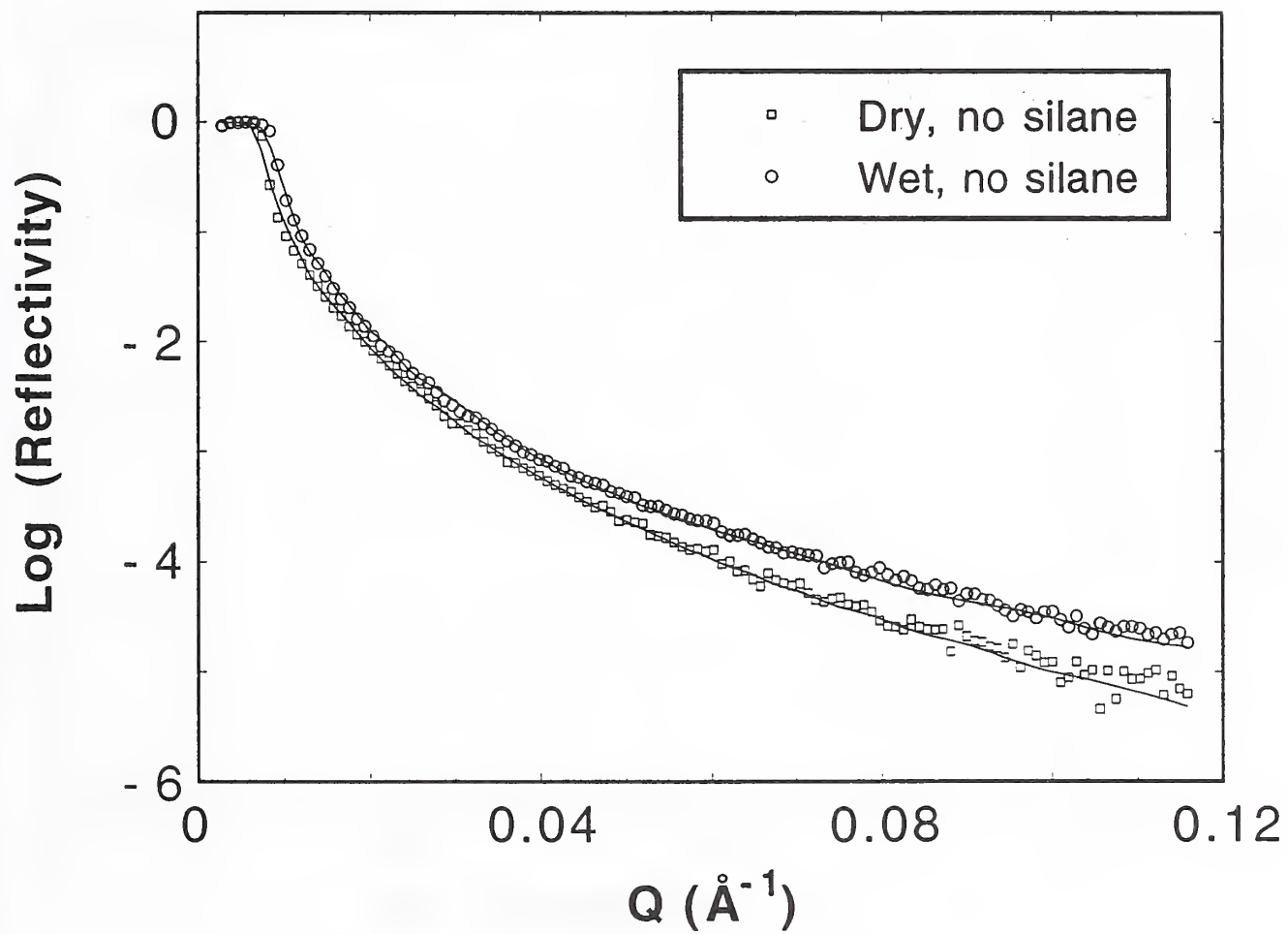
- Figure 1. Raw data from neutron reflectivity measurements of dry (solid circles) and "wet" (open circles) PI on silicon wafers. No silane coupling agent was used in these samples. The inset shows an enlarged view of the data at low angle, highlighting differences in the critical angle.
- Figure 2. Neutron reflectivity results from samples without silane coupling agent which are dry (open squares) and wet (open circles). Theoretical fits are given as solid lines.
- Figure 3. Potential energy profiles, in terms of Q_c^2 , of a dry PI/Si interface (•) and the corresponding wet interface (o). No coupling agent was used for this sample pair.
- Figure 4. Moisture concentration profiles for PI/Si interfaces without silane (o) and with silane (•) coupling agent.
- Figure 5. Potential energy profiles, in terms of Q_c^2 , of a dry PI/Si interface (•) and the corresponding wet interface (o). An aminosilane coupling agent was used for this sample pair.
- Figure 6. Transverse scan results from the PI/Si interfaces under dry (•) and wet (o) conditions. The detector was fixed at 0.4 throughout these measurements and the sample was rocked from 0.1 to 0.3 .

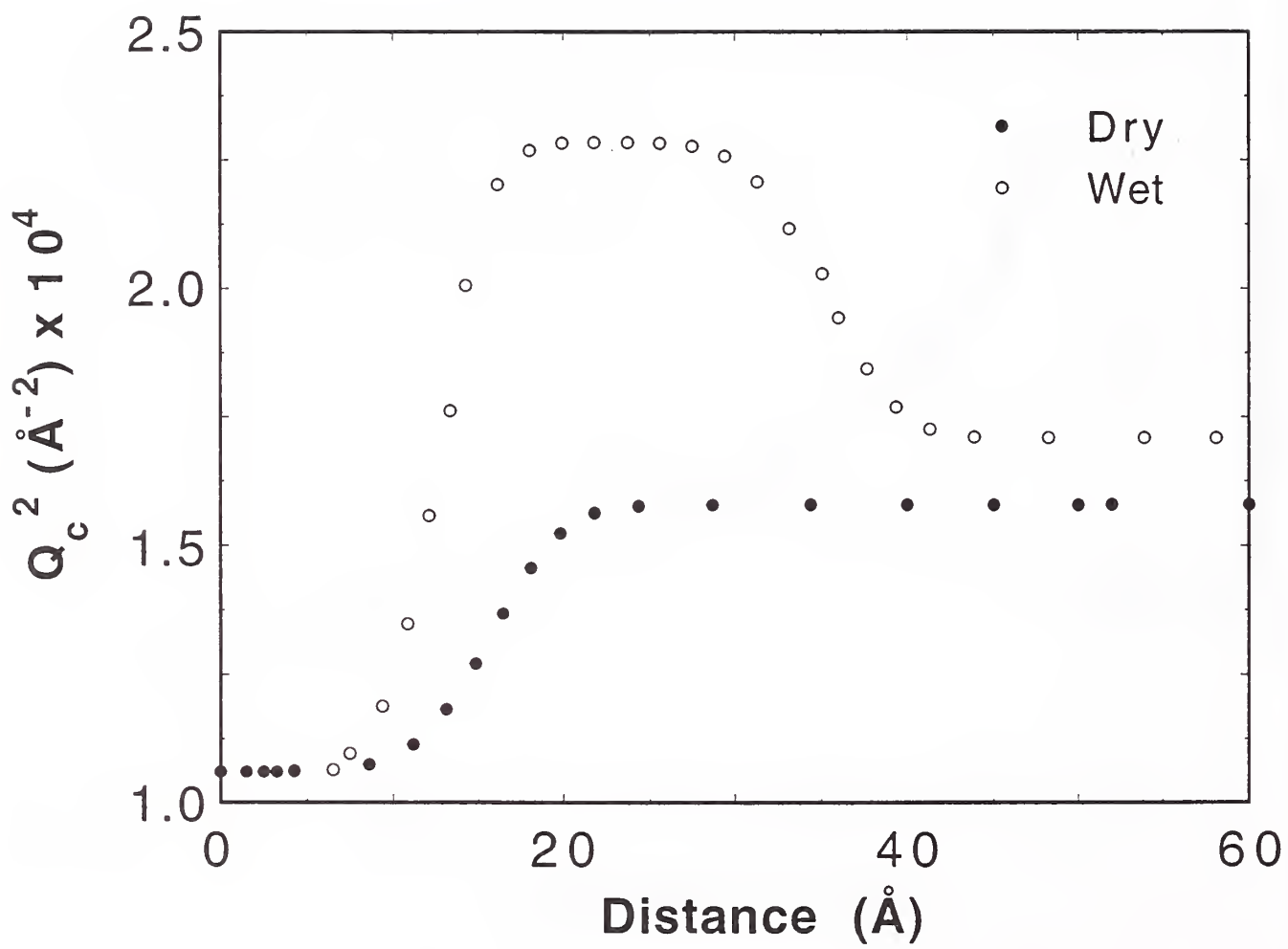
Typically, polyimides absorb a few percent moisture at room temperature. If an excess amount of water exists at the interfaces between PI and the components within an electronic or optoelectronic device, there can be damage to the underlying substrates or even total debonding at the interfaces.

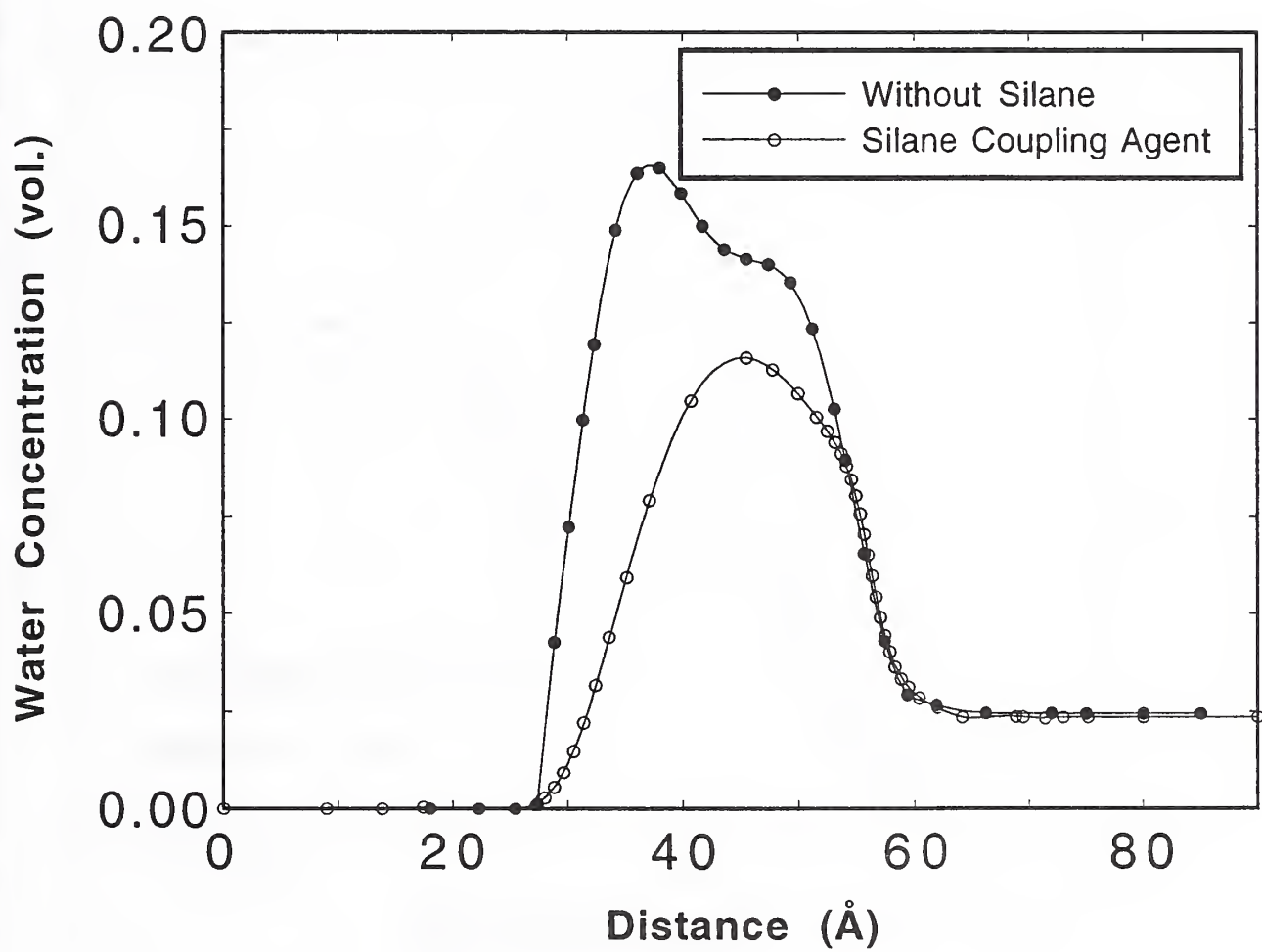
NR has the capability to characterize water at buried interfaces due to its high spatial resolution, which is of the order of the neutron wavelength of 2.35 Å used in this work, and due to the penetration power of neutrons to a variety of single crystals. Silicon single crystal wafers with a diameter of 11 cm were used here. With an attenuation factor of less than 15% for a beam path of 11 cm, the wafer is essentially transparent to the neutron beam, which enables the study of the buried interfaces.

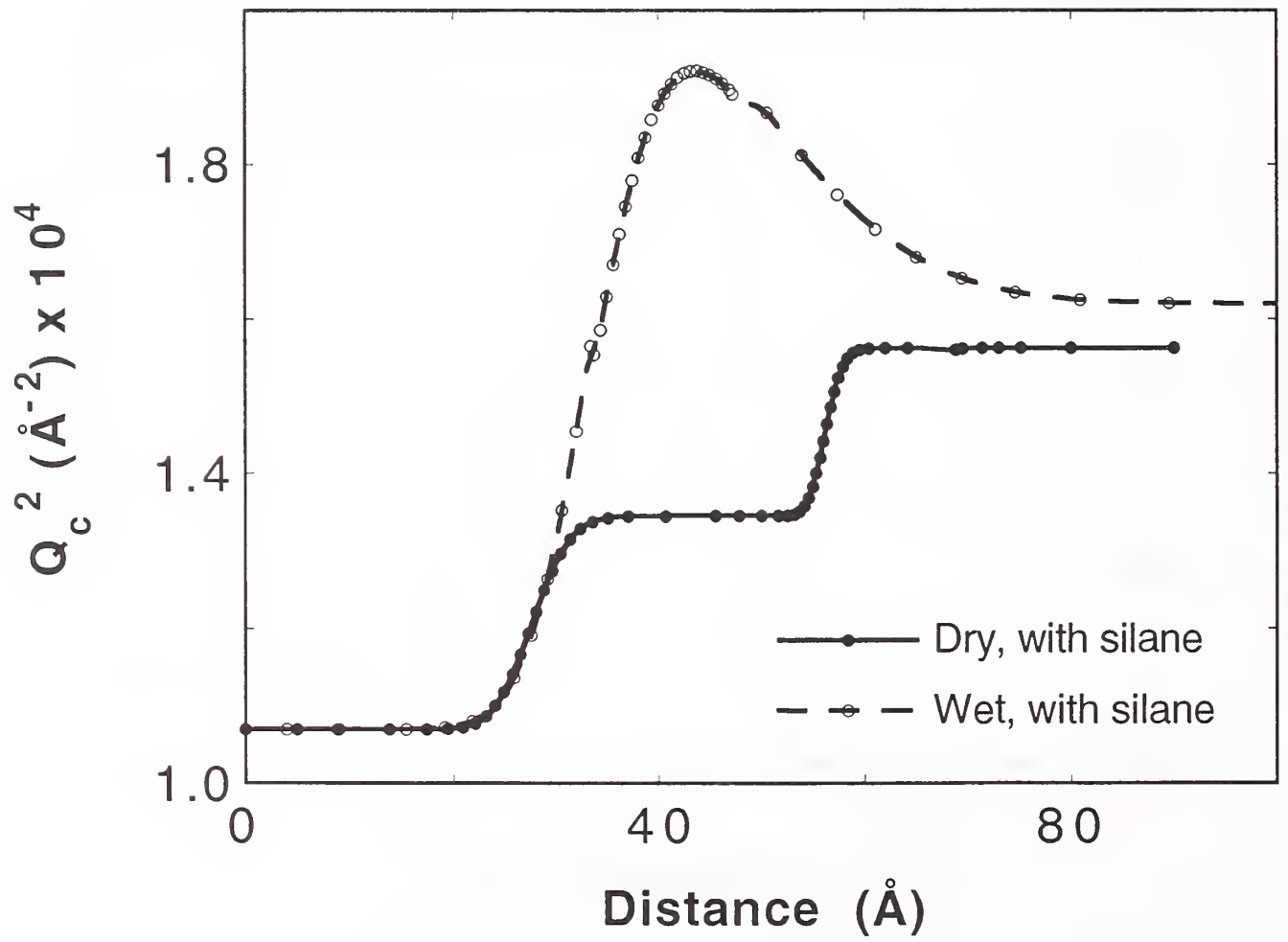
An important material constant which needs to be clarified for this discussion is the elastic cohesive scattering length per unit volume designated as Q_c^2 . This name derives from the fact that Q_c^2 is proportional to the second power of the critical angle defined in terms of the magnitude of the momentum transfer $Q_c = (4\pi/\lambda) \sin\Theta_c$. Total reflection of neutrons with wavelength λ will occur if the incident angle is less than Θ_c . It is noteworthy that in the above definition of Q_c or Θ_c , the interface between the material and vacuum is considered. Q_c^2 can be regarded as the height of the potential energy "barrier" for the surface. If the energy of the neutron beam transverse to the surface is less than Q_c^2 , total reflection occurs. More explicitly, $Q_c^2 = 16\pi Nb$ where N is the number density of

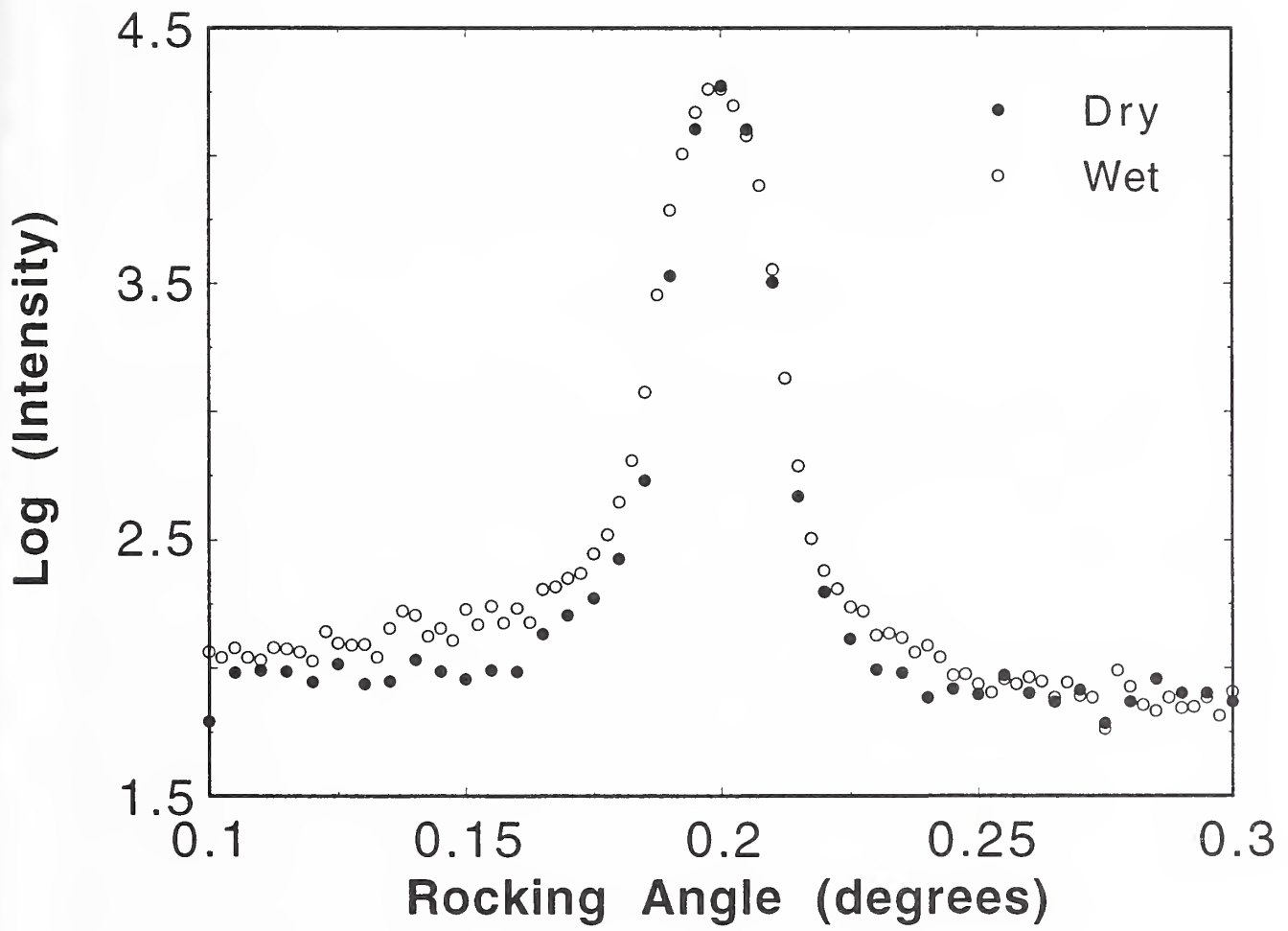












Session V

Analytical Techniques

AN EVALUATION OF THE MOISTURE CONTENT OF HERMETICALLY SEALED T05 METALLIC CANS AS A FUNCTION OF ANALYSIS TEMPERATURE

by

Jack H. Linn and Josh Daar
Harris Semiconductor
Melbourne, FL

ABSTRACT

Abstract: T05 headers, with no die attached, were welded with nickel lids. Twenty randomly selected units from this 'lot' were analyzed by mass spectrometry with the component holder temperature set at 50°C, 100°C, 125°C, and 150°C. The results indicate that the mean values are statistically similar for the units analyzed with the component holder at 50°C and at 100°C. However, the mean values for the units analyzed at 125°C and 150°C were approximately 2x to 3x that of units analyzed at 50°C and 100°C. X-ray photoelectron spectroscopy (XPS) from the inside surface of the nickel lids shows a distinct O(1s) peak with oxide, hydroxide, and water components. Monitoring the O(1s) data from nickel surfaces heated to various temperatures shows a large release of water and hydroxide between 115°C and 125°C. The amount of desorbed water and hydroxide begins to equilibrate as surface temperatures reach 140°C.

1. INTRODUCTION

Integrated circuit (IC) operating temperatures have continued to rise over the past few years. It is not at all uncommon for parts to be designed to operate at temperatures approaching 150°C. Higher operating temperatures pose the possibility of increased water vapor in the package due to the release of chemisorbed water from the package surfaces. Higher water vapor levels can result in the increased transport of contaminants (e.g. ionic species and particles), possibly leading to corrosion. Packages which are insufficiently cleaned or have residual foreign material trapped within the unit are most susceptible to this type of enhanced corrosion. The additional available moisture can also lead to increased electrical instability issues. Previous surface analysis studies have shown that 'physisorbed' water on metallic surfaces can be released at temperatures below 100°C, but temperatures above 120°C are required to release the chemically bonded water (1-3). Since current residual gas (RGA) methods employ a component holder maintained at 100°C, the measured water vapor is probably less than the actual water vapor available in a part operating at elevated temperatures.

This paper will present the residual gas analysis (RGA) data from a variable temperature study designed to determine moisture levels as a function of IC temperature. Surface analysis data

from nickel surfaces at elevated temperatures will also be presented to support the RGA findings. The data suggests that units should be analyzed at temperatures close to where they are expected to operate, not just arbitrarily at 100°C.

2. EXPERIMENTAL

Two hundred gold plated T05 headers and two hundred nickel lids were vacuum baked at 150°C for 2 hours at a pressure of 10 mtorr. The lids were subsequently seam welded to the headers, which contained no die, in a backfilled dry nitrogen ambient at about 1 atm pressure. The units were fine and gross leaked checked with helium and fluorinert solution, respectively.

The TO's were analyzed with a Pernicka Corporation mass spectrometer, which was specially built for the residual gas analysis of IC packages. The analysis method was based on a slow gas leak into the quadrupole mass spectrometer after the unit was punctured. The gas was leaked through a valve containing a 1 mil orifice. The mass analysis system employed was a Balzer's QMA 140 quadruple and QMG 311 quadrupole controller, capable of scanning from 0-100 amu. An IBM PC-XT with an 8088 microprocessor was used to acquire, quantitate, and store the data. The mass spectrometer was calibrated daily using 0.1 cc and 0.01 cc volume gas bursts of humidified nitrogen. The nitrogen gas pressure was set to deliver a 5000 ppm water in nitrogen stream, as read by a General Eastern hygrometer. The block containing the puncture needle and the inlet to the quadrupole mass spectrometer were set and maintained throughout the analyses at 125°C.

The units were not prebaked prior to analysis. One day each week for a period of five weeks, sixteen randomly selected units were analyzed. Four of the sixteen units were analyzed at each of the following component holder temperatures: 50°C, 100°C, 125°C and 150°C. The units were allowed to equilibrate in the component holder for 20 minutes before the analysis was begun. The order in which the analyses were performed was varied each day. A total of twenty units were analyzed at each of the component holder temperatures.

Five randomly selected units from the original two hundred were delidded prior to analysis or thermal treatment. The lids from these units were used for the X-ray photoelectron spectroscopy (XPS) analysis. The XPS data was obtained with a Physical Electronics (Phi) model 15-255G Double Pass Cylindrical Mirror Analyzer (CMA) attached to a PHI Model 590 Scanning Auger. The spectra were generated with Mg K-alpha X-rays at a power of 400 W. The analysis area was about 1mm². The pass energy was typically set at 50 eV for multiplex data and 200 eV for survey scans. Samples were positioned at a fixed 30° tilt angle. The base pressure in the system was maintained below 1 X 10⁻⁸ torr.

3. RESULTS AND DISCUSSION

Table 1 shows the results of the eighty analyses at the various component holder temperatures. Note that none of the units analyzed at 125°C or 150°C have water values below 1000 ppm. However, several of the units analyzed at 50°C and 100°C have water values significantly below 1000 ppm. In addition, several of the high temperature samples have water values above 2000 ppm, while none of the low temperature samples have any water values above 2000 ppm. The averages and standard deviations for each of the analysis temperatures are shown in Table 2. Note that the average values for the 125°C and 150°C sample sets are approximately 2X to 3X those of the 50°C and 100°C samples, while the standard deviation values are similar for each of the sample sets.

T-test data at a confidence level of 0.05 indicates that there is no statistically significant difference between the group of samples analyzed at 50°C and 100°C. The t-test data also indicates that there is no statistically significant difference between the group of parts analyzed at 125°C and 150°C at a 0.05 significance level. However, t-tests between the 100°C and 125°C sample sets shows that there is a statistically significant difference between the two groups of data.

This data indicates that additional moisture becomes available in the hermetically sealed package at temperatures above 100°C. Since the units were analyzed at a mass spectrometer pressure lower than 1×10^{-8} torr, the water must be chemisorbed, or chemisorbed, to the surfaces inside the TO can. If the water was not chemically bound, it would freely evolve from the package surfaces at 100°C, the boiling point of water at 1 atm pressure. Additionally, the boiling point of water is lowered significantly below 100°C in a vacuum. It appears that a certain activation energy is required to overcome the chemical bonds between the chemisorbed water molecules and the package surfaces before this water can become 'free' vapor.

This assertion is well supported by the fact that heating the parts from 50°C to 100°C has no statistical affect on the observed water content. The available water that is not chemisorbed to the package surfaces freely evolves off the surfaces at both of these analysis temperatures. However, at 125°C and 150°C, the observed water value rises significantly. The additional temperature must supply sufficient thermal energy to break the chemical bonds between the surfaces inside the package and the chemisorbed water molecules. The water must be chemically bonded either to the nickel lid or the gold plated header, as these packages contained no die or bond wires.

Past studies have indicated that water can both physisorb and chemisorb to nickel surfaces containing passive or native oxide layers (2,3). However, the same studies demonstrated that there is no chemisorption of water to gold surfaces (1). Water can

only physically adsorb to the gold. XPS O(1s) data from a typical nickel surface, containing a normal passivating layer after air exposure, shows that the chemisorbed layer of water exists as both molecular water and as hydroxides and peroxides. These species are most likely bonded to the oxygen associated with the native nickel oxide layer through hydrogen bonding. This helps to explain the fact that water does not chemically bond to gold surfaces. There is no native oxide layer formed on the surface of the gold, so there is no hydrogen bonding of the water and hydroxide to the gold surface. It is also hypothesized that many of the hydroxyl groups are actually bonded to the nickel atoms, creating a $\text{Ni}(\text{OH})_x$ or $\text{NiO}(\text{OH})$. Gold surfaces also do not form hydroxide or peroxide species. This layer of water and hydroxide on the nickel surfaces was found to be about 5 angstroms by variable angle XPS (1).

To test the theory that residual moisture was chemically bonded to the nickel lids, similar XPS analyses to the above studies were performed on the inside of delidded nickel lids. Figure 1 shows the XPS O(1s) spectrum from the inside of an unheated nickel lid. Note the components for water, hydroxide, and oxide. These peak locations were established in the previous studies by freezing water on a surface and from literature values. The ratios of each component are quite similar to those observed in the previously documented studies.

In the previous study, a nickel sample was heated to 125°C and analyzed. The O(1s) spectrum from this analysis is shown in Figure 2. A distinct drop in the water and hydroxide components is observed. Figure 3 shows the O(1s) spectrum from the same sample after it was heated to 150°C . A gradual continuation of the drop-off of the oxide and hydroxide components is noted. This sample was then cooled and moist room air was backfilled into the vacuum chamber to a pressure of 1×10^{-4} torr. The sample was allowed to stand in the system overnight and the sample was again subjected to XPS analysis. Figure 5 shows the O(1s) spectrum from this sample. The water and hydroxide components have risen back to nearly the same level as before the thermal treatment. This data establishes that the water can be released from the nickel surface at temperatures above 120°C and is easily re-adsorbed on to the surface of the nickel when it is cooled.

Figure 4 shows the composite plot of the changes in the water and hydroxide components, as observed in the XPS O(1s) spectra, as a function of sample temperature. Clearly, the beginning of the release of the majority of the chemisorbed water and hydroxide begins at about 120°C . This data supports the observed increase in water content as the units were analyzed at temperatures above 120°C . In addition, the curve shows a general leveling of the released water and hydroxide above temperatures of 140°C . Again, this correlates with the residual gas analysis which shows no statistically significant difference between the samples analyzed at 125°C and 150°C . The sample that was cooled and exposed to

the moist room air (Figure 5) is represented by the square in Figure 4.

In an analogous manner to the test surfaces, water vapor inside the sealed package will readily adsorb to the nickel lid when it is cool (e.g. after seal) and then be released at operating temperatures above 120°C (e.g. when the IC is active). Many IC operating temperatures can easily approach these conditions. When the IC is no longer active and begins to cool, the water will then be reabsorbed onto the lid surface or onto other materials, such as the die surface, bond wires or bond posts. This movement of the water from a condensed liquid to a gas and back to a condensed liquid can easily function as a transport mechanism for contaminants. Isolated surfaces, such as the lid surface, many times contain residual contamination containing ionic contaminants and particles. These can be transported throughout the inner cavity by the increased water vapor. Corrosion at the die surface, bonding wires, and bonding posts is often initiated by increased levels of ionic contaminants. The possibility of particles, in addition to water condensing on the die surface, can also lead to increased electrical instability (e.g. inversion).

The data clearly demonstrates that there is chemically bonded water and hydroxide in TO metal cans which is not now analyzed under the current test parameters of MIL-STD 883, Method 1018 (e.g. 100°C). All water that is not chemically bonded will readily be released for analysis at temperatures as low as 50°C. However, the water content available in IC's operating at temperatures above 100°C can be substantially higher. Two identically sealed packages subjected to two different environmental conditions, one operating at 50°C and one operating at 125°C, will have differing levels of available water vapor. More water vapor is available in the IC operating at the higher temperature. This increased water vapor can enhance the prospects of contaminant transport, which can lead to the possibility of corrosion, as well as increased electrical instability problems.

There is preliminary evidence to indicate that ceramic body packages may actually have even more chemisorbed water bonded to the internal package surfaces than the nickel lidded TO headers. In an analogous manner to the thin nickel oxide layer, the water and hydroxide can easily chemically bond to the increased surface area and roughness of the aluminum oxide.

If one is interested in the total water available to interact with the materials inside an IC package, the analysis conditions must be matched to the actual operational conditions of the IC. If the units are not operated or exposed to temperatures above 115°C, current methods of analysis are sufficient. In fact, it would be possible to analyze these types of devices at temperatures as low as 50°C. However, if the IC is operated or exposed to temperatures above 115°C, it is recommended that the

analysis temperature be at least 125°C to assure that the actual quantity of water vapor under operational conditions is known.

CONCLUSIONS

- Residual gas analysis using mass spectroscopy has demonstrated that T05 metallic cans show a marked increase in internal water vapor at elevated analysis temperatures.
- Mean water values increase by a factor of 2x to 3x at analysis temperatures above 125°C when compared to the normal analysis temperature of 100°C.
- XPS surface analysis studies indicate that metallic surfaces which form native, passivating oxides, will readily chemisorb water. Gold surfaces do not.
- XPS data indicates that the chemisorbed water is present as molecular water and as some type of hydroxide species.
- The chemisorbed water will not readily desorb from the metallic surfaces inside the IC package at temperatures below 115°C.
- A significant leveling in the release of these adsorbed water and hydroxide species occurs at temperatures above 140°C.
- The water vapor released inside the sealed units at elevated temperatures will readily chemisorb to the package surfaces, and possibly the die, as they cool.
- The dynamic action of the increased water vapor can aid in the transportation of contaminants from one area to another, leading to the increased possibility of corrosion.
- It is recommended that the operating temperature of the IC be considered when the internal water vapor measurements are conducted.

REFERENCES

1. J.H. Linn and W.E Swartz, Jr., Applied Surface Science **19**, 1984.
2. L.M. Moroney, M.W. Roberts, J. Chem Soc Faraday Trans I **79**, 1983.
3. W.E. Swartz, Jr., J.H. Linn, J.M. Ammons, M. Kovac, Proceedings of the 21st International Reliability Physics Symposium, 1983.

TABLE 1

Individual water values (ppm) for each of the twenty units analyzed at the four different analysis temperatures.

50°C	100°C	125°C	150°C
1110	700	1840	1680
100	620	1250	1840
1370	1230	1360	1730
270	1460	1090	1830
1190	1380	2330	2560
100	990	2570	2670
780	1050	2880	1970
1260	430	2720	2040
230	1010	1860	1810
1310	1230	2380	2670
800	1080	1160	1890
650	1190	1900	1950
1120	880	1810	1830
240	500	2410	1860
670	410	2140	2080
940	950	2600	2500
1140	1110	1450	1950
600	640	1990	1990
740	670	2450	2550
880	910	2550	2370

TABLE 2

Average and standard deviation values for the twenty IC packages analyzed at each temperature.

Analysis Temperature (°C)	Mean	Std Deviation
50	775	414
100	922	309
125	2037	552
150	2088	360

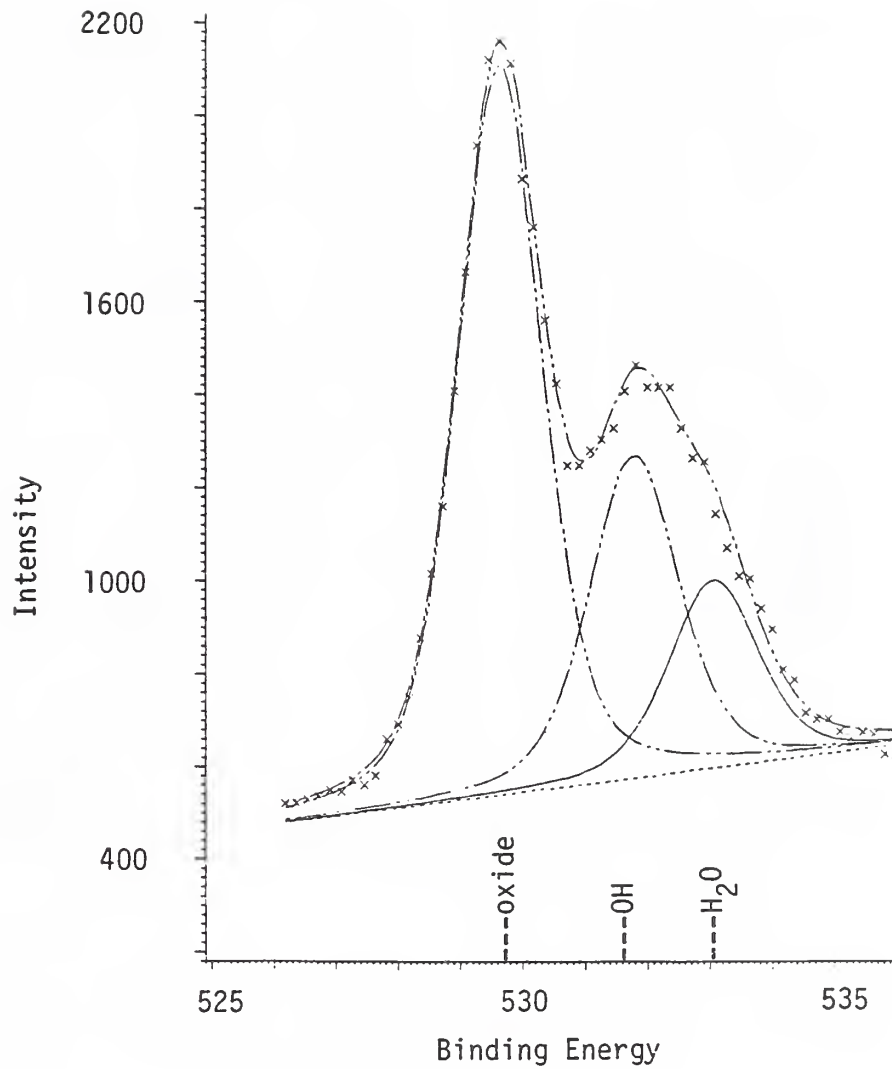


Figure 1. XPS O(1s) spectrum from a delidded nickel lid at 25 degrees celcius.

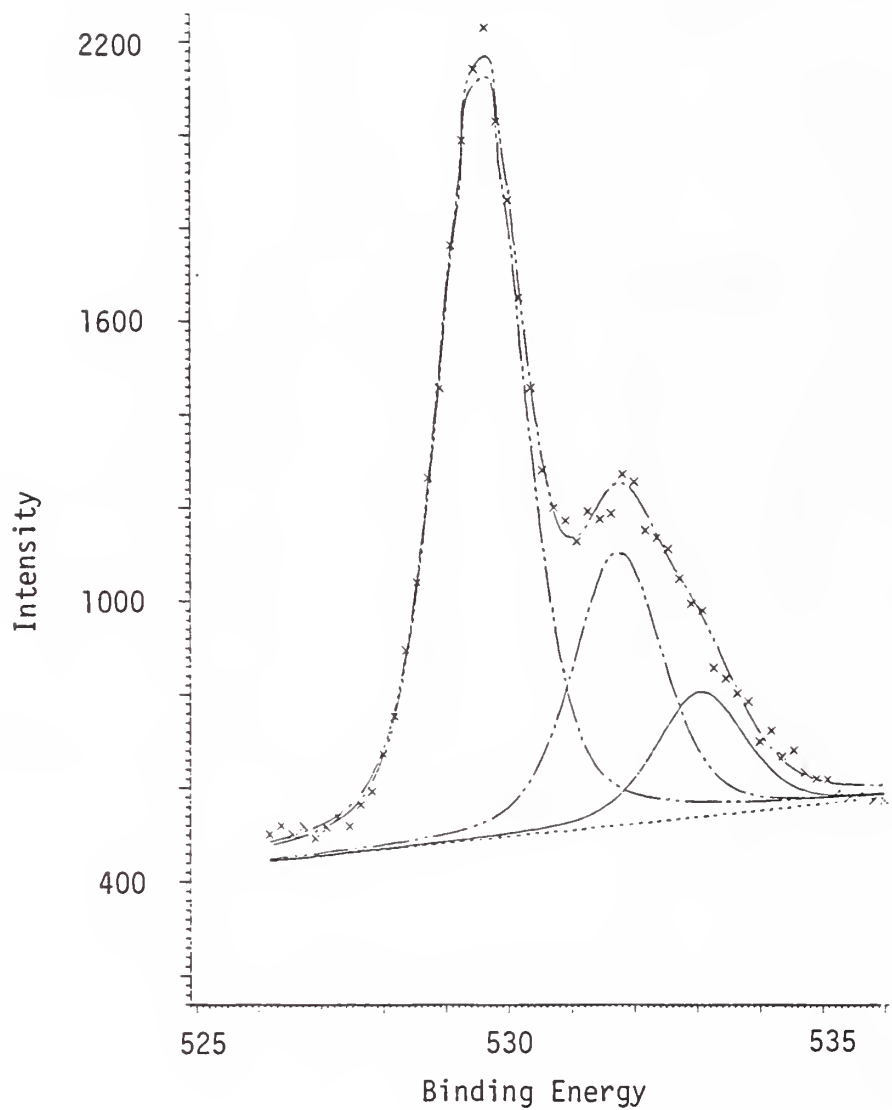


Figure 2. XPS O(1s) spectrum from a nickel surface heated to 125 degrees celcius.

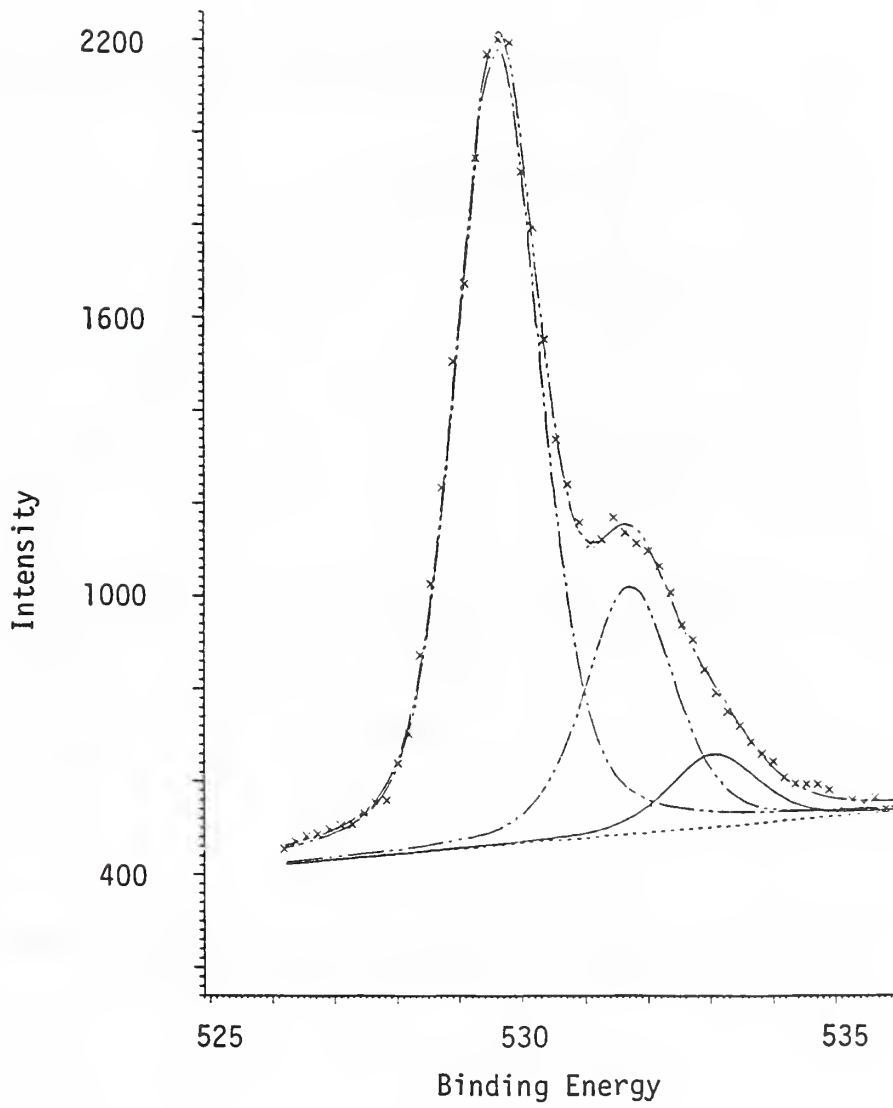


Figure 3. XPS O(1s) spectrum from a nickel surface heated to 150 degrees celcius.

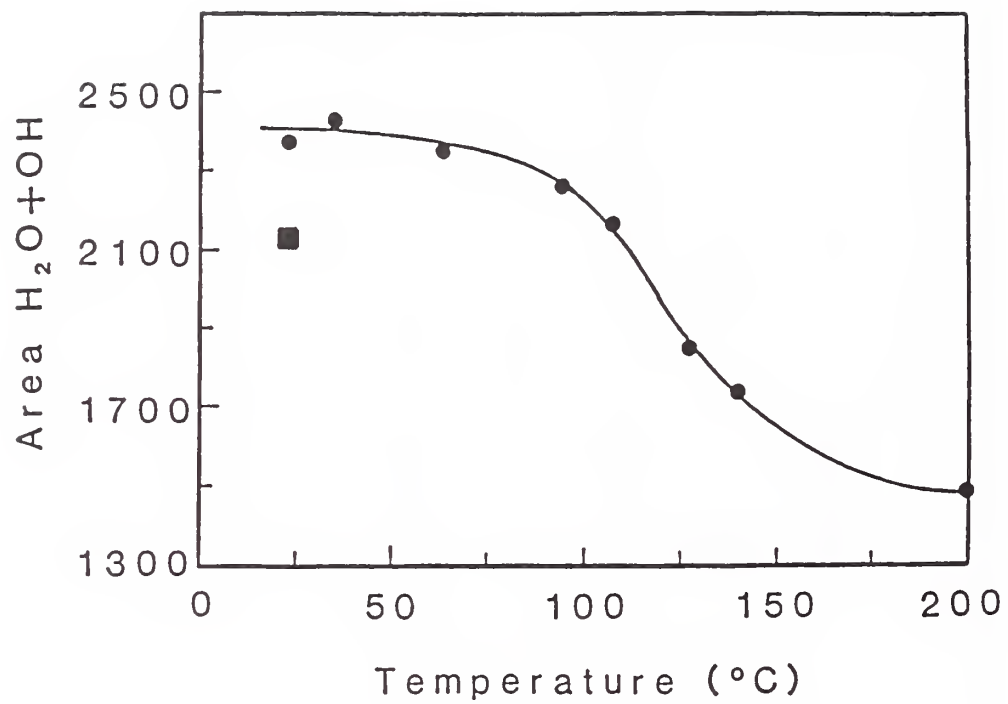


Figure 4. Composite plot of the area under the water and hydroxide peaks as a function of temperature.

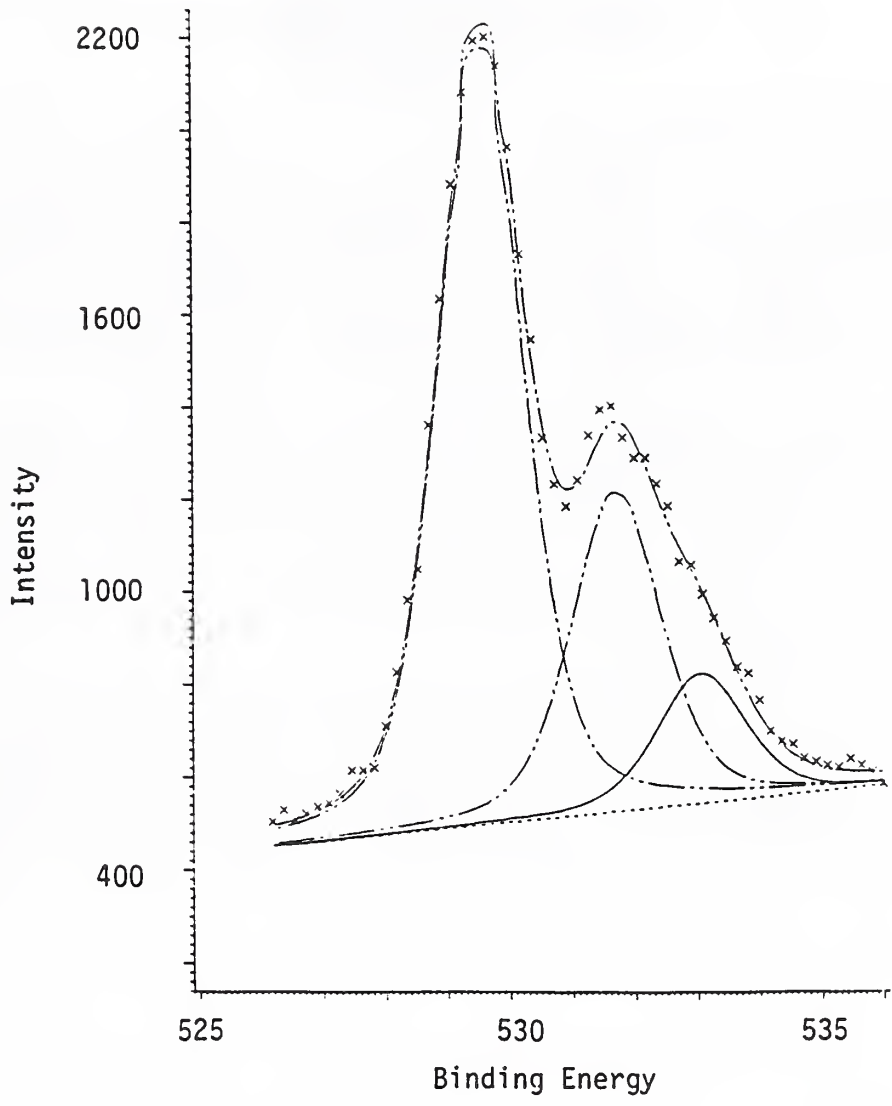


Figure 5. XPS O(1s) spectrum from a nickel surface after being heated and then cooled in vacuum at 1 E-4 torr.

RELIABLE MOISTURE DETERMINATION IN THE PRESENCE OF HYDROGEN OR OXYGEN USING METHOD 1018.2

by

Bruce J. Gollob
Atlantic Analytical Laboratory, Inc.
Whitehouse, NJ

The basis for establishing the absolute accuracy of the moisture determination in Method 1018.2 is to calibrate the mass spectrometer in a manner that closely duplicates the puncture of a semiconductor device and the subsequent analysis of the released gases. The goal of the calibration, therefore, is to introduce a known gas sample into the mass spectrometer that is of similar size to the unknown sample, at the same rate of introduction as the unknown, and of similar composition to the unknown.

The standard procedure in Method 1018.2 for calibrating for moisture is to pass nitrogen with a known amount of moisture through a three or five volume calibration valve into the mass spectrometer. This procedure satisfies the goal of introducing a moisture standard in a manner similar to the analysis of the unknown. However, many analysts have noted anomalous moisture results when the unknown sample had been sealed in an air or in a forming gas atmosphere.

A series of experiments has been performed at Atlantic Analytical which indicates that concentrations of oxygen or hydrogen above 3% in the package atmosphere can cause falsely high results for the moisture determination. This effect, and an analytical procedure that can compensate for these interferences, will be discussed.

GAS COMPOSITION ANALYSIS OF HERMETIC STRUCTURES AS A NON-DESTRUCTIVE TEST

by

John C. Pernicka
Pernicka Corporation
Ft. Collins, Colorado

Since 1967 the author has been engaged in the gas analysis of hermetically sealed structures. Historically this test procedure has been a destructive test and is specified as such in MIL-STD 883D, Method 1018.2, Procedure 1. During the past fifteen years experiments using a laser drill have been conducted to demonstrate the feasibility of analyzing gases in hermetic structures, backfilling the structure, and then resealing the structure. This paper presents a brief history of the evolution of the test procedure, comparison of the standard method verses the laser method, and recommendation for implementation of the test method.

I. INTRODUCTION

The "RGA Test", "Moisture Test", or sometimes fondly referred to as the "Kiss of Death Test" is basically the procedure used to measure the amount of moisture as a percentage per unit volume contained in a hermetically sealed semiconductor package.

Tests of this type, first conducted in 1967 by the author using a large double focused magnetic sector mass spectrometer, have been considered to be a destructive test even when applied to DPA or failure analysis. Once the hermetic integrity of the package is breached in order to extract the gas sample, the package is usually discarded unless further physical or electrical examination is required.

As the value of the semiconductor device increases the motivation to reuse the package increases. The author had developed ESD handling procedures such that a high value package can be reprocessed after the moisture test but this procedure amounts to remanufacturing the device with very little savings in time or cost.

A considerable amount of interest and encouragement was received from RADC, TRW, Litton, JPL and Lockheed to proceed with experiments designed to reduce the cost of reprocessing.

The following experiments were designed to test the feasibility of analyzing the contents of a hermetic package using MIL-STD 883 Method 1018.2, Procedure 1, then backfilling the package with a clean dry gas and resealing the package. The basis for this work

originated in 1975 when the author designed, manufactured and tested a similar system for Argonne National Laboratory to analyze fission gases in nuclear reactor fuel rods. This procedure consisted of:

1. Fixturing the fuel rod and forming a vacuum tight seal to the surface,
2. Laser drilling a hole to release the gas sample,
3. Analyzing the gas sample,
4. Backfilling the rod with a tag gas,
5. Welding the hole closed with 95% material thickness in weld area,
6. Leak testing the weld area.

II. APPLICATION QUESTIONS

Applying the above procedure to semiconductor packages seems straight forward, however, a number of questions had to be answered, namely:

1. Would laser drilling and/or rewelding create particulates which would impact the reliability and operation of the device under test?
2. Can the various materials used to package semiconductor devices be laser drilled and rewelded reliably to insure hermeticity?
3. Would laser drilling and/or rewelding damage the semiconductor device?
4. Would laser drilling impact the accuracy of the moisture measurement?
5. What moisture level can be expected in the resealed package?
6. Is the procedure economically viable?

III. EXPERIMENTS

The following four experiments were conducted over the past two years with lots of encouragement and little or no funding from any of the parties involved: 1, test of particulate generation, reweldability, and circuit damage; 2, test of reweldability, circuit damage, and performance of the resealed device; 3, test

of moisture data accuracy; 4, test of moisture level in resealed package.

1. Experiment 1.

The author received two lids and three large hybrid packages (approximately 4.0cc in volume). Two of the sealed packages were empty and the third contained a scrap circuit on a large substrate which filled the entire package. Pin tests had been performed on all three packages as well as fine and gross leak tests. A series of 200 holes were drilled and rewelded on the two sample lids in order to optimize the laser operating parameters. Next six holes were drilled and rewelded in each of the three packages using the optimum settings on the laser. Pin tests were then performed on the resealed packages. The packages were then opened and the rewelds and substrate were examined. The results of the pin tests and visual examination indicated that the procedure for drilling and rewelding would not create any particulates, the hermeticity could be maintained after the reweld, and the location of the penetration is critical to prevent damage to the circuitry.

2. Experiment 2.

The second experiment consisted of analyzing ten devices whose performance was particularly sensitive to high moisture levels. Five of the samples exhibited normal performance and five were electrically unstable. All ten devices were subjected to laser drilling, analysis of the gas mixture, backfilling with grade 4.5 nitrogen, and rewelding. The results of this experiment indicated that those packages with high moisture levels were unstable and all rewelded packages exhibited normal performance.

3. Experiments 3.

The third experiment consisted of analyzing 96 packages (MCL 420G XKOREAJHBIK) randomly selected from a lot of 1200 packages, which were manufactured about 18 years ago for Pernicka Corporation. The packages were divided into 4 groups. The first group of 24 were to be analyzed using an external test fixture and mechanical puncture device. The second group of 24 were to be analyzed using a batch fixture and mechanical puncture device. The third and fourth group of 24 each were to be laser drilled using an external fixture and batch fixture respectively. Each group was further divided into A and B subgroups of 12 packages which represented approximately one days work on the mass spectrometer.

Prior to each days analysis the mass spectrometer moisture calibration was checked using a high pressure saturator and General Eastern Model 1500 which was calibrated by GEI against their NIST transfer standard. The uncertainty of the transfer standard was reported at $\pm 0.04^{\circ}\text{C}$ in the measurement range of interest and our instrument difference reading varied from -0.02°C to -0.08°C over the same range. Converting the above dewpoints to ppm per unit volume yields an accuracy of -18.4ppm - 9.2ppm to -36.8ppm . A series

of ten measurements were made each morning and the mean and standard deviation for each subgroup are summarized in the Table(1) below:

SUBGROUP	DEWPOINT MEASURED	MASS SPECTROMETER READING
1A	5280ppm \pm 18ppm	5305ppm \pm 25ppm
1B	5177ppm \pm 25ppm	5160ppm \pm 30ppm
2A	5220ppm \pm 15ppm	5210ppm \pm 27ppm
2B	5152ppm \pm 20ppm	5151ppm \pm 28ppm
3A	5210ppm \pm 23ppm	5200ppm \pm 22ppm
3B	5230ppm \pm 20ppm	5243ppm \pm 29ppm
4A	5212ppm \pm 24ppm	5210ppm \pm 30ppm
4B	5198ppm \pm 26ppm	5205ppm \pm 28ppm

Table 1. Subgroup Moisture Calibration Summary

After the ten calibration checks were made, 12 packages of each respective subgroups were analyzed per the requirements of MIL-STD 883D, Method 1018.2, Procedure 1. The results of these tests are summarized in Table(2) below:

SUBGROUP	MEAN VALUE IN %	STANDARD DEVIATION
1A	1.2229	.6398
1B	1.1531	.6523
2A	1.2374	.7511
2B	1.1003	.6887
3A	1.2577	.8012
3B	1.3049	.7212
4A	1.2168	.6656
4B	1.2446	.7143

Table 2. Subgroup Moisture Measurements Summary.

Careful review of Table(1) and Table(2) suggests that the packages selected for this experiment were by no means optimum. However, one might conclude that variations in the mean value measured in each subgroup were considerably less than the standard deviation and therefore acceptable under the MIL-STD.

4. Experiment 4.

The packages laser drilled in the above experiment were backfilled with Grade 4.5 Nitrogen after each package was analyzed except that those packages analyzed in the batch mode were also filled as a batch and then rewelded. The packages in subgroups 3A and 3B were remixed and randomly divided into 3A1 and 3B1. Similarly 4A and 4B

were redivided into 4A1 and 4B1. Subgroups 3A1 and 4A1 were analyzed by mechanical puncture in the batch and external fixture mode respectively. Where as subgroups 3B1 and 4B1 were analyzed using the laser drill in the batch and external fixture mode respectively. The following Table(3) summarizes the test results of the rewelded packages:

SUBGROUP	MEAN VALUE IN PPM	STANDARD DEVEATION
3A1	2280	759
3B1	2850	612
4A1	2631	937
4B1	2174	453

Table 3. Rewelded Subgroup Moisture Measurement Summary.

Examination of Table(3) might suggest that the packages under test benefitted from the test procedure even though they would have been rejected as failures when first analyzed. The variation measured between subgroups is within the same order of magnitude as the calculated Standard Deveation and certainly less than the accuracy guidelines (± 1000 ppm) required by the MIL-STD.

IV. CONCLUSION

The laser drill and reweld procedure as applied to the moisture analysis test can be applied without apparent distortion of the test result, or damage to the performance of the device under test provided that extreme caution is exercised in selecting the location of the puncture site. The economic benefit of applying this technique to analyze packages and/or rework packages depends entirely on the cost of the original package and retesting requirements. Not all package configurations lend themselves to this procedure, however, designers can incorporate the requirements of this procedure into new designs.

New Microelectronics Package Atmosphere Analysis System: Sample Analysis and Calibration Standards

Stephen A. Ruatta, Julius Perel and John F. Mahoney
Phrasor Scientific, Inc. 1536 Highland Ave, Duarte, CA 91010

An instrument designed to analyze the ambient components inside of microelectronics and other small hermetically sealed packages has been constructed and is in operation. This instrument allows the gas contents of the package to expand into a 0.01cm^3 volume and then into a mass spectrometer after the package is punctured. This arrangement minimizes adsorption of analytes onto extraneous surfaces; reducing contamination and increasing sample throughput. Of equal interest, we are working on the development of a method for calibration of moisture measurements. This method utilizes saturated solution of salts to generate known humidity gases inside of small volume containers. Using this technique, we have generated concentrations of moisture ranging from 1590 ppmV to 18300 ppmV to compare with the results expected using a two pressure humidity generator and measurements of the humidity in the calibration flow using a solid state sensor.

Keywords: Failure analysis, Humidity measurement, Mass spectrometry, Semiconductor package, Water vapor measurement.

1. INTRODUCTION

The presence of moisture in a package atmosphere can be an important factor in the premature failure of semiconductor devices [1, 2] and references therein). Determining the sources of this moisture is an area of ongoing research which may attribute it to any of the following; water somehow trapped at sealing, die attach produced moisture (either simply outgassed or derived from chemical reactions), moisture produced by chemical reactions of various gaseous components or other unknown mechanisms.

Determining the concentration of moisture in the ambient atmosphere of a package volume is complex. Compared to most gases, water has a relatively low vapor pressure (Appendix B5 in [3]) which makes extracting it out of a package and into an analyzer a challenging task. Finally, measuring the concentration of any compound requires that reference materials be available during the analyses. In most analytical techniques, calibration curves of standards over a range of concentrations are used for the analysis of samples containing concentrations of analytes between maximum and minimum concentrations of interest. By bracketing the sample concentration with known standards, the true sample concentration may be calculated with greater confidence. Ideally, the standards should be as similar to the sample as possible. In the case of semiconductor package analysis, the internal volume, internal pressure and temperature should be matched as closely as possible by the standard. The standard should be readily available to all laboratories (and their customers!) for both interlab comparisons and blind standards. This paper provides us with an opportunity to discuss a system for analysis of moisture in semiconductor packages. This system exposes a very small surface area to the water containing gas, thus minimizing

contamination and loss of analyte water. The manner in which packages are sampled allows us to also pursue development of a set of moisture standards for determining the accuracy and precision of this instrument.

2. PROCEDURE

A. Package Interface and Mass Spectrometry

A system for the mass spectrometric analysis of the gaseous components contained within a small volume package has been constructed to comply with MIL-STD 883C Method 1018.2. The key features of the interface between the package and the mass spectrometer is shown schematically in figure 1. This design minimizes the surface area exposed to the analyte water vapor thus reducing adsorption and outgassing effects that could lead to systematic errors.

As is evident from figure 1, puncturing of a package releases the gas into about a 0.01cm^3 volume connected to a fused silica transfer line. This transfer line ($40\mu\text{mID}$) utilizes viscous (laminar) flow to reduce contact of the analyte vapors with the walls of the tubing as it flows into the Millipore/Extrel Questor III quadrupole mass spectrometer source. The gas is then ionized by electron bombardment with the resulting ions up to 200 Daltons (amu) mass analyzed and detected by a Faraday cup and/or an electron multiplier. Data is collected automatically by a computer which also controls the mass spectrometer hardware.

Gas flow in a tube can be thought of as one of two basically different types or an intermediate between the two. At low pressures where few molecules are present, the mean free path between gas molecules is long compared with the dimension of its container. In this molecular flow regime, there are many interactions between a gas species and the container walls as shown in figure 2a.

Here the mean free path is inversely proportional to the gas density or pressure. A convenient formula for mean free path is given by O'Hanlon[3]:

$$\lambda(\text{cm}) = \frac{5}{P(\text{micron})}$$

As the pressure increases, the mean free path decreases, eventually becoming less than the distance to the walls of the tubing through which it is flowing. When the mean free path is much less than this distance, the character of the gas flow is determined mainly by gas-gas interactions while gas-wall interactions occur relatively infrequently. This viscous flow regime is shown schematically in figure 2b and can be theoretically described by the Poiseuille equation[4]:

$$Q = \frac{\pi a^4}{8\eta l} P_a (P_2 - P_1) \quad (\text{micron-liters-sec}^{-1})$$

where,

Q = flow rate
 $P_a = (P_1 + P_2)/2$

a = tube radius
 P_2 = high pressure

η = gas viscosity
 P_1 = low pressure

l = tube length

assuming that the following four conditions are met:

- 1.) The gas must be "incompressible" or the flow must be slow compared to the speed of sound.
- 2.) The gas must flow into the tube such that viscous flow is established in a short distance.
- 3.) Turbulent flow must not exist.
- 4.) The flow velocity at the walls must be zero.

A complete discussion of this equations and its assumptions is beyond the scope of this paper. The interested reader may find this material well covered in Dushman[4].

An interesting use of this phenomenon was demonstrated in a recent paper by Lin and Sunner[5] showing that transfer of gas phase ions across long distances(up to 50 meters) in metal capillaries without complete neutralization is possible. Efficiencies of up to 35% were reported for ions transferred through tubes of varying lengths(0.6-50m).

B. Calibration Standards

A major problem in the analysis of moisture inside of semiconductor packages is the lack of standards with which to calibrate a particular instrument or group of instruments. While samples are available for certification purposes, it would be ideal for laboratories to have a standard that could be utilized daily or as needed. One possibility which we have begun to investigate is to utilize saturated salt solutions to generate known moisture levels in air or nitrogen inside of small metal and/or Teflon packages.

The use of saturated salt solutions to provide constant humidity gases is not new. Tables of humidity vs. temperature for different salts can be readily found[6, 7, 8, 9]. Although these references usually provide humidity in terms of %Rh, converting to ppmV may be done if the temperature is known. Such solutions are also used commercially as secondary standards for calibrating solid state hygrometers in the field[10].

Preparation of such a solution is straightforward. A saturated salt solution has an excess of solute (ie. 99.9+%NaCl (Aldrich)) added to distilled water and is allowed to equilibrate to ensure that an excess is present. The concentration of salt in the solution defines the solubility product (K_{sp}) for that salt and depends on the particular salt used.



where

$$K_{sp} = [Na^+][Cl^-]/[H_2O]$$

It is only for dilute solutions of sparingly soluble salts (unlike NaCl) that the concentration of water (kg/liter) is close to 1. Since the concentration of the water in the liquid phase is determined by the solubility of the salt (as listed in tables of concentrative properties of aqueous solutions[9]), the equilibrium concentration of the water in the gas phase is similarly determined by this concentration[7, 11] at a given temperature.

The task of adapting this idea to the production of a useful calibration tool for semiconductor packages should be possible. The best possible design should look as much like the package under test as possible. Because of the wide variety of packages possible, and the preliminary nature of this work, we have not included this in the design criteria. We have included the following qualities:

- 1). The humidity should be variable.
- 2). The volume should be variable.
- 3). Inert materials that are comparable to real packages (Teflon, glass, ceramics, stainless steel) should be used that do not react with the concentrated salt solutions.

A schematic diagram of a reference device is shown in figure 3 . This device is based on a stainless steel Whitey valve, with the addition of a glass salt solution holder and a stainless steel or aluminum reference volume. When the valve is in the open position, the vapor above the solution can easily equilibrate throughout the valve and the gas chamber. This results in all the surfaces being wetted so as to be in equilibrium with the moisture containing gas. Just prior to sampling, the valve is closed, isolating the gas chamber from the salt solution, without moving the solution containing bulb. Closure is maintained by a spring pushing the Teflon plunger onto the valve seat. This action reduces perturbation of the water equilibrated surfaces to a minimum, especially in the gas chamber. The reference device can then be easily mounted for subsequent puncturing and sampling of the gas chamber.

C. Results

There are currently two installed instruments utilizing the technique of minimizing the surface area that analytes are exposed to. Both of these instruments are in the certification process.

Preliminary results of the multiple analysis of four different solutions are shown in table 1 and plotted in figure 4. Figure 4 shows the results plotted with the expected results based on the reference humidity values for each of the salts used. If we consider only the concentrations between 10,000 and 2000ppm, the agreement is fair, even considering the scatter in the data. This is reasonable considering that for these preliminary experiments, the system was only calibrated for 5000ppm water vapor content. Given this calibration concentration, it is not unlikely that the measured values for NaCl, which should be about 18,000ppmV[7], are off simply because the mass spectrometer and inlet system had not been calibrated for concentrations in this range. If this is in fact the case, then this fortuitous result is a good example of why calibration curves are necessary for determining the true concentration of an analyte in an unknown sample.

3. CONCLUSIONS

Improvements to the mass spectrometer and inlet system in terms of improved software, automated and multiple sample analysis and more automated calibration at different moisture concentrations are in progress. Future work on the calibration standards will include making them easier to use on a regular basis and improving their reproducibility.

REFERENCES

1. Cohen, E.C., Ruthberg, S., Eds., *NBS/RADC Workshop Moisture Measurement Technology for Hermetic Semiconductor Devices, II*, Washington, DC, (1980).
2. Schafft, H.A., Ruthberg S., Cohen, E.C., Eds., *ARPA/NBS Workshop V, Moisture Measurement Technology for Hermetic Semiconductor Devices*, Washington, DC, (1978).

3. O'Hanlon, J.F., *A User's Guide to Vacuum Technology* (John Wiley and Sons, New York, NY, 1980).
4. Dushman, S., Lafferty, J.M., *Scientific Foundations of Vacuum Technique* (John Wiley and Sons, New York, NY, 1962).
5. Lin B., Sunner J., Electrospray ionization and ion transport through high pressure capillaries, *Proc. Am. Soc. Mass Spect.* Washington, DC, 1992, pp 1661-2.
6. J. A. Dean, *Lange's Handbook of Chemistry* (McGraw-Hill, New York, 1992).
7. L. Greenspan, Humidity fixed points of binary saturated aqueous solutions, *J. Res. NBS* **81A**, 89-95 (1976).
8. H. M. Spencer, in *International Critical Tables* E. W. Washburn, Ed. (McGraw-Hill, New York, 1926), vol. 1, pp. 67-68.
9. R. C. Weast, Ed., *Handbook of Chemistry and Physics* (Chemical Rubber Co., Cleveland, OH, 1989).
10. Hy-Cal Engineering, Inc., El Monte, CA.
11. A. N. Kirgintsev, A. V. Luk'yanov, Thermodynamic characteristics of saturated aqueous solutions of salts, *Russ. J. Inorg. Chem.* **12**, 1070-1072 (1967).

Table 1 -- Preliminary results of the analysis of four different salt solutions at 25°C.

Salt	ppmV(predicted ^a)	ppmV(exp)	ave. ppmV(exp)
LiCl	2800	3212 2020 3616 4250	3274
LiBr	1590	3985	-----
NaI	9300	7790 8970 11370 6690	9377
NaCl	18300	9134 12520	10827

^aValues converted from relative humidities given in [7].

FIGURES

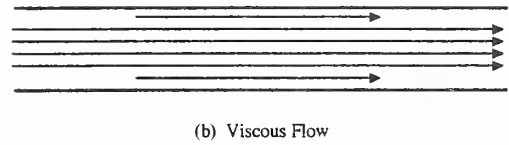
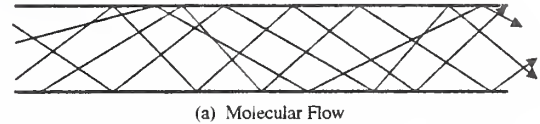
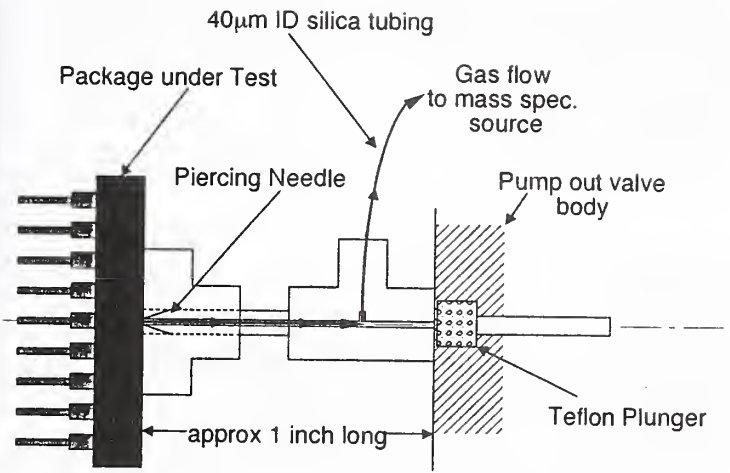


Figure 1. Schematic of the inlet portion of instrument.

Figure 2. Two basic flow regimes.

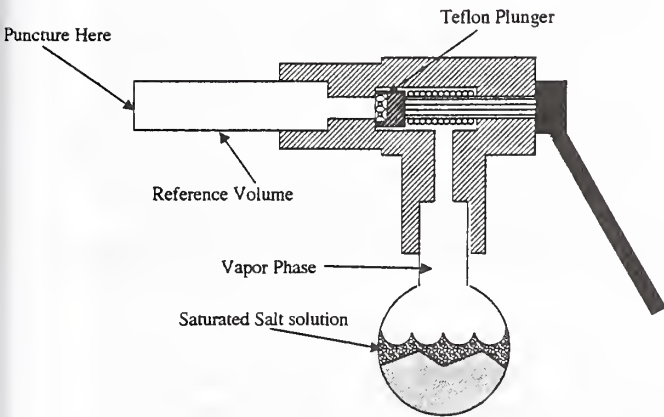


Figure 3. Schematic diagram of a reference device (Valve closed).

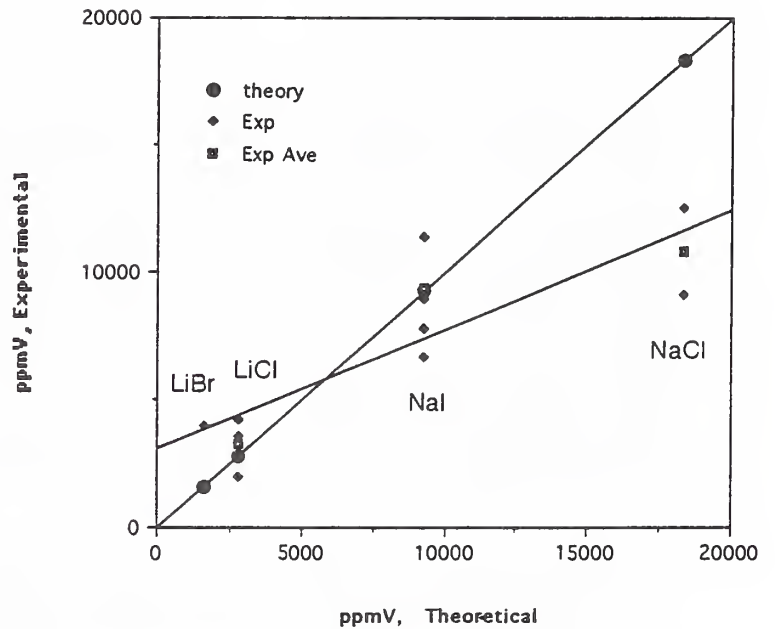


Figure 4. Plot of preliminary results of the analysis of four different salt solutions.

MICROCIRCUIT HERMETICITY TESTING USING THE BERGQUIST METHOD

Scot K. Anderson and Thomas J. Green
Martin Marietta Astronautics Group
P.O. BOX 179 M/S 0350
Denver, Colorado 80201

ABSTRACT

This paper describes the Bergquist hermeticity test technique. Leak test data is presented for a variety of package styles with volumes ranging from .01 to .2 cubic centimeters. This data are compared with conventional MIL-STD-883 test data. Additional data are presented for a large volume (approx. 1 cc) gold plated kovar flatpack.

KEY WORDS; Hermeticity, Fine Leak, Gross Leak, Bergquist, Helium

INTRODUCTION

Hermeticity testing of electronic components is becoming an ever more critical aspect of manufacturing modern high reliability systems. As component complexity and expected life increase, the requirements imposed on a leak detection system become very demanding. In addition, anticipated changes to MIL-STD-883 TM1014 (SEAL) [1] will drive the industry to manufacturer devices with equivalent standard air leak rates below 10^{-8} atm cc/sec. Several years ago a new type of leak detector was developed to leak test components with leak requirements of 10^{-8} atm-cc/sec. This new leak detector design performs both gross and fine leak tests during the same test cycle, using helium as the tracer gas for both test ranges.

In leak detecting components several concerns may arise. First, fine leak techniques do not lend themselves to gross leak detection and may in fact produce passing results for parts with major seal defects. Second, gross leak techniques often require a skilled operator and do not offer an objective pass/fail criterion. Third, testing methods that submerge a component in a fluid may introduce contaminants that cause other failures or even temporarily seal the leak. Fourth, bombing a part in helium may prove too insensitive or require extensive bombing to detect the small leak rates required for long life components.

This paper presents leak test data for a variety of package styles with volumes ranging from 0.01 cc to 0.2 cc. The 32 parts tested were supplied by A. DerMarderosian of Raytheon. All 32 packages were known to have leaks. Additional data are presented using the new leak detector design to optimize a sealing schedule for a typical hybrid package.

THE LEAK TEST TECHNIQUE

To reduce risk in testing costly hybrids, especially optical devices, a new methodology for leak testing components was required. The method discussed in this report was developed by L. Bergquist and others [2] and allows for a greater fine leak dynamic range and performs a gross leak test during the same test cycle. A complete test cycle takes approximately 8 minutes to complete and offers a more objective gross leak test.

In standard, helium mass spectrometer fine leak detectors, the helium inside the component volume may be removed from the part during the initial pump down prior to leak measurement. When the partial pressure of helium is then measured, very low, possibly passing, leak rates may be observed. The new test method used for these measurements operates on the principle that if the leak detector's vacuum system removes the air from the test chamber without also removing the helium, a gross leak test could be made before the fine leak test. A specially modified cryopump evacuates the gas from the test chamber. The modifications prevent the helium leaking from the component from being removed from the vacuum chamber volume. Therefore, as soon as the test chamber is closed any helium escaping from the part is captured for subsequent measurement. This technique has been proven sensitive enough to detect gross leakers in parts (.15cc volume) backfilled with room air.

There are, as expected, limits to the ability to sense large leaks in small component volumes. Further, the pass/fail criterion must be established for each package type to be tested. Once this data has been accumulated, a non-ambiguous partial pressure reading may be used to reject parts with gross leaks. The dwell time from bomb to test chamber is of critical importance for components with very small internal volumes. For large leaks in small components (Vol. < 0.15 cc), a dwell time of 30 minutes may reduce helium pressure below rejection limits. If an arbitrary limit of 99% helium loss during the dwell time is assumed to be too great, then an approximate detection limit may be computed. Figure 1 shows how detectable leak rate varies with component volume. The sloped lines from top to bottom are for dwell times of 1, 30, and 60 minutes respectively.

Figure 2 illustrates how excessive dwell time can effect the fine leak reading obtained. In this figure the measured leak rate is plotted against actual leak rate for 1 cc package volume and a 2 minute dwell time. This effect is much worse for small package volumes or longer dwell times. This is believed to be the reason many of the packages passed when tested using standard 883D methods on the Bergquist leak detector.

Fine leaks are measured by the rate of rise of helium in the vacuum chamber. Since the modified cryopump does not pump helium, any helium leaking from the package accumulates in the test manifold volume. The partial pressure of helium in the vacuum chamber may be determined by the following expression:

$$P_{\text{He}} = \frac{Lt}{V}$$

Where:

L is the helium leak rate
t is time
V is the total test manifold volume

This relationship applies to measurements that do not significantly reduce the helium pressure in the component during the fine leak test.

To determine an unknown leak rate, helium is introduced into the test manifold from a standard helium leak. The rate of rise of helium in the vacuum manifold is proportional to its volume. Hence, the unknown leak rate may then be determined using the following relationship:

$$L_{\text{unk}} = \frac{m_{\text{unk}}}{m_{\text{std}}} L_{\text{std}}$$

Where:

L_{unk} is the unknown leak rate
 L_{std} is the standard leak rate
 m_{unk} is the rate of rise of helium from the unknown
 m_{std} is the rate of rise of helium from the standard leak

A straight line is sufficient to determine the leak rate for a fine leak. Further accuracy may be achieved by performing a least squares fit to several data points allowing improved statistical significance for the test and the computation of standard deviations and the correlation. Using this technique, leak rate background as small as 10^{-13} std-cc/sec have been observed. In fact, the helium entering a glass ion gauge is detectable.

Obviously, care must be exercised to prevent false readings. Our leak detector utilizes all metal seals and has provisions for valving the ion gauge out of the system. Helium retention in elastomers is also a concern so all metal valves are used. Atmospheric helium is prevented from entering the test chamber during part introduction with a strong nitrogen purge.

Figure 3 is a block diagram of the leak detector. A turbomolecular pump is used to evacuate the helium after a test. The quadrupole is used to measure helium partial pressures. The cryopump has been specially modified to pump all gasses except helium. These modifications also enable the pump to absorb a large volume of nitrogen at atmospheric pressure. Total pressure is monitored with an ion gauge. As in conventional leak detection calibration is performed using a standard helium leak.

The leak detector is computer controlled, including the valve sequencing and data display. The leak detector is divided into four sections: the sample chamber, the cryo/roughing pump, the detection system, and the helium pump. A component is introduced by closing valve V3 and opening valves V1 and V2. Purge gas enters V2 and exits through the sample port, V1. Once the part is inside the sample chamber V1 and V2 are closed. Valve V4 is now closed to isolate the cryopump. This done, V3 is opened and the gas inside the sample chamber is dumped to the cryopump. Once the cryopump has removed the nitrogen purge gas, valve V5 is closed and V4 is opened. During this gross leak test any helium evolved from a leaking component is measured by the mass spectrometer. After completion of the gross leak test, V5 is opened to exhaust the collected helium. Valve V5 is again closed to make the fine leak test. During the fine leak test many measurements are made to establish the slope of the accumulating helium. At completion of the fine leak test valve V5 is opened, V3 is closed, and V1 and V2 are opened. The component is removed and a background measurement is made on the now empty chamber. Figure 4 is a flow chart of this process.

LEAK TEST RESULTS (SMALL VOLUME)

The Bergquist leak detector described above was designed to test large volume hybrid packages. From the beginning it was realized that characteristic leak behavior from small volume parts would be different than the leak behavior expected from large parts. To date, little data existed for small components. A series of tests were conducted to compare this leak detector to the standard 883D tests. When making these comparisons no changes were made to the baseline configuration of the leak detector or the control software for valve sequencing. Modifications to the leak detector and control software would improve sensitivity and reduce test time.

Before testing began, all packages were cleaned, baked and initial baseline background measurements were taken using the Bergquist leak detector. This was followed by testing after helium bombing per 883D TM 1014. All packages were then bombed again and tested using a conventional leak detector for fine leaks. In both Bergquist and conventional leak tests the packages were bombed in a helium atmosphere at 60 psig for two to four hours as required. A "simple" bubble test was performed immediately after removal of the component from the conventional fine leak test. Packages that passed this test, or were questionable, were retested using the formal 883D TM1014 condition C1 bubble test. After analyzing this data several inconsistencies were noted. A weight gain test and a second 883D bubble test were performed on parts exhibiting these inconsistencies. Finally, packages that passed the initial Bergquist leak test were retested using a modified helium bomb technique that improved gross leak accuracy. Figure 5 shows a flowchart of the tests schedule.

To elucidate the nature of the leaks and gauge their approximate size two parts were destructively analyzed. Both were found to contain large voids in the glass seal between the two ceramic package halves. One of the packages had a clearly defined leak channel corresponding to a computed helium leak rate of $6 \cdot 10^{-4}$ std cc/sec. As can be seen from Figure 1, a leak this size might be missed after a dwell time of 10 to 15 minutes.

In the initial tests, components were bombed and tested using the Bergquist leak detector in accordance with 883D methods. This method allows up to a one hour dwell time between bombing and insertion into the leak detector. If gross leak detection in small volume components is to be performed using helium as a tracer, shorter dwell times are required.

To reduce the effect of long dwell times in the second set of Bergquist leak tests, the packages were kept in one atmosphere of helium after bombing. This insured that helium inside the component volume could not dissipate into the air because of the short dwell time. To predict how this change in procedure changes the fine leak computation, the Howl-Mann equation must be adjusted to account for the time spent under one atmosphere of helium. This is a small effect if the exposure to one atmosphere is less than an hour. Only packages that passed the original fine and gross leak test were retested using this method.

Table 1 shows the results of all tests. In table 1, the sample numbers are arbitrary numbers assigned to the packages before they were received. The next two columns are the package internal volume and the reported weight gains or leak rates. Gross leak data taken with the Bergquist leak detector were considered to be failures if the helium partial pressure was seven times greater when the component was present than the background measurement taken after

component removal. Fine leak data were considered failures if the leak rate was greater than 10^{-7} std-cc/sec helium. Columns four and five are the results from the first tests performed on the Bergquist leak detector, the column labeled dwell time refers to these tests. No attempt was made to correct these data for dwell time. The columns labeled Bubble and Conventional refer to standard gross and fine leak detection methods as described in TM 1014. Again no attempt was made to correct for dwell time. The last four columns refer to the bubble, weight gain and Bergquist retests respectively.

A comparison of the data in table 1 produces several interesting observations. Parts 14, 28, and 29 passed the initial Bergquist test but failed during the retest. Data on these parts showed massive leaks that passed both fine and gross leak tests for long dwell times. This supports the conclusion that dwell time is a critical factor in gross leak checking components using helium as a tracer. It should also be noted that the large amount of helium introduced by the short dwell technique significantly increased the pressure in the test manifold.

Of the 13 components that passed the initial Bergquist test only four passed the retest in which the dwell time was shortened. Table 2 shows the data for the four components that passed the final leak test. The data for 147996 is not complete and has been eliminated from this analysis. Only 161124 would have failed conventional 883D test methods, excluding weight gain. Serial number 161129 failed initial Bergquist testing but passed the second test. Examination of the actual data revealed that the component failed marginally during the first test. This could have been caused by the introduction of parasitic helium during component introduction to the sample chamber. Sample 161130 passed all leak tests performed, including weight gain. It should be noted that these two samples and 161124 were all the same package type and these results could be indicative of an unknown feature of this package. Further, the history of these packages is not known to the authors, previous tests and handling could have sealed the leaks or reduced the internal package volume. Also of significance is the discrepancy between the weight gain test results for these packages and the reported weight gain results supplied with the components. This clearly indicates some, as yet unknown, common factor effecting the results for these components.

All of the eight components that passed the first test but failed the second were subjected to long dwell times. The shortest dwell time was 17 minutes for serial number 148954, suggesting a leak rate greater than 10^{-4} std cc/sec. Serial number 148946 was one of the packages destructively analyzed and had an estimated leak rate of $6 \cdot 10^{-4}$ std cc/sec. All of the other components that passed the initial test were subjected to much longer dwell times.

A total of 33 components were tested and 66% were found to have leaks using a non-optimized test method. Using the modified bomb technique, 87% failed, discounting the two packages that were destroyed. The remaining 13% that passed exhibited unusual behavior in both the Bergquist and conventional leak tests.

LEAK TEST RESULTS (LARGE VOLUME)

Besides collecting data on small volume components the leak detector was used to develop a seam welding schedule for a gold-plated .75 x .75-in. (.787cm³) flatpack. A design of experiments (DOE) approach was used [3]. The objective of the experiment was to understand the main effects and significant factor interactions that effect the seamwelding process. The DOEs described here use helium leak rate as the primary response or dependent variable. Using the Bergquist leak detector it is possible to repeatedly measure leak rates in the 10⁻¹²std cc/sec range and provide the test sensitivity needed to optimize the sealing process. In addition, it is possible to measure both gross and fine leaks in the same test cycle, thus providing quantitative data for leaks above 6.4* 10⁻⁶ std cc/sec.

The seam sealing operation uses two copper electrodes that roll along the package edge at preprogrammed settings. Electrode roller speed, power, and force, along with other factors, all work together to liquefy the metal between the lid and package and form a weld. The weld is actually a braze in which the plating material is reflowed to form the seal.

To be sure the Bergquist detector would find gross leaks, small holes were drilled in several hermetic packages, bombed in helium for 2 hours at 30 psig and checked for leaks. The results are shown in table 3. It was clear that even packages with a hole 13 mils in diameter could be detected. In this case a rate was not derived but the unusually high current reading indicated the part had a gross leak. Run # 101 is data for a package that had a hole made during an RGA test. Knowing that visual leaks were easily detectable allowed the use of only the Bergquist test for measuring hermeticity.

From the Bergquist leak detector, the measured value (L) is really a measure of the leak at the weld (R_W), plus the leak at the glass seals (R_S), plus the rate at which helium desorbs from the surface of the package (R_P), plus the atmospheric helium in the chamber initially (R_{Atm}), so:

$$L = R_W + R_S + R_P + R_{Atm}$$

It's difficult to separate R_S from R_W , so in these experiments the objective is to minimize the term $(R_W + R_S)$. RA_{tm} is minimized by the nitrogen purge. The amount of helium that desorbs from the package, R_p , can be measured and factored in for data collected immediately after helium bombing. Figure 6 shows actual measurements from an unlidded package that had been bombed for 2 hours at 30 psig. An empty, unlidded package roughly approximates the total surface area of a sealed package. Also shown are actual data for a sealed package (T13). As Figure 6 shows most of the helium escapes from the surface after the first 2 hours. The part then approaches its true leak rate $(R_S + R_W)$.

The first experiment was designed to identify a suitable range from which to conduct further experiments. The results of this simple two level fractional factorial are shown in table 4.

After review of the data from the fractional factorial, the range for each of the significant variables was reduced and a computer generated D-optimal design matrix was created. The results of the experiment are shown in table 5.

The leak rates recorded for packages T6 through T17 were taken from measurements made about 3 weeks after the parts underwent a 2 hour helium bomb at 30 psig. Packages T18 through T29 measurements were made about 7 weeks after a 2 hour helium bomb at 30 psig. Similar results were achieved when the measurements were made 1 to 2 hours after bombing and adsorbed helium was corrected for using the data in figure 6. With the exception of T11, the data indicates that very little helium was forced into the packages and the helium leak measurements recorded are more a reflection of the background helium in the atmosphere and are near the background limits of the leak detector as it is presently configured and operated. All 24 parts showed visually acceptable welds, hence the response data lies on the flat part of the optimization curve. Except for the low power, high speed, low force setting for T11, it does not matter what combination is chosen within the limits tested, a good weld is formed. The fact that the T11 settings were the worst case makes sense, because low power and high roller speed produces less of a melt and therefore increases the probability for leaks.

The results from the D-optimal design and subsequent confirmation runs identified an optimal working range for the package sealer. An additional eight-run two-level full factorial was set up to understand the limits of the seal schedule. The factor settings chosen were outside the range of the D-optimal, but inside the limits of the fractional factorial. The response data are shown in table 6. The first set of measurements were made after a 2-hr bomb at 30 psig. The parts were then retested a week later with no additional bombing. The same general trends emerged from this second set of data. In the case of T64, all the helium leaked from the package. From these data the following regression equation was generated, which has an adjusted R-squared of 0.91.

$$-\text{Log}(\text{Leak rate}) = 6.86 + 0.73(S) - 0.29(P) + 0.74(F) + 1.72(S)(P) + 0.53(S)(F) - 0.94(P)(F)$$

Note that the coefficient for S*P is greater than the others, which indicates a strong interaction as suspected.

Figure 7 is a graphic illustration that compares the data collected using the Bergquist technique vs. data obtained using the conventional 883 TM1014 testing techniques. As can be seen the Bergquist technique provides reliable, quantitative leak test data from 10^{-12} std cc/sec through 10^{-4} std cc/sec whereas, conventional test technique have little or no visibility below 10^{-10} std cc/sec and provide only qualitative pass fail information above 10^{-6} std cc/sec. This extended dynamic range provides the opportunity to explore ways to improve the seal process.

There were approximately 100 parts that were sealed and leak tested as part of this experiment. Many of the parts were tested more than once in the Bergquist leak detector and these results were compared to conventional 883 techniques. In every case where the Bergquist indicated a gross leak the part also failed the 883 bubble test. And in every case where the Bergquist test result indicated a low helium leak rate (e.g. see table 5), the 883 fine leak test method also indicated a small leak.

CONCLUSIONS

The testing of small volume parts is still problematic. Completely unambiguous tests for gross leaks are close but have not yet been realized. The test methods described here do have several significant advantages over current techniques. A single test is used for both fine and gross leaks. In larger packages (volume > 0.15 cc) this method has been shown to be adequate and unambiguous. Helium is used as a tracer for both tests resulting in complete freedom from contamination and the masking effects present in many gross leak test methods. Costly optical components sensitive to contamination are readily tested using this method. The dynamic range of the fine leak test ranges from 10^{-4} std-cc/sec to 10^{-12} std-cc/sec, are possible. This dynamic range allows for greater sensitivity and better process control. Further, the system used to make these measurements is completely automated which reduces training time and chance for error.

Other techniques to enhance reliability discussed here improved the performance of the system. Specifically, allowing the devices to remain under helium purge prior to leak testing caught virtually all the packages with gross or fine leaks. Of the four that passed three exhibited unusual behavior and

might have been passed by the current 883D test methods. The results of the tests performed on these packages illustrate the need for improved leak detection equipment and practices.

Perhaps the easiest method of improving fine leak sensitivity is adding helium to the fill gas used when sealing components. Using a technique such as this in conjunction with the Bergquist method completely eliminates bombing and the need for individual gross and fine leak tests. Further, the greater sensitivity to fine leaks allows for better seal process optimization and control.

REFERENCES

- [1] MIL-STD-883, Test Methods and Procedures for Microelectronics, TM 1014 (SEAL).
- [2] L.E. Bergquist, "Small Component He Leak Detector," U.S. Patent 4,608,866 (2 Sept 1986).
- [3] Green, T.J., Duncan C., Using DOE to Optimize Hermetic Package Seamwelding, *Proceedings of the International Society for Hybrid Microelectronics*, San Francisco, California, OCT, 1992.

Sample #	Vol. cc	Reported Wt. Gain mg	Gross		Dwell Time	Bubble	Conventio	Bubble Retest	Weight Gain mg	Gross		Fine
			Bergquist	Fine						Bergquist	Fine	
1	0.20	362	FAIL	PASS	26	FAIL	PASS					
14	0.20	113	PASS	PASS	43	FAIL	FAIL			FAIL	FAIL	FAIL
28	0.20	368	PASS	PASS	34	FAIL	PASS			FAIL	FAIL	PASS
29	0.20	349	PASS	PASS	51	FAIL	PASS		347.6	FAIL	FAIL	FAIL
31	0.20	345	FAIL	FAIL	2	FAIL	PASS		341.9	FAIL		
147818	0.01	17	PASS	PASS	57	FAIL	PASS		16.1	PASS		
147994	0.01	16	FAIL	PASS	65	FAIL	PASS		17.5	PASS		
147996	0.01	18	PASS	PASS	48		PASS			PASS	PASS	PASS
147998	0.01	15	FAIL	PASS	40	??????	PASS		9.8	FAIL		
148919	0.02	>1E-7	FAIL	FAIL	33	PASS	FAIL		2.7	PASS		
148920	0.02	>1E-7	FAIL	FAIL	37	PASS	FAIL		1.8	PASS		
148921	0.02	>1E-7	FAIL	FAIL	46	PASS	FAIL		0.6	PASS		
148922	0.02	>1E-7	FAIL	FAIL	12	PASS	FAIL		2.2	PASS		
148923	0.02	>1E-7	FAIL	FAIL	20	PASS	FAIL		1	PASS		
148924	0.02	>1E-7	FAIL	FAIL	34	FAIL	PASS					
148946	0.02	17	FAIL	PASS	54		PASS					
148952	0.02	32	PASS	PASS	6		PASS					
148954	0.02	32	PASS	PASS	17	FAIL	PASS			FAIL	FAIL	PASS
149183	0.05	77	FAIL	PASS	57	FAIL	PASS					
149190	0.05	79	FAIL	PASS	42	FAIL	PASS					
155056	0.04	88	PASS	PASS	65	FAIL	PASS					
155057	0.04	>1E-7	FAIL	FAIL	2	PASS	FAIL		3.1	PASS		FAIL
161123	0.06	90	FAIL	FAIL	9	FAIL	PASS					
161124	0.06	90	PASS	PASS	33	FAIL	FAIL		4.4	PASS	PASS	PASS
161127	0.06	90	FAIL	FAIL	23	FAIL	FAIL					
161129	0.06	90	FAIL	FAIL	18	PASS	PASS		6	PASS	PASS	PASS
161130	0.03	90	PASS	PASS	57	PASS	PASS		-0.1	PASS	PASS	PASS
161176	0.02	12	FAIL	FAIL	14	PASS	FAIL		20	PASS		
161177	0.02	12	FAIL	FAIL	47	FAIL	FAIL		34.2	PASS		
161182	0.02	12	FAIL	FAIL	23	FAIL	FAIL		91.4	FAIL		
161183	0.02	12	PASS	PASS	31	FAIL	FAIL				FAIL	FAIL
161184			PASS	PASS	39	FAIL	PASS				FAIL	FAIL
161224	0.01	14	PASS	PASS	21	FAIL	PASS				FAIL	PASS

Table 1; Bergquist leak test results vs. other hermeticity test techniques.

Sample	Vol.	Reported	Gross	Fine	Dwell	Bubble	Fine	Bubble	Weight	Gross	Fine
	cc	Wt. Gain	Bergquist		Time	Conventional		Retest	Gain	Bergquist	Retest
		mg							mg		
147996	0.01	18	PASS	PASS	48		PASS			PASS	PASS
161124	0.06	90	PASS	PASS	33	FAIL	FAIL	PASS	4.4	PASS	PASS
161129	0.06	90	FAIL	FAIL	18	PASS	PASS	PASS	6	PASS	PASS
161130	0.03	90	PASS	PASS	57	PASS	PASS	PASS	-0.1	PASS	PASS

Table 2; Leak test results for selected parts.

Run #	Hole Diam. (in.)	Dwell Time	Leak Rate (Bergquist)	Leak Rate (TM1014)
T104	.0033	10 seconds	1.16E-05	FAIL
T105	.0031	5 seconds	1.28E-05	FAIL
T109	.0032	3 minutes	2.64E-05	FAIL
T124	.0029	28 minutes	9.95E-05	FAIL
T125	.0024	16 minutes	8.45E-05	FAIL
T129	.0019	89 minutes	1.04E-04	FAIL
T101	.0137	1 minutes	high current	FAIL

Table 3; Leak rates from packages with laser drilled holes.

Run #	Bergquist	1014 (Fine)	1014 (gross)	Description of weld
T1	5.52E-05	6.40E-06	FAIL	Minimum melt at weld
T2	4.50E-06	6.40E-06	FAIL	Minimum melt at weld
T3	4.50E-05	6.40E-06	FAIL	Too hot, Au depletion
T4	-----	2.20E-09	PASS	Too hot
T5	5.33E-05	6.40E-06	FAIL	O.K.

Table 4; Measured leak rates from first package sealing experiment.

Run #	Power % of Max	Speed in./sec.	Force Newtons	Measured He Leak Rate	
				He cc/sec (T6-T17)	(T18-T19)
T6/T18	30	1.5	30	7.46E-12	2.50E-11
T7/T19	30	.5	14	9.11E-12	1.10E-12
T8/T20	40	1.5	14	1.07E-11	2.70E-11
T9/T21	40	.5	30	8.45E-10	2.83E-11
T10/T22	40	1.5	30	6.41E-12	1.39E-11
T11/T23	30	1.5	14	1.38E-09	9.50E-12
T12/T24	30	.5	30	4.42E-12	7.60E-12
T13/T25	40	1.0	22	5.92E-12	5.60E-12
T14/T26	35	1.0	30	6.25E-12	2.50E-12
T15/T27	35	1.5	22	6.13E-12	2.40E-11
T16/T28	40	.5	14	4.34E-12	1.93E-11
T17/T29	35	.5	14	3.32E-10	3.20E-12

Table 5; Measured leak rates from D-Optimal experimental test run.

Run #	Power % of Max	Speed in./sec.	Force Newtons	Leak Rate He cc/sec <i>2 hr bomb 30 PSIG</i>	Dwell min	Leak Rate He cc/sec <i>no bomb one week later</i>	Dwell
T60	25	.4	10	5.49E-08	2	4.84E-08	1 week
T61	25	.4	25	9.06E-10	9	2.00E-11	1 week
T62	55	.4	10	2.60E-05	15	1.87E-09	1 week
T63	55	.4	25	2.18E-04	52	1.32E-09	1 week
T64	25	1.6	10	2.08E-04	45	1.76E-11	1 week
T65	25	1.6	25	2.46E-09	60	5.37E-11	1 week
T66	55	1.6	10	1.07E-09	66	2.64E-11	1 week
T67	55	1.6	25	7.99E-10	72	2.00E-11	1 week

Table 6; Results from the full factorial sealing experiment.

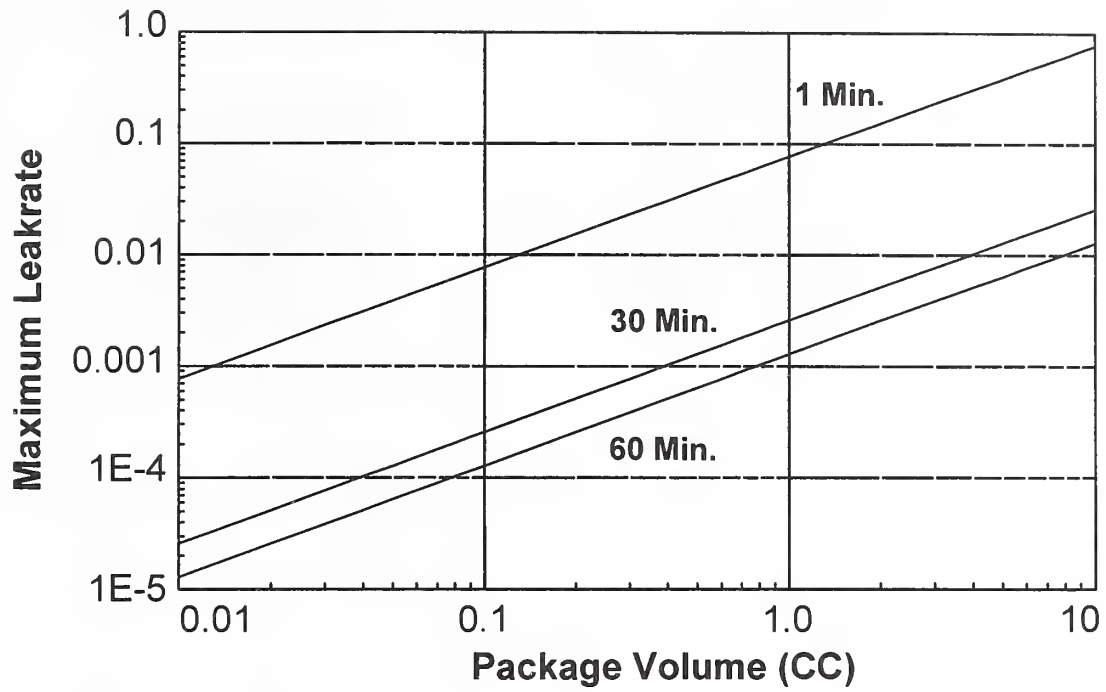


Figure 1. Detectable leakrate as a function of package volume for dwell times of 1, 30, and 60 minutes

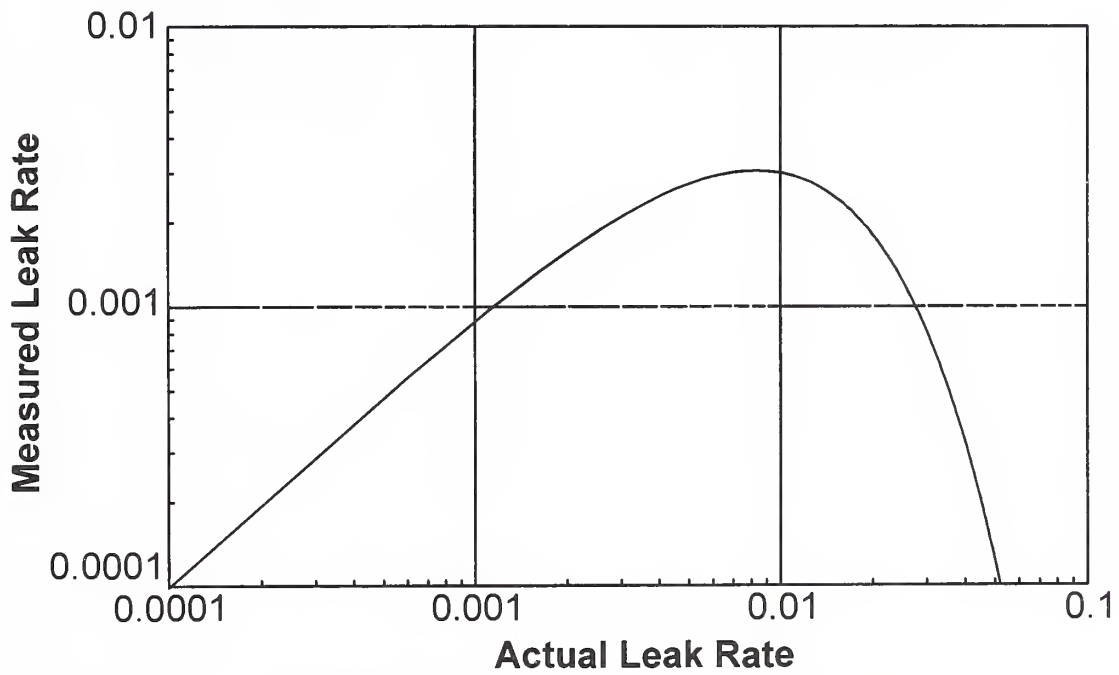


Figure 2. Measured leak rate vs. actual leak rate for a 1 cc package volume and 2 minute dwell time

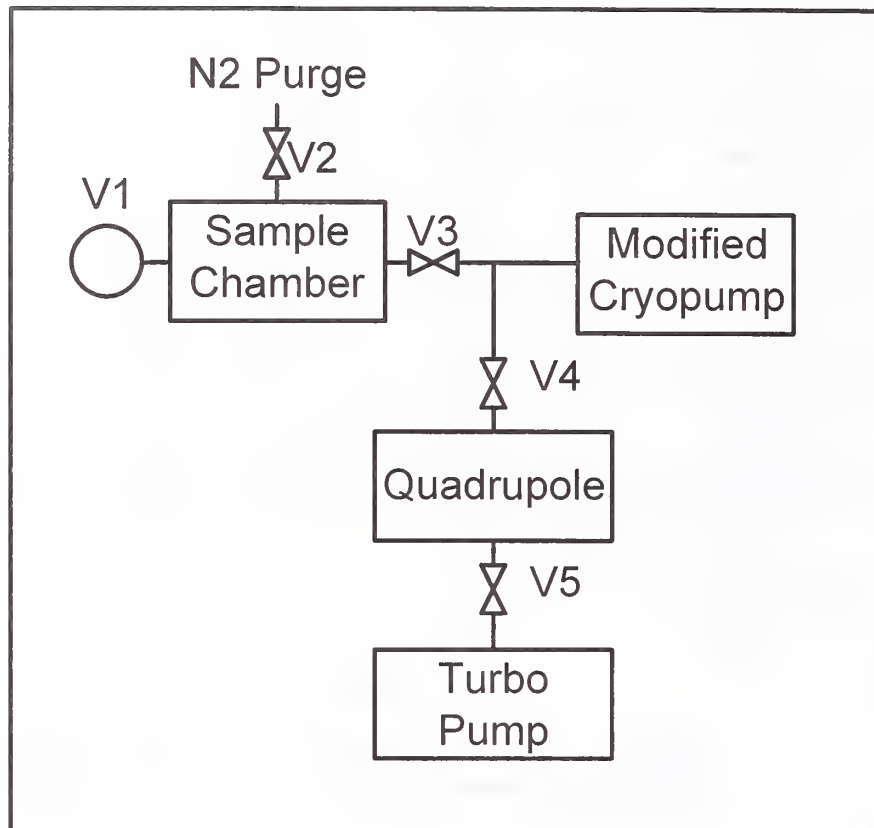


Figure 3. Leak Detector Block Diagram

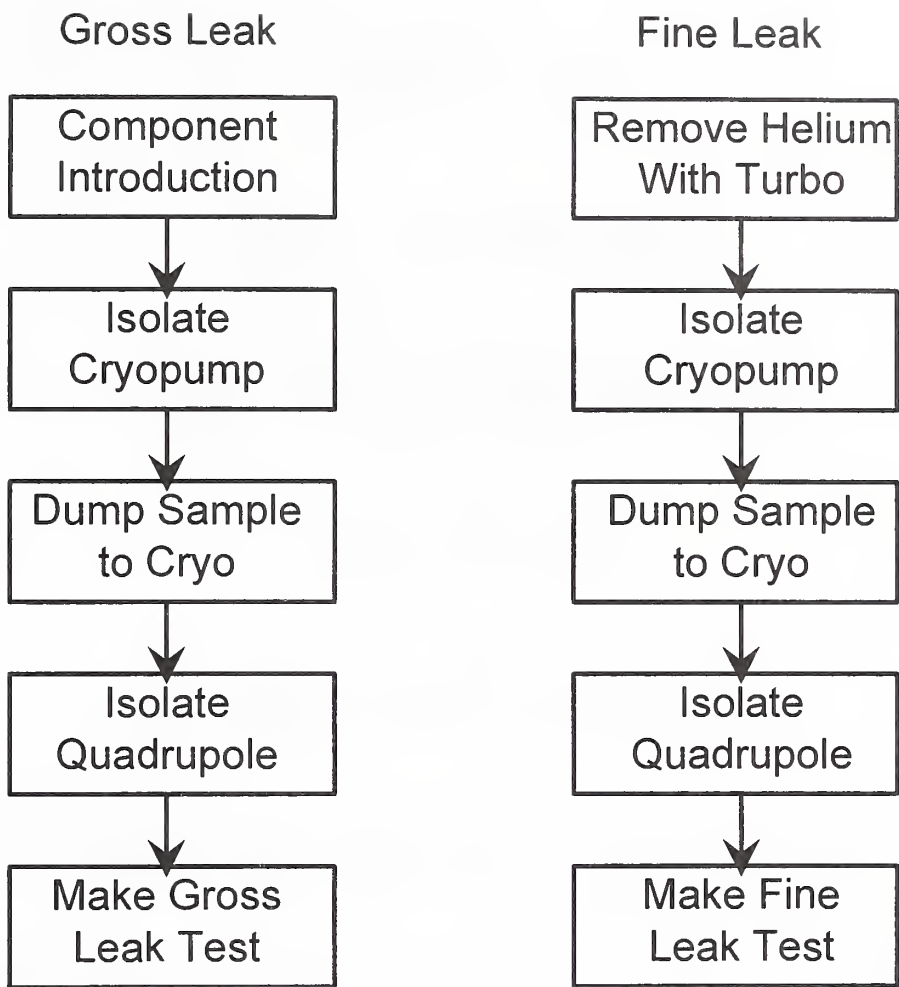


Figure 4. Leak Test Flow

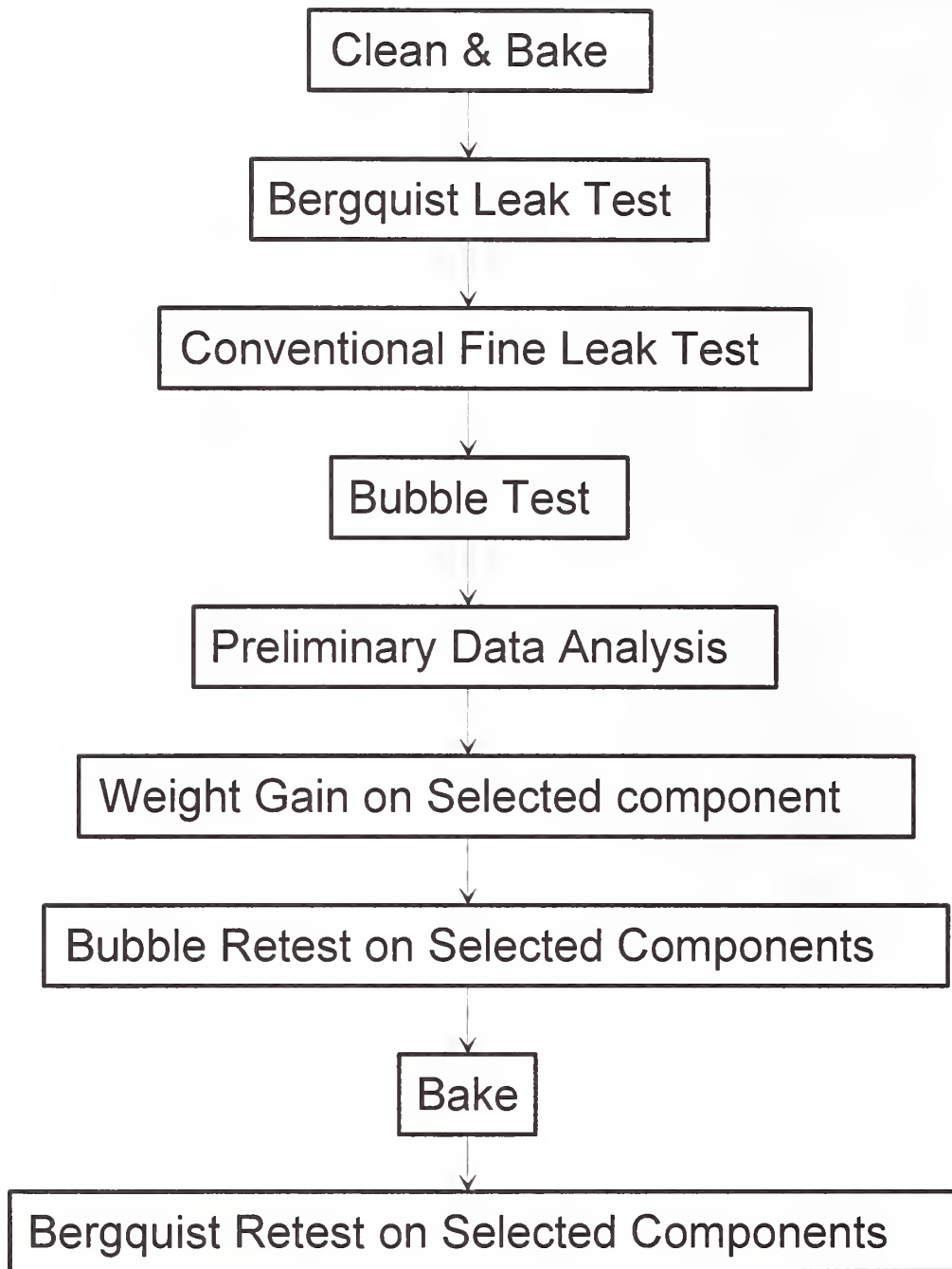


Figure 5 Leak Test Flow

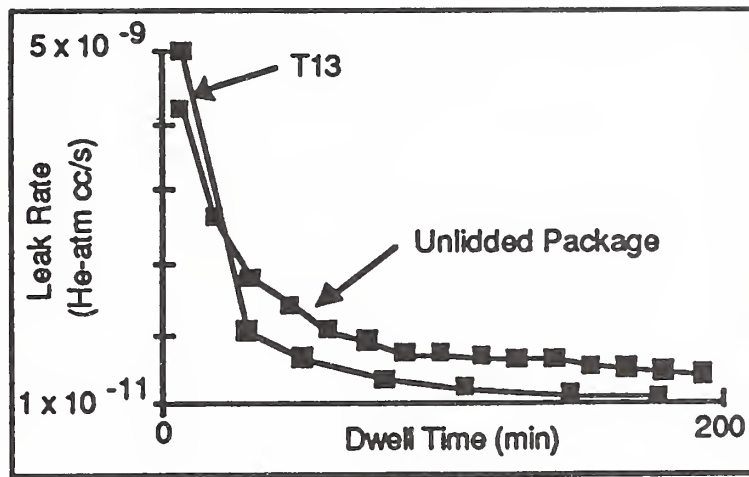


Figure 6; Leak rate as a function of dwell time for a .8 cc package volume

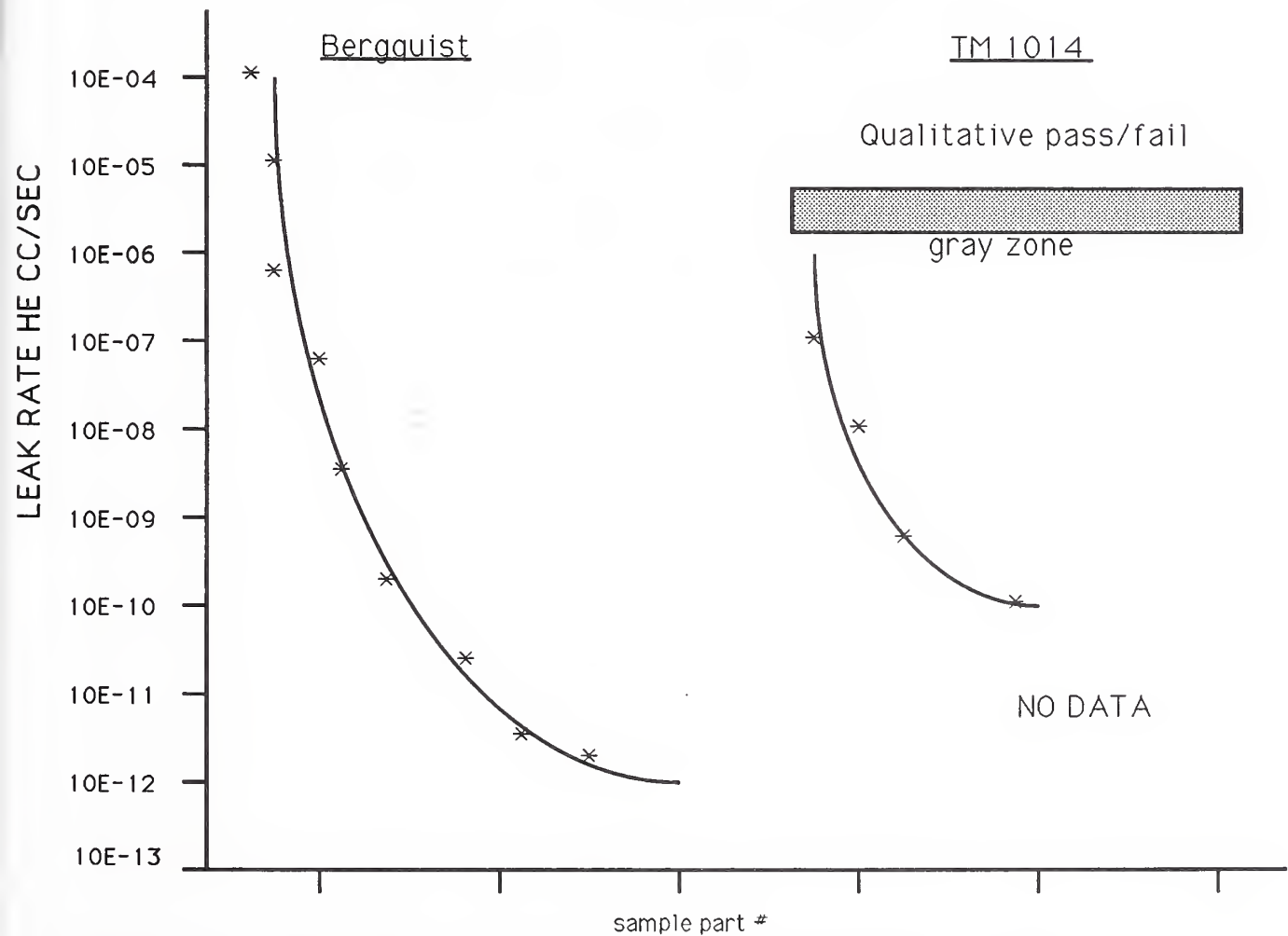


Figure 7; Illustrates the range of leak test data that is possible using the Bergquist technique vs conventional TM 1014 test techniques.









